CRANFIELD UNIVERSITY

College of Aeronautics

PhD Thesis

K H LOH

An Investigation into the Hovering Flight Dynamics and Control of a Flapping Wing Micro Air Vehicle

Supervisor : MIKE V COOK

Feb 2003

This Thesis is submitted for the Degree of Doctor of Philosophy

PAGE NUMBERS CLOSE TO THE EDGE OF THE PAGE
SOME ARE CUT OFF

In memory of my father,
who instilled in me the desire to learn

ACKNOWLEDGEMENTS

I would like to thank the Ministry of Defence and the Defence Science Organisation of Singapore, who sponsored me on this long and arduous journey.

I would like to thank Mr Mike Cook and Mr Pete Thomasson who provided the high level of supervision and constructive comments during the entire research.

A special thanks goes also to Professor Charles Ellington of Cambridge University, who provided valuable advice and information during the experimental phase of this research.

Mention must be made of the wonder-kid Dr Simon Wiedermeier, whom I used to jokingly refer to as my 'research assistant' because he assisted me (in fact directed me) when faced with the problems in the electronics of the test-rig.

The help provided by Clive, Trevor, Paul, Julie and Malcolm in the manufacture of the components are also appreciated.

Most importantly, I must thank my wife and children, without whom I would not be able to embark on and complete this piece of work.

ABSTRACT

The hovering flight of a micro air vehicle was investigated. Various flight control concepts, inspired by observation of insect and bird flight, were investigated in some detail. The concepts make use of flap frequency or phase between the flap and pitch attitudes of the wing to control the force magnitude. Tilt of the stroke plane or fuselage was used to vector the force. A flight control system was designed for each concept investigated.

The investigation has revealed that the preferred control concept is one in which force vectoring is achieved by the fuselage tilt through a shift in the centre of gravity location while the force magnitude is controlled by the phase between pitch and flap attitudes. This has the advantage of reducing the vehicle weight while at the same time relaxing the demand of extremely high frequency actuators.

The equations of motion based on a multi-body representation of a flapping wing micro air vehicle were derived and these form the basis for the SIMULINK flight simulation program used to carry out the above investigation.

The aerodynamic model used for the simulation was obtained from force measurements with a flapping mechanism that allows the model wing to oscillate with two degrees of freedom (flap and pitch). During these measurements, the phase angle between the flap and pitch angles of the model wing was varied to determine the effects on the force magnitude and direction.

Contents

Nomenclature

$\mathbf{a}$	Vector $[a_x \ a_y \ a_z]^T$
$\mathbf{a}^x$	Skew symmetric form of vector $\mathbf{a}$ $\begin{bmatrix} 0 & -a_z & a_y \\ a_z & 0 & -a_x \\ -a_y & a_x & 0 \end{bmatrix}$
$\mathbf{B}$	3x3 matrix
a_j, b_j	Fourier coefficients of the j-th harmonic
$\mathbf{b}_i$	Position vector of joint P_i from the origin of the reference system of R_h
$\mathbf{C}_{ij}$	Direction cosine matrix from j-th reference frame to the i-th reference frame
C_{xi}, C_{yi}, C_{zi}	Aerodynamic force coefficients in the x-, y- and z-directions of the i-th reference frame
C	Damping
$\bar{c}$	Wing mean chord
$\mathbf{c}_w$	Column vector of the first moment of inertia for the wing
c_α, s_α	Cosine and sine of the angle α
D	Drag
$\mathbf{d}_w$	Vector from the pivot of the flapper (flap axis) to the CG of the flapping arm including wing
$\mathbf{f}_i$	column vector of external forces acting on R_i
F_{xi}, F_{yi}, F_{zi}	Aerodynamic forces in x-, y- and z-directions of the i-th reference frame
${}^i\mathbf{F}$	Column vector of forces in the i-th reference frame
$\mathbf{F}$	Column vector of externally applied forces
$\mathcal{F}_i$	Reference frame of R_i
$\mathbf{g}_i$	External torque acting on body R_i
$\mathbf{g}_{pi}$	Internal torque acting on body R_i
$\mathbf{h}_i$	Angular momentum of R_i
$\mathbf{I}$	Identity matrix
I	Second moment of inertia
$\mathbf{J}$	Tensor of second mass moment of inertia
k_{dir}	Factor accounting for stroke direction
K	Stiffness
k	Feedback gain

l	Model scale length, R_{mod} / R_{moth} or R_{mod} / R_{veh}
$\boldsymbol{l}_{cp}$	Position vector of wing centre of pressure from the origin of the wing reference frame
L, S, D	Lift, side force and drag of wing
m	Mass
n	Number of harmonics in Fourier series
n	Flap frequency
N	Number of points per cycle
P_1	Position vector of the origin of fuselage reference frame given in the inertial frame $\boldsymbol{F}_0$
$P_{req,aero}$	Aerodynamic power requirement of model wing
$P^*_{req,aero}$	Aerodynamic power requirement per unit mass of micro air vehicle or moth
p_i	Linear momentum of R_i
p	Roll rate of fuselage
q	Pitch rate of fuselage
R	Wing span
R_e	Reynolds' number
r	Yaw rate of fuselage
s	Laplace variable
$\hat{t}$	Non-dimensionalised time, t/T
T	Periodic time of flapping cycle, time constant
T	Transformation matrix
u	Input vector
u_b	Velocity of fuselage along its P_1x_1 axis
V	Velocity
v_b	Velocity of fuselage along its P_1y_1 axis
w_b	Velocity of fuselage along its P_1z_1 axis
x	State vector
y	Output vector

Greek Symbols

$\bar{\alpha}, \hat{\alpha}, \dot{\alpha}, \ddot{\alpha}$	mean, amplitude, first time derivative and second time derivative of angle α
β_{SPA}	Angle between time-averaged resultant aerodynamic force and stroke plane
β^*	Angle between stroke plane and horizontal plane

Greek Symbols (cont'd)

ε	Error signal
χ	Pitch angle
δ	Flap angle
κ	Stroke plane angle
λ	Eigenvector
μ	Absolute viscosity of air or coefficient of friction
τ	Non-dimensionalised periodic time
ρ	Density of air
φ	Phase lead between pitch and flap
ϕ	Fuselage bank angle
$\mathbf{\Phi}$	Vector of wing Euler angles, $[\kappa\ \delta\ \chi]^T$
θ	Pitch attitude of flapper or of fuselage
$\boldsymbol{\vartheta}$	Vector of fuselage Euler angles, $[\phi\ \theta\ \psi]^T$
ψ	Yaw angle of flapper
ζ	Damping ratio
ω	Damped natural frequency
ω_n	Undamped natural frequency
ω_{pi}	Column vector of relative angular velocity of R_i with respect to R_h, $\omega_i - \omega_h$

Indices

aero	Aerodynamic component
B	Balance axes system
calc	calculated
dmd	demanded
E	Euler
F	Flapper axes system
grav	Gravity
L	LSD axes system
l	roll moment
m	pitch moment
mod	Model
n	yaw moment
p	port
q	pitch rate
s	starboard
T	Tunnel system, transpose

Indices (cont'd)

V	RVF axes system
veh	Vehicle
W	Wing axes system
0	Inertial frame, initial state
1	Fuselage
2	Port stroke plane actuator motor
3	Starboard stroke plane actuator motor
4	Port wing
5	Starboard wing

List of Acronyms

A/D	Analog to Digital
CFD	Computational fluid dynamics
DoD	Department of Defense
DCM	Direction cosine matrix
GPS	Global positional system
LDS	Lift drag system
MAV	Micro air vehicle
MEMS	Micro-electro-mechanical systems
NED	North-East down system
PC	Personal computer
RVF	Resultant vertical force

List Of Figures

Chapter 1

Chapter 2

Chapter 3

Chapter 4

Chapter 5

Chapter 7

Chapter 8

Chapter 9

List of Tables

Chapter 2

Chapter 5

Chapter 7

Chapter 8

Chapter 9

CHAPTER 1

INTRODUCTION

1.1 MOTIVATION

This thesis describes an investigation of the flight dynamics and controllability of a micro air vehicle (MAV) during hovering flight in which the principal source of weight support and thrust is its wings that flap like the birds, bats and insects. In general, this type of vehicles is called a flapping wing MAV.

MAVs are small autonomous vehicles identified by the National Defence Research Institute in the United States in the endless pursuit of the advantage provided by the possession of high-technology systems over those who do not.

MAVs are to traverse large distances to carry out surveillance, search and locate missions in adverse conditions, such as the aftermath of an earthquake, when fitted with a micro-camera. When properly equipped, it could carry out attack missions to seek out the infantryman and deliver a non-lethal dose of incapacitating agent thus immobilising him to be apprehended.

The current official US Department of Defence (DoD) requirement limits the size of an MAV to less than 15 cm in any dimension and to a maximum weight of 110 grams, so that it can be carried and deployed by a foot soldier. The vehicle is to have an endurance of between 20 to 60 minutes, whilst carrying a payload of around 56 grams at speeds in the range of 32 to 64 km/h and a maximum range of 4.8 km.

By 1999, at least 4 prototypes had flown for the first time in the USA. The Black Widow of AeroVironment, the MicroStar of Lockheed Sanders, the Trochoid and the Bat of MLB are all fixed wing configurations. However, the Microbat is a flapping wing design of AeroVironment. Other concepts, some innovative like ducted fan-body and a multi-mode (flying / crawling) vehicle employing flapping flight are also under consideration. Less revolutionary types employing rotary wing technology are also being investigated.

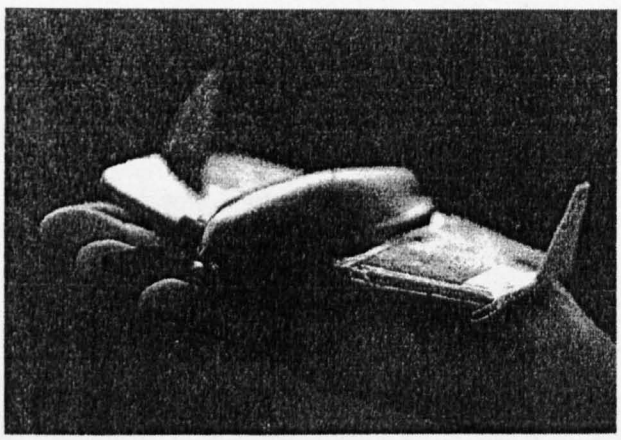

Fig 1.1 **The MicroStar from Sanders has flown for 15 mins under manual control (Courtesy of Lockheed Sanders)**

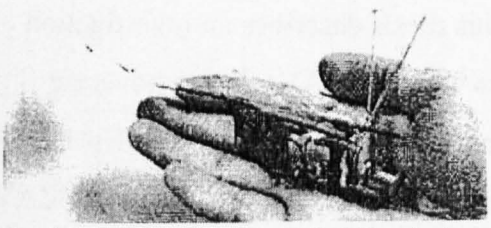

Fig 1.2 **AeroVironment's Microbat ornithopter (Photo, AeroVironment)**

The typical MAV mission requires it to fly inside a confined space, such as inside a building, where the size and location of obstacles are often unknown at the outset. This requires stealthiness as well as a limit on the maximum airspeed for better agility. An MAV based on the rotary wing design with a rotor running in excess of a thousand Hz, or a fixed wing powered by a propeller running at 30,000 rpm (500 Hz) would generate a

high noise signature. The Trochoid and the Black Widow are audible within 30 metres and fly at airspeeds above 16 km/h. At lower airspeeds, small wing areas utilising conventional airfoils are not able to generate sufficient lift to support the weight of the vehicle. Alternative weight support, such as thrust vectoring, will increase power consumption and weight, and thus limit range and endurance.

The disadvantages of the fixed and rotary wing designs make flapping flight an interesting alternative. The flapping wings of birds and insects, on the other hand, are hardly audible. Power requirement is much lower than for both fixed and rotary wing designs. Insects employing flapping wing flight require a maximum of only 70W/kg [Dudley and Ellington, 1990, Tennekes, 1997] compared to 150W/kg for aeroplanes [Zbikowski, 1999]. With wings flapping, insects and birds generate additional lift through unsteady aerodynamic effects to provide the support, thus enabling them to fly at airspeeds below 11 km/h.

Another advantage of flapping flight is the capability to hover. Although fixed wing designs can hover if the propeller can generate thrust higher than the weight, these often require a large change in body attitude from close to horizontal to a vertical orientation. This would mean that the target of surveillance might be out of the field of view of the video camera. Hovering at a spot for a limited time is generally not a problem for most insects and some birds, while others are capable of hovering for extended durations. They also do so without much change in body orientation.

1.2 HISTORICAL DEVELOPMENT OF FLAPPING FLIGHT

Man has always been awed by the ease with which birds and insects fly. From primitive times he has watched these creatures and yearned to fly like them. It seems so natural and easy to flap the wings and be airborne. Without any other form of power than his own muscles, it was only instinctive to don feather-covered wings and flap his arms in the hope to soar like the birds. History records that this approach was doomed to failure from its outset.

Man's interest in flight was first registered as early as 843 B.C. when Bladud, the ninth king of Britain, was killed when he attempted to fly in Trivanatum (London) using wings covered with feathers. Between this time and the first record by Marco Polo in the 14th century of man becoming airborne on kites in Cathay (China), numerous experimenters must have been killed just like King Bladud when their attempts to fly failed.

Fig 1.3 King Bladud of Trivanatum (Taylor, 1989)

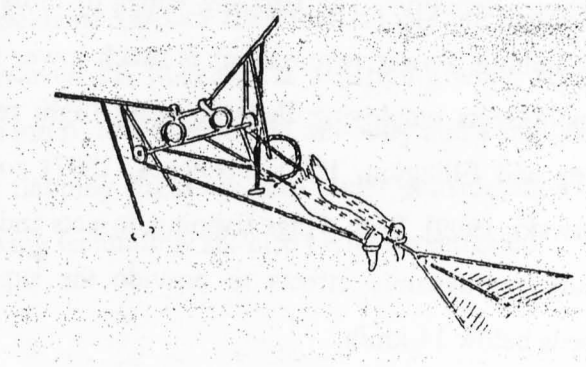

Fig 1.4 Leonardo da Vinci's invention (Chanute, 1976)

Despite these setbacks, Man's fascination with flight, and especially flapping flight, was undaunted. In 1250, an English Franciscan monk made a reference, in his book entitled '*Secrets of Art and Nature*', to a flying machine that has '*artificiall Wings made to beat the Aire*' known today as an ornithopter.

Although the Italian artist Leonardo da Vinci had designed various types of flying machine such as the parachute, ornithopter, helicopter and powered aeroplane between 1483 and 1497, it was not until 1647 that the first flying machine was produced and flown by Italian Titus Livio Burattini, who was at the Polish court of King Wladyslaw IV. It had four sets of wings, two sets beating as those of an ornithopter. In 1772, Canon Desfarges constructed an ornithopter but this proved unsuccessful. However, close to a decade later in 1781, Karl Friedrich Meerwein of Austria designed and built an advanced form of glider, for which a proper area of wing was calculated for manned flight. It was

said to have flown on at least two occasions whereby an up-and-down movement of the oval wing provided some form of propulsion.

Herzafen Celebi of Turkey accomplished gliding as early as the 17th century and followed later by George Cayley's full-size unmanned glider in 1809. Although much effort and design talent were engaged in getting airborne solely by imitating the flapping of wings by birds and insects, there was no success. When the early inventors resorted to human power to flap the wings, they failed to realise that not only are human beings not as strong as birds, weight for weight, humans were also not able to develop energy fast and long enough to flap the wings at the necessary frequency to generate sufficient lift. Attempts, such as the one made by Albrecht Berblinger of Germany to fly across the Danube in 1811, were always unsuccessful (although in 1929, Alexander Lippisch [1960] showed that extended glide but not sustained flight was possible when a human powered ornithopter was first towed to altitude).

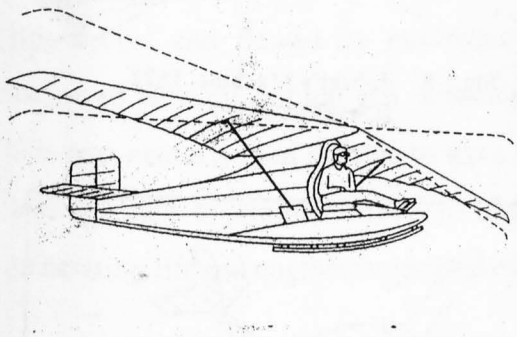

Fig 1.5 Lippisch's 1929 Human powered ornithopter (DeLaurier, 1994)

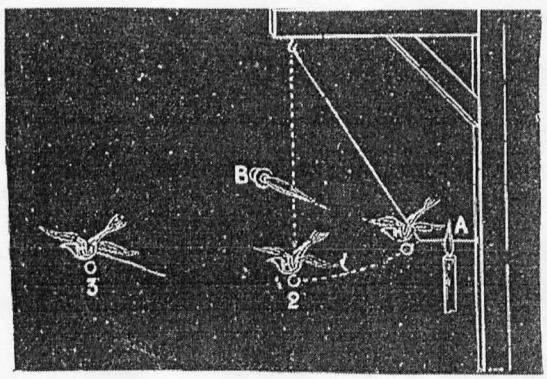

Fig 1.6 Gustav Trouve's model ornithopter, 1870 (Chanute, 1976)

On the front of power for flight, attempts to make use of the steam engine to power the wings were futile. The earlier steam engines were unreliable in operation while others suffered from vibration. Later engines usually weighed too much for the power that they delivered.

Other inventors then looked at the smaller scale and started developing models, making use of energy stored in gunpowder and later in twisted rubber strip as alternative sources of power. In 1870, Gustav Trouvé successfully flew a model ornithopter using revolver parts to beat the wings up and down. Two years later in 1872, Hureau de Villeneuve, the permanent Secretary of the French Aeronautical Society, flew his mechanical bird powered by twisted rubber. The model was able to start direct from the ground, but owing to the limited power of the rubber spring, it managed to rise to a height of only 4 feet. In the same year, Jobert managed to fly his ornithopter, which had four wings beating alternately in pairs, powered also by twisted elastic band.

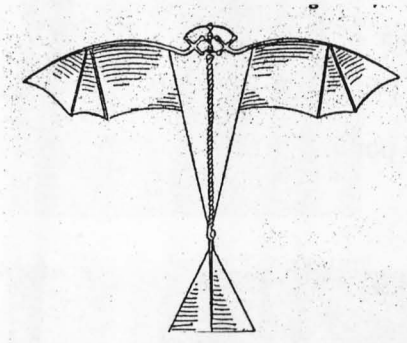

Fig 1.7 Hureau de Villeneuve's Machine, 1872 (Chanute, 1976)

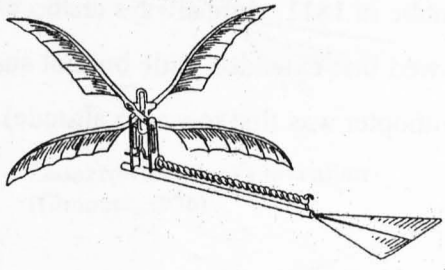

Fig 1.8 Jobert's Machine, 1872 (Chanute, 1976)

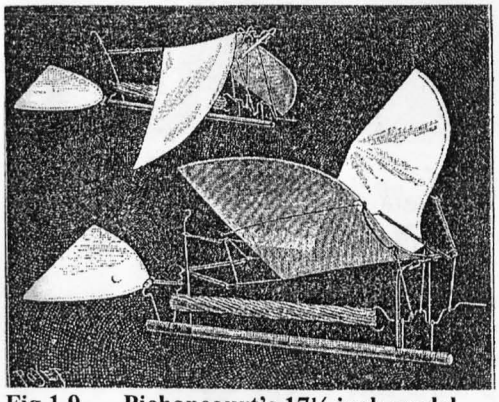

Fig 1.9 Pichancourt's 17½ inch model 1889 (Chanute, 1976)

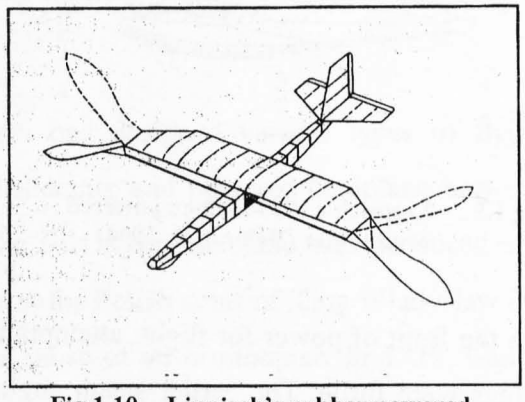

Fig 1.10 Lippisch's rubber powered ornithopter, 1938 (Chanute, 1976)

In 1889, Pichancourt's 17½-inch model flew up to a height of 25 feet and to a distance of 70 feet against a slightly adverse wind. More recent designers, as quoted by DeLaurier

[1994] included Lippisch in 1935 and Kieser in 1985. Both ornithopters are rubber powered.

Prior to the first manned, powered, sustained and controlled flight of December 17, 1903 at Kitty Hawk by the Wright brothers, numerous designs of various types of flying machine from flapping wings (employing flapping flight) to screws (now known as propellers) to aeroplanes (or fixed wing aircraft) were tried. As it turned out, none designed before the Wright brothers proved successful to carry the weight of the airframe, the power source and the man on board. Since the memorable twelve-second flight of over 120 feet by Orville Wright, the entire 20th century saw rapid development in aeronautics and astronautics. It was transformed to an era where supersonic aeroplanes zoom hundreds of passengers across the world and where helicopters and thrust vectoring fixed wing and swing-wing aircraft demonstrated extreme agility while performing air combat manoeuvres. Flapping wings as a mode of flight almost faded into oblivion.

What appeared to be a natural form of flight performed by hundreds of bird species and thousands of insect species with such ease of flapping their wings, seemed to prove impractical and flawed by numerous engineering limitations and left best to beings endowed with the natural gift. Looking at the aeronautical research and development of this past century, man seemed to have abandoned the more complicated method of flight and resorted to simpler forms of flight offered by the aeroplane (with fixed wings generating lift and engines or propellers producing the forward thrust) or helicopters.

In the meantime, while the aeronautical interests were directed towards the development and improvement of fixed wing and rotary wing technologies, zoologists and biologists world-wide were, and still are, fascinated at answering questions on avian and insect flight. They have made use of tools developed for the aeronautical industry such as the wind tunnel, computational fluid dynamics methods and the aerodynamic knowledge in their studies. High-speed photography and videography have allowed them to study the kinematics of the insect and avian wing as they perform their manoeuvres.

Man has in his possession today, tools and knowledge that were unavailable even 50 years ago. The flapping mode of flight that was impractical then may seem achievable now. The 19th century designers and inventors were not supported by modern day technology. Today, we have high performance computers to help optimise design of lightweight structures, which are less susceptible to mechanical destruction when under the action of powerful engines, which generate high power per unit mass. Computer technology allows us to develop our knowledge of aerodynamics, structural dynamics and their interaction.

It was only towards the end of the 20th century that DeLaurier [1993a] of the University of Toronto and his students successfully demonstrated that flapping wing flight would still be possible on a scale larger than those tested in the 19th century. A 25% scale proof-of-concept model of the ornithopter with a nine-foot span and weighing approximately 9 lbs flew via radio control a total of 38 powered flights in 1991, the longest of which lasting 2 minutes and 46 seconds. Taxi trials on the full-scale model have shown that the ornithopter can be propelled forward through the flapping wings alone [Anon, 1999a].

Although less sophisticated, the 'Tim Bird', which is a rubber-powered ornithopter sold as a toy, demonstrates that the complexity of flapping flight will some day be overcome.

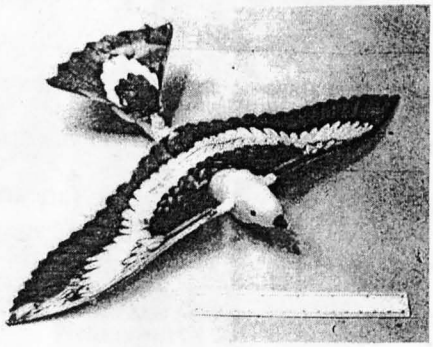

Fig 1.11 'Tim' bird, rubber powered ornithopter (DeLaurier, 1994)

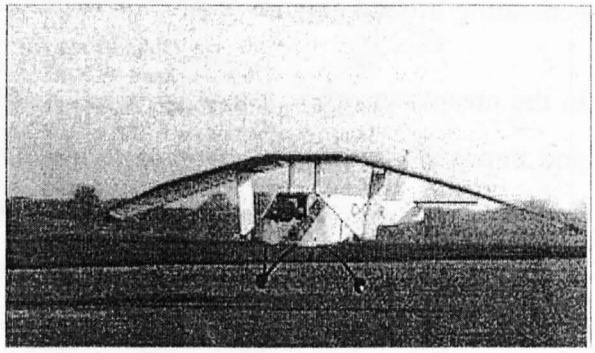

Fig 1.12 DeLaurier's full-sized engine powered ornithopter in taxi-trial, 1997 (DeLaurier, 1999)

1.3 CHALLENGES AND ENABLING TECHNOLOGIES FOR THE MICRO AIR VEHICLE

Despite the available technology and knowledge in the field of structure, aerodynamics, structural dynamics and their interplay, the micro-air vehicle still faces a whole range of challenges. The main challenge faced arises mainly from its small size requirement and relatively high take-off weight.

Due to its small size and relative low flight speed, the airflow around the vehicle is in the low Reynolds number regime where viscous forces are significant. The aerodynamic community is fully aware that boundary layer behaviour and its separation are significantly different from those large scale airfoils and conditions tested to date. Very little experimental data is therefore available for design purposes and wind tunnel testing is difficult. The forces being measured are so slight and even acoustic noise and vibration have been found to affect the repeatability of the tests [Grundy et al, 2000].

Numerical solution of the full Navier-Stokes equations will be necessary for computational aerodynamics to be meaningful and generation of a complete database is time consuming. Furthermore, the flow can no longer be assumed to be two-dimensional and many effects such as the transient sideways momentum on the stability of vortices become important. However, some research into the area of computational fluid dynamics is well under way as seen in some research works described later.

Propulsion in such minute scale is another challenge. With a wingspan of not more than 15 cm, it would be desirable to limit the diameter of the motor or engine to about 3 cm. Also, it should also be light or the designer of micro air vehicles will be doomed with the same failure faced by their predecessors in powered flight before the Wright brothers. Standard model aeroplane engines are too big for the micro air vehicle. Various research and development efforts have yielded miniature prototypes. Micro-electro-mechanical systems (MEMS) technology allowed MIT to develop a micro-turbine [Drake, 1998]. Similar efforts at DERA proposes a hydrogen-peroxide powered jet engine [Tilston and Cheung, 2000].

Ashley [1998] reported that a company in the United States named M-DOT, Inc used off-the-shelf parts like dental drill bearings to develop a 4 cm diameter turbine weighing 85 grams capable of delivering some 6N thrust. Engineers at MIT's Lincoln Labs in the United States feel that internal combustion engines seem to hold great promises [Ashley, 1998 and Mraz, 1998] in the near term future. However, one of the main disadvantages currently is the low thermal cycle efficiency at this scale with fuel flow being very high.

Electric motors are also available with better efficiency and reliability. However, much higher energy density is required to allow hover flight. Current off-the shelf electric motors using lithium batteries power some of the flying micro air vehicles such as the Black Widow [Dornheim, 1999]. RMB, a company in Switzerland, has produced the smallest electric micro-motor with a diameter of only 3 mm and a mass of 8 grams. Three of these are used as the flap control actuators in the Black Widow [Ashley, 1998]. Some other newer developments include piezoelectric ultrasonic motors [Ueha and Tomikawa, 1993] with diameters of about 8mm, which are used in the camera and watch industries.

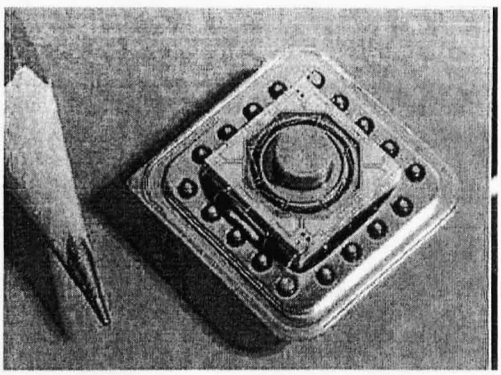

Fig 1.13 Micro-gyro is one of the enabling technologies for MAVs (Courtesy : University of Wisconsin)

Research on micro sensors and actuators, necessary for the guidance, navigation and control systems, are also well underway. Most of these apply MEMS manufacturing technology and are used quite extensively in the automotive industry. MEMS sensors have been employed in airbag systems, active suspension systems, automatic door lock systems and anti-lock braking systems of vehicles [Anon, 2000a]. Micro gyroscopes

[Anon, 2000b] are currently being developed by various research institutes and universities engaged in MEMS research. The Black Widow is equipped with a flight control system that features pitch, roll and yaw gyros and a GPS receiver. The University of Wisconsin has also developed linear actuators [Anon, 1999] about 5mm long and another version with higher force and larger throw. Integration of both sensor and actuator into a single device is also being researched.

There is certainly sufficient research and development work being carried out currently to make the micro air vehicle, which employs either fixed, rotary or flapping wing flight, to be a reality. It is just a matter of time before these mechanical birds and insects become fact rather than fiction.

1.4 CURRENT FLAPPING WING FLIGHT RESEARCH UNDERTAKEN WORLDWIDE

Research on flapping wing flight since the 1950s, has been carried out by both the aeronautical and the zoological community, and some of these are interdisciplinary in nature. With the invention of the video camera and high-speed photography, zoologists could observe the wing beat kinematics of birds [Tobalske et al, 1999 and Warrick et al, 1998] and insects [Willmott and Ellington, 1997a, b and Lehmann and Dickinson, 1998] in flight aimed at developing an understanding of how these may affect lift generation. They have identified novelties in insects to generate lift exploiting unsteady aerodynamics such as the "clap-and-fling", the "near-fling" or the "clap-and-peel" mechanisms.

Wakeling and Ellington [1997a] were able to deduce how the beat amplitude of the hind wings of the dragonfly shows good regression with the thrust generated and is probably used in flight control while the forewings were responsible for lift generation. Flapping frequencies and the phase differences between the fore and hind wings have also been estimated.

Zoologists have also measured the steady state contribution to forces and moments experienced by the wings of insects in the wind tunnel [Sato and Azuma, 1997] in an attempt to obtain performance related parameters and to estimate power requirement, flight speeds for minimum power, maximum endurance or maximum range [Okamoto et al, 1996, Sunada et al, 1993a, Wakeling and Ellington, 1997b]. Some attempts by others have been made to understand mechanisms for manoeuvring flight [Robertson and Johnson, 1993, Wortmann and Zarnack, 1993].

Concurrently, researchers have also developed theoretical models of the aerodynamics ranging from simple lifting line theory [Phlips et al, 1981], lifting surface theory [Sunada et al, 1993b], momentum jet theory [Hall and Pigott, 1998] and blade element method or strip theory [DeLaurier, 1993b] to more complicated CFD models incorporating unsteady aerodynamics using unsteady panel methods [Vest and Katz, 1996, Smith, 1996] and the solution of the 3-dimensional, incompressible, unsteady Navier-Stokes equations [Liu et al, 1998]. Findings by the zoologists in wing beat kinematics form the basis of wing motion in some of these theoretical works.

Early attempts have been made to collect aerodynamic data experimentally by Katzmayr [1922]. More recent researchers like Archer, Sappupo and Betteridge [1979] tested half wing models that flap only in the plane normal to flight. Fejtek and Nehera [1980] collected aerodynamic data to study the effects of changes of flapping amplitude, flapping plane angle, wing incidence and wind speed. Jones and Platzer [1999] investigated the thrust generated by an airfoil undergoing pitch and 'plunge' motion and correlated the experimentally obtained data with a previously developed, unsteady panel method. Vest and Katz [1999] measured the forces generated by the single degree of freedom flapping using a mechanical replica of the pigeon in the wind tunnel and compared them with those predicted by their CFD results. Van den Berg and Ellington [1997] performed flow visualisation studies of a mechanical flapping moth wing. This was then compared with the findings by Liu et al [1998]. Wilkin and Williams [1993] derived the forces experienced by live moths in flight, which Smith [1996] made use of to validate his theoretical model.

Research works by Michelson and Reece [1998] in the United States and Zbikowski [1999] in the United Kingdom focus in the area of wing aerodynamic design or overall vehicle design. The challenge of generating sufficient lift for sustained flight and manoeuvre requires more than mere mimicry of Nature. In a way, these vehicles must outperform Nature just like the conventional aircraft has.

Fig 1.14 Georgia Tech Research Institute's multi-mode Entomopter (Michelson and Reece, 1998)

DeLaurier and Harris [DeLaurier, 1999] have been able to demonstrate sustained flight with the ornithopter. However, this aircraft relied on the roll-yaw coupling provided by the wings and cruciform tail for lateral-directional control. In order to reduce the drag penalty, removal of the vertical fin would be desirable to enable true flapping flight in a manner practiced by the birds and insects.

Current research as shown in the available literature is focused on the design criteria of the wing and the development of more accurate CFD models to predict the aerodynamic flow around the wing. The flight dynamics and control of a vehicle employing flapping wing flight has, until recently, received very little attention. Although qualitative accounts on the stability and control [Ellington, 1999] and papers based on the observation of insect flight [Robertson and Johnson, 1993] were available, the only document on the mathematical modelling and simulation at the start of the research for this thesis in 1999 was the thesis by Rashid [1995] who studied the open-loop flight dynamics of the ornithopter designed by DeLaurier and Harris. By the time this research was nearing

completion, a number of articles on the stability and control of flapping wing MAVs [Deng et al, 2001 and Schenato et al 2001a, b] were published.

In his September 1901 lecture entitled *Some Aeronautical Experiments* to the Western Society of Engineers in Chicago, Wilbur Wright clearly understood that when the stability and control '*is worked out the age of flying machines will have arrived, for all other difficulties are of minor importance*' [quoted by MacFarland, 1953]. This opening statement applies to both the aeroplane then as well as the flapping wing flying machine of the future. As Ellington [1999] puts it, '*more will be understood of flapping flight from future work on machines than from birds or insects*'.

1.5 OBJECTIVES OF PRESENT RESEARCH PROGRAM

The overall aim of this research program is to study the flight dynamics and control of a micro air vehicle that employs flapping wing flight during the hover. To achieve the goal, the following sub-objectives are set out:

a. A mathematical model of the multi-body system representation of the dynamics of a virtual flapping wing MAV will be developed

b. A simulation program based on the above mathematical modelling shall be developed and tested.

c. A mechanical flapper for the experimental determination of the aerodynamics of the flapping wing will be designed.

d. Aerodynamic data will be collected for the flapping wing to be used in the simulation program.

e. The flight dynamics of the flapping wing MAV will be analysed

f. Various control strategies shall be analysed and compared for the control of the vehicle at the hover.

CHAPTER 2

MATHEMATICAL MODELLING

2.1 DESCRIPTION OF THE VIRTUAL VEHICLE

The subject used in this research shall be a virtual flapping wing micro air vehicle (FMAV). While the author acknowledges the limitations of current technology, it is assumed that the technology will eventually become available for a prototype to be manufactured.

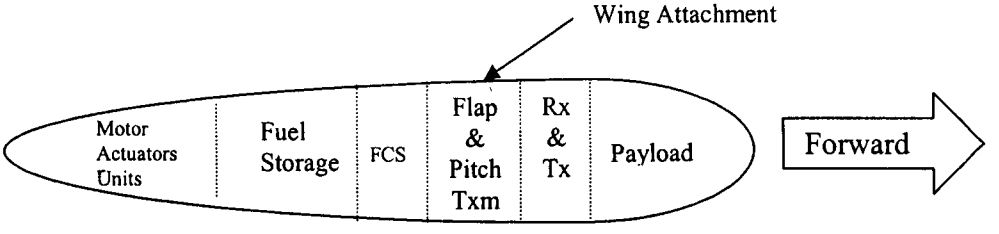

Fig 2.1 General layout of essential equipment in fuselage of FMAV

The vehicle comprises of a cigar shaped fuselage, which houses all the essential equipment, and Fig 2.1 shows a possible arrangement of the equipment. The payload, presumably a micro video camera or other micro sensors and transmitter, is assumed to be carried at the forward section in order to have unobstructed view. The locations of the power, transmission and fuel units, which are expected to form the bulk of the mass of

the vehicle, have a significant effect on the pitch inertia of the vehicle. Having low pitch inertia, the vehicle is more responsive about this axis. It also means that oscillation about this axis is of higher magnitude, resulting in possibly poorer picture quality. A compromise has to be made between responsiveness in vehicle pitch and its effect on picture quality. While the transmission units have to be placed near the wing attachment points, the power units and fuel cells are located in the aft sections. This arrangement increases the pitch inertia of the fuselage. The flight control computer is assumed to be located between the fuel compartment and the transmission units.

Referring to Fig 2.2, each of the two wings of the vehicle, shown at the bottom of the stroke, has two degrees of freedom. The main motion of the wing is the large amplitude flapping. The wing can also rotate about its own longitudinal axis. This degree of freedom is the wing pitch.

Fig 2.2 Illustration of Wing Degrees of Freedom

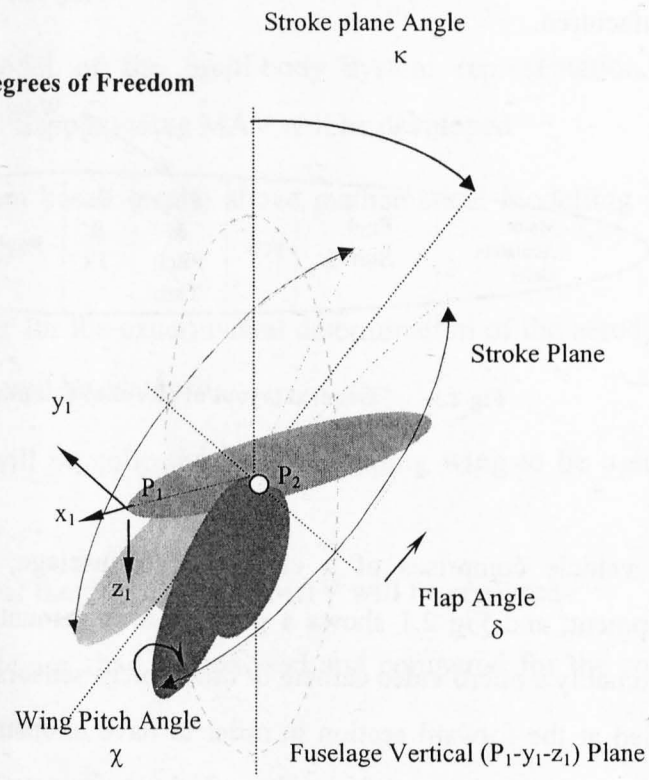

As the wing flaps, the locus of its longitudinal axis forms a plane called the stroke plane. In addition to the flap and pitch, the stroke plane can also be rotated about an axis parallel to the fuselage lateral axis. The stroke plane angle is the angle between the y-z plane of the fuselage and the stroke plane.

In the present study, each degree of freedom of each wing is assumed to be driven by a separate actuator motor. No particular design has been developed or assumed to be capable of the task but this actuator motor can, in the future, take the form of reciprocating chemical muscles, electric motors, ultrasonic motors or any other form currently under research.

The vehicle is assumed to measure 108 mm from wing tip to wing tip when the wings are level. The nominal flapping frequency is assumed to be 40 Hz, with a total vehicle mass of 4 grams based on the net aerodynamic force measured in the experiments carried out in this research. The break down of mass is assumed to be similar to the 56-gram first generation Black Widow MAV as given by Grasmeyer and Keenon [2001] and shown in Table 2.1. Its mass distribution and effects on the inertia are estimated in Appendix B.

Elements	Percentage of Total Mass of FMAV	Percentage of Total Mass of Black Widow
Fuselage and Structure	14	17
Wings	5	
Power Units	25	62
Transmission Units	25	
Fuel Units	10	
Flight Control Computer	9	9
Payload	10	12
Transmitter	2	

Table 2.1 Mass breakdown estimation based on first generation Black Widow

2.2 DEFINITION OF AXES SYSTEMS

The MAV can be modelled by linking the fuselage (R_1), two stroke plane actuators (R_2 and R_3) and two wings (R_4 and R_5) as shown in Fig 2.3. Each of the five individual bodies R_i (i = 1 to 5) has a dextral orthonormal axes system ($P_i x_i y_i z_i$) affixed to it at P_i, which is an arbitrarily selected, convenient point on the body R_i.

In addition, the spatial North-East-Down (NED) reference system $Ox_0y_0z_0$ is defined with the axes pointing towards the North (Ox_0), East (Oy_0) directions and downwards to the centre of the Earth (Oz_0). This is a Galilean system, ie it is non-rotational and fixed in space.

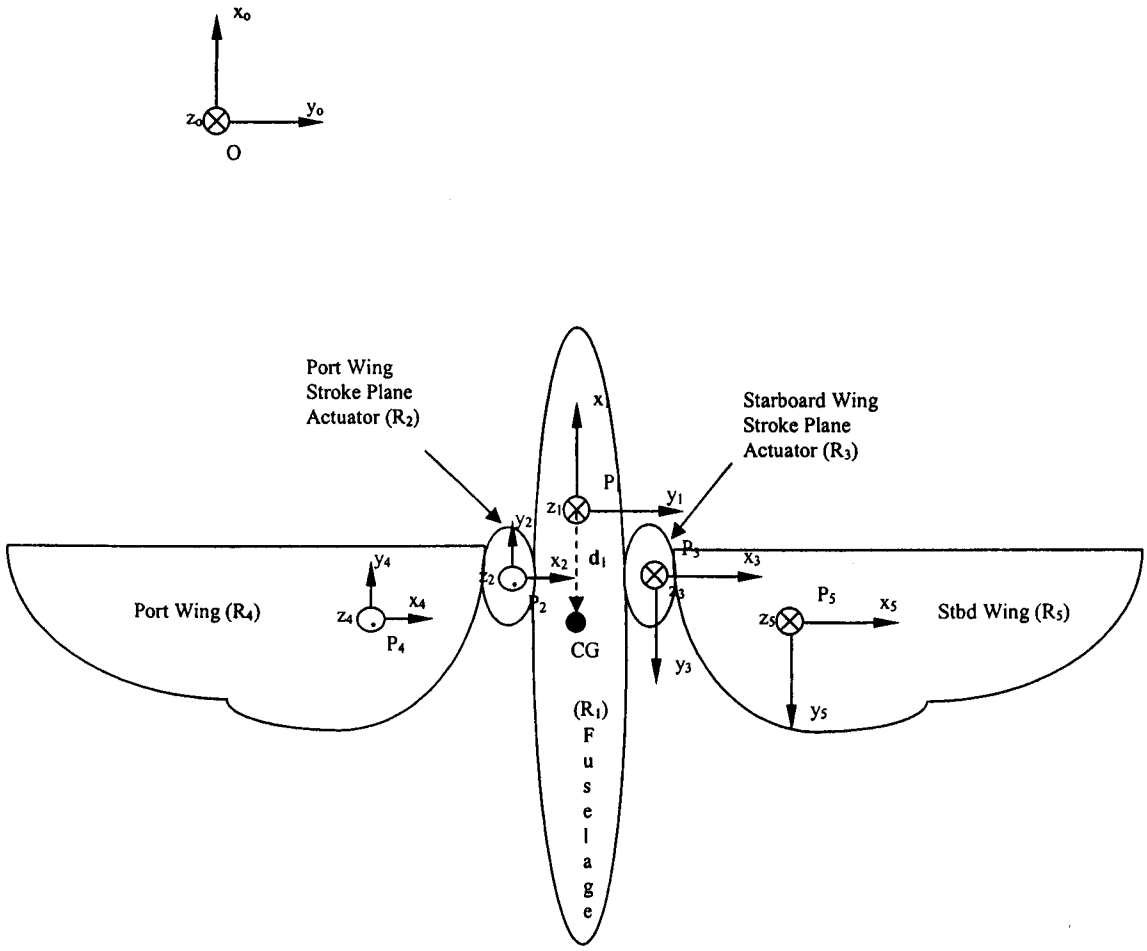

Fig 2.3 Definition of Coordinate Systems for the MAV Model

The fuselage has six degrees of freedom defined by its position $\mathbf{P}_1 = [x_b\ y_b\ z_b]^T$ and its Euler orientation in bank, pitch and azimuth $\vartheta = [\phi\ \theta\ \psi]^T$. Each of the two stroke plane actuators has a single degree of freedom (stroke plane angles κ_p and κ_s). Each wing has two degrees of freedom in pitch (χ) and flap (δ). The orientation of the wing is defined by the orientation vectors $\Phi_p = [\kappa_p\ \delta_p\ \chi_p]^T$ for the port wing and $\Phi_s = [\kappa_s\ \delta_s\ \chi_s]^T$ for starboard wing.

The orientations for the NED and fuselage axes-systems are consistent with aircraft representation. The orientations for axes systems of the wings and the stroke plane actuators are determined by the need for a consistent convention for the stroke plane angle (κ), flap (δ) and pitch (χ) angles about the axes of the wing coordinate systems for both wings. Table 2.2 defines positive deflections in each of the variables in the above notation.

The transformation of a vector from the i-th axes system ($^i\mathbf{a}$) to the j-th axes system ($^j\mathbf{a}$) is governed by the following equation

$$^j\mathbf{a} = \mathbf{C}_{ji}\,{}^i\mathbf{a} \qquad \text{Eqn 2.1}$$

where $\mathbf{C}_{ji}$ is the direction cosine matrix.

Variable	
X_0	Vehicle CG is north of the origin of the NED system
Y_0	Vehicle CG is east of the origin of the NED system
Z_0	Vehicle CG is below of the origin of the NED system
X_1	The referred point is forward of the origin of the fuselage axes system
Y_1	The referred point is on the starboard side of the origin of the fuselage axes system
Z_1	The referred point is below of the origin of the fuselage axes system
ϕ	If both wings have the same orientation, the vehicle is banked with port wing higher than the starboard wing
θ	The vehicle has a nose up pitch attitude
ψ	The vehicle is yawed clockwise about the Down axes of the NED system
κ_p, κ_s	The stroke plane is tilted from the vertical such that with the wing at the extreme upstroke position, it is behind the wing attachment point P_2 or P_3
δ_p, δ_s	The wing is flapped with the wings above the wing level position
χ_p, χ_s	The wing is pitched with the leading edge up and trailing edge down

Table 2.2 Sign Convention for Variables

2.3 DIRECTION COSINE MATRICES, DCMs

2.3.1 FUSELAGE R_1

The fuselage (body R_1) has three translational and three rotational degrees of freedom defined with respect to the inertial NED reference system. Its position is given by the vector $\mathbf{P}_1 = [x_B \; y_B \; z_B]^T$ and its orientation is defined by the Euler angles ϕ, θ and ψ. The DCMs between the body and the inertial reference frame $\mathbf{C}_{01}$ and $\mathbf{C}_{10}$ are readily found in standard textbooks (e.g. Nelson [1990]) and given by

$$\mathbf{C}_{01} = \begin{bmatrix} c_\theta c_\psi & s_\varphi s_\theta c_\psi - c_\varphi s_\psi & c_\varphi s_\theta c_\psi + s_\varphi s_\psi \\ c_\theta s_\psi & s_\varphi s_\theta s_\psi + c_\varphi c_\psi & c_\varphi s_\theta s_\psi - s_\varphi c_\psi \\ -s_\theta & s_\varphi c_\theta & c_\varphi c_\theta \end{bmatrix} \qquad \text{Eqn 2.2}$$

and

$$\mathbf{C}_{10} = \mathbf{C}_{01}^{\,T} \qquad \text{Eqn 2.3}$$

with $c_\theta = \cos\theta$, $s_\theta = \sin\theta$, $t_\theta = \tan\theta$ and so on for the above and subsequent expressions.

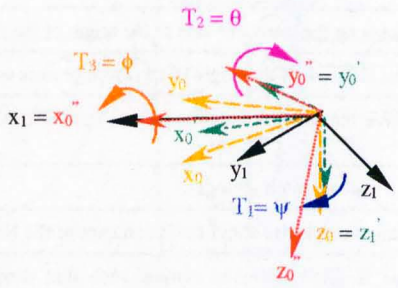

Fig 2.4 Transformation from $\mathcal{F}_0$ to $\mathcal{F}_1$

2.3.2 PORT WING STROKE PLANE ACTUATOR

The port wing actuator (body R_2) has a single degree of freedom defined by the stroke plane angle κ_p and is measured from the vehicle vertical plane or the $P_1y_1z_1$ plane. The angle κ_p is a rotation about the x_2 axis.

The transformation from the fuselage axes system to the port wing actuator system is achieved through three successive rotations. First, it is rotated -90° about the z_1-axis resulting in the x'_1-y'_1-z_1 axes system. This is followed by a 180° about the y'_1-axis resulting in the x''_1-y'_1-z''_1 axes system. Finally, it is rotated by the angle κ_p about x''_1-axis resulting in the x_2-y_2-z_2 axes system.

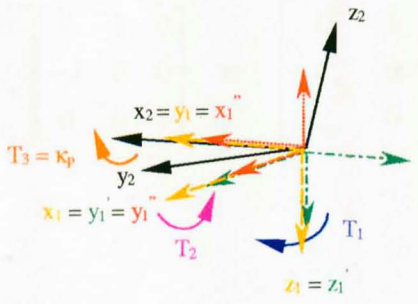

Fig 2.5 Transformation from $\mathcal{F}_1$ to $\mathcal{F}_2$

$$C_{21} = T_3T_2T_1 = T_{\kappa_p x_1''}T_{180y_1'}T_{-90z_1}$$

$$= \begin{bmatrix} 1 & 0 & 0 \\ 0 & c_{\kappa_p} & s_{\kappa_p} \\ 0 & -s_{\kappa_p} & c_{\kappa_p} \end{bmatrix} \begin{bmatrix} -1 & 0 & 0 \\ 0 & 1 & 0 \\ 0 & 0 & -1 \end{bmatrix} \begin{bmatrix} 0 & -1 & 0 \\ 1 & 0 & 0 \\ 0 & 0 & 1 \end{bmatrix} \qquad \text{Eqn 2.4}$$

$$= \begin{bmatrix} 0 & 1 & 0 \\ c_{\kappa_p} & 0 & -s_{\kappa_p} \\ -s_{\kappa_p} & 0 & -c_{\kappa_p} \end{bmatrix}$$

2.3.3 STARBOARD WING STROKE PLANE ACTUATOR

The starboard wing actuator (body R_3) also has a single degree of freedom defined by the stroke plane angle κ_s and is measured from the vehicle vertical plane or the $P_1y_1z_1$ plane. The angle κ_s is a rotation about the x_3 axis.

The transformation from the fuselage axes system to the starboard wing actuator system is achieved through only two successive rotations. First, it is rotated 90° about the z_1-axis resulting in the interim x'_1-y'_1-z_1 axes system. This is followed by a rotation through an angle κ_s about the x'_1-axis resulting in the x_3-y_3-z_3 axes system.

$$C_{31} = T_{\kappa_s x_1'} T_{90 z_1}$$

$$= \begin{bmatrix} 1 & 0 & 0 \\ 0 & c_{\kappa_s} & s_{\kappa_s} \\ 0 & -s_{\kappa_s} & c_{\kappa_s} \end{bmatrix} \begin{bmatrix} 0 & 1 & 0 \\ -1 & 0 & 0 \\ 0 & 0 & 1 \end{bmatrix} = \begin{bmatrix} 0 & 1 & 0 \\ -c_{\kappa_p} & 0 & s_{\kappa_p} \\ s_{\kappa_p} & 0 & c_{\kappa_p} \end{bmatrix} \qquad \text{Eqn 2.5}$$

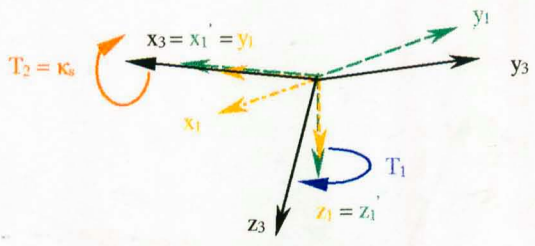

Fig 2.6 Transformation from $\mathcal{F}_1$ to $\mathcal{F}_3$

2.3.4 PORT AND STARBOARD WINGS

The wings (body R_i, i = 4,5) have two rotational degrees of freedom each, defined by the flap (δ_k) and pitch (χ_k) angles, where the subscript k = p,s. The transformation from the actuator axes system to the wing axes system comprises of two successive rotations. Starting with the wing axes system congruent to the actuator axes system, the wing is rotated about the y_2-axis through the flap angle (δ_k), resulting in the x'_2-y_2-z'_2 axes system. It is then followed by a rotation about the x'_2-axis through the pitch angle (χ_k).

The DCM for the actuator to wing transformation $\mathbf{C}_{ih}$ is thus given by the following matrix operation

$$\mathbf{C}_{ih} = T_{\chi_k x'_h} T_{\delta_k y_h}$$

$$= \begin{bmatrix} 1 & 0 & 0 \\ 0 & c_{\chi_k} & s_{\chi_k} \\ 0 & -s_{\chi_k} & c_{\chi_k} \end{bmatrix} \begin{bmatrix} c_{\delta_k} & 0 & -s_{\delta_k} \\ 0 & 1 & 0 \\ s_{\delta_k} & 0 & c_{\delta_k} \end{bmatrix} \qquad \text{Eqn 2.6}$$

$$= \begin{bmatrix} c_{\delta_k} & 0 & -s_{\delta_k} \\ s_{\chi_k} s_{\delta_k} & c_{\chi_k} & s_{\chi_k} c_{\delta_k} \\ c_{\chi_k} s_{\delta_k} & -s_{\chi_k} & c_{\chi_k} c_{\delta_k} \end{bmatrix}$$

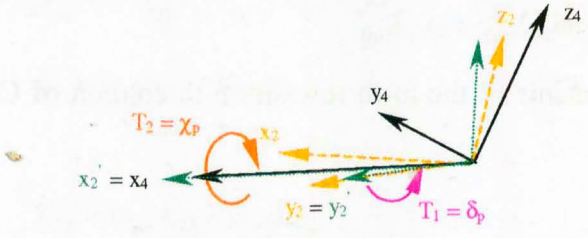

Fig 2.7 Transformation from $\mathcal{F}_2$ to $\mathcal{F}_4$

The wing to fuselage transformation matrix $\mathbf{C}_{1i}$ is thus given by the operation $\mathbf{C}_{1h}[\mathbf{C}_{ih}]^T$ or

$$\mathbf{C}_{14} = \begin{bmatrix} s_{\delta_s} s_{\kappa_s} & c_{\chi_s} c_{\kappa_s} - s_{\chi_s} c_{\delta_s} s_{\kappa_s} & -s_{\chi_s} c_{\kappa_s} - c_{\chi_s} s_{\delta_s} s_{\kappa_s} \\ c_{\delta_s} & s_{\chi_s} s_{\delta_s} & c_{\chi_s} s_{\delta_s} \\ s_{\delta_s} c_{\kappa_s} & -c_{\chi_s} s_{\kappa_s} - s_{\chi_s} c_{\delta_s} c_{\kappa_s} & s_{\chi_s} s_{\kappa_s} - c_{\chi_s} c_{\delta_s} c_{\kappa_s} \end{bmatrix} \qquad \text{Eqn 2.7}$$

and

$$\mathbf{C}_{15} = \begin{bmatrix} -s_{\delta_s} s_{\kappa_s} & -c_{\chi_s} c_{\kappa_s} + s_{\chi_s} c_{\delta_s} s_{\kappa_s} & s_{\chi_s} c_{\kappa_s} + c_{\chi_s} s_{\delta_s} s_{\kappa_s} \\ c_{\delta_s} & s_{\chi_s} s_{\delta_s} & c_{\chi_s} s_{\delta_s} \\ -s_{\delta_s} c_{\kappa_s} & c_{\chi_s} s_{\kappa_s} + s_{\chi_s} c_{\delta_s} c_{\kappa_s} & -s_{\chi_s} s_{\kappa_s} + c_{\chi_s} c_{\delta_s} c_{\kappa_s} \end{bmatrix} \qquad \text{Eqn 2.8}$$

2.4 RELATIONSHIP BETWEEN EULER AND BODY RATES

2.4.1 FUSELAGE

The relationship between the Euler rates $\dot{\vartheta} = [\dot{\phi} \quad \dot{\theta} \quad \dot{\psi}]^T$ and the body rates $[p \quad q \quad r]^T$ or $[\omega_{1x} \quad \omega_{1y} \quad \omega_{1z}]^T$ for the fuselage are given by evaluating the Poisson's kinematic equations

$$\begin{aligned} \dot{\lambda}_{m1} &= -\omega_{1y}\lambda_{m3} + \omega_{1z}\lambda_{m2} \\ \dot{\lambda}_{m2} &= \omega_{1x}\lambda_{m3} - \omega_{1z}\lambda_{m1} \\ \dot{\lambda}_{m3} &= -\omega_{1x}\lambda_{m2} + \omega_{1y}\lambda_{m1} \end{aligned} \qquad \text{Eqn 2.9}$$

where λ_{mn} are the elements of the m-th row and n-th column of $\mathbf{C}_{01}$. This results in the following relationship

$$\begin{bmatrix} \dot{\phi} \\ \dot{\theta} \\ \dot{\psi} \end{bmatrix} = \begin{bmatrix} 1 & s_\phi t_\theta & c_\phi t_\theta \\ 0 & c_\phi & -s_\phi \\ 0 & s_\phi \sec_\theta & c_\phi \sec_\theta \end{bmatrix} \begin{bmatrix} p \\ q \\ r \end{bmatrix} \qquad \text{Eqn 2.10}$$

2.4.2 STROKE PLANE ACTUATORS

The relationship between $\dot{\kappa}_k$ (k = p,s) and the relative angular velocity $\omega_{pi} = \omega_i - \omega_h$ (where h and i represent the fuselage frame and the frame of stroke plane actuator motor respectively) can be obtained from Eqn 2.9 again, this time replacing the components of ω_l with those of ω_{pi}. The elements of $\mathbf{C}_{li}$ shall now be λ_{mn}.

This results in the expression

$$\dot{\lambda}_{1i} = -\dot{\kappa}_k s_{\kappa_k} = -\omega_{pix} s_{\kappa_k}$$
$$\Rightarrow \quad \dot{\kappa}_k = \omega_{pix} \qquad \text{Eqn 2.11}$$

2.4.3 WINGS

For the wings, the relationship between the Euler rates ($\dot{\chi}_k$ and $\dot{\delta}_k$, k = p,s) and the relative angular velocities between the stroke plane actuators and the wings ω_{pi} (i = 4,5) can also be obtained by evaluating the Eqn 2.9 using the elements of C_{hi} (where h and i now represent the stroke plane actuator motor frame and the frame of the wing respectively). We can thus show that

$$\dot{\lambda}_{11} = -\omega_{piy}\lambda_{13} + \omega_{piz}\lambda_{12}$$
$$-\dot{\delta}_k s_{\delta_k} = -\omega_{piy} c_{\chi_k} s_{\delta_k} + \omega_{piz} s_{\chi_k} s_{\delta_k} \qquad \text{Eqn 2.12}$$
$$\Rightarrow \quad \dot{\delta}_k = \omega_{piy} c_{\chi_p} - \omega_{piz} s_{\chi_k}$$

$$\dot{\lambda}_{22} = \omega_{pix}\lambda_{23} - \omega_{piz}\lambda_{21}$$
$$-\dot{\chi}_k s_{\chi_k} = -\omega_{pix} s_{\chi_k} \qquad \text{Eqn 2.13}$$
$$\Rightarrow \quad \dot{\chi}_k = \omega_{pix}$$

2.5 DEVELOPMENT OF MULTI-BODY EQUATIONS OF MOTION

The development of the equations of motion for the multi-body representation of the flapping wing MAV is described in detail in Appendix C. This is summarised in the following sub-sections.

As shown in Fig 2.3, the vehicle is modelled as 5 rigid bodies, namely R_1 (fuselage), R_2 (port stroke plane actuator), R_3 (starboard stroke plane actuator), R_4 (port wing) and R_5 (starboard wing).

The fuselage has 6 degrees of freedom (D.O.F.) defined by its position $\mathbf{P}_1$ in the NED frame of reference and its Euler orientation ϑ. Each wing, able to flap and pitch, is attached to the fuselage via the stroke plane actuator. Each stroke plane actuator has a single degree of freedom such that the stroke plane can be adjusted with respect to the fuselage axes system. The orientation of the wing is collectively defined by the vectors $\Phi_p = [\kappa_p \; \delta_p \; \chi_p]^T$ and $\Phi_s = [\kappa_s \; \delta_s \; \chi_s]^T$. Fig 2.2 illustrates the degrees of freedom of the vehicle.

The bodies form an open chain with each body linked to a maximum of two other bodies. The stroke plane actuators R_2 and R_3 are each linked to the fuselage R_1 at the inboard joint and a wing at the outboard joint. For any body R_i, a body lying just outboard of it will have a higher index and will be denoted as R_j and the joint will be P_j while the body lying just inboard of it will be denoted R_h and the joint will be P_i. A right-handed, orthogonal, body-fixed axes system $P_i x_i y_i z_i$ or frame $\mathcal{F}_i$ is defined for R_i with origin at P_i.

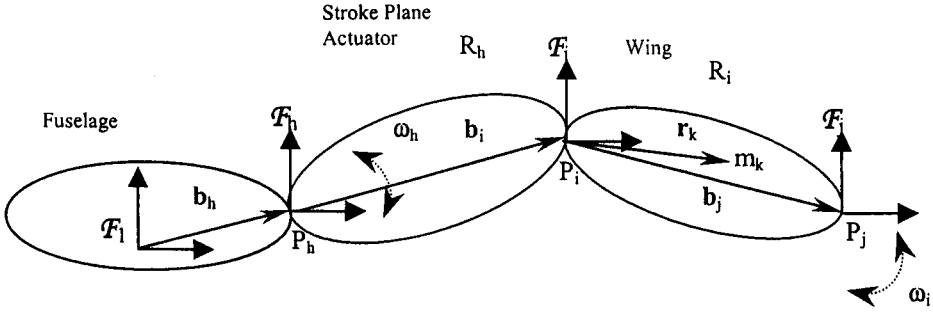

Fig 2.8 Schematic Representation of Three of Five Bodies of FMAV

Let $\vec{v}_i$ and $\vec{\omega}_i$ denote the absolute linear and angular velocities of R_i. Further, with $\vec{\omega}_{pi} = \vec{\omega}_i - \vec{\omega}_h$ defined as the relative angular velocity of R_i with respect to the adjoining body R_h), the absolute linear and angular velocities of a particle Δm_i in R_i at a distance $\vec{r}_i$ from P_i is given for i = 1..5 by

$$\vec{v}_k = \vec{v}_1 + \vec{\omega}_1 \times \left(\vec{b}_h + \vec{b}_i + \vec{r}_k\right) + \vec{\omega}_{ph} \times \left(\vec{b}_i + \vec{r}_k\right) + \vec{\omega}_{pi} \times \vec{r}_k \qquad \text{Eqn 2.14}$$

where $\vec{b}_i$ is the position vector of P_i from the origin of the frame of P_h.

In the above equation and subsequent equations, terms associated with the index *h* are zero if $i \leq 3$. Similarly, terms associated with the index j are zero if $i \geq 4$. Also, $\vec{b}_1 = \vec{0}$.

The linear momentum of the individual body R_i, i = 1..5, can be written as follows:

$$\begin{aligned} \vec{p}_i &= \int \vec{v}_k dm_k \\ &= m_i\left[\vec{v}_1 - \vec{b}_h \times \vec{\omega}_1 - \vec{b}_i \times \left(\vec{\omega}_1 + \vec{\omega}_{ph}\right)\right] - \vec{c}_i \times \left(\vec{\omega}_1 + \vec{\omega}_{ph} + \vec{\omega}_{pi}\right) \end{aligned} \qquad \text{Eqn 2.15}$$

For the system of bodies, the linear momentum is the sum of the individual linear momenta and this is shown to be

$$\begin{aligned} \vec{p} &= \sum \vec{p}_i \\ &= \sum_{i=1}^{5} m_i \vec{v}_1 - \vec{c} \times \vec{\omega}_1 - \sum_{i=2}^{5} \left(\vec{c}_i + \vec{c}_j + m_i \vec{b}_j\right) \times \vec{\omega}_{pi} \end{aligned} \qquad \text{Eqn 2.16}$$

with

$$\vec{c} = \sum_{i=1}^{5} \left[\vec{c}_i + m_i\left(\vec{b}_i + \vec{b}_h\right)\right] \qquad \text{Eqn 2.17}$$

Similarly, the angular momentum of the individual body R_i is

$$\vec{\mathbf{h}}_i = \vec{\mathbf{c}}_i \times \vec{\mathbf{v}}_1 + \tilde{\mathbf{J}}_{i1} \cdot \vec{\boldsymbol{\omega}}_1 + \tilde{\mathbf{J}}_{ih} \cdot \vec{\boldsymbol{\omega}}_{ph} + \tilde{\mathbf{J}}_i \cdot \vec{\boldsymbol{\omega}}_{pi} \qquad \text{Eqn 2.18}$$

where the terms on the right hand side (RHS) of the above equations and those to follow are the masses and moments of inertia tensors, which, for simplicity, are not reproduced here but have been evaluated and summarized in Appendices D and E.

The system angular momentum about P_1 is again the sum of the individual angular momenta and is given by

$$\vec{\mathbf{h}}_{P_1} = \vec{\mathbf{c}} \times \vec{\mathbf{v}}_1 + \tilde{\mathbf{J}} \cdot \vec{\boldsymbol{\omega}}_1 + \sum_{i=4}^{5} \left(\tilde{\mathbf{J}}_{1h} + \tilde{\mathbf{J}}_{1ih} \right) \cdot \vec{\boldsymbol{\omega}}_{ph} + \sum_{i=4}^{5} \tilde{\mathbf{J}}_{1i} \cdot \vec{\boldsymbol{\omega}}_{pi} \qquad \text{Eqn 2.19}$$

Applying Newton's law of motion, the externally applied forces and moments can be equated to the time rate of change of the linear and angular momentum of the system respectively. This results in

$$\overset{*}{\vec{\mathbf{p}}} = \sum_{i=1}^{5} \vec{\mathbf{f}}_i \qquad \text{Eqn 2.20}$$

and

$$\overset{*}{\vec{\mathbf{h}}}_{P_1} = \sum_{i=1}^{5} \vec{\mathbf{g}}_i + \sum_{i=2}^{5} \left(\vec{\mathbf{b}}_i + \vec{\mathbf{b}}_h \right) \times \vec{\mathbf{f}}_i - \vec{\mathbf{v}}_1 \times \sum_{i=1}^{5} \vec{\mathbf{p}}_i \qquad \text{Eqn 2.21}$$

The time derivative of the vector $\vec{\mathbf{a}}$ is denoted

- in the inertial frame $\mathcal{F}_0$ by $\overset{*}{\vec{\mathbf{a}}}$,
- in the R_1 frame by $\dot{\vec{\mathbf{a}}}$,
- in the frame of R_2 or R_3 by $\overset{o}{\vec{\mathbf{a}}}$,
- in the frame of R_4 or R_5 by $\overset{+}{\vec{\mathbf{a}}}$.

The time derivative of a vector can be transformed from one frame to another by observing the following rules:

$$\overset{o}{\vec{a}}_i = \overset{+}{\vec{a}}_i + \vec{\omega}_{pn} \times \vec{a}_i$$

$$\dot{\vec{a}}_i = \overset{o}{\vec{a}}_i + \vec{\omega}_{pm} \times \vec{a}_i = \overset{+}{\vec{a}}_i + (\vec{\omega}_{pm} + \vec{\omega}_{pn}) \times \vec{a}_i \qquad \text{Eqn 2.22}$$

$$\overset{*}{\vec{a}}_i = \dot{\vec{a}}_i + \vec{\omega}_1 \times \vec{a}_i = \overset{o}{\vec{a}}_i + (\vec{\omega}_1 + \vec{\omega}_{pm}) \times \vec{a}_i = \overset{+}{\vec{a}}_i + (\vec{\omega}_1 + \vec{\omega}_{pm} + \vec{\omega}_{pn}) \times \vec{a}_i$$

where i, m and n have the following relationship shown in Table 2.3.

i	h	m	n
1	-	-	-
2	1	2	-
3	1	3	-
4	2	2	4
5	3	3	5

Table 2.3 Relationships between Indices h, i, m and n

Hence the linear momentum of the system given in Eqn 2.20 can be rewritten as

$$\dot{\vec{p}} = \vec{f} - \vec{\omega}_1 \times \vec{p} \qquad \text{Eqn 2.23}$$

The angular momentum of the system is then

$$\dot{\vec{h}}_{P_1} = \sum_{i=1}^{5} \vec{g}_i + \sum_{i=2}^{5} (\vec{b}_i + \vec{b}_{ih}) \times \vec{f}_i - \vec{v}_1 \times \sum_{i=1}^{5} \vec{p}_i - \vec{\omega}_i \times \vec{h}_{P_1} \qquad \text{Eqn 2.24}$$

The angular momentum of R_2 or R_3 are given by

$$\overset{o}{\vec{\mathbf{h}}}_i = \left(\vec{\mathbf{h}}_i + \vec{\mathbf{h}}_j\right)\times\left(\vec{\omega}_1 + \vec{\omega}_{pm}\right) - \overset{o}{\vec{\mathbf{h}}}_j + \vec{\mathbf{g}}_i + \vec{\mathbf{g}}_{pi} + \vec{\mathbf{g}}_j - \vec{\mathbf{b}}_j \times \left(\dot{\vec{\mathbf{p}}}_j + \vec{\omega}_1 \times \vec{\mathbf{p}}_j - \vec{\mathbf{f}}_j\right)$$

$$+\left[\vec{\mathbf{v}}_1 + \vec{\omega}_1 \times \left(\vec{\mathbf{b}}_h + \vec{\mathbf{b}}_i\right) + \vec{\omega}_{ph} \times \vec{\mathbf{b}}_i\right] \times \left[\vec{\mathbf{c}}_i \times \left(\vec{\omega}_1 + \vec{\omega}_{ph} + \vec{\omega}_{pi}\right)\right] \quad \text{Eqn 2.25}$$

$$+\left[\vec{\mathbf{v}}_1 + \vec{\omega}_1 \times \left(\vec{\mathbf{b}}_i + \vec{\mathbf{b}}_j\right) + \vec{\omega}_{pi} \times \vec{\mathbf{b}}_j\right] \times \left[\vec{\mathbf{c}}_j \times \left(\vec{\omega}_1 + \vec{\omega}_{pi} + \vec{\omega}_{pj}\right)\right]$$

and for R_4 or R_5, it is

$$\overset{+}{\vec{\mathbf{h}}}_i + \left(\vec{\omega}_1 + \vec{\omega}_{pm} + \vec{\omega}_{pn}\right) \times \vec{\mathbf{h}}_i + \left[\vec{\mathbf{v}}_1 + \vec{\omega}_1 \times \left(\vec{\mathbf{b}}_h + \vec{\mathbf{b}}_i\right) + \vec{\omega}_{ph} \times \vec{\mathbf{b}}_i\right] \times \vec{\mathbf{p}}_i = \vec{\mathbf{g}}_i + \vec{\mathbf{g}}_{pi} - \vec{\mathbf{g}}_{pj} - \vec{\mathbf{b}}_j \times \vec{\mathbf{f}}_{pj} \quad \text{Eqn 2.26}$$

The above vector formulation of the momentum equations (Eqns 2.23 to 2.26) can now be expressed in scalar form.

By differentiating Eqn 2.16 and then substituting the results into Eqn 2.23, the linear momentum of the system can be represented as

$$m\dot{\mathbf{v}}_1 - \mathbf{c}^{\times}\dot{\vec{\omega}}_1 - \sum_{i=1}^{5}\left[m_i\mathbf{C}_{1h}\mathbf{b}_i^{\times} + \mathbf{C}_{1i}\mathbf{c}_i^{\times}\mathbf{C}_{ih}\right]\dot{\vec{\omega}}_{ph} - \sum_{i=1}^{5}\mathbf{C}_{1i}\mathbf{c}_i^{\times}\dot{\vec{\omega}}_{pi} = \sum_{i=1}^{5}\mathbf{C}_{1i}\mathbf{f}_i - \omega_1^{\times}\mathbf{p} + \mathbf{BB} \quad \text{Eqn 2.27}$$

where

$$\mathbf{BB} = \sum_{i=1}^{5}\left[\left\{\left(\mathbf{C}_{1m}\boldsymbol{\omega}_{pm}\right) + \left(\mathbf{C}_{1n}\boldsymbol{\omega}_{pn}\right)\right\}^{\times}\mathbf{C}_{1i}\mathbf{c}_i\right]^{\times}\left(\boldsymbol{\omega}_1 + \mathbf{C}_{1h}\boldsymbol{\omega}_{ph} + \mathbf{C}_{1i}\boldsymbol{\omega}_{pi}\right) - \sum_{i=1}^{5}m_i\left(\boldsymbol{\omega}_1 + \mathbf{C}_{1h}\boldsymbol{\omega}_{ph}\right)^{\times}\mathbf{C}_{1h}\boldsymbol{\omega}_{ph}^{\times}\mathbf{b}_i \quad \text{Eqn 2.28}$$

Similarly, the angular momentum of the system of bodies can be represented in scalar form as

$$\mathbf{c}^{\times}\dot{\mathbf{v}}_1 + \mathbf{J}\dot{\boldsymbol{\omega}}_1 + \sum_{i=4}^{5}\left(\mathbf{J}_{1h} + \mathbf{J}_{1ih}\right)\mathbf{C}_{1h}\dot{\boldsymbol{\omega}}_{ph} + \sum_{i=4}^{5}\mathbf{J}_{1i}\mathbf{C}_{1i}\dot{\boldsymbol{\omega}}_{pi}$$

$$= \sum_{i=1}^{5}\mathbf{C}_{1i}\mathbf{g}_i + \sum_{i=1}^{5}\left(\mathbf{C}_{1g}\mathbf{b}_h^{\times}\mathbf{C}_{1i} + \mathbf{C}_{1h}\mathbf{b}_i^{\times}\mathbf{C}_{hi}\right)\mathbf{f}_i - \boldsymbol{\omega}_1^{\times}\mathbf{h}_{P_1} - \mathbf{v}_1^{\times}\mathbf{p} - \dot{\mathbf{c}}^{\times}\mathbf{v}_1 - \mathbf{J}\dot{\boldsymbol{\omega}}_1 \qquad \text{Eqn 2.29}$$

$$- \sum_{i=4}^{5}\left(\dot{\mathbf{J}}_{1h} + \dot{\mathbf{J}}_{1ih}\right)\mathbf{C}_{1h}\boldsymbol{\omega}_{ph} - \sum_{i=4}^{5}\dot{\mathbf{J}}_{1h}\mathbf{C}_{1i}\boldsymbol{\omega}_{pi}$$

and those of the stroke plane actuator as

$$\left(\mathbf{c}_i^{\times}\mathbf{C}_{i1} + \mathrm{m}_j\mathbf{b}_j^{\times}\mathbf{C}_{i1}\right)\dot{\mathbf{v}}_1 + \left[\mathbf{J}_{i1}\mathbf{C}_{i1} - \mathrm{m}_j\mathbf{b}_j^{\times}\mathbf{C}_{i1}\left(\mathbf{b}_i^{\times} + \mathbf{C}_{1i}\mathbf{b}_j^{\times}\mathbf{C}_{i1}\right) - \mathbf{b}_j^{\times}\mathbf{C}_{ij}\mathbf{c}_j^{\times}\mathbf{C}_{j1}\right]\dot{\boldsymbol{\omega}}_1$$
$$+ \left(\mathbf{J}_i - \mathbf{b}_j^{\times}\mathbf{C}_{ij}\mathbf{c}_j^{\times}\mathbf{C}_{ji}\right)\dot{\boldsymbol{\omega}}_{pi} - \mathbf{b}_j^{\times}\mathbf{C}_{ij}\mathbf{c}_j^{\times}\dot{\boldsymbol{\omega}}_{pj}$$
$$= \mathbf{g}_i + \mathbf{g}_{pi} - \mathbf{C}_{ij}\mathbf{g}_{pj} + \mathbf{b}_j^{\times}\mathbf{C}_{ij}\mathbf{f}_j + \left[\mathbf{h}_i^{\times} + \mathbf{C}_{i1}\left(\mathbf{v}_0 + \boldsymbol{\omega}_1^{\times}\mathbf{b}_i\right)^{\times}\mathbf{C}_{1i}\mathbf{c}_i^{\times}\right]\left(\mathbf{C}_{i1}\boldsymbol{\omega}_1 + \boldsymbol{\omega}_{pi}\right)$$
$$- \mathbf{b}_j^{\times}\mathbf{C}_{i1}\boldsymbol{\omega}_1^{\times}\mathbf{C}_{1j}\mathbf{p}_j - \mathbf{A}_1 - \mathbf{A}_2$$

Eqn 2.30

with

$$\mathbf{A}_1 = +\mathrm{m}_j\mathbf{b}_j^{\times}\mathbf{C}_{i1}\left(\boldsymbol{\omega}_1 + \mathbf{C}_{1i}\boldsymbol{\omega}_{pi}\right)^{\times}\left(\boldsymbol{\omega}_{pi}^{\times}\mathbf{b}_j\right)$$
$$- \mathbf{b}_j^{\times}\mathbf{C}_{i1}\left[\left(\boldsymbol{\omega}_1^{\times}\mathbf{C}_{1j} + \mathbf{C}_{1i}\boldsymbol{\omega}_{pi}^{\times}\mathbf{C}_{ij} + \mathbf{C}_{1j}\boldsymbol{\omega}_{pj}^{\times}\right)\mathbf{c}_j\right]^{\times}\left(\mathbf{C}_{jm}\boldsymbol{\omega}_{pm} + \mathbf{C}_{jn}\boldsymbol{\omega}_{pn}\right) \qquad \text{Eqn 2.31}$$

and

$$\mathbf{A}_2 = -\mathbf{c}_i^{\times}\boldsymbol{\omega}_{pm}^{\times}\mathbf{C}_{i1}\mathbf{v}_0 + \dot{\mathbf{J}}_{i1}\mathbf{C}_{i1}\boldsymbol{\omega}_1 - \mathbf{J}_{i1}\boldsymbol{\omega}_{pm}^{\times}\mathbf{C}_{i1}\boldsymbol{\omega}_1 \qquad \text{Eqn 2.32}$$

Finally, the wing angular momentum is given by

$$\mathbf{c}_i^{\times}\mathbf{C}_{i1}\dot{\mathbf{v}}_0 + \mathbf{J}_{i1}\mathbf{C}_{i1}\dot{\boldsymbol{\omega}}_1 + \mathbf{J}_{ih}\mathbf{C}_{ih}\dot{\boldsymbol{\omega}}_{ph} + \mathbf{J}_i \cdot \dot{\boldsymbol{\omega}}_{pi}$$

$$\begin{aligned} &= \left\{\mathbf{C}_{i1}\left[\mathbf{v}_0^{\times} + \left(\boldsymbol{\omega}_1^{\times}\mathbf{b}_h\right)^{\times} + \left(\boldsymbol{\omega}_1^{\times}\mathbf{C}_{1h}\mathbf{b}_i\right)^{\times}\right]\mathbf{C}_{1i}\mathbf{c}_i^{\times}\right\}\left(\mathbf{C}_{i1}\boldsymbol{\omega}_1 + \mathbf{C}_{im}\boldsymbol{\omega}_{pm} + \mathbf{C}_{in}\boldsymbol{\omega}_{pn}\right) \\ &+ \left\{\mathbf{C}_{1h}\left(\boldsymbol{\omega}_{ph}^{\times}\mathbf{b}_i\right)^{\times}\mathbf{C}_{hi}\mathbf{c}_i^{\times}\right\}\left(\mathbf{C}_{i1}\boldsymbol{\omega}_1 + \mathbf{C}_{im}\boldsymbol{\omega}_{pm} + \mathbf{C}_{in}\boldsymbol{\omega}_{pn}\right) \\ &+ \mathbf{h}_i^{\times}\left(\mathbf{C}_{i1}\boldsymbol{\omega}_1 + \mathbf{C}_{im}\boldsymbol{\omega}_{pm} + \mathbf{C}_{in}\boldsymbol{\omega}_{pn}\right) + \mathbf{g}_i + \mathbf{g}_{pi} + \mathbf{A}_3 \end{aligned} \qquad \text{Eqn 2.33}$$

with

$$\begin{aligned} \mathbf{A}_3 = \mathbf{c}_i^{\times}\Big[&\left(\mathbf{C}_{im}\boldsymbol{\omega}_{pm} + \mathbf{C}_{in}\boldsymbol{\omega}_{pn}\right)^{\times}\mathbf{C}_{i1}\mathbf{v}_0\Big] - \dot{\mathbf{J}}_{i1}\mathbf{C}_{i1}\boldsymbol{\omega}_1 - \mathbf{J}_{i1}\left(\mathbf{C}_{i1}\boldsymbol{\omega}_1\right)^{\times}\left(\mathbf{C}_{im}\boldsymbol{\omega}_{pm} + \mathbf{C}_{in}\boldsymbol{\omega}_{pn}\right) \\ &- \dot{\mathbf{J}}_{ih}\mathbf{C}_{ih}\boldsymbol{\omega}_{ph} - \mathbf{J}_{ih}\mathbf{C}_{ih}\left(\boldsymbol{\omega}_{ph}^{\times}\mathbf{C}_{hn}\boldsymbol{\omega}_{pn}\right) - \mathbf{J}_i\boldsymbol{\omega}_{pi}^{\times}\mathbf{C}_{im}\boldsymbol{\omega}_{pm} \end{aligned}$$

Eqn 2.34

Eqns 2.27, 2.29, 2.30 and 2.33 represent the system linear momentum, the system angular momentum, the angular momentum of the stroke plane actuator and the angular momentum of the wing respectively. They can be summarized in matrix form as

$$\dot{\mathbf{V}} = \mathbf{M}^{-1}\left(\mathbf{F} + \mathbf{F}_{dyn}\right) \qquad \text{Eqn 2.35}$$

with

$$\dot{\mathbf{V}} = \begin{bmatrix} \dot{\mathbf{v}}_1 & \dot{\boldsymbol{\omega}}_1 & \dot{\boldsymbol{\omega}}_{p2} & \dot{\boldsymbol{\omega}}_{p3} & \dot{\boldsymbol{\omega}}_{p4} & \dot{\boldsymbol{\omega}}_{p5} \end{bmatrix}^T \qquad \text{Eqn 2.36}$$

$$\mathbf{F} = \begin{bmatrix} \sum_{i=1}^{5}\mathbf{C}_{1i}\mathbf{f}_i \\ \sum_{i=1}^{5}\mathbf{C}_{1i}\mathbf{g}_i + \sum_{i=1}^{5}\left(\mathbf{C}_{1g}\mathbf{b}_h^{\times}\mathbf{C}_{1i} + \mathbf{C}_{1h}\mathbf{b}_i^{\times}\mathbf{C}_{hi}\right)\mathbf{f}_i \\ \mathbf{g}_2 + \mathbf{g}_{p2} - \mathbf{C}_{24}\mathbf{g}_{p4} + \mathbf{b}_4^{\times}\mathbf{C}_{24}\mathbf{f}_4 \\ \mathbf{g}_3 + \mathbf{g}_{p3} - \mathbf{C}_{35}\mathbf{g}_{p5} + \mathbf{b}_5^{\times}\mathbf{C}_{35}\mathbf{f}_5 \\ \mathbf{g}_4 + \mathbf{g}_{p4} \\ \mathbf{g}_5 + \mathbf{g}_{p5} \end{bmatrix} \qquad \text{Eqn 2.37}$$

$$\mathbf{F}_{dyn} = \begin{bmatrix} -\omega_1^{\times}\ddot{\mathbf{p}} + \mathbf{BB} \\ -\omega_1^{\times}\mathbf{h}_{P_1} - \mathbf{v}_1^{\times}\mathbf{p} - \dot{\mathbf{c}}^{\times}\mathbf{v}_1 - \dot{\mathbf{J}}\omega_1 - \left(\dot{\mathbf{J}}_{12} + \dot{\mathbf{J}}_{142}\right)\mathbf{C}_{12}\omega_{p2} - \left(\dot{\mathbf{J}}_{13} + \dot{\mathbf{J}}_{153}\right)\mathbf{C}_{13}\omega_{p3} - \dot{\mathbf{J}}_{14}\mathbf{C}_{14}\omega_{p4} - \dot{\mathbf{J}}_{15}\mathbf{C}_{15}\omega_{p5} \\ \left\{\mathbf{h}_2^{\times} + \mathbf{C}_{21}\left(\mathbf{v}_1 + \omega_1^{\times}\mathbf{b}_2\right)^{\times}\mathbf{C}_{12}\mathbf{c}_4^{\times}\right\}\left(\mathbf{C}_{21}\omega_1 + \omega_{p2}\right) - \mathbf{b}_4^{\times}\mathbf{C}_{21}\omega_1^{\times}\mathbf{C}_{14}\mathbf{p}_4 - \mathbf{A}_{1,2} - \mathbf{A}_{2,2} \\ \left\{\mathbf{h}_3^{\times} + \mathbf{C}_{31}\left(\mathbf{v}_1 + \omega_1^{\times}\mathbf{b}_3\right)^{\times}\mathbf{C}_{13}\mathbf{c}_5^{\times}\right\}\left(\mathbf{C}_{31}\omega_1 + \omega_{p3}\right) - \mathbf{b}_5^{\times}\mathbf{C}_{31}\omega_1^{\times}\mathbf{C}_{15}\mathbf{p}_5 - \mathbf{A}_{1,3} - \mathbf{A}_{2,3} \\ \left\{\mathbf{h}_4^{\times} + \left[\mathbf{C}_{41}\left(\mathbf{v}_1 + \omega_1^{\times}\mathbf{b}_2 + \omega_1^{\times}\mathbf{C}_{12}\mathbf{b}_4\right)^{\times}\mathbf{C}_{14} + \mathbf{C}_{42}\left(\omega_{p2}^{\times}\mathbf{b}_4\right)^{\times}\mathbf{C}_{24}\right]\mathbf{c}_4^{\times}\right\}\left(\mathbf{C}_{41}\omega_1 + \mathbf{C}_{42}\omega_{p2} + \omega_{p4}\right) + \mathbf{A}_{3,4} \\ \left\{\mathbf{h}_5^{\times} + \left[\mathbf{C}_{51}\left(\mathbf{v}_1 + \omega_1^{\times}\mathbf{b}_3 + \omega_1^{\times}\mathbf{C}_{13}\mathbf{b}_5\right)^{\times}\mathbf{C}_{15} + \mathbf{C}_{53}\left(\omega_{p3}^{\times}\mathbf{b}_5\right)^{\times}\mathbf{C}_{25}\right]\mathbf{c}_5^{\times}\right\}\left(\mathbf{C}_{51}\omega_1 + \mathbf{C}_{53}\omega_{p3} + \omega_{p5}\right) + \mathbf{A}_{3,5} \end{bmatrix}$$

Eqn 2.38

$$\mathbf{M} = \begin{bmatrix} \mathbf{m} & -\mathbf{c}^{\times} & -\left\{\mathbf{C}_{12}\left(\mathbf{m}_2\mathbf{b}_4^{\times} + \mathbf{c}_2^{\times}\right) + \mathbf{C}_{14}\mathbf{c}_4^{\times}\mathbf{C}_{42}\right\} & -\left\{\mathbf{C}_{13}\left(\mathbf{m}_3\mathbf{b}_5^{\times} + \mathbf{c}_3^{\times}\right) + \mathbf{C}_{15}\mathbf{c}_5^{\times}\mathbf{C}_{53}\right\} & -\mathbf{C}_{14}\mathbf{c}_4^{\times} & -\mathbf{C}_{15}\mathbf{c}_5^{\times} \\ \mathbf{c}^{\times} & \mathbf{J} & \left(\mathbf{J}_{12} + \mathbf{J}_{142}\right) & \left(\mathbf{J}_{13} + \mathbf{J}_{153}\right) & \mathbf{J}_{14}\mathbf{C}_{14} & \mathbf{J}_{15}\mathbf{C}_{15} \\ \mathbf{c}_2^{\times}\mathbf{C}_{21} + \mathbf{m}_2\mathbf{b}_4^{\times}\mathbf{C}_{21} & \mathbf{J}_{21}\mathbf{C}_{21} - \mathbf{m}_4\mathbf{b}_4^{\times}\mathbf{C}_{21}\mathbf{b}_2^{\times} - \mathbf{b}_4^{\times}\mathbf{C}_{24}\mathbf{c}_4^{\times}\mathbf{C}_{41} & \mathbf{J}_2 - \mathbf{b}_4^{\times}\mathbf{C}_{24}\mathbf{c}_4^{\times}\mathbf{C}_{42} & 0 & -\mathbf{b}_4^{\times}\mathbf{C}_{24}\mathbf{c}_4^{\times} & 0 \\ \mathbf{c}_3^{\times}\mathbf{C}_{31} + \mathbf{m}_3\mathbf{b}_5^{\times}\mathbf{C}_{31} & \mathbf{J}_{31}\mathbf{C}_{31} - \mathbf{m}_5\mathbf{b}_5^{\times}\mathbf{C}_{31}\mathbf{b}_3^{\times} - \mathbf{b}_5^{\times}\mathbf{C}_{35}\mathbf{c}_5^{\times}\mathbf{C}_{51} & 0 & \mathbf{J}_3 - \mathbf{b}_5^{\times}\mathbf{C}_{35}\mathbf{c}_5^{\times}\mathbf{C}_{53} & 0 & -\mathbf{b}_5^{\times}\mathbf{C}_{35}\mathbf{c}_5^{\times} \\ \mathbf{c}_4^{\times}\mathbf{C}_{41} & \mathbf{J}_{41}\mathbf{C}_{41} & \mathbf{J}_{42}\mathbf{C}_{42} & 0 & \mathbf{J}_4 & 0 \\ \mathbf{c}_5^{\times}\mathbf{C}_{51} & \mathbf{J}_{51}\mathbf{C}_{51} & 0 & \mathbf{J}_{53}\mathbf{C}_{53} & 0 & \mathbf{J}_5 \end{bmatrix}$$

Eqn 2.39

Eqn 2.35 represents the non-linear equations of motion of order 12 of the multi-body representation of the flapping wing MAV. The state derivative vector $\dot{\mathbf{V}}$ can be calculated at each time step, provided the terms on the right hand side of Eqn 2.35 are known. $\dot{\mathbf{V}}$ can then integrated by standard integration routines (such as the Runge-Kutta 4th order routine) to obtain the state vector **V**. This can then be transformed using the relations given in section 2.4, resulting in the vehicle velocities $\dot{\mathbf{P}}_1$ and Euler rates $\dot{\vartheta}$ and wing orientation rates $\dot{\Phi}$. Further integration will result in the vehicle position and orientation and wing orientation.

2.6 FORCES AND MOMENTS MODEL

The forces and moments due to the dynamics of the system are summarised in the generalised force vector $\mathbf{F}_{dyn}$ in Eqn 2.36 and can be calculated once the mass and inertia properties and the motion parameters of the individual bodies are known. The generalised force vector **F** in Eqn 2.37 is an eighteen-component vector comprising of forces $\mathbf{f}_1 = [f_{1x}\ f_{1y}\ f_{1z}]^T$ that act on the fuselage at P_1 along the axes P_1x_1, P_1y_1 and P_1z_1, the moments $\mathbf{g}_1 = [g_{1x}\ g_{1y}\ g_{1z}]^T$ acting on the fuselage about these axes, and the 12 moments $\mathbf{g}_i = [g_{ix}\ g_{iy}\ g_{iz}]^T$ ($i = 2..5$) about the axes of the wings and the stroke plane actuators.

2.6.1 SOURCES OF FORCES AND MOMENTS

These forces and moments result from the aerodynamics of the wings, the friction at the joints, the driving torques of the motors, the constraint forces, gravity and dynamics of the system. The externally applied forces and moments as well as the constraint forces and moments shall be developed here.

2.6.1.1 Aerodynamic Forces

It is assumed that only the aerodynamic effects originate from the wings alone. The low speed flight investigated in this research makes it reasonable to assume that the fuselage as well as the stroke plane actuators has negligible effects on the aerodynamics. It is further assumed that perturbations of the fuselage in pitch, roll and yaw are small enough to have negligible effects on the wing aerodynamics.

These assumptions seem reasonable for a vehicle with wing length from root to tip of about 50 mm flapping at 40 Hz. The flap velocity is then about 6.8 $m.s^{-1}$ at the wing tip. A roll rate of about 2.5 $rad.s^{-1}$ would cause less than 1% increase in the flap velocity on one wing and a corresponding reduction on the other. As a roll rate higher than this magnitude is generally not expected at the trimmed hover and position control analysis to be carried out later, the assumption is justifiable.

The aerodynamic forces experienced by the wing were obtained experimentally as will be described in Chapter 4. The data is expressed in the axes system $P_F x_F y_F z_F$ (see Fig 4.5) defined for the mechanical flapper in the experiment and given as Fourier coefficients. The aerodynamic force coefficient for the k-th axis (k = x, y or z) is given by Eqn 2.40 in the frame of the flapper axes

$$ {}^{i}C_k(\hat{t}) = \frac{\Delta F_k(\hat{t})}{\frac{1}{2}\rho(\overline{V}_{flap})^2 S_{wing}} \qquad \text{Eqn 2.40} $$

where $F_k(\hat{t}) = a_{k0} + \sum_{j=1}^{n}\{a_{kj}\cos(2\pi j\hat{t}) + b_{kj}\sin(2\pi j\hat{t})\}$.

As the experiment collected data from the port wing only, the span-wise force coefficient of the starboard wing ($^{Flapper}C_{y,s}$) is given by

$$ {}^{Flapper}C_{y,s} = - {}^{Flapper}C_{y,p} \qquad \text{Eqn 2.41} $$

The experiment was also conducted for zero mean flap angle $\bar{\delta}$. As the flapper axes system is congruent to the fuselage axes system for $\kappa = 0°$ and $\bar{\delta} = 0°$, the aerodynamic data has to be transformed for other non-zero values κ and $\bar{\delta}$ with the direction cosine matrix $\mathbf{C}_{1\bar{\delta}}$.

$$ {}^{R_1}C_k = \mathbf{C}_{1\bar{\delta}} {}^{Flapper}C_k \qquad \text{Eqn 2.42} $$

where

$$ \mathbf{C}_{1\bar{\delta}_p} = \begin{bmatrix} c_{\kappa_p} & 0 & s_{\kappa_p} \\ 0 & 1 & 0 \\ -s_{\kappa_p} & 0 & c_{\kappa_p} \end{bmatrix} \begin{bmatrix} 1 & 0 & 0 \\ 0 & c_{\bar{\delta}_p} & -s_{\bar{\delta}_p} \\ 0 & s_{\bar{\delta}_p} & c_{\bar{\delta}_p} \end{bmatrix} = \begin{bmatrix} c_{\kappa_p} & s_{\kappa_p}s_{\bar{\delta}_p} & s_{\kappa_p}c_{\bar{\delta}_p} \\ 0 & c_{\bar{\delta}_p} & -s_{\bar{\delta}_p} \\ -s_{\kappa_p} & c_{\kappa_p}s_{\bar{\delta}_p} & c_{\kappa_p}c_{\bar{\delta}_p} \end{bmatrix} \qquad \text{Eqn 2.43} $$

and

$$ \mathbf{C}_{1\bar{\delta}_s} = \begin{bmatrix} c_{\kappa_s} & 0 & s_{\kappa_s} \\ 0 & 1 & 0 \\ -s_{\kappa_s} & 0 & c_{\kappa_s} \end{bmatrix} \begin{bmatrix} 1 & 0 & 0 \\ 0 & c_{\bar{\delta}_s} & s_{\bar{\delta}_s} \\ 0 & -s_{\bar{\delta}_s} & c_{\bar{\delta}_s} \end{bmatrix} = \begin{bmatrix} c_{\kappa_s} & -s_{\kappa_s}s_{\bar{\delta}_s} & s_{\kappa_s}c_{\bar{\delta}_s} \\ 0 & c_{\bar{\delta}_s} & s_{\bar{\delta}_s} \\ -s_{\kappa_s} & -c_{\kappa_s}s_{\bar{\delta}_s} & c_{\kappa_s}c_{\bar{\delta}_s} \end{bmatrix} \qquad \text{Eqn 2.44} $$

2.6.1.2 Frictional Torque

Friction exists in the joints P_i (i = 2..5) and acts in opposition to the motion. For simplicity, the coefficient of friction μ_i assumed to be constant for all the axes of the body R_i. The frictional torque is given by

$$^{R_i}\mathbf{g}_{friction,i} = -\mu_i \mathbf{I} \mathbf{J}_i \omega_{pi} \qquad \text{Eqn 2.45}$$

where **I** is the identity matrix.

2.6.1.3 Motor Torque

In order to control the stroke plane angle, it is assumed that R_2 and R_3 are to be fitted with an actuator motor each with the axes of rotation in the P_2x_2 and P_3x_3 axes respectively. Similarly, R_4 and R_5 would be driven in the pitch and flap degrees of freedom by two motors in the pitch and flap axes. Each of the actuator motors has an individual control loop but the loops are similar in design. Fig 2.9 shows the stroke plane angle control loop.

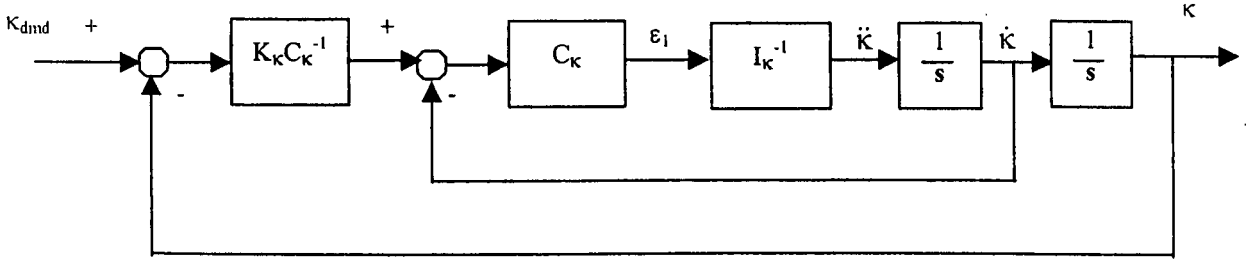

Fig 2.9 Stroke Plane Actuator Control Loop

The controlled variables are the stroke plane angle κ, the flap angle δ and the pitch angle χ of each wing. The response of each of these variables can be represented as a second order system. For the stroke plane angle, this can be written as

$$I_\kappa \ddot{\kappa} + C_\kappa \dot{\kappa} + K_\kappa \kappa = Q_{motor,\kappa} \qquad \text{Eqn 2.46}$$

where $Q_{motor,\kappa}$ is the stroke plane actuator motor torque, I_κ is the inertia of the stroke plane, K_κ is the actuator motor gain and C_κ is the damping provided by the control loop. Chapter 3.2.2 will provide more details on the determination of the gains in the block diagrams.

The torque required to drive the stroke plane (i = 2,3) is given by the following expression:

$$^{R_i}\mathbf{g}_{motor,i} = \begin{bmatrix} Q_{motor,\kappa} \\ 0 \\ 0 \end{bmatrix} \qquad \text{Eqn 2.47}$$

and for the flap and pitch degrees of freedom of the wings (i = 4,5),

$$^{R_i}\mathbf{g}_{motor,i} = \begin{bmatrix} Q_{motor,\chi} \\ Q_{motor,\delta} \\ 0 \end{bmatrix} \qquad \text{Eqn 2.48}$$

2.6.1.4 Gravity

The gravity force for the body R_i (i=1..5), when expressed in the inertial frame $Ox_oy_oz_o$, has a vertical component in the direction Oz_o only. It is hence easier to specify the force vector in this frame. It can then be transformed into the required frame $\mathcal{F}_i$ as necessary. In the frame of R_1, the gravity force of the body R_i (i=1..5) is given by

$$^{1}\mathbf{f}_{grav,i} = \mathbf{C}_{10}\begin{bmatrix} 0 \\ 0 \\ m_i g \end{bmatrix} \qquad \text{Eqn 2.49}$$

2.6.1.5 Constraint Moments

The relative angular velocities ω_{pi} (i = 1..5) all have three components. The stroke plane actuators have only one degree of freedom each while the wings have two degrees of freedom each. In order to reconcile this, R_2 and R_3 will have two degrees of freedom frozen while R_4 and R_5 will each have one frozen degree of freedom. This result in constraint moments acting at the joints P_i (i = 2..5) and these shall be developed for the stroke plane actuators and wings in the following sub-sections.

2.6.1.5.1 Stroke Plane Actuators

The moments acting on the stroke plane actuator R_i (i = 2,3) expressed in its own frame shall be

$$^{R_i}\mathbf{g}_{ext,i} = {}^{R_i}\mathbf{g}_{grav,i} + {}^{R_i}\mathbf{g}_{dyn,i} + {}^{R_i}\mathbf{g}_{friction,i} + {}^{R_i}\mathbf{g}_{motor,i} \qquad \text{Eqn 2.50}$$

Since the only degree of freedom is κ about the P_ix_i-axis, the constraint moment vector must be

$$^{R_i}\mathbf{g}_{con,i} = {}^{R_i}\begin{bmatrix} 0 \\ -g_{ext,iy} \\ -g_{ext,iz} \end{bmatrix} \qquad \text{Eqn 2.51}$$

2.6.1.5.2 Wings

The moments acting on the wing R_i (i = 4,5) expressed in its own frame are very similar to those acting on R_2 and R_3, except that it now includes the aerodynamic term

$$^{R_i}\mathbf{g}_{ext,i} = {}^{R_i}\mathbf{g}_{grav,i} + {}^{R_i}\mathbf{g}_{dyn,i} + {}^{R_i}\mathbf{g}_{friction,i} + {}^{R_i}\mathbf{g}_{motor,i} + {}^{R_i}\mathbf{g}_{aero,i} \qquad \text{Eqn 2.52}$$

Each wing has two degrees of freedom is χ and δ about the P_ix_i- and P_iy_i-axes respectively. Consequently, the degree of freedom about the P_iz_i-axis must be frozen and the constraint moment vector must be

$$ {}^{R_i}\mathbf{g}_{con,i} = {}^{R_i}\begin{bmatrix} 0 \\ 0 \\ -g_{ext,iz} \end{bmatrix} \qquad \text{Eqn 2.53} $$

2.6.2 FORCES ACTING ON FUSELAGE R_1

The forces $\mathbf{f}_1$ acting on the fuselage is given by the sum of the weights of all five bodies and the aerodynamic forces of the wings. As the fuselage is not constrained in any way, there is no term due to motor torque, friction or constraint forces. Hence, we can write

$$ \begin{aligned} {}^1\mathbf{f}_1 &= \sum_{i=1}^{5}\sum_{s} {}^1\mathbf{f}_{si} \\ &= {}^1\mathbf{f}_{aero,1} + \sum_{i=4}^{5} \mathbf{C}_{1\bar{\delta}}{}^{Flapper}\mathbf{f}_{aero,i} + \sum_{i=1}^{5} \mathbf{C}_{10}{}^{0}\mathbf{f}_{grav,i} \end{aligned} \qquad \text{Eqn 2.54} $$

where the index s refers to the sources of the forces, ie aerodynamic and gravity.

2.6.3 MOMENTS ACTING ON FUSELAGE R_1

The fuselage R_1 is theoretically linked to the inertial reference frame $\mathcal{F}_0$ by the virtual joint at P_1. Although this is a frictionless unconstrained joint and there is no driving torque, the vector sum of the constraint and frictional torques at the shoulders P_2 and P_3 causes an equal and opposite reaction torque and this has to be accounted for. Consequently, the moment acting at P_1 is given by

2.6.4 MOMENTS ACTING ON STROKE PLANE ACTUATORS AND WINGS

For the stroke plane actuators R_i (i = 2,3), the moments are due to gravity, motor torque, friction, dynamics and constraints at the joints. For the wings R_i (i = 4,5), there is the additional aerodynamic moment. The total moment is the sum of externally applied moments and the constraint moment, given in Eqns 2.50 to 2.53. This is expressed explicitly as follows:

$$\begin{aligned} {}^{i}\mathbf{g}_i = \mathbf{d}_i^{\times}\mathbf{C}_{i0}\,{}^{0}\mathbf{f}_{grav,i} + {}^{i}\mathbf{g}_{motor,i} - \mathbf{C}_{ij}\,{}^{j}\mathbf{g}_{motor,j} + \mu_i \mathbf{I}\omega_{pi} + {}^{i}\mathbf{g}_{dyn,i} \\ + \mathbf{C}_{i1}\left(\mathbf{C}_{1i}\boldsymbol{l}_{cp,i}\right)^{\times}\left(\mathbf{C}_{1\bar{\delta}}\,{}^{Flapper}\mathbf{f}_{aero,i}\right) + {}^{i}\mathbf{g}_{con,i} + {}^{i}\mathbf{g}_{friction,i} \end{aligned} \qquad \text{Eqn 2.56}$$

2.6.5 GENERALISED FORCE VECTOR

The generalised force vector in Eqn 2.37 is the vector of all externally applied forces and moments on the fuselage, stroke plane actuators and wings. It has eighteen components, which can be subdivided into 6 groups, namely the forces and moments acting on the fuselage (${}^{1}\mathbf{f}_1$and ${}^{1}\mathbf{g}_1$), the moments acting on the stroke plane actuators at P_2 and P_3 (${}^{2}\mathbf{g}_2$ and ${}^{3}\mathbf{g}_3$) and the moments acting on the wings at P_4 and P_5 (${}^{4}\mathbf{g}_4$ and ${}^{5}\mathbf{g}_5$). These are given in Eqns 2.54 to 2.56, which can be summarised in the following equation

$$F = [{}^{1}\mathbf{f}_1 \;\; {}^{1}\mathbf{g}_1 \;\; {}^{2}\mathbf{g}_2 \;\; {}^{3}\mathbf{g}_3 \;\; {}^{4}\mathbf{g}_4 \;\; {}^{5}\mathbf{g}_5]^{T} \qquad \text{Eqn 2.57}$$

2.7 SUMMARY

The equations of motion for the multi-body representation of a flapping wing vehicle comprising of five bodies R_i (i = 1..5) linked together at the joints P_k (k = 2..5) to form an open chain as shown in Fig 2.8 have been derived in the preceding sections.

The equations of motion can be summarised in matrix-vector formulation as follows:

$$\dot{\mathbf{V}} = \mathbf{M}^{-1}\left(\mathbf{F} + \mathbf{F}_{dyn}\right) \qquad \text{Eqn 2.35}$$

with

$$\dot{\mathbf{V}} = \begin{bmatrix} \dot{\mathbf{v}}_1 & \dot{\boldsymbol{\omega}}_1 & \dot{\boldsymbol{\omega}}_{p2} & \dot{\boldsymbol{\omega}}_{p3} & \dot{\boldsymbol{\omega}}_{p4} & \dot{\boldsymbol{\omega}}_{p5} \end{bmatrix}^T \qquad \text{Eqn 2.36}$$

$$\mathbf{F} = \begin{bmatrix} \sum_{i=1}^{5} \mathbf{C}_{1i}\mathbf{f}_i \\ \sum_{i=1}^{5} \mathbf{C}_{1i}\mathbf{g}_i + \sum_{i=1}^{5}\left(\mathbf{C}_{1g}\mathbf{b}_h^{\times}\mathbf{C}_{1i} + \mathbf{C}_{1h}\mathbf{b}_i^{\times}\mathbf{C}_{hi}\right)\mathbf{f}_i \\ \mathbf{g}_2 + \mathbf{g}_{p2} - \mathbf{C}_{24}\mathbf{g}_{p4} + \mathbf{b}_4^{\times}\mathbf{C}_{24}\mathbf{f}_4 \\ \mathbf{g}_3 + \mathbf{g}_{p3} - \mathbf{C}_{35}\mathbf{g}_{p5} + \mathbf{b}_5^{\times}\mathbf{C}_{35}\mathbf{f}_5 \\ \mathbf{g}_4 + \mathbf{g}_{p4} \\ \mathbf{g}_5 + \mathbf{g}_{p5} \end{bmatrix} \qquad \text{Eqn 2.37}$$

$$\mathbf{F}_{dyn} = \begin{bmatrix} -\boldsymbol{\omega}_1^{\times}\mathbf{p} + \mathbf{BB} \\ -\boldsymbol{\omega}_1^{\times}\mathbf{h}_{P_1} - \mathbf{v}_1^{\times}\mathbf{p} - \dot{\mathbf{c}}^{\times}\mathbf{v}_1 - \dot{\mathbf{J}}\boldsymbol{\omega}_1 - \left(\dot{\mathbf{J}}_{12} + \dot{\mathbf{J}}_{142}\right)\mathbf{C}_{12}\boldsymbol{\omega}_{p2} - \left(\dot{\mathbf{J}}_{13} + \dot{\mathbf{J}}_{153}\right)\mathbf{C}_{13}\boldsymbol{\omega}_{p3} - \dot{\mathbf{J}}_{14}\mathbf{C}_{14}\boldsymbol{\omega}_{p4} - \dot{\mathbf{J}}_{15}\mathbf{C}_{15}\boldsymbol{\omega}_{p5} \\ \left\{\mathbf{h}_2^{\times} + \mathbf{C}_{21}\left(\mathbf{v}_1 + \boldsymbol{\omega}_1^{\times}\mathbf{b}_2\right)^{\times}\mathbf{C}_{12}\mathbf{c}_4^{\times}\right\}\left(\mathbf{C}_{21}\boldsymbol{\omega}_1 + \boldsymbol{\omega}_{p2}\right) - \mathbf{b}_4^{\times}\mathbf{C}_{21}\boldsymbol{\omega}_1^{\times}\mathbf{C}_{14}\mathbf{p}_4 - \mathbf{A}_{1,2} - \mathbf{A}_{2,2} \\ \left\{\mathbf{h}_3^{\times} + \mathbf{C}_{31}\left(\mathbf{v}_1 + \boldsymbol{\omega}_1^{\times}\mathbf{b}_3\right)^{\times}\mathbf{C}_{13}\mathbf{c}_5^{\times}\right\}\left(\mathbf{C}_{31}\boldsymbol{\omega}_1 + \boldsymbol{\omega}_{p3}\right) - \mathbf{b}_5^{\times}\mathbf{C}_{31}\boldsymbol{\omega}_1^{\times}\mathbf{C}_{15}\mathbf{p}_5 - \mathbf{A}_{1,3} - \mathbf{A}_{2,3} \\ \left\{\mathbf{h}_4^{\times} + \left[\mathbf{C}_{41}\left(\mathbf{v}_1 + \boldsymbol{\omega}_1^{\times}\mathbf{b}_2 + \boldsymbol{\omega}_1^{\times}\mathbf{C}_{12}\mathbf{b}_4\right)^{\times}\mathbf{C}_{14} + \mathbf{C}_{42}\left(\boldsymbol{\omega}_{p2}^{\times}\mathbf{b}_4\right)^{\times}\mathbf{C}_{24}\right]\mathbf{c}_4^{\times}\right\}\left(\mathbf{C}_{41}\boldsymbol{\omega}_1 + \mathbf{C}_{42}\boldsymbol{\omega}_{p2} + \boldsymbol{\omega}_{p4}\right) + \mathbf{A}_{3,4} \\ \left\{\mathbf{h}_5^{\times} + \left[\mathbf{C}_{51}\left(\mathbf{v}_1 + \boldsymbol{\omega}_1^{\times}\mathbf{b}_3 + \boldsymbol{\omega}_1^{\times}\mathbf{C}_{13}\mathbf{b}_5\right)^{\times}\mathbf{C}_{15} + \mathbf{C}_{53}\left(\boldsymbol{\omega}_{p3}^{\times}\mathbf{b}_5\right)^{\times}\mathbf{C}_{25}\right]\mathbf{c}_5^{\times}\right\}\left(\mathbf{C}_{51}\boldsymbol{\omega}_1 + \mathbf{C}_{53}\boldsymbol{\omega}_{p3} + \boldsymbol{\omega}_{p5}\right) + \mathbf{A}_{3,5} \end{bmatrix}$$

Eqn 2.38

$$\mathbf{M}=\begin{bmatrix} \mathbf{m} & -\mathbf{c}^{\times} & -\left\{\mathbf{C}_{12}\left(m_2\mathbf{b}_4^{\times}+\mathbf{c}_2^{\times}\right)+\mathbf{C}_{14}\mathbf{c}_4^{\times}\mathbf{C}_{42}\right\} & -\left\{\mathbf{C}_{13}\left(m_3\mathbf{b}_5^{\times}+\mathbf{c}_3^{\times}\right)+\mathbf{C}_{15}\mathbf{c}_5^{\times}\mathbf{C}_{53}\right\} & -\mathbf{C}_{14}\mathbf{c}_4^{\times} & -\mathbf{C}_{15}\mathbf{c}_5^{\times} \\ \mathbf{c}^{\times} & \mathbf{J} & \left(J_{12}+J_{142}\right) & \left(J_{13}+J_{153}\right) & J_{14}\mathbf{C}_{14} & J_{15}\mathbf{C}_{15} \\ \mathbf{c}_2^{\times}\mathbf{C}_{21}+m_2\mathbf{b}_4^{\times}\mathbf{C}_{21} & J_{21}\mathbf{C}_{21}-m_4\mathbf{b}_4^{\times}\mathbf{C}_{21}\mathbf{b}_2^{\times}-\mathbf{b}_4^{\times}\mathbf{C}_{24}\mathbf{c}_4^{\times}\mathbf{C}_{41} & J_2-\mathbf{b}_4^{\times}\mathbf{C}_{24}\mathbf{c}_4^{\times}\mathbf{C}_{42} & \mathbf{0} & -\mathbf{b}_4^{\times}\mathbf{C}_{24}\mathbf{c}_4^{\times} & \mathbf{0} \\ \mathbf{c}_3^{\times}\mathbf{C}_{31}+m_3\mathbf{b}_5^{\times}\mathbf{C}_{31} & J_{31}\mathbf{C}_{31}-m_5\mathbf{b}_5^{\times}\mathbf{C}_{31}\mathbf{b}_3^{\times}-\mathbf{b}_5^{\times}\mathbf{C}_{35}\mathbf{c}_5^{\times}\mathbf{C}_{51} & \mathbf{0} & J_3-\mathbf{b}_5^{\times}\mathbf{C}_{35}\mathbf{c}_5^{\times}\mathbf{C}_{53} & \mathbf{0} & -\mathbf{b}_5^{\times}\mathbf{C}_{35}\mathbf{c}_5^{\times} \\ \mathbf{c}_4^{\times}\mathbf{C}_{41} & J_{41}\mathbf{C}_{41} & J_{42}\mathbf{C}_{42} & \mathbf{0} & J_4 & \mathbf{0} \\ \mathbf{c}_5^{\times}\mathbf{C}_{51} & J_{51}\mathbf{C}_{51} & \mathbf{0} & J_{53}\mathbf{C}_{53} & \mathbf{0} & J_5 \end{bmatrix} \qquad \text{Eqn 2.39}$$

The components of the generalised force vector in Eqn 2.37 are given by

$$\begin{aligned} {}^{1}\mathbf{f}_1 &= \sum_{i=1}^{5}\sum_{s}{}^{1}\mathbf{f}_{si} \\ &= {}^{1}\mathbf{f}_{aero,1}+\sum_{i=4}^{5}\mathbf{C}_{1\bar{\delta}}{}^{Flapper}\mathbf{f}_{aero,i}+\sum_{i=1}^{5}\mathbf{C}_{1E}{}^{E}\mathbf{f}_{grav,i} \end{aligned} \qquad \text{Eqn 2.54}$$

$$\begin{aligned} {}^{1}\mathbf{g}_1 &= \sum_{i=1}^{5}\sum_{s}{}^{1}\mathbf{g}_{si} \\ &= {}^{1}\mathbf{g}_{aero,1}+\boldsymbol{l}_{ac1}^{\times}\mathbf{f}_{aero,1}+\sum_{i=4}^{5}\left(\mathbf{b}_h+\mathbf{C}_{1h}\mathbf{b}_i+\mathbf{C}_{1i}\boldsymbol{l}_i\right)^{\times}\mathbf{C}_{1\bar{\delta}}{}^{Flapper}\mathbf{f}_{aero,i} \\ &\quad +\mathbf{d}_1^{\times}\mathbf{f}_{grav,1}+\sum_{i=2}^{5}\left(\mathbf{b}_h+\mathbf{C}_{1h}\mathbf{b}_i\right)^{\times}\mathbf{C}_{1E}{}^{E}\mathbf{f}_{grav,i} \end{aligned} \qquad \text{Eqn 2.55}$$

and for the wings and stroke plane actuators

$$\begin{aligned} {}^{i}\mathbf{g}_i &= \mathbf{d}_i^{\times}\mathbf{C}_{i0}{}^{0}\mathbf{f}_{grav,i}+{}^{i}\mathbf{g}_{motor,i}-\mathbf{C}_{ij}{}^{j}\mathbf{g}_{motor,j}+\mu_i\mathbf{I}\boldsymbol{\omega}_{pi}+{}^{i}\mathbf{g}_{dyn,i} \\ &\quad +\mathbf{C}_{i1}\left(\mathbf{C}_{1i}\boldsymbol{l}_{cp,i}\right)^{\times}\left(\mathbf{C}_{1\bar{\delta}}{}^{Flapper}\mathbf{f}_{aero,i}\right)+{}^{i}\mathbf{g}_{con,i}+{}^{i}\mathbf{g}_{friction,i} \end{aligned} \qquad \text{Eqn 2.56}$$

The forces and moments due to aerodynamics, friction, motor, gravity and constraints from the joints were described in Chapter 2.6.

The state derivatives given by Eqn 2.36 can be found by solving Eqn 2.35. Integrating with respect to time results in the state vector. The vehicle position can be obtained by carrying out the following operations

$$\mathbf{P}_1=\int\dot{\mathbf{P}}_1\mathrm{d}t=\mathbf{C}_{01}\int\mathbf{v}_1\mathrm{d}t \qquad \text{Eqn 2.58}$$

The orientation of the vehicle can be found by integrating the vehicle Euler rates given by Eqn 2.10

$$\begin{bmatrix} \dot{\phi} \\ \dot{\theta} \\ \dot{\psi} \end{bmatrix} = \begin{bmatrix} 1 & s_\phi t_\theta & c_\phi t_\theta \\ 0 & c_\phi & -s_\phi \\ 0 & s_\phi \sec_\theta & c_\phi \sec_\theta \end{bmatrix} \begin{bmatrix} p \\ q \\ r \end{bmatrix} \qquad \text{Eqn 2.10}$$

where $[p\ q\ r]^T = \omega_l$.

Finally, the stroke plane actuator and wing degrees of freedom are obtained by integrating the wing Euler rates given by Eqns 2.11 to 2.13

$$\dot{\kappa}_k = \omega_{ix} \qquad (\text{for } i = 2,3) \qquad \text{Eqn 2.11}$$

$$\dot{\delta}_p = \omega_{iy} c_{\chi_p} - \omega_{iz} s_{\chi_k} \qquad (\text{for } i = 4,5) \qquad \text{Eqn 2.12}$$

$$\dot{\chi}_k = \omega_{ix} \qquad (\text{for } i = 4,5) \qquad \text{Eqn 2.13}$$

CHAPTER 3

DEVELOPMENT OF THE SIMULATION MODEL

3.1 SIMULATION ENVIRONMENT

The simulation model for the flapping wing micro air vehicle was developed in the MATLAB and SIMULINK environment. SIMULINK allows non-linear simulation models to be created readily. The building blocks can be taken from the software library and put together to form the models. When the system becomes complicated, it is possible for a few blocks to be grouped together to form subsystems. Hence, even for complicated models, it is easy to maintain good overview through these subsystems and also from the graphical block diagram structures of the systems.

MATLAB also allows custom-built modules to be interfaced with the SIMULINK library blocks. Many methods are available to incorporate such modules, one of which is through the use of *S-functions*. These are codes written in MATLAB or in the C programming language and embedded in a block, which can be imported to and assimilated by the simulation model.

One of the main advantages of SIMULINK is that sub-routines or sub-programs representing standard components of control systems such as limiters, integrators, n-order systems are already available in the library and need not be developed and tested.

However, SIMULINK also has its disadvantages. It is found that by incorporating *S-functions* and by using small-step integration as required in the simulation of high frequency systems, the program speed rapidly deteriorates.

3.2 OPEN LOOP SIMULATION MODEL

The simulation model of the flapping wing micro air vehicle consists of six main subsystems as shown in Fig 3.1.

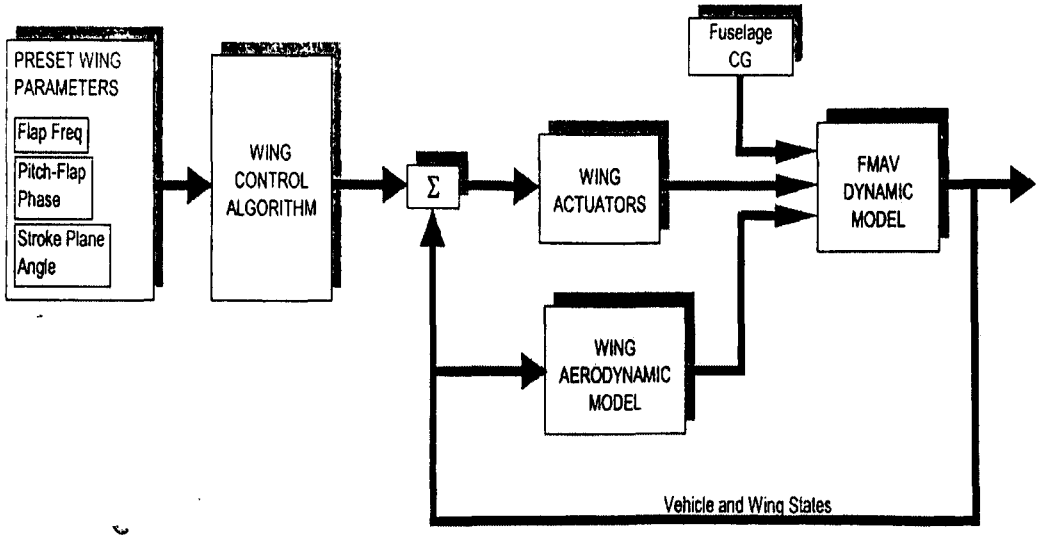

Fig 3.1 Open Loop MAV Simulation Model

The subsystems 'Preset Wing Parameters' and 'Fuselage CG' are inputs for the open loop simulation. The former is a consolidation of the wing parameters, namely the flap frequency, the phase between the wing pitch and flap degrees of freedom and the stroke plane angle. The other wing parameters such as flap and pitch amplitudes, mean flap and pitch angles are also defined in this block as constants.

'Fuselage CG' is a single input, which is the vector defining the location of the fuselage centre of gravity from the origin of the fuselage reference frame at P_1, see Fig 2.3.

The subsystem 'Wing Control Algorithm' obtains the prescribed wing beat kinematics from 'Preset Wing Parameters' and determines the time history of the orientation of each wing. This information is then passed on to the 'Wing Actuators' block, which compares the actual and the demanded states of the wings to determine the motor torques required to drive the stroke plane actuators and the wings to follow the prescribed motion.

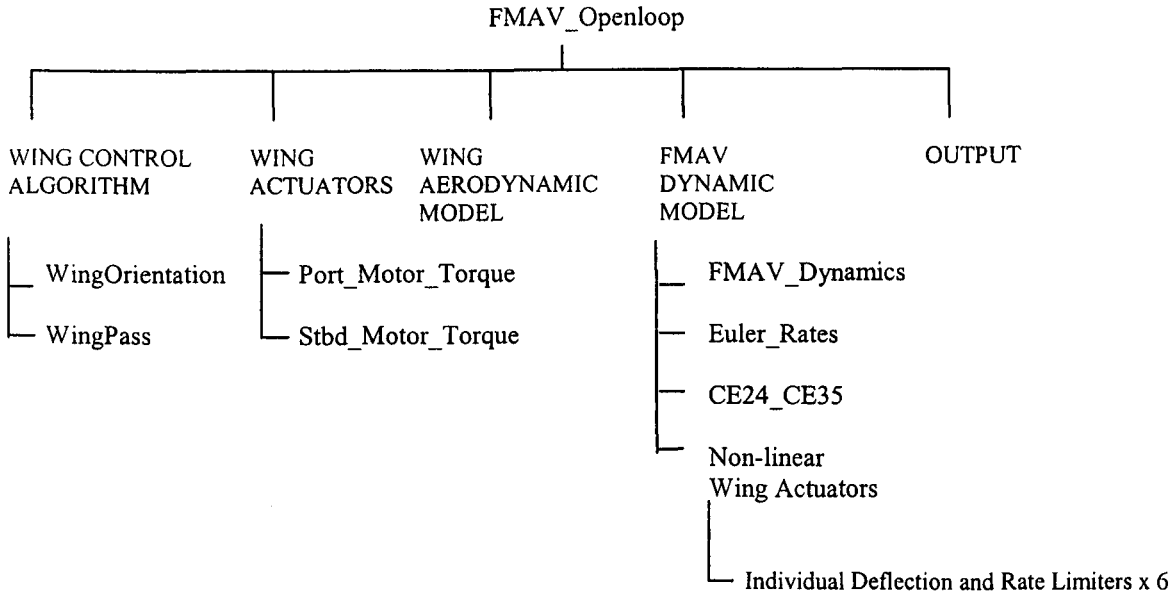

Fig 3.2 Hierarchy of Open Loop SIMULINK Model '*FMAV_Openloop*'

'FMAV Dynamic Model' consolidates the functions that include the calculation in the equations of motion for the vehicle, the coordinate transformations and the simulation of the non-linear actuators with rate limitations.

Fig 3.2 shows the sub-division of the simulation model into a maximum of three further levels of subsystems. The input blocks 'Preset Wing Parameters' and 'Fuselage CG' are not illustrated here.

The 'Wing Control Algorithm' subsystem contains two further subsystems. The subsystem *WingOrientation* specifies the demanded time histories of the wing orientation parameters $\Phi_p = [\kappa_p \; \delta_p \; \chi_p]^T$ for the port wing and $\Phi_s = [\kappa_s \; \delta_s \; \chi_s]^T$ for the starboard wing, where κ is the instantaneous stroke plane angle, χ is the instantaneous pitch angle and δ is the instantaneous flap angle of the wing. The subsystem *WingPass* simply consolidates the input parameters and the newly calculated wing orientation and passes them on to the 'Wing Actuators' subsystem.

The 'Wing Actuators' subsystem consists of two *S-functions*, that calculate the required torques for the port and starboard motors. These are the *Port_Motor_Torque* and *Stbd_Motor_Torque*,

The 'Wing Aerodynamic Model' is itself an *S-function* that delivers the aerodynamic force and moment coefficients of the wings in the fuselage axes system.

The 'FMAV Dynamic Model' consists of four subsystems as shown in Fig 3.3. The *S-function FMAV_Dynamics* contains the multi-body equations of motion developed in Chapter 2.5 and 2.6. The *S-function Euler_Rates* performs the transformation from the fuselage body rates to the Euler rates as described in Chapter 2.4. *CE24_CE35* performs the coordinate transformations as described in Chapter 2.3. The subsystem *Non-linear Wing Actuators* models the individual rate- and deflection-limited actuators.

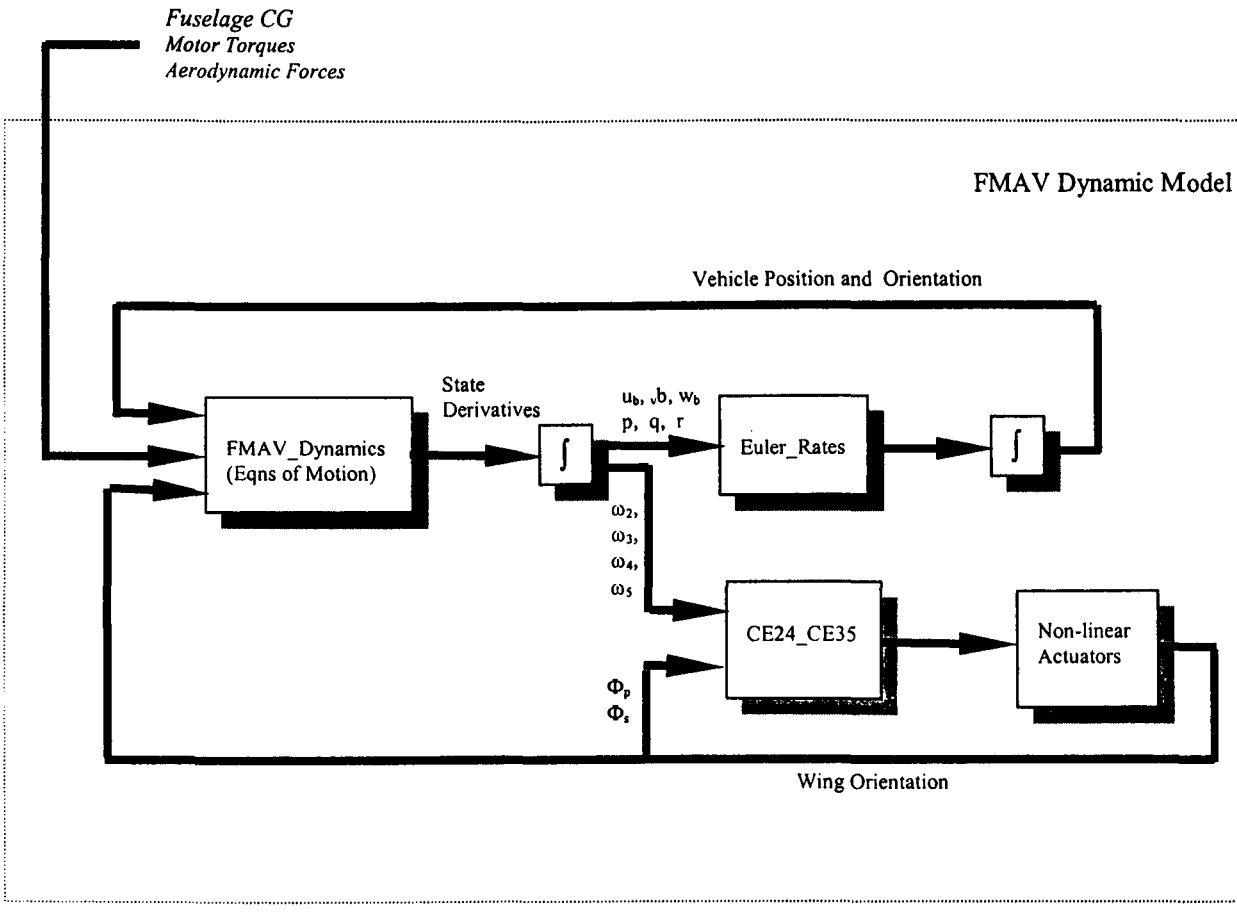

Fig 3.3 Details of FMAV Dynamic Model

Finally, the subsystem `Output` prepares the calculated data and parameters in output format to the MATLAB workspace for off-line processing and graph plotting.

3.2.1 SUBSYSTEM *WINGORIENTATION*

The input to this subsystem is the preset wing parameters, namely the flap and pitch amplitudes, flap frequency, mean angles and the phase between the flap and pitch attitudes of the wings. Once these are defined, the wing orientation $\delta_p(t)$, $\chi_p(t)$, $\delta_s(t)$ and $\chi_s(t)$ at the instant t are calculated in this *S-function* according to Eqns 3.1 and 3.2 and forms the output of the subsystem.

$$\delta = \hat{\delta}\cos(2\pi\tau) + \overline{\delta} \qquad \text{Eqn 3.1}$$

and

$$\chi = \hat{\chi}\cos(2\pi\tau + \varphi) + \overline{\chi} \qquad \text{Eqn 3.2}$$

3.2.2 SUBSYSTEMS *PORT_MOTOR_TORQUE* AND *STBD_MOTOR_TORQUE*

There are three motors responsible for the motion of each wing, namely the pitch, flap and rotation of the stroke plane. Each of the actuator motors has an individual control loop but the loops are similar in design and were described in Chapter 2.6.1.3.

The controlled variables are the stroke plane angle κ, the flap angle δ and the pitch angle χ of each wing. The response of each of these variables can be represented as a second order system. The stroke plane angle, for example was shown in Eqn 2.46 to be

$$I_\kappa \ddot{\kappa} + C\dot{\kappa} + K\kappa = Q_{motor,\kappa} \qquad \text{Eqn 2.46}$$

where $Q_{motor,\kappa}$ is the stroke plane actuator motor torque, I_κ is the inertia in the stroke plane, K_κ is the actuator motor gain and C_κ is the damping provided by the control loop as shown in Fig 2.5 and repeated below as Fig 3.4.

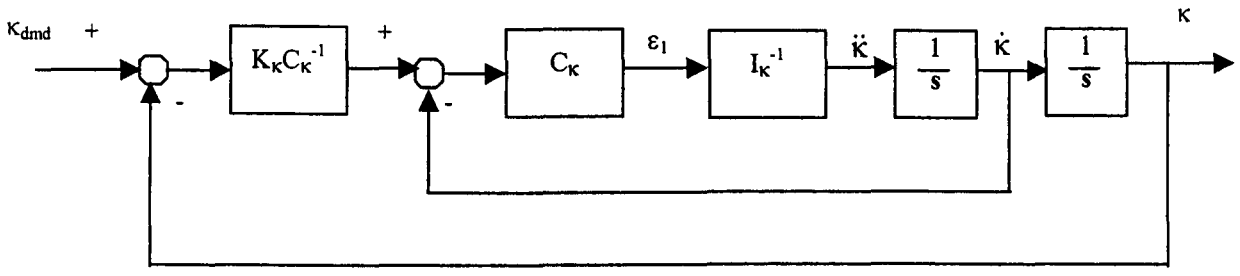

Fig 3.4 Stroke Plane Actuator Control Loop

The equation of motion for the stroke plane angle degree of freedom can be developed as follows:

$$I_\kappa \ddot{\kappa} = \varepsilon_1 \qquad \text{Eqn 3.3}$$

or

$$\ddot{\kappa} = I_\kappa^{-1}\varepsilon_1 = I_\kappa^{-1}\left[K(\kappa_{dmd} - \kappa) - C\dot{\kappa}\right] \qquad \text{Eqn 3.4}$$

Taking the Laplace transform, this can be rearranged to yield

$$\frac{\kappa}{\kappa_{dmd}} = \frac{K}{I_\kappa s^2 + Cs + K} \qquad \text{Eqn 3.5}$$

The closed loop characteristic equation for the above control system is thus

$$s^2 + \frac{C}{I_\kappa}s + \frac{K}{I_\kappa} = 0 \qquad \text{Eqn 3.6}$$

3.2.3 SUBSYSTEM *WING AERODYNAMIC MODEL*

This *S-function* computes the aerodynamic forces and moments experienced by the wing. The input to this subsystem is the flap frequency, wing orientation and rates, as well as the fuselage orientation and rates, both linear and rotational.

The dynamic pressure is given by

$$\bar{q} = \frac{1}{2}\rho\left(V_{flap}^2 + V_o^2\right) \qquad \text{Eqn 3.7}$$

If the aerodynamic force coefficients are represented generally as C_k and the moment coefficients as $C_{m,k}$, then the aerodynamic forces can be calculated by

$$F_k = \bar{q} S_{ref} C_k \qquad \text{Eqn 3.8}$$

and the aerodynamic moments are given by

$$M_k = \bar{q} S_{ref} b_{ref} C_{m,k} \qquad \text{Eqn 3.9}$$

The experimental determination of the aerodynamic coefficients will be described in Chapter 4. The transformation of the aerodynamic forces and moments from the reference frame of the experimental data to that of the fuselage will be described in Chapter 5.

3.3 TEST AND EVALUATION STRATEGY

The equations of motion are of order 18 and are non-linear and highly coupled. The task of obtaining an analytical model of the dynamics of the vehicle is enormous, if not impossible. This can be avoided if the equations are solved numerically. In order to ensure that the numerical solution of these equations is correct, the complexity of the model requires that a series of tests be carried out and the results interpreted intuitively to check the coherence of the model with the physical expectations. These tests increase in complexity and allow an overall picture of the simulation model to be built up gradually.

In order to avoid further complication to the interpretation of the results, the tests are carried with the aerodynamic forces and moments omitted. The effects of the aerodynamics will be tested in Chapter 5 and Chapter 7.

The test can be built up as follows:

(i) Testing fuselage and wing motion in absence of motor control

a. allowing the wings to drop without joint friction

b. allowing the wings to drop with joint friction

c. allowing the vehicle to spin about an axis parallel to the P_1z_1-axis, refer to Fig 2.3, and passing through the vehicle CG. This allows the effects of centrifugal forces on the wings to be observed

(ii) Testing the effects of motor driving torque by

a. keeping the wings level against the action of gravity

b. rotating the stroke plane

c. demanding pure flapping motion of the wing

d. demanding pure pitching motion of the wing

e. demanding simultaneous flapping and pitching of the wing

f. demanding simultaneous flapping and pitching of the wing, while at the same time changing the stroke plane angles

(iii) Testing the unrestrained vehicle motion

a. Vehicle imparted with initial vertical velocity

b. Vehicle imparted with initial vertical velocity and rotational rates with wings flapping demanded and with them free

3.4 TEST RESULTS

The test results are shown and analysed in the following paragraphs. Each set of results is reproduced in a set of 12 graphs representing position and orientation of the wings and fuselage. For example, with reference to Fig 3.5, the first column represents the time history of the position of P_1, the origin of the fuselage reference systems (x_b, y_b and z_b in metres). The next column shows the orientation of the fuselage (ϕ, θ and ψ in degrees). The third and last columns represent the wing orientation of the port (κ_p, δ_p and χ_p in degrees) and starboard (κ_s, δ_s and χ_s in degrees) wings respectively.

3.4.1 ABSENCE OF MOTOR CONTROL

In these tests, the motor torques $\mathbf{g_{motor}}$ developed in Chapter 2.6.1.3 are set to zero.

In the first test, the vehicle was initiated with the wings level ($\delta_p = \delta_s = 0°$). Friction was also omitted by setting $\mathbf{g_{friction}}$ in Eqn 2.45 to zero. The wings are then released and the time histories of the flap angles were plotted as in Fig 3.5. The charts at the centre of the third and fourth columns from the right show that the flap angles oscillated without any damping between 0° and 180°. The physical interference between wing and fuselage was ignored in this simulation and hence the wings were able to reach flap angles of 180°.

Energy was conserved as the oscillations returned to these values at the beginning and end of each of the flap cycles. The results were anticipated in a physical model except that it was expected that the fuselage should move upwards when the wings flap down and vice versa. This was not the case because the fuselage z_b-degree of freedom was inhibited in this and all subsequent tests to prevent the vehicle from descending below ground level.

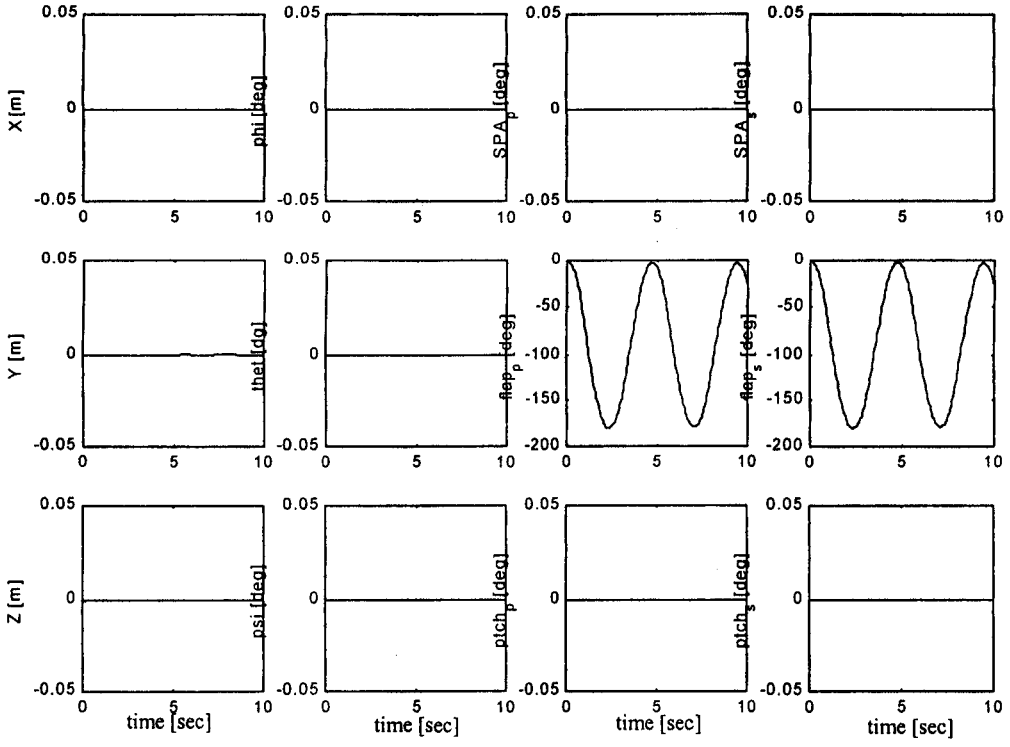

Fig 3.5 Wing drop with no joint friction

In the next test, the vehicle was initiated again with wings level but this time, a coefficient of friction of $\mu_i = 0.025$ ($i = 2..5$) was used. The simulation results in Fig 3.6 show that the initial potential energy of the wings when held level was gradually dissipated and that they tend gradually to the vertical position (i.e. $\delta_p = \delta_s = -90°$) corresponding to the position with minimum potential energy. This is the equilibrium position of the wings.

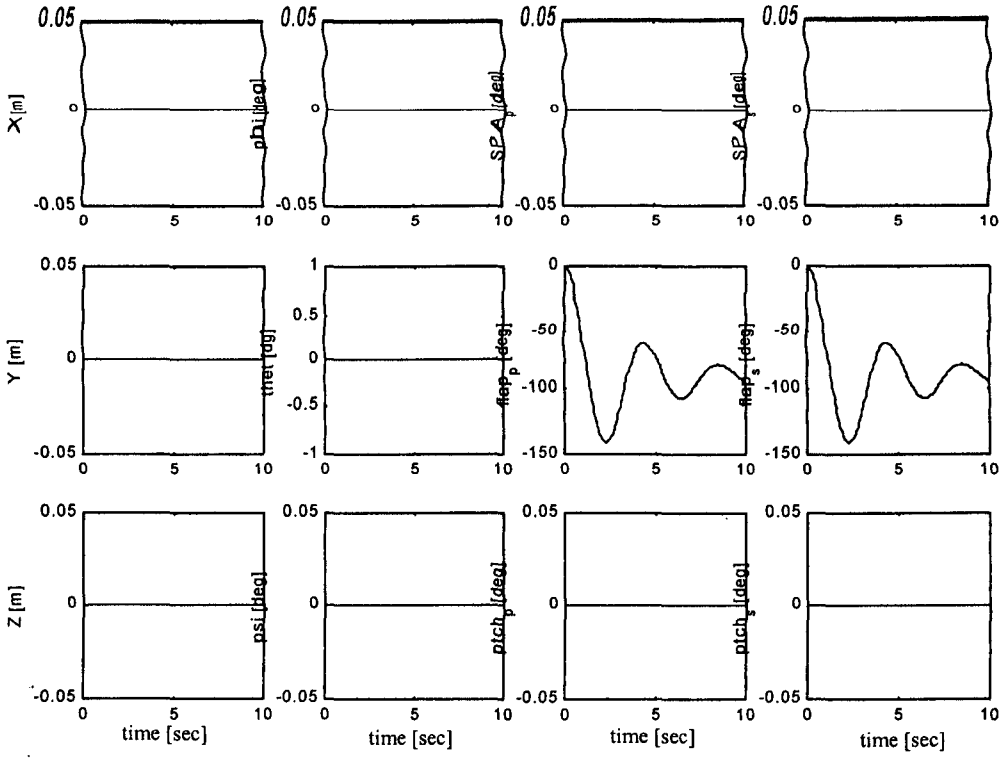

Fig 3.6 Wing drop with joint friction (μ = 0.025)

Next, the vehicle was initiated with wings first pointing vertically down ($\delta_p = \delta_s = -90°$). The fuselage was then given an initial rotational rate $\omega_z = 6$ rad s^{-1} about its vertical P_1z_1-axis. Friction was included only for the wing joints with $\mu_i = 0.025$ (i = 4,5). In the absence of friction between the fuselage and the ground, it continued to spin steadily about its vertical axis as seen in its azimuth time history (ψ) in Fig 3.7. The wings are seen to seek an equilibrium position with ($\delta_p = \delta_s = -70°$) after some initial overshoot. This position balances the moments due to the centrifugal force and the weights of the wings, the moments about the wing joints due to centrifugal forces tend to force the wings out while the moments due to the weight of the wings tend to force them down.

In the above test, the stroke plane actuator degrees of freedom were frozen. They would have otherwise introduced coupling between the wing and the effects of the centrifugal force would not be that obvious.

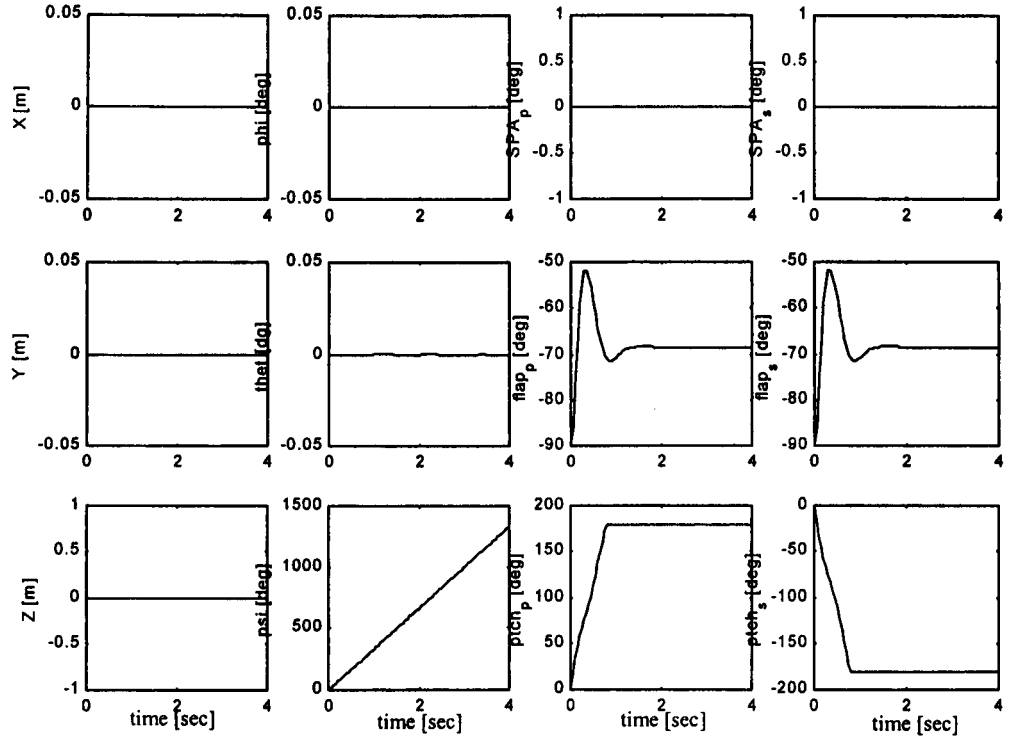

Fig 3.7 Rotation of Vehicle about Z_1-axis ω_z=6 rad/s, SPA frozen, no motor torque, μ=0.025

3.4.2 EFFECTS OF MOTOR CONTROL

In the tests described in this section, the motor torque $\mathbf{g_{motor}}$ prescribed by the demanded wing kinematics determined in the subsystem `WingOrientation` are now included in the simulation.

In the first test, wings level attitude was demanded by setting $\delta_{pdmd} = \delta_{sdmd} = 0°$. It can be seen that the wings initially drooped slightly to -0.4° due to its own weight and the flap motors then corrected this to slightly less than –0.4°, as seen in Fig 3.8. An absolute zero is not achieved because the motors require an error reading in order to generate holding torque or an integrator in the control loop to cancel the error signal.

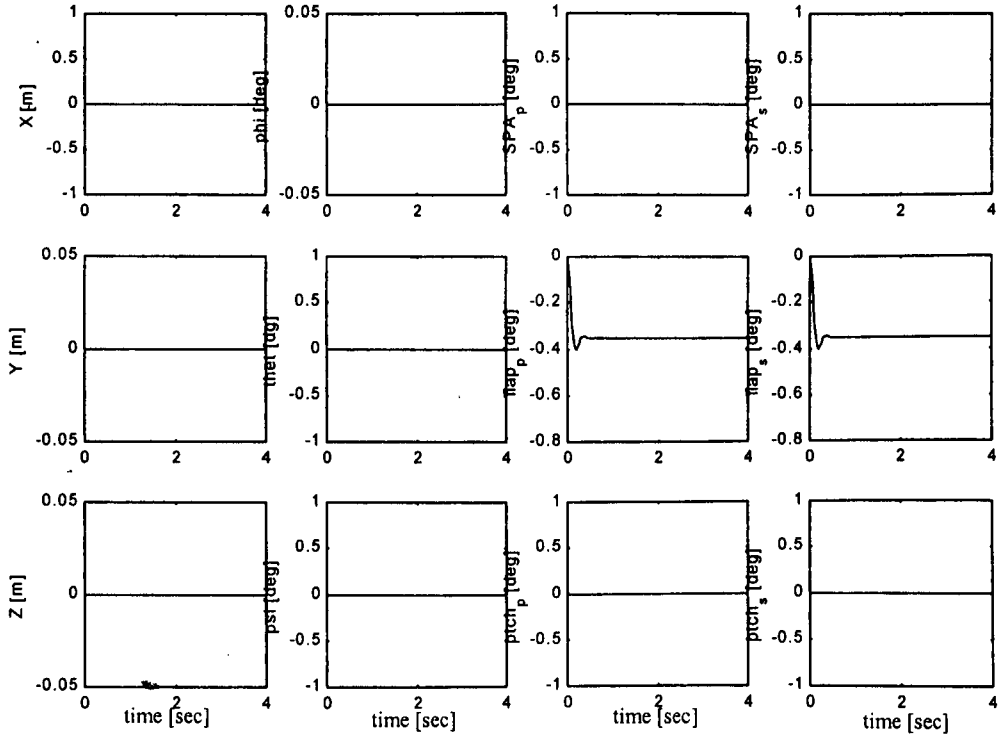

Fig 3.8 Holding Wings at κ=δ=χ=0°

Next, beginning with $\kappa_p = \kappa_s = 0°$, a demand of $\kappa_p = \kappa_s = 57.3°$ (or 1 radian) was generated. The results are shown in Fig 3.9. It can be seen that the final positions are reached after some overshoot. The wings also responded by first rotating in pitch in the opposite sense until the error signal was large enough for the pitch motors to begin to generate a counter-torque, returning the pitch attitudes to the demanded zero value. At the same time, the fuselage also pitched nose down due to the conservation of momentum about this axis. As there was no friction or restoring moment between the fuselage and the ground, it continued pitching nose down after given an initial nose down pitch acceleration.

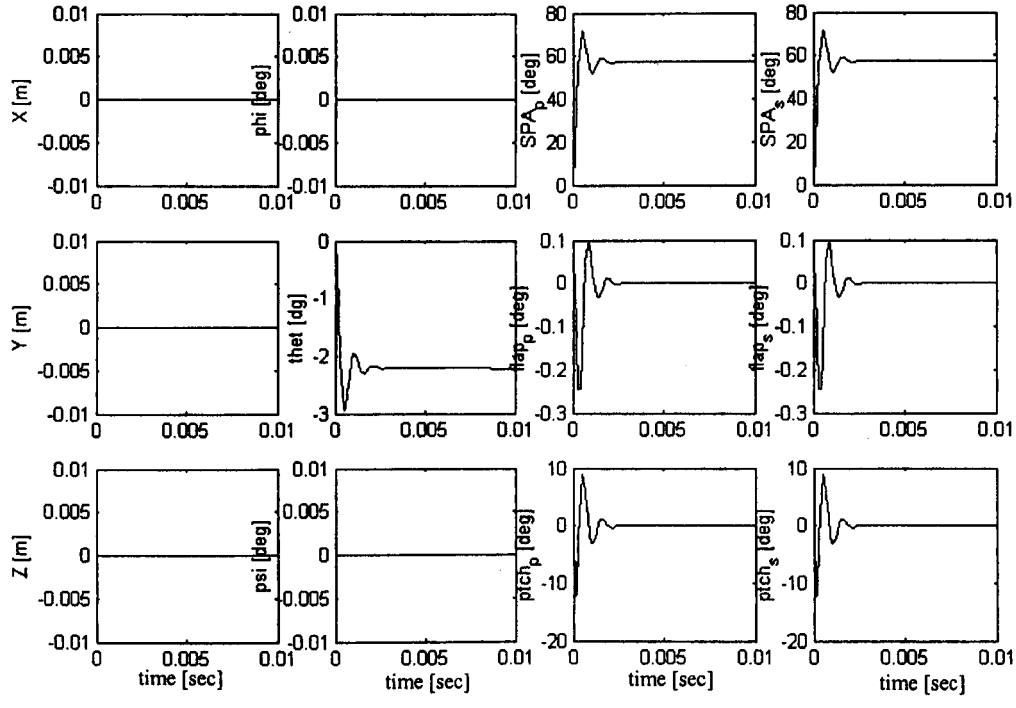

Fig 3.9 Rotating the Stroke Plane from 0° to 57.3°

The above test was repeated with the port and starboard actuators being commanded to equal magnitudes but in opposite sense, Fig 3.10. This time, the wings responded as in the previous test. However, the pitch momentum due to the port wing is equal and opposite that of the starboard wing and the sum of momentum about the fuselage pitch axis is therefore zero. The fuselage does not pitch.

The port wing drooped due to its weight at the same time as the stroke plane was rotated to +45°. This combined motion effectively brought the centre of gravity of the wing forward due to the kinematics of the motion. Similarly, the centre of gravity of the starboard wing was brought backwards due to the stroke plane rotating to -45° as the wing drooped. The motion of the wing centres of gravity caused a positive yaw of the fuselage. In the absence of friction between fuselage and ground, it continued to rotate about the fuselage yaw axis P_1z_1.

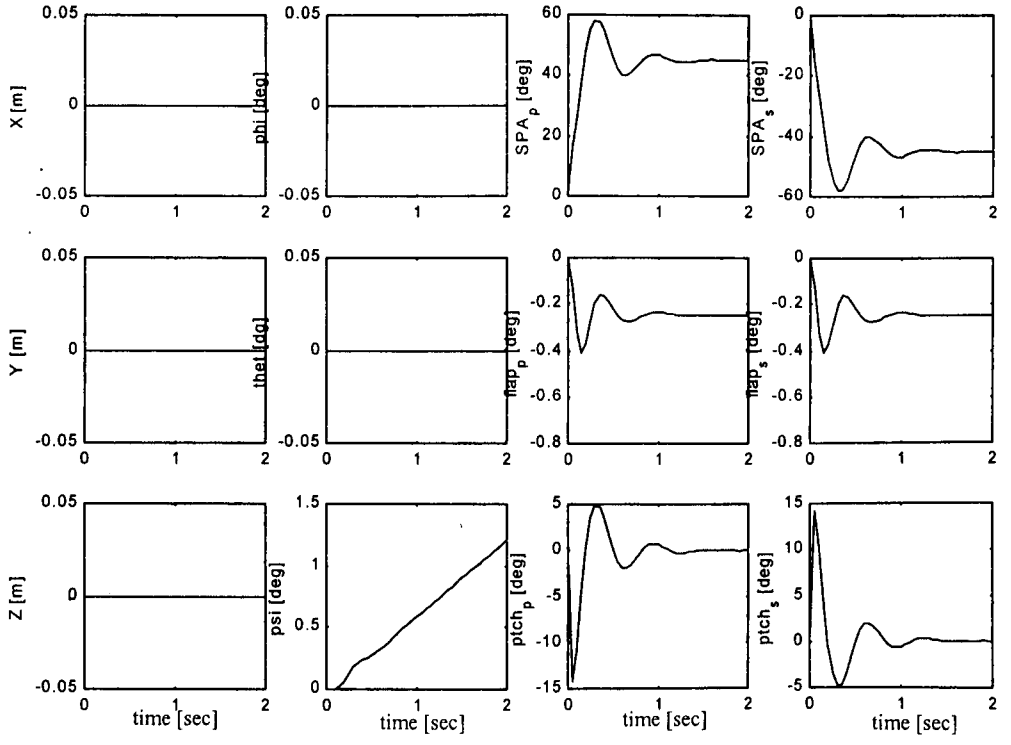

Fig 3.10 Rotating Stroke Plane Angle from 0° to 45° (port) and 0° to –45° (starboard)

In the next test, the demanded wing beat was pure flapping with amplitude of 110° (±55°) at a frequency of 0.5 Hz. As the wing attachment point was specified to be at the same position as the CG of the fuselage in this test, there was no oscillation of the fuselage and the wings responded to the demand as seen in Fig 3.11.

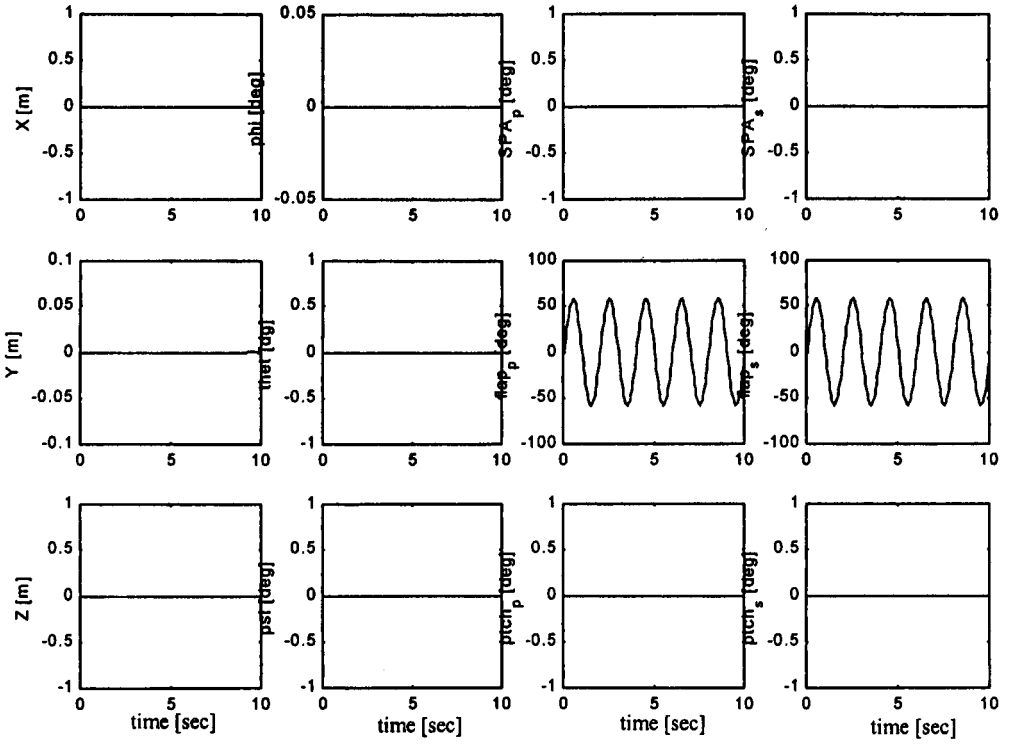

Fig 3.11 Pure Flapping at 0.5 Hz

Fig 3.12 shows the response of the vehicle when pure pitching of the wings was demanded. The fuselage oscillated in pitch in the opposite sense due to the conservation of momentum as explained earlier.

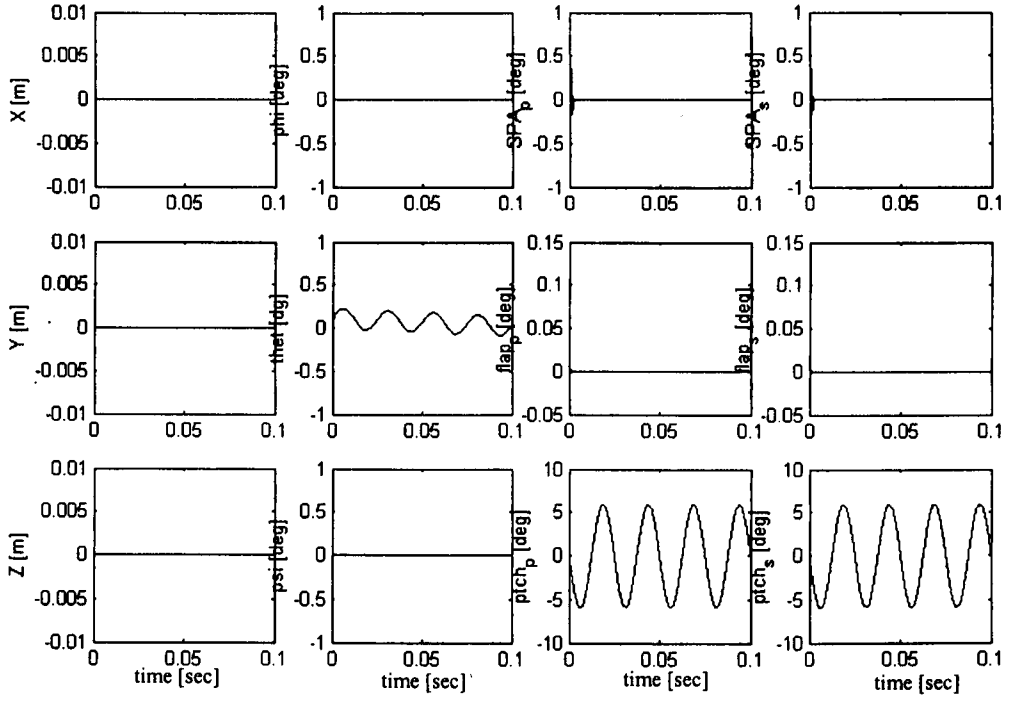

Fig 3.12 Pure Pitching of the Wings at 40 Hz

Next, the vehicle was subjected to simultaneous flap and pitch demand. The frequency was at 40 Hz, flap amplitude was 100° (±50°), pitch amplitude was 10° (±5°) and the phase between pitch and flap was 90°. Figure 3.13 shows the results of the simulation. It was seen that the fuselage oscillated in pitch as before.

In the inhibition of the z_b degree of freedom, a tolerance was specified for z_b. The algorithm would only inhibit z_b only upon exceeding this tolerance. This was the reason for the slight increment ($1x10^{-4}$ m) observed in z_b in the figure.

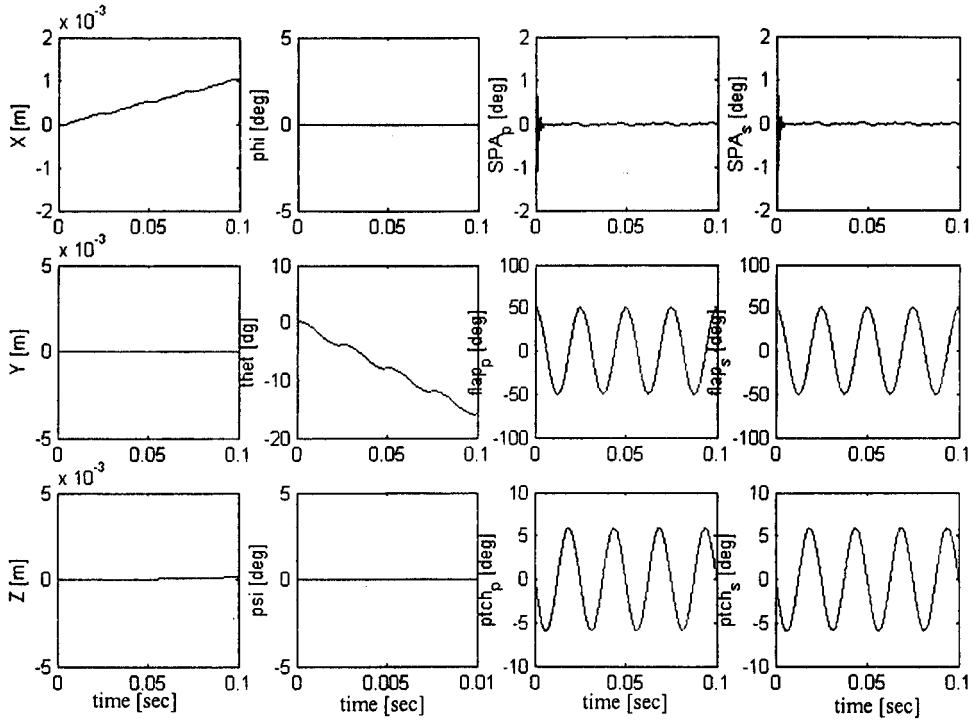

Fig 3.13 Flapping and Pitching at 40Hz with SPA controlled at 0°

The initial values of the states were then calculated. For example, the flap and pitch rates are known based on the wing beat kinematics. The relationship between the wing Euler rates and ω_{pi} (i = 4,5) are given by the equations in Chapter 2.4.3. The fuselage states are still unknown. If the wing beat of both the port and starboard wings is symmetrical, the lateral-directional states can be set to zero. The longitudinal states u_b, z_b and q_b are then adjusted such that the time-averaged rates are zero. Repeating the test again with values of the states set to appropriate levels, we see that although the body pitched and moved fore and aft periodically, there is no drift from the initial position, Fig 3.14.

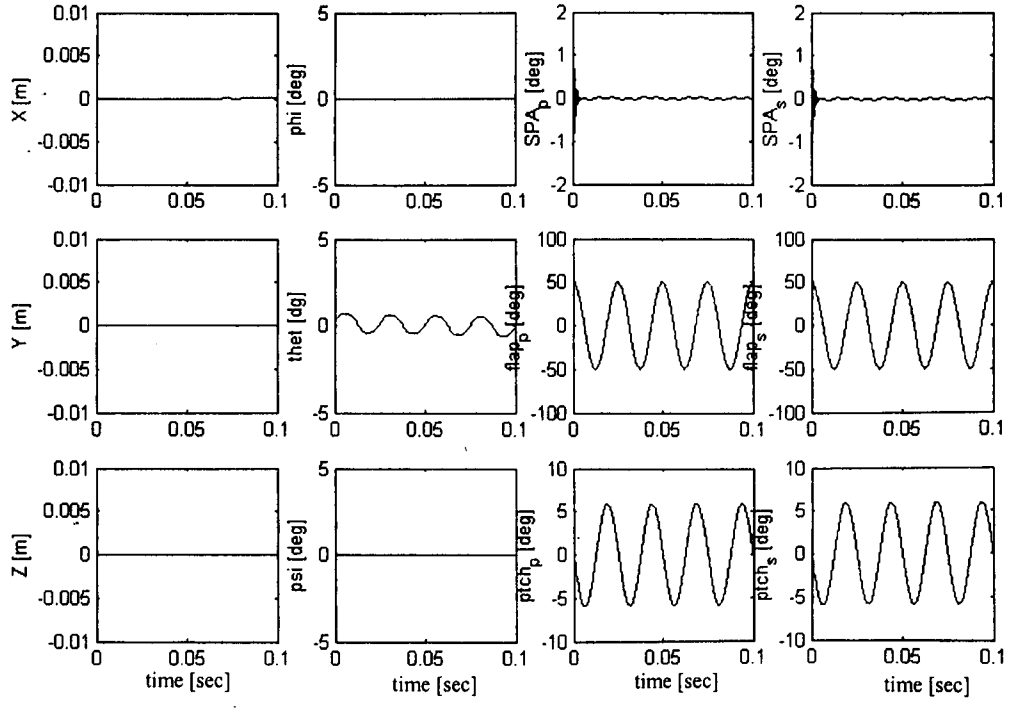

Fig 3.14 Flapping and Pitching at 40 Hz with SPA controlled at 0° and initial conditions determined for 'no-drift'.

The final test in this section was to demand a stroke plane angle change from 0° to 10° while the wings are flapping and pitching at the same time. Fig 3.15 shows the results. The stroke plane angles (SPA_p and SPA_s, charts on the first row, third and fourth column) tend to 10°. There is strong coupling between the wings and the actuators and hence the shape of the curves. It can be seen that the stroke plane angles oscillated about the demanded position 10°. The resultant fuselage position and pitch attitude are again attributed to untrimmed initial settings.

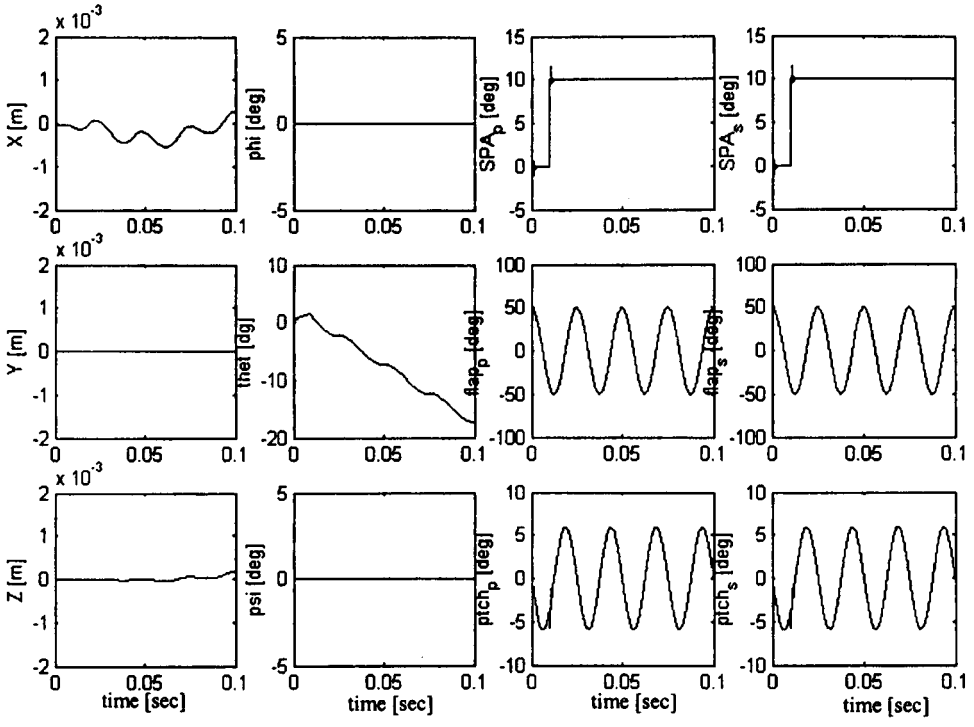

Fig 3.15 Flapping and pitching with rotation of stroke plane from 0° to 10°

3.4.3 UNRESTRAINED VEHICLE MOTION

All the foregoing tests were conducted with the vehicle in contact with the ground. It has shown that the simulation is satisfactory and that the results correspond to a physical model subjected to the same inputs. The next phase of tests were chosen to confirm the vehicle behaviour when it is not in contact with the ground. The objectives of the tests were to check the effect of gravity on the vehicle and to check that the simulation runs properly when subjected to large changes in the variables without the program terminating prematurely.

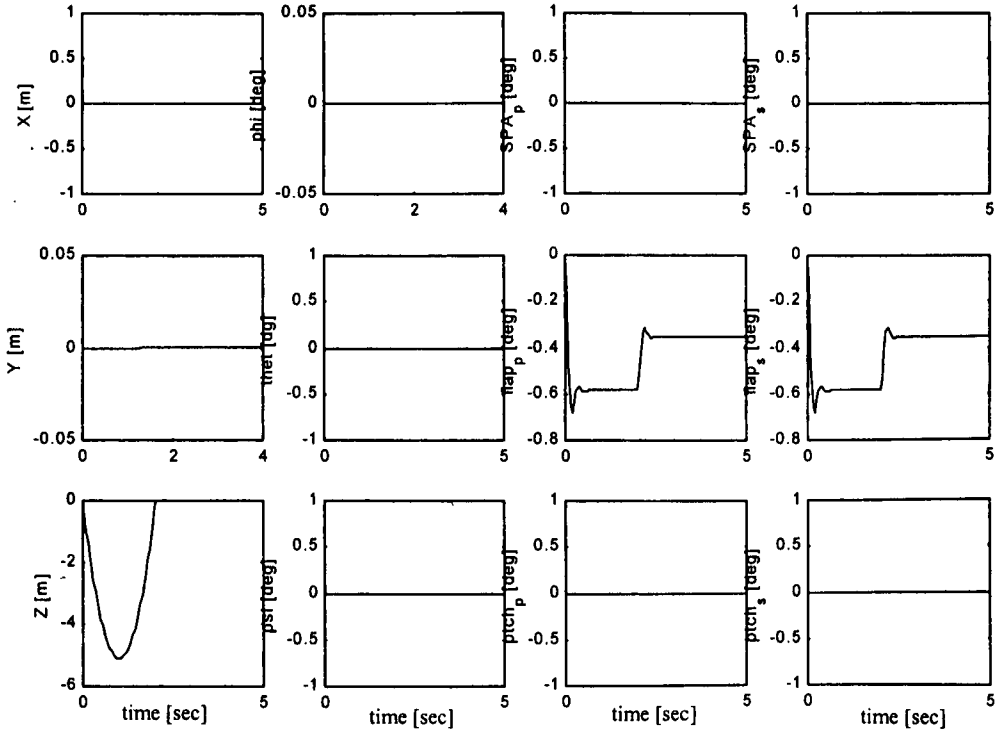

Fig 3.16 Vehicle thrown upwards with w=-10m/s and wings controlled at zero deflection

Fig 3.16 shows the results when the vehicle was given an initial vertical velocity with its wings fixed at $\delta_p = \delta_s = 0°$. The vehicle rises vertically to a height of about 5m before falling back to its initial point. The wings fall down to $\delta_p = \delta_s = -0.6°$ as compared with

the -0.4° observed when the vehicle was stationary on the ground. As it hits the ground again, it can be seen that an impulse was experienced and the wings returned to the -0.4° as in the test in section 3.4.2.

Fig 3.17 shows the time histories when the vehicle was thrown vertically upwards and at the same time given initial rotational rates about all the fuselage axes. The wings are not driven and are free about its degrees of freedom. It is interesting to note that now the vehicle does not fall vertically back to its launch point but has traversed a slight distance forward and to the side as shown in the x_b and y_b positions. This is because the coupling between the rotational rates and the vertical velocity results in motion away from the vertical.

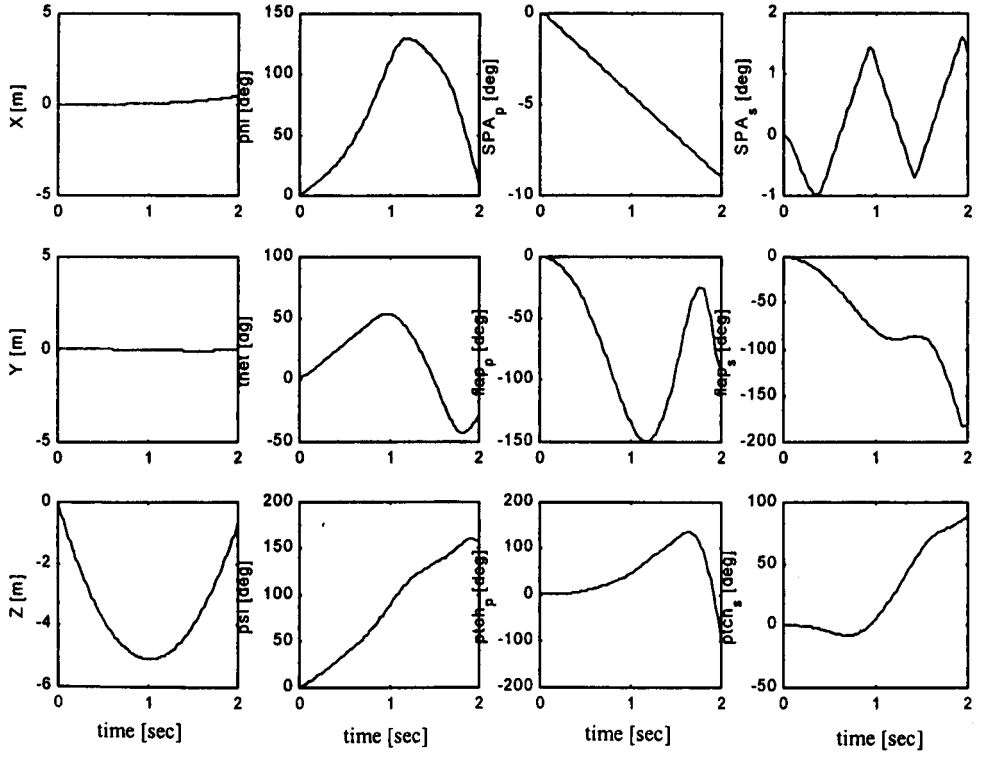

Fig 3.17 **Vehicle thrown vertically upwards at 10 m/s with initial rotational rates of 1 rad/s about all axes, wings are not driven**

The test was repeated with wings flapping and pitching at 2 Hz and the results are shown in Fig 3.18. The motion was asymmetric and coupling between all axes was evident, making the interpretation of the results difficult. However, the run was completed and did not terminate prematurely.

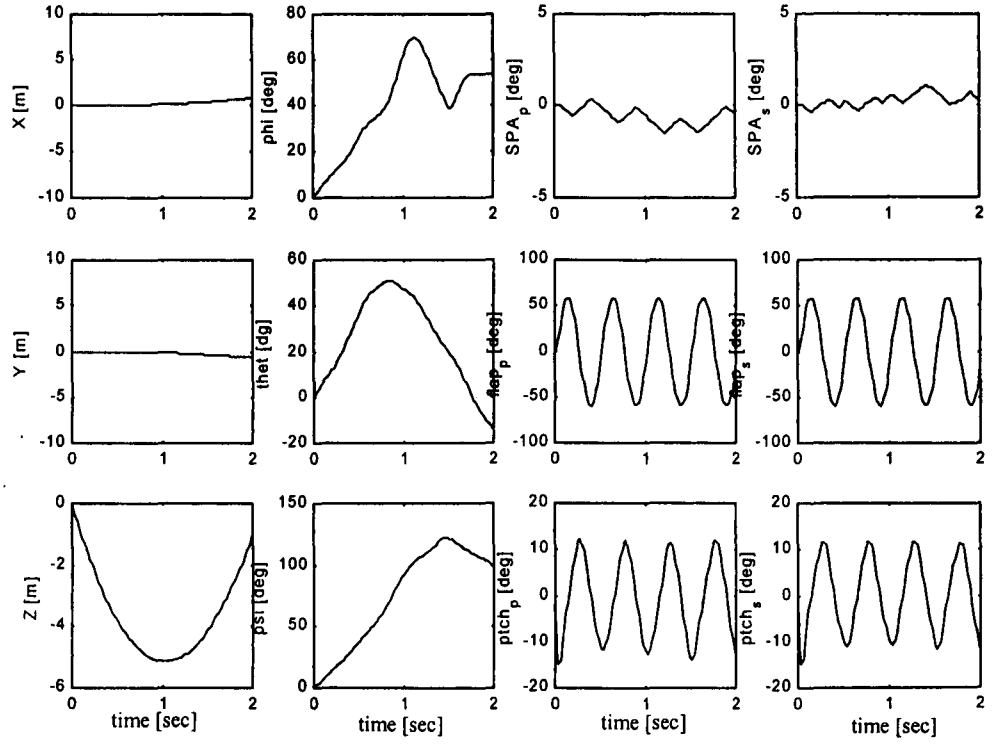

Fig 3.18 **Vehicle thrown vertically up with 1 rad/s inital rotation rates about all axes and wings driven at 2 Hz**

CHAPTER 4

DETERMINATION OF AERODYNAMIC CHARACTERISTICS OF FLAPPING WING

4.1 INTRODUCTION

Experiments were carried out during the course of this thesis to obtain the aerodynamic forces of the wing flapping in still air under simulated hover condition to build up a data base for the flight simulation of the flapping wing MAV can be simulated. The beat kinematics of the wing in terms of the amplitude and mean flap and pitch angles as well as the phase between the flap and pitch angles were varied to study their effects on the force magnitude and direction with respect to the stroke plane.

Although some works have been published by other researchers, either the numerical results were not available in sufficient detail or they are specific to a single test condition.

Vest [1996], for example, published his PhD thesis in which he developed a CFD model for the flow field around the flapping wing of a pigeon in forward flight. In his model, the flow field was solved in two parts. Firstly, the inviscid solution for the external pressure and velocity field was found. Then, from these results, the inner viscous problem would be solved. The numerical solution of only a single point was available but insufficient for our purpose.

Smith et al [1996] developed a similar CFD model of a hawk moth wing but included the flexibility of the wing in his solution. Again, the results assumed non-viscous flow and a single data point was available.

Liu et al [1998] worked on a set of CFD codes that included the viscosity of the fluid in which the wing flaps. By so doing, he was able to model the presence of a leading edge vortex discovered by van den Berg and Ellington [1997] in their flow visualisation experiment.

On the experimental front, Archer et al [1979] made use of a flapping mechanism that allows single degree of freedom flapping in a plane normal to the direction of flight in order to concentrate their attention on the thrust producing mechanism.

Fejtek and Nehera [1980] used a Scotch-yoke mechanism in combination with a rack and spur gear to flap their model wings with a single degree of freedom at frequencies between 2.6 and 3.3 Hz. The Reynolds' number ranged from 7.2×10^4 to 12×10^4. Their experiments charted time-averaged lift and drag coefficients lying between 0.2 and 0.5 over a range of advance ratio between 5 and 20 for stroke plane angles of 0°, 15° and 30°.

Dickinson [1994] designed a mechanism that flaps and rotates the model wing in a water tunnel and measured the forces experienced. The wing flaps through large angles and is rotated at the end of the stroke. By varying the timing of the rotation, he was able to study its effect on the unsteady aerodynamic performance of the wing. He was able to measure instantaneous peak values of up to 4 for the force coefficients.

Vest and Katz [1999] built a model of a pigeon with wings that flap with a single degree of freedom to measure the forces experienced in a wind tunnel. The measurements were compared with the theoretical prediction from their CFD model described above.

The above works are of limited use for the current research as it was hoped that by parameter variation it might be possible to devise a control strategy for the micro air vehicle, hence the motivation to conduct experiments to collect the aerodynamic data for the wing.

From the beginning, it was anticipated that the experiment would not be a simple task. The design of the flapping mechanism to achieve flapping frequencies high enough for measurable aerodynamic force would be limited by the sizing of the motors and the moving components. Indirect drives through the use of gearboxes may allow higher frequencies to be achieved for a given motor but may introduce backlash problems that may affect the force measurements.

The very small magnitude of the forces, which is dependent on the flap frequency, also poses another problem. The balance available for the task may not be able to measure forces that momentarily fall below its resolution threshold.

4.2 EXPERIMENTAL SET-UP

4.2.1 DESIGN OF MECHANICAL FLAPPER

A mechanical flapper with two degrees of freedom about the pitch and flap axes as shown in Fig 4.1 was designed and built for this experiment.

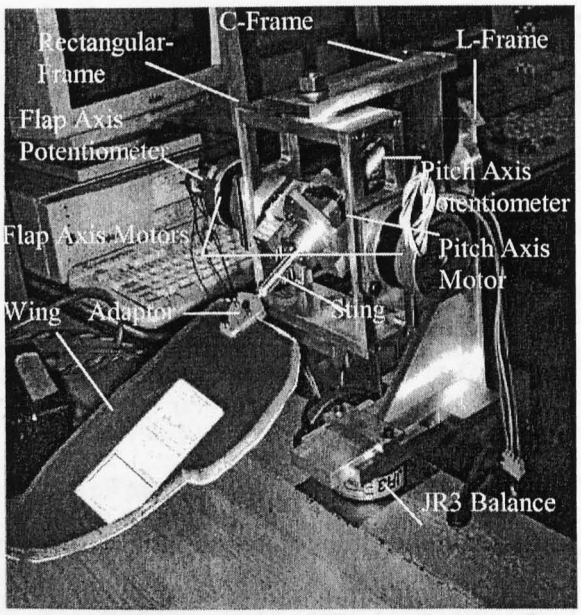

Fig 4.1 Mechanical Flapper Design

It consists of an L-shaped support, to which a C-frame is attached by bolt and nut. A rectangular frame is supported by the C-frame as shown in Fig 4.2. Two stepper motors (RS 440-442 and RS 440-458), attached to the rectangular frame, drive the flapping arm. A single stepper motor (RS 440-436) is attached to the flapping arm and this drives the pitch degree of freedom.

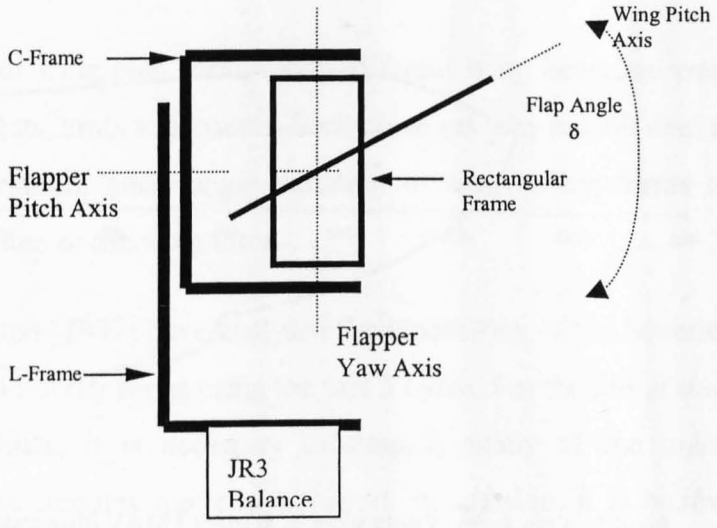

Fig 4.2 General Component Layout of Flapper

The wing is attached to the flapper arm via an adaptor and a short cylindrical sting of 8 mm diameter. The distance between the root of the wing and the flap axis of rotation in the final design is 40 mm or 18% of the root to tip dimension of the wing.

The 3 frames are secured in place by bolts and nuts. The design allows stroke plane angle to be adjusted the by rotating the C-frame about its attachment to the L-frame (i.e. flapper pitch-axis). The sideslip angle can be varied by rotating the rectangular frame with respect to the C-frame (i.e. flapper yaw-axis). The tests are conducted with a vertical stroke plane and as the tests simulate the hovering condition, sideslip angle was also not relevant.

4.2.2 WING PLAN FORM

Nature has presented a large variety of wing plan forms, each probably best suited for its intended purposes. There are currently some researches being carried out to identify the design criteria for micro air vehicle wing plan forms. It was not the intention of these experiments to identify the ideal plan form for the vehicle being investigated.

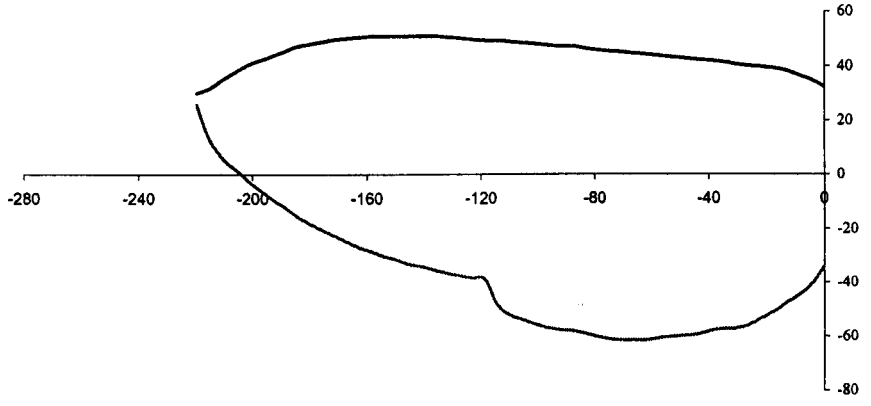

Fig 4.3 Plan form of port wing of subject FMAV [dimensions in mm]

The plan form of the wing of the hawk moth *Manduca sexta* as shown in Fig 4.3 was selected for the test wing due to the significant research work carried out by many researchers that included two different computational fluid dynamics (CFD) models by Vest [1996] and Liu and Kawachi [1999], and flow visualisation using a low frequency flapper by van den Berg and Ellington [1997].

It was hoped that the current tests would generate a database for comparison with the predictions by the CFD models. Unfortunately, the resolution of the force sensor was not sufficiently fine to measure the forces produced by test wing at the corresponding flap frequency.

In order to increase the magnitude of the forces, the wing was flapped at a frequency that was about 45% higher. Even at this increased frequency, the data accuracy is also questionable, at best, for one series of the tests. This made the comparison of the collected data with the CFD models inappropriate. As the comparison was only one of the

objectives of the tests, conduct of the tests with the selected plan form did not affect the primary aim of collecting aerodynamic data of the flapping wing for flight simulation purposes.

4.2.3 WING BEAT KINEMATICS

Just as in the case of wing plan form, many different wing beats are employed by the different species of bats, birds and insects. Such creatures may exhibit clap and fling, clap and peel, phase variation, mean angle variation or many other forms to control the magnitude and direction or the wing force.

Willmott and Ellington [1997] have analysed the kinematics of the hovering hawk moth and quantified it as a Fourier series using the first 3 terms. For the initial study of flapping wing micro air vehicle, it is necessary to simplify many of the unknowns to aid understanding of this complex mode of transport. In addition, it is believed that in an implementation of a flight control system for a practical MAV, a simplified kinematics would be advantageous, provided the force generation capability is not compromised. It is for this reason that the wing beat kinematics in the tests are simplified to sinusoidal motion defined by the amplitude and mean values for each of the two degrees of freedom, the phase between them and the flap frequency, with the pitch frequency identical to the flap frequency. Hence, the wing beat kinematics is fully defined by the following equations for the flap and pitch degrees of freedom:

$$\delta = \hat{\delta} \cos(2\pi\tau) + \overline{\delta} \qquad \text{Eqn 4.1}$$

and

$$\chi = \hat{\chi} \cos(2\pi\tau + \varphi) + \overline{\chi} \qquad \text{Eqn 4.2}$$

4.2.4 EXPERIMENTAL HARDWARE

Fig 4.4 shows schematically the experimental set-up. The flapper is controlled via the custom-built stepper motor control system (Cortex S649) that generates the required motion for the wing and is configurable from a program residing in PC #1.

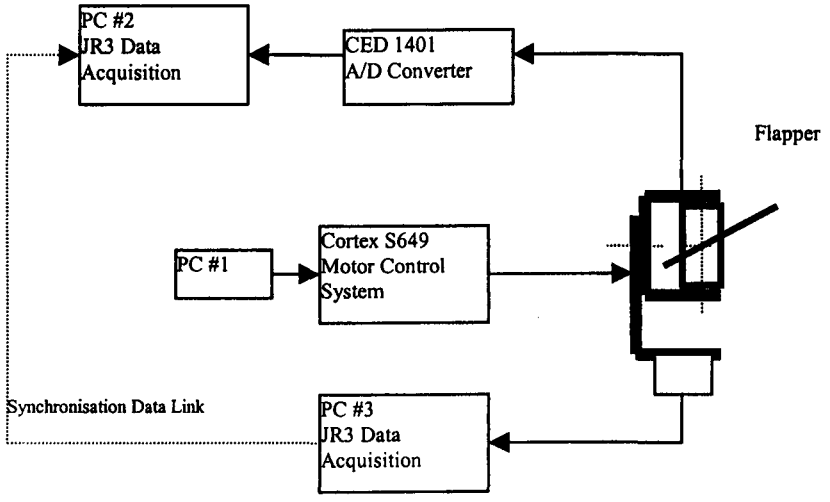

Fig 4.4 Schematic diagram of Experimental Set-up

The orientation of the wing is sensed by potentiometers (RS 173-760 2) attached directly to the rear shafts of the pitch stepper motor and to one of the flap stepper motors. These signals are recorded by PC #2 via an analogue to digital (A/D) converter (CED 1401). A The six-component balance from JR3 Inc (Model 67M25A-I40 capable of measuring forces of milli-Newton magnitude) measures the forces experienced by the flapper, which are effectively those experienced by the wing. The data from the force balance are transmitted to PC #3 via a built-in A/D converter card.

As the information on the wing orientation and the measured forces are recorded on two different computers, there is a need for synchronisation. Hardwiring the two keyboards to a single throw switch that activates both data collection programs simultaneously achieve this. A further synchronisation signal from the software that collects the force data was sent to the A/D converter at the beginning of the run. The data reduction program will search for this signal to synchronise the two sets of data.

4.2.5 TEST CONDITIONS

The actual wing of the hawk moth has a span (root to tip length) of 48.67 mm. The model wing is 4.52 times larger at 220 mm.

Originally, the tests were intended to represent the condition for the hovering hawk moth, conducted under conditions of similar Reynolds' number R_e, one possible definition of which is based on the reference wing chord as defined by Ellington [1999]:

$$R_e = \frac{\rho \overline{V}_{flap} \overline{c}}{\mu} \qquad \text{Eqn 4.3}$$

with the density (ρ) and absolute viscosity (μ) of air and the reference chord of the wing ($\overline{c}$). The mean flap velocity $\overline{V}_{flap}$ is given by

$$V_{flap} = 2n\hat{\delta}R \qquad \text{Eqn 4.4}$$

The relation between the flapping frequency of the moth and the model wing will therefore be

$$\frac{n_{moth}}{n_{mod}} = \frac{\overline{c}_{mod}}{\overline{c}_{moth}} \frac{R_{mod}}{R_{moth}} = l^2 \qquad \text{Eqn 4.5}$$

with flap frequency (n), wing span (R) and scale factor of the model (l=R_{mod}/R_{veh}). The Reynolds' number is a mean value since the mean flap velocity at wing tip and not the instantaneous value was used.

Since the model wing is 4.52 times larger than the hawk moth wing, the flapper frequency of the model needs to be 20.4 times slower. With the hawk moth flapping at 26.1 Hz, the flapper frequency shall be 1.28 Hz.

However, the tests at this frequency show that the force in the P_BX_B-axis (see section 4.3.1 for definition of the axes system) was too small to be sensed by the JR3-balance. The

alternative of using force sensors with higher resolution and lower threshold was considered but this was found to be not only a very costly option but would bring with it the problem of noise to signal ratio. More powerful motors (Mclennan 34HSX-208 and 34HSX-208E) for the flap axis have also been tested but these are also heavier. The existing structure was found to be too flexible, resulting in vibration noises. Stiffening the structure might be a solution but due to a possible delay of the schedule, this was not implemented.

Instead, the frequency was increased to 1.86 Hz using the existing flapper design and motors, a compromise between the achievable flap frequency constrained by motor torque and the measurable forces in the $P_B x_B$-axis.

The following are the parameters for the tests conducted:

flap amplitude $\hat{\delta} = \pm 50°$ mean flap angle $\overline{\delta} = 0°$

pitch amplitude $\hat{\chi} = \pm 45°$ mean pitch angle $\overline{\chi} = 0°$, 15° or 30°

pitch-flap phase $\varphi = 30°..120°$ with $\Delta\varphi = 15°$ or 30°

The Reynolds' number at 1.86 Hz (18000) compared with the 1.28 Hz is about 45% higher and exact correlation to the case of the hawk moth may not be possible. As the comparison is not the primary objective of the tests, the compromise was deemed an acceptable solution.

4.3 DATA REDUCTION PROCEDURES

4.3.1 AXES SYSTEMS

The test object was a port wing, with the axes system $P_4x_4y_4z_4$ as defined in Chapter 2.2. The origin P_4 lies along pitch axis at the root of the wing. In addition to the axes systems for the mathematical model of the vehicle and wings, the following right-handed orthogonal axes systems pertaining to the tests must be defined, see Fig 4.5:

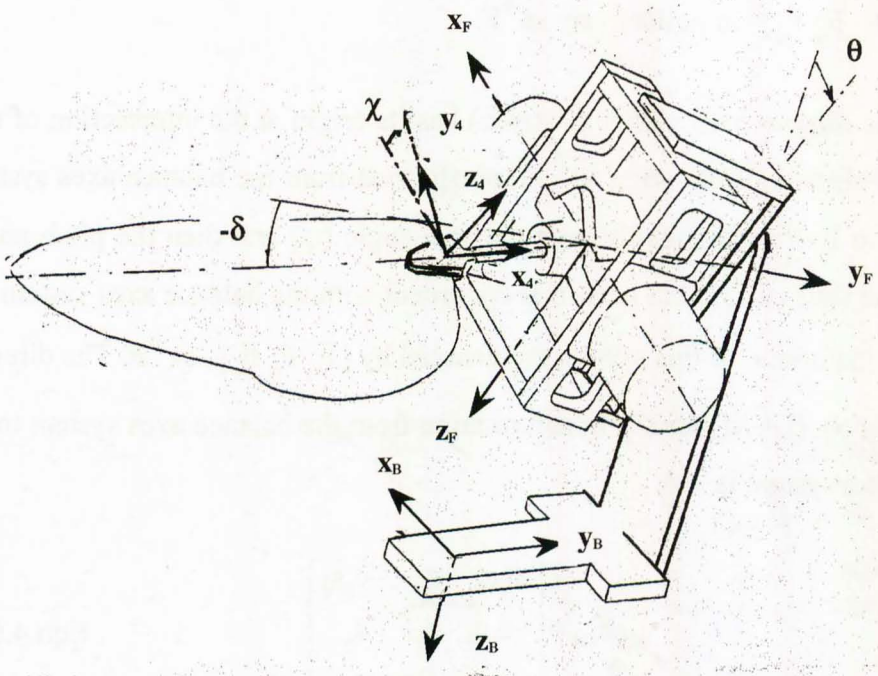

Fig 4.5 Definition of Axes Systems in Experiment

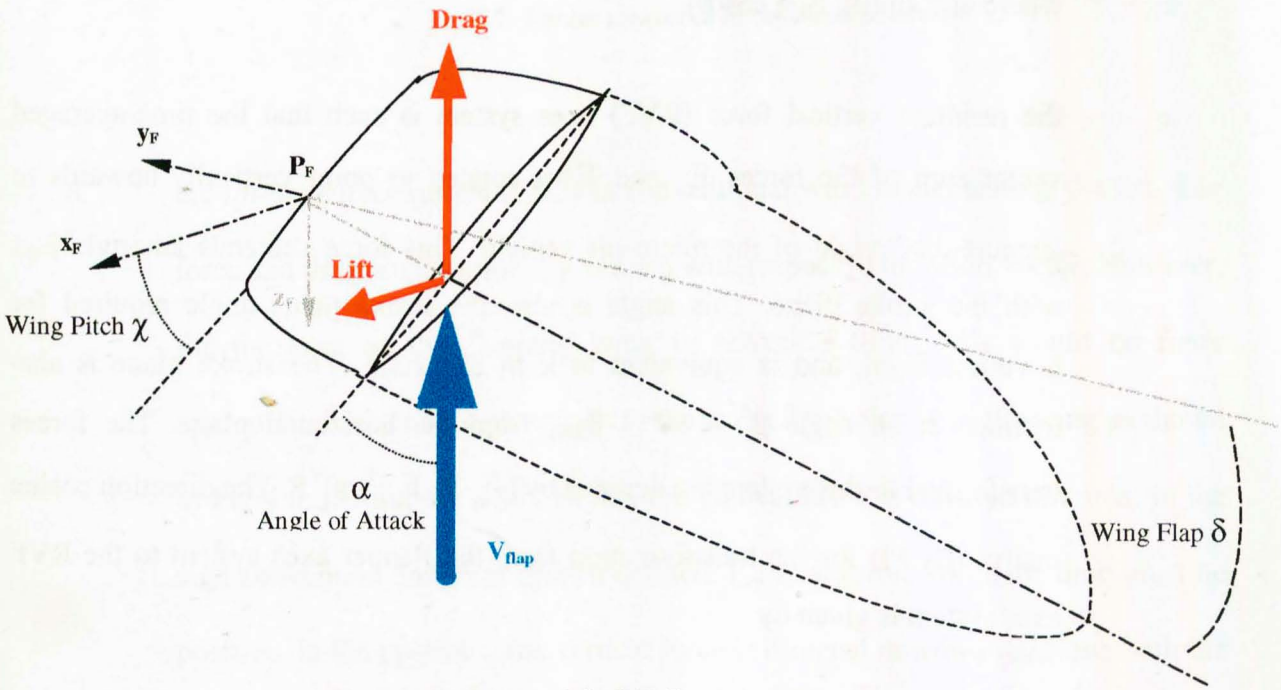

Fig 4.6 Definition of the Lift-Drag Axes System

a. the *balance axes system* ($P_BX_By_BZ_B$) has its origin at the centre of the top surface of the cylindrical balance. The axes P_BX_B and P_By_B point radially outwards while the axis points downwards. The forces measured by the balance are denoted by $[F_{X_B}\ F_{Y_B}\ F_{Z_B}]^T$ or collectively as ${}^B\mathbf{F}$.

b. the *flapper axes system* ($P_FX_Fy_FZ_F$) has its origin at the intersection of the flap and pitch axis of the wing and is transformed from the balance axes system through two Euler rotations through the yaw angle (ψ) and then the pitch angle (θ). For the tests carried out here, it is congruent with the balance axes system. The forces transformed to this system are denoted by $[F_{X_F}\ F_{Y_F}\ F_{Z_F}]^T$ or ${}^F\mathbf{F}$. The direction cosine matrix (DCM) for the transformation from the balance axes system to the flapper axes system is

$$\mathbf{C}_{FB}=\begin{bmatrix} c_\psi c_\theta & s_\psi & -c_\psi s_\theta \\ -s_\psi c_\theta & c_\psi & s_\psi \\ s_\theta & 0 & c_\theta \end{bmatrix} \qquad \text{Eqn 4.6}$$

where $s_\theta = \sin(\theta)$, $c_\theta = \cos(\theta)$.

c. the resultant vertical force (RVF) axes system is such that the time-averaged vector sum of the forces F_{X_F} and F_{Z_F} is rotated to point vertically upwards to support the weight of the micro air vehicle. This force subtends an angle β_{SPA} with the stroke plane. This angle is also the stroke plane angle required for hovering flight, and is equivalent to κ in Fig 2.1.2. The stroke plane is also inclined at an angle $\beta^* = 90^\circ - \beta_{SPA}$ from the horizontal plane. The forces transformed to this system are denoted by $[F_{X_V}\ F_{Y_V}\ F_{Z_V}]^T$ or ${}^V\mathbf{F}$. The direction cosine matrix (DCM) for the transformation from the flapper axes system to the RVF axes system is given by

$$\mathbf{C}_{VF} = \begin{bmatrix} c_{\beta_{SPA}} & 0_{,,} & s_{\beta_{SPA}} \\ 0 & 1 & 0 \\ s_{\beta_{SPA}} & 0 & -c_{\beta_{SPA}} \end{bmatrix} \qquad \text{Eqn 4.7}$$

where

$$\kappa = \quad \beta_{SPA} = \tan^{-1} \frac{F_{x_F}}{F_{z_F}} \qquad \text{Eqn 4.8}$$

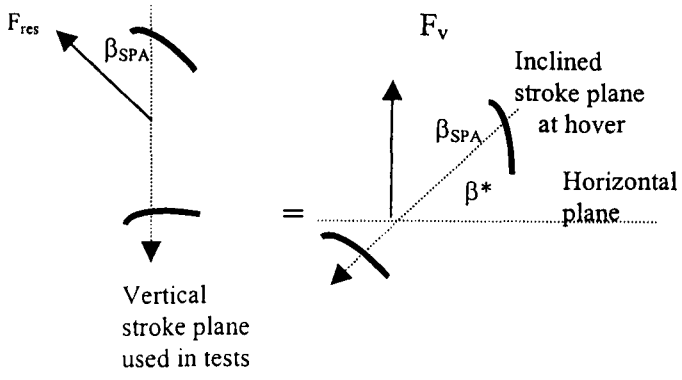

Fig 4.7 Forces measured in tests and at hover

d. the *lift-drag axes system* (LDS) In conventional wind tunnel testing, the lift, side force and drag are traditionally defined with respect to the wind vector. However, for the case of the flapping wing in hovering flight, this would be more appropriately defined with respect to the mean flap velocity of the wing as shown in Fig 4.6. During the down stroke, the vertical force is directed upwards. In the sign convention and axes system defined, F_{ZB} is negative while the drag must be positive. In the upstroke, the vertical force is directed downwards. Now, both the

drag and F_{zB} are positive. Thus, as the flap velocity changes direction from the down stroke to the upstroke, the transformation of the force vector in the balance axes system to the LDS system has to account for this through a factor k_{dir}, which is 1 for the upstroke and –1 for the down stroke.

$$^{L}\mathbf{F}_{aero} = [L\ S\ D]^{T} = [\ F_{xB}\ -F_{yB}\ k_{dir}F_{xB}] \qquad \text{Eqn 4.9}$$

In the above equation, $\mathbf{F}_{aero}$ refers to the aerodynamic force vector, while L, S and D denote the lift, side force and drag.

In the tests, the orientation angles of the flapping mechanism are all set to 0°. The DCM to transform from the balance axes to the wing axes system is thus given by

$$\mathbf{C}_{B4} = \begin{bmatrix} 0 & c_{\chi} & -s_{\chi} \\ c_{\delta} & s_{\chi}s_{\delta} & c_{\chi}s_{\delta} \\ s_{\delta} & -s_{\chi}c_{\delta} & -c_{\chi}c_{\delta} \end{bmatrix} \qquad \text{Eqn 4.10}$$

where δ and χ are the wing flap and pitch angles respectively and where $s_{\delta}=\sin(\delta)$, $c_{\delta}=\cos(\delta)$, etc.

4.3.2 DATA REDUCTION PROCESS

In dynamic wind tunnel tests, the measured forces are of gravitational, inertial and aerodynamic nature. In order to extract pure aerodynamic forces from these tests, the gravitational and inertial components must be known. In rotational tests for fixed wing aircraft, the gravitational forces in the rotating axes system of the vehicle body are cyclical and are removed by integrating and averaging the signal. Inertial components are assumed to be constant wind-on and wind-off for the same rotational speed so that the aerodynamic component is the difference between wind-on and wind-off measurements [O'Leary 1984].

For the current experiment, the gravitational component acting on the balance in its non-rotating axes system is constant and it can be zeroed to eliminate the gravity forces. The wind-off measurement for the flapping wing contains aerodynamic components and cannot be extracted in the same manner as mentioned above. It was intended that the aerodynamic components be obtained from the difference of two sets of tests, one with the wing attached and another with a mass replacement. However, while the total force (sum of inertial and aerodynamic components) at 1.86 Hz exceeded the threshold of the JR3, it was found that the inertial component alone in the direction of the x_B-axis even at this higher frequency was still too low to be sensed accurately. Hence, the aerodynamic component was then obtained by subtracting the calculated inertial forces from the experimental forces. It is therefore necessary to verify the mathematical model used to compute the inertial forces. This is discussed in the next section.

Once the aerodynamic components are determined, they can then be transformed to any co-ordinate system as required. The aerodynamic force coefficients can also be computed.

In order to have confidence in the measurements taken during the tests, at least 3 sets of readings were taken for every test point. The force time histories were compared and if there was a large variation, the test was repeated. Measurements from at least 2 readings were used to obtain the average instantaneous force value.

4.3.2.1 Calibration of Force Sensor

The JR3 force and moment sensor is a six-component sensor. Only the force channels are of interest in the experiments in order to reduce the complexity of the experiment. The forces are sensed by pre-calibrated strain gauges and converted to digital format by the built-in D/A conversion card.

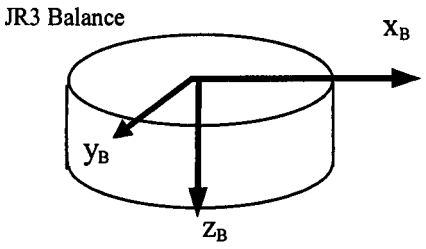

Fig 4.8 Axes System of JR3 Balance

The sensor has a threshold of 5 grams. The sensitivity of each of the three force axes is identical. Hence, it was necessary to check the calibration and sensitivity of just one of the axes by placing calibrated lead weights on the P_BZ_B axis. By plotting the output of the sensor against the calibration masses as shown in Fig 4.9 below, the calibration equation and its regression can be found. Although a linear trend was observed, the accuracy based on the measurements of about 10% does not meet the standard requirements. However, due to the constraints imposed on the project, this level of accuracy is acknowledged and the uncertainty of the aerodynamic data must be taken into account later in the simulation.

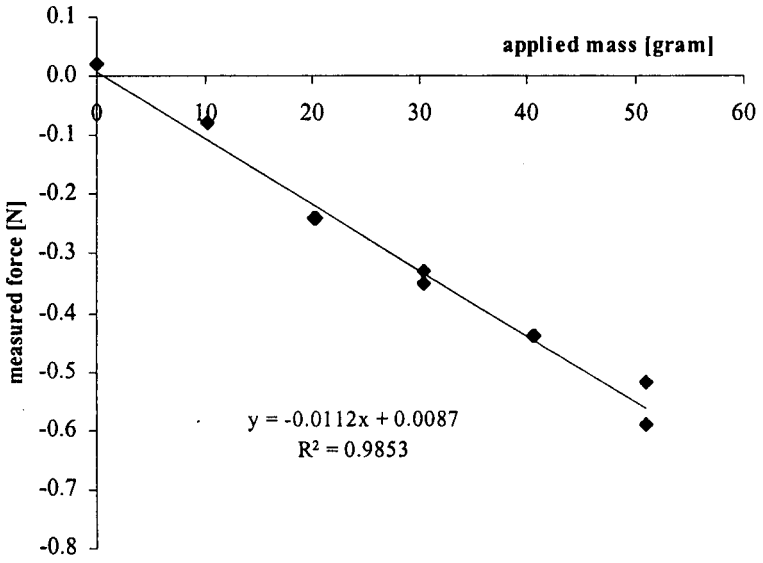

Fig 4.9 Calibration of P_BZ_B-axis of JR3

4.3.2.2 Reduction To Cyclic Force Variation

Each set of readings was long enough to record about 10 cycles on the average (6 seconds). The sampling frequency is constant at 500Hz (sampling time of 0.002 second).

A data reduction package FDDR (Flapper Dynamic Data Reduction) was written in MATLAB. The functions of the package are as follows:

- The files containing the wing orientation and forces are loaded.
- The recording (both wing orientation and forces) are then filtered with a 50 point averaging non-causal filter.
- Dropouts are removed from the filtered data.
- The periodic time of the flap cycle is then calculated from the wing orientation time history.
- The start and end of each cycle are then identified for the force data, which are synchronised with the wing orientation data through the synchronisation signal recorded in both files.
- The lag introduced by the filter in the JR3 data acquisition card is also taken into account.
- The periodical forces are then averaged and represented by a Fourier series with n coefficients:

$$F_k(\hat{t}) = a_{k0} + \sum_{j=1}^{n} \{a_{kj}\cos(2\pi j\hat{t}) + b_{kj}\sin(2\pi j\hat{t})\} \qquad \text{Eqn 4.11}$$

In the above equation for the force in the direction of the axis k (where where $k = x_i$, y_i or z_i) of the I-th axes system and n is the number of harmonics considered. The time history was found to be adequately represented with n = 5. Here, $\hat{t}$ has a value between 0 and 1.

4.3.2.3 Inertial Forces

The mathematical model developed in Chapter 2 can be used to compute the inertial forces if the relevant modifications are made. R_1 would represent the structure of the mechanical flapper, R_2 can be removed and R_4 would represent the sting, adapter and test wing assembly. By doing so, the equations of motion (Eqns 2.35 to 2.39) can be simplified to

$$-\mathbf{C}_{14}\mathbf{c}_4^{\times}\dot{\boldsymbol{\omega}}_{p4} = \mathbf{f}_{grav} + \mathbf{C}_{14}\left(\boldsymbol{\omega}_{p4}^{\times}\mathbf{c}_4\right)^{\times}\boldsymbol{\omega}_{p4} \qquad \text{Eqn 4.12}$$

where $\mathbf{c}_4^{\times}$ is the skew symmetric 3×3 matrix of the first moment of inertia of the wing assembly $\mathbf{c}_4$. The relative angular velocity of the wing assembly is $\boldsymbol{\omega}_{p4}$. The gravity force vector f_{grav} can be zeroed and eliminated by the force balance, leaving

$$\mathbf{C}_{14}\mathbf{c}_4^{\times}\dot{\boldsymbol{\omega}}_{p4} + \mathbf{C}_{14}\left(\boldsymbol{\omega}_{p4}^{\times}\mathbf{c}_4\right)^{\times}\boldsymbol{\omega}_{p4} = 0 \qquad \text{Eqn 4.13}$$

The relation between the flap and pitch degrees of freedom of the flapper and the vector $\boldsymbol{\omega}_{p4}$ can be written as

$$\boldsymbol{\omega}_{p4} = \mathbf{C}_{4E}\begin{bmatrix}\dot{\chi}\\ \dot{\delta}\\ 0\end{bmatrix} = \mathbf{C}_{4E}\dot{\Phi} \qquad \text{Eqn 4.14}$$

where $\Phi = [\chi \quad \delta \quad 0]^T$ and $\mathbf{C}_{4E}$ is obtained by consolidating Eqn 2.12 and 2.13.

$$\mathbf{C}_{4E} = \begin{bmatrix}1 & 0 & -s_\delta\\ 0 & c_\chi & c_\delta s_\chi\\ 0 & -s_\chi & c_\delta c_\chi\end{bmatrix} \qquad \text{Eqn 4.15}$$

The angular acceleration of the wing (or in this case, the wing attachment or sting) is given by differentiating Eqn 4.14

$$\dot{\boldsymbol{\omega}}_{p4} = \mathbf{C}_{4E}\ddot{\Phi} + \dot{\mathbf{C}}_{4E}\dot{\Phi} = \mathbf{C}_{4E}\ddot{\Phi} \qquad \text{Eqn 4.16}$$

since it can be shown also that

$$\dot{\mathbf{C}}_{4E}\dot{\Phi} = \boldsymbol{\omega}^{x}\mathbf{C}_{4E}\dot{\Phi} = \boldsymbol{\omega}^{x}\boldsymbol{\omega} = 0 \qquad \text{Eqn 4.17}$$

Finally, $\mathbf{c}_4$ is given by

$$\mathbf{c}_4 = m_4\mathbf{d}_4 \qquad \text{Eqn 4.18}$$

where m_4 is the mass of the flapping arm including the wing and $\mathbf{d}_4$ is the vector from the origin of the wing axes system to the CG of the flapping arm including the wing.

The orientation of the wing (flap and pitch angles, δ and χ) is given by Eqns 4.1 and 4.2. The rates and accelerations are obtained by differentiating them analytically.

Fig 4.10 shows the comparison of the experimentally measured forces (dotted line) experienced by the flapper with a lead mass attached to the adaptor such that the CG of the flapping arm lies 1.5mm off the pitch axis, and 1mm from the flap axis or

$$\mathbf{d}_4 = [-1.5e^{-3}\ -1e^{-3}\ \ 0]^T \qquad \text{Eqn 4.19}$$

with dimensions given in S.I. units, i.e. in metres.

The mass of the flapping arm is 0.396 kg. The inertial forces, calculated using Eqn 4.13 are shown in full lines. It is seen that there is an extremely good match between the mathematical model and the experimental data, thus verifying not only the mathematical model but also the data reduction methodology.

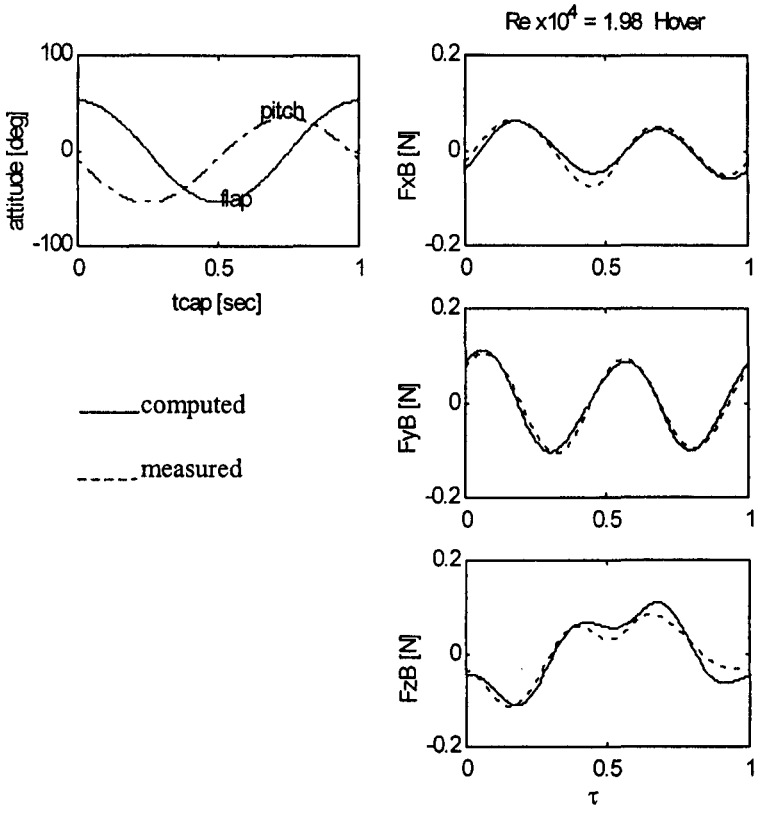

Fig 4.10 Comparison of measured and computed inertial forces

4.3.2.4 Extraction Of Aerodynamic Forces

The difference between the experimental data with the wing and the calculated inertial forces is then obtained using the respective Fourier coefficients.

$$\Delta F_k(\hat{t}) = F_k(\hat{t})_{wing} - F_k(\hat{t})_{calc} \qquad \text{Eqn 4.20}$$

The time dependent aerodynamic coefficient in the k-direction in *i*-th axis system is given by

$${}^{i}C_k(\hat{t}) = \frac{\Delta F_k(\hat{t})}{\frac{1}{2}\rho(\overline{V}_{flap})^2 S_{wing}} \qquad \text{Eqn 4.21}$$

The aerodynamic coefficients in another axes system j is given by

$$^{j}[C_x \; C_y \; C_z]^T = \mathbf{C_{ji}} \; ^{i}[C_x \; C_y \; C_z]^T \qquad \text{Eqn 4.22}$$

where the DCMs $[\mathbf{C}_{ji}]$ are already given in earlier in Chapter 4.3.1.

4.3.2.5 Estimation of Aerodynamic Power

The instantaneous power to overcome the aerodynamic resistance is given by the product of the instantaneous wing drag and instantaneous flap velocity. The total power required is the work done per cycle (integral sum of instantaneous power) divided by the period T of the cycle and given as

$$P_{aero} = \frac{W_{cycle}}{T} = \frac{\int_{\hat{t}} D_{wing}(\hat{t}) V_{flap}(\hat{t}) d\hat{t}}{N d\hat{t}} = \frac{0.3R \sum_{\hat{t}=0}^{\hat{t}=1} D_{wing}(\hat{t}) \left|\dot{\delta}(\hat{t})\right|}{N} \qquad \text{Eqn 4.23}$$

assuming that the aerodynamic force acts at 30% wingspan, i.e. 0.3R. This is close to the centre of area of a triangle, to which the wing plan form is approximated. The wing drag (D_{wing}) is obtained from Eqn 4.9.

4.3.3 RESULTS

The experiments were designed to investigate the effects of

(a) the phase φ between the pitch and flap degrees of freedom and

(b) the mean pitch angle on force magnitude and direction as well as on aerodynamic power requirement.

By varying the phase φ, the pitch attitude at a given instantaneous flap angle is changed. This will thus modify the angle of attack experienced by the wing. By so doing, it is believed that the aerodynamic force variation within the cycle may be altered, making force magnitude and direction modulation possible.

The motivation for variation of mean pitch is best seen by comparison of Fig 4.11(a) and (b), which shows the schematic view of the experiment in the $P_FX_FZ_F$-plane. Each line represents the wing chord at an instant in time. For ease of illustration, the wing chord is advanced with time. Hence, although the stroke has a V-shape, they actually collapse on a vertical stroke plane, perpendicular to the page.

At zero mean pitch as shown in Fig 4.11(a), the angle of attack of the wing is more or less symmetrical during both up and down strokes. As such, the forces in the flapper vertical axis will more or less cancel out and the time-averaged resultant along this axis will be small. The main component used to support the vehicle weight would be the force along the horizontal flapper axis P_FX_F. Although the vertical forces are not contributing to weight support, energy has to be expended to overcome them as they manifest themselves as wing drag. It will be shown later that this is the reason for higher aerodynamic power per unit lift generated.

On the other hand, by having a non-zero mean pitch angle as shown in Fig 4.11(b), the angle of attack at the upstroke is smaller than at down stroke. Hence, the aerodynamic force in the vertical flapper axis during the upstroke will be smaller in magnitude than that of the down stroke. The resultant over the cycle would therefore be directed upwards. In this case, the force along the vertical flapper axis P_FZ_F could contribute significantly to the total force for weight support.

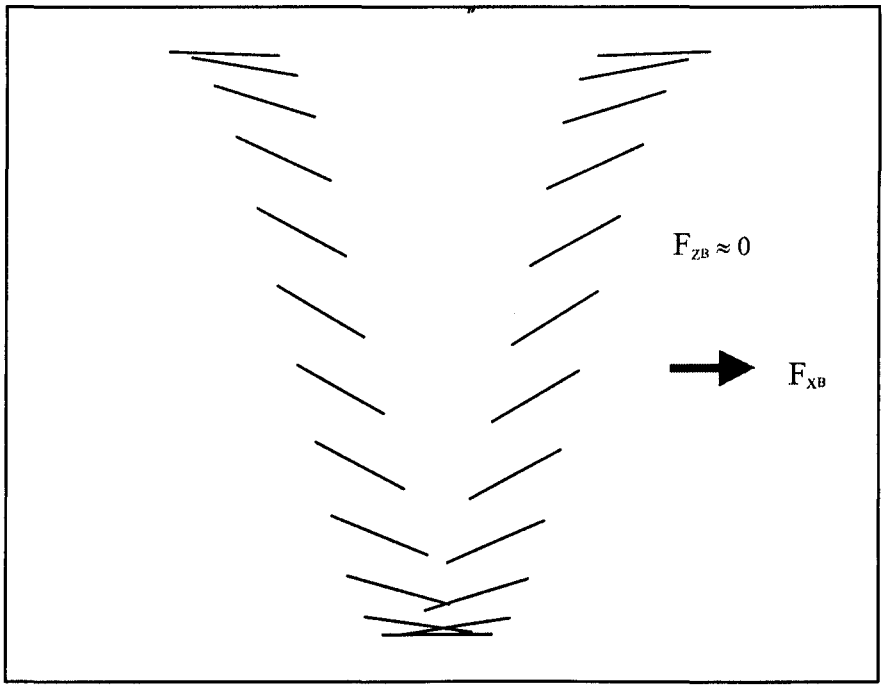

Fig 4.11(a) **Wing Attitude at $\varphi = 90°$, $\bar{\chi} = 0°$.**

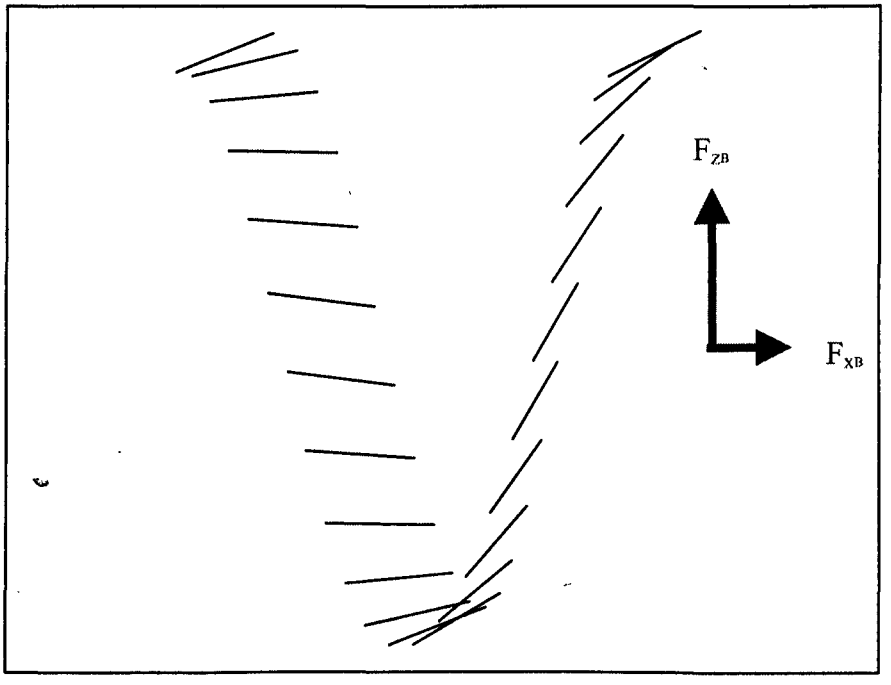

Fig 4.11(b) **Wing Attitude at $\varphi = 90°$, $\bar{\chi} = 30°$.**

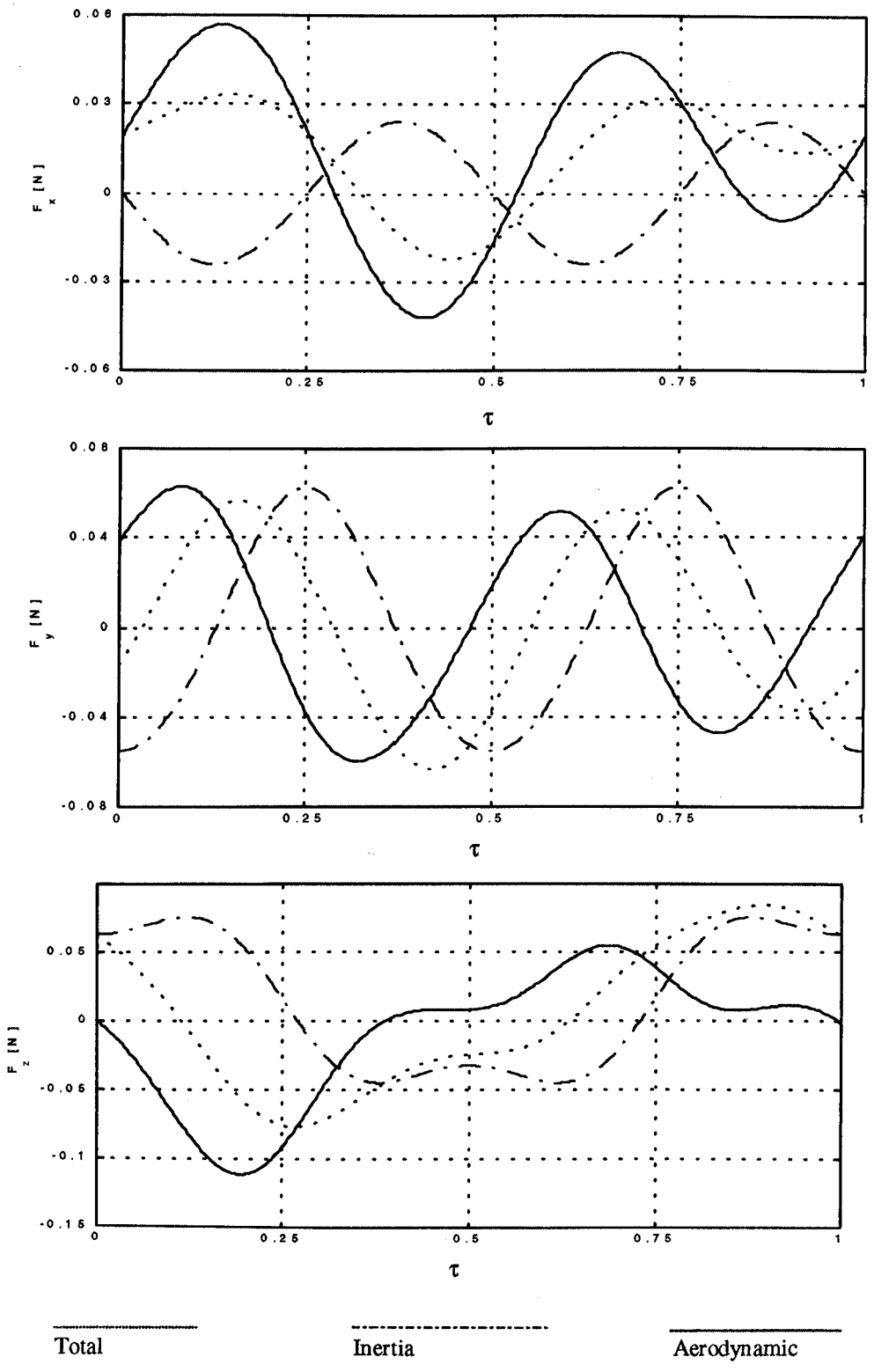

Fig 4.12 Forces at f = 1.86 Hz φ = 90°, $\hat{\chi}$ = 90°, $\overline{\chi}$ = 0°, $\hat{\delta}$ = 100° and $\overline{\delta}$ = 0°.

4.3.3.1 Effects of Phase Variation at Zero Mean Pitch

Data was first collected for pitch amplitude of 90° (i.e. ±45°) and flap amplitude of 100° (i.e. ±50°). The mean pitch and flap angles were both 0° and the flapping frequency was 1.86 Hz. The phase φ between the flap and pitch angles was varied between 30° and 120° at steps of 30°.

Fig 4.12 shows the results of the experiment in the balance axes system for the case φ=90°. It is typical for all other values of φ, the results of which are reproduced in Appendix E.

The period of the flap cycle has been non-dimensionalised and is represented by τ, which has a value between 0 and 1 with 0.5 representing the end of the down stroke and the begin of the upstroke.

4.3.3.1.1 Force Magnitude

It is seen in Fig 4.12 that a negative F_{zB} peak occurs at $\tau = 0.25$ (the middle of the down stroke) and close to $\tau = 0.75$ (the middle of the upstroke). These correspond to maximum flap velocity and hence maximum dynamic pressure. Consequently, the aerodynamic force is also at maximum as expected.

The side force F_{yB} is the projection of the resultant force on the horizontal axis and its magnitude and direction of depends on both the magnitude of the resultant force as well as the flap angle of the wing. It can be seen that the magnitude is zero at $\tau \approx 0.25$ and $\tau \approx 0.75$, during which the flap angle $\delta = 0°$. F_{yB} is also expected to be zero when the wing is at the end of stroke where the flap velocity is zero. The time history shows that F_{yB} has non-zero values at the end of the strokes ($\tau = 0$, 0.5 and 1). Although the accuracy of the measurement may be one of the causes, the experiments of Dickinson [1999, 2001] seem to suggest that at the end of stroke rotation, the starting vortex remained above the upper

surface of the wing, which may be the cause of a non-zero force, as illustrated below in Fig 4.13. This generated a low pressure at the upper surface and thus an aerodynamic force although the wing is not in translational motion.

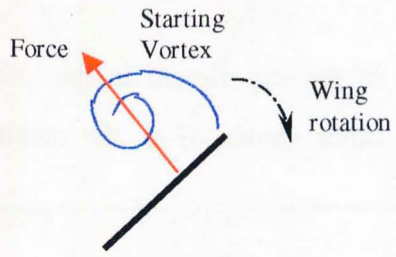

Fig 4.13 Force at End-of-Stroke Rotation

The force F_{XB} is the wing lift. As the wing flaps through the cycle, its angle of attack is positive. Due to the construction of the flapper and to avoid mechanical interference between the wing and the flapper, the pitch angle of the wing has to be limited to ±45° in the experiments. This results in angles of attack of more than 55°, which is above the stall angle of a typical flat plate. The lift generated is not expected to be high and this constitutes one of the main problems in the measurement of this component. The marginal performance of the force sensor in this direction may make the measurement questionable.

The top chart of Fig 4.12 shows a negative force of up to 0.03N was evident for τ between 0.375 and 0.6. Although negative force magnitude is not expected since the angle of attack remained positive throughout the flap cycle, this phenomenon was also evident if the CFD results from Liu and Kawachi [1999] were transformed to the flapper axes system used here. Fig 4.14 shows that the coefficient C_{xF} has a negative value close to the end of upstroke and at the end of down stroke.

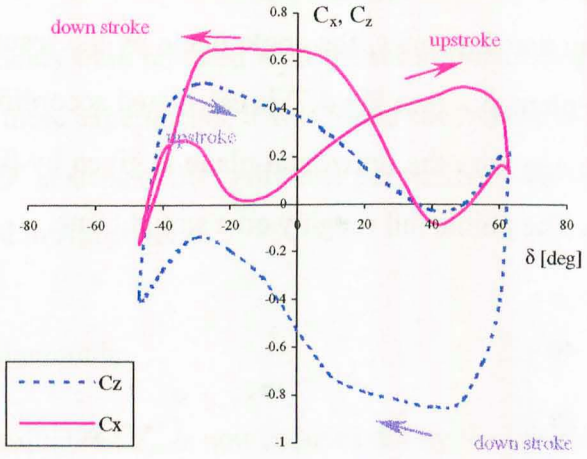

Fig 4.14 Force Coefficients obtained from CFD models of hovering *Manduca sexta* wing [Liu and Kawachi, 1999]

Notwithstanding the doubt cast upon the accuracy of the measurement of F_{XB}, the time-averaged resultant force in the RVF axes system was calculated for the series of experiments and plotted against φ in Fig 4.15. It can be seen that the vertical force coefficient C_v varies linearly with the phase angle for the points tested.

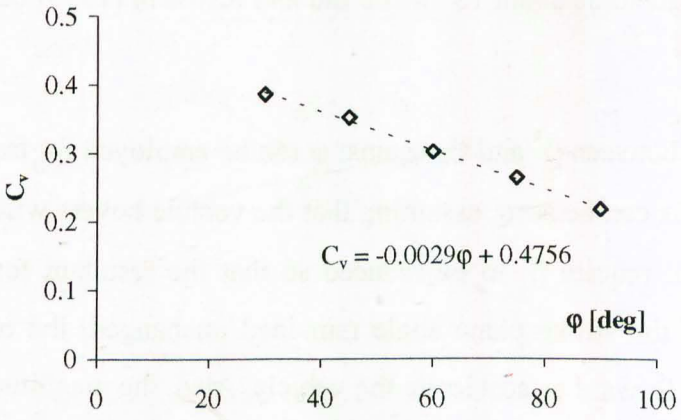

Fig 4.15 Variation of Vertical Force Coefficient C_v with Flap-Pitch Phase φ

4.3.3.1.2 Force Direction

Assuming that the measurements of F_{XB} were accurate and that the peculiarities can be explained by the wing aerodynamics, the angle made by the resultant force in the $P_BX_BZ_B$ plane with the stroke plane β_{SPA} (see Fig 4.7) is calculated according to Eqn 4.8. The angle made by the stroke plane with the horizontal plane is given by $\beta^* = 90° - \beta_{SPA}$ is plotted against φ in Fig 4.16. The points fall roughly on a straight line.

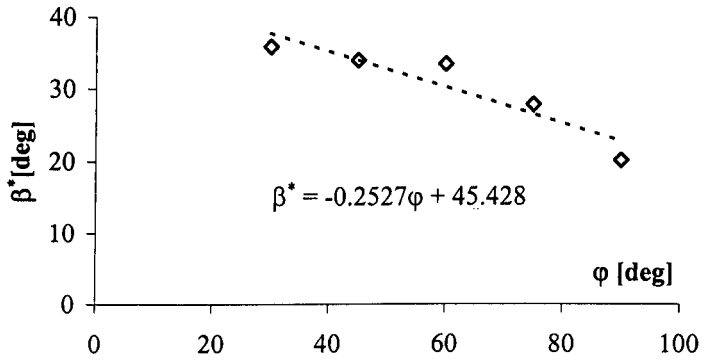

Fig 4.16 Variation of Stroke Plane Attitude β^* with Pitch-Flap Phase φ

It is appropriate to note that the present results correspond closest to the hawk moth case at $\varphi = 90°$ (1.57 rad). It is seen that β^* was found here to be 20°. Willmott [1997] estimated the angle to be about 15° while Liu and Kawachi [1999] calculated the angle β^* to be about 23.6°.

The linear trend between β^* and C_V against φ can be employed for transition to low speed forward flight. As can be seen, assuming that the vehicle hovers with $\varphi = 60°$, a increase in the phase will require β^* to be reduced so that the resultant force remains vertical. Alternatively, if the stroke plane angle remained unchanged, the resultant force would then be directed forward to accelerate the vehicle. Also, the magnitude is also reduced. A combination of the stroke plane angle tilt and phase change can thus be found to maintain a level transition to forward flight.

4.3.3.2 Effects of Phase Variation at Non-zero Mean Pitch

The foregoing experiments were repeated with the mean pitch being set first at 15° and then again at 30°. For these experiments, it was found convenient to conduct the tests for ϕ between 30° and 120° at steps of 30°. All other parameters were unchanged. The force time histories are found in Appendix E.

4.3.3.2.1 Force Magnitude

The instantaneous magnitude of F_{ZB} is now reduced during the upstroke, especially for the cases when φ = 60° and φ = 90° due to the 'feathering' of the wing, thus reducing the angle of attack and the wing drag. Consequently, there is a resultant time-averaged force directed upwards. The wing is thus generating a weight supporting force through the drag rather than through the lift as in the case of the experiments with zero mean pitch. Fig 4.18 shows the variation of the magnitude of the time-averaged resultant force F_v with the phase φ.

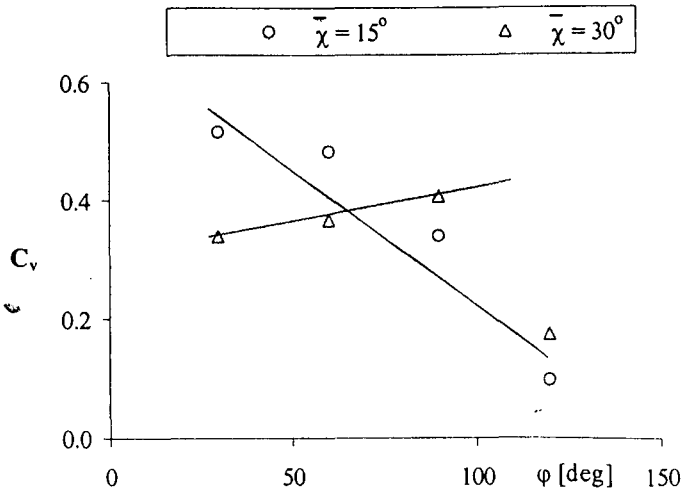

Fig 4.18 Variation of Vertical Force Coefficient C_v with Flap-Pitch Phase φ

4.3.3.1.3 Aerodynamic Power

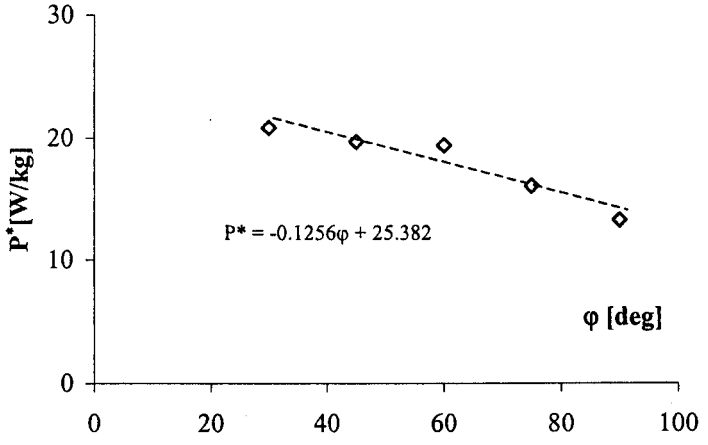

Fig 4.17 Variation of Specific Power P^* With Pitch-Flap Phase φ

The aerodynamic power required to overcome the drag of the wing during the flap cycle can be calculated using Eqn 4.23. Dividing by F_v, the specific power P^* or power per unit force can be obtained. This is plotted in Fig 4.17. The chart shows that the specific power follows a linear trend for φ between 30° and 90°.

The above chart shows a surprising behaviour of the wing in that the increase in phase results in an increase in the force coefficient for mean pitch angle of 30° but results in a decrease when the mean pitch angle was 15°. If only F_{ZB} is plotted against φ as shown in Fig 4.19, and ignoring the values at φ = 120°, then a consistent decrease in the magnitude is seen.

This could be another indication of poor accuracy of the measurement of F_{XB} and the confidence for the F_{ZB} measurement, since with increasing φ, the feathering during the upstroke is significant giving rise to smaller downward force and a higher time-averaged upward force.

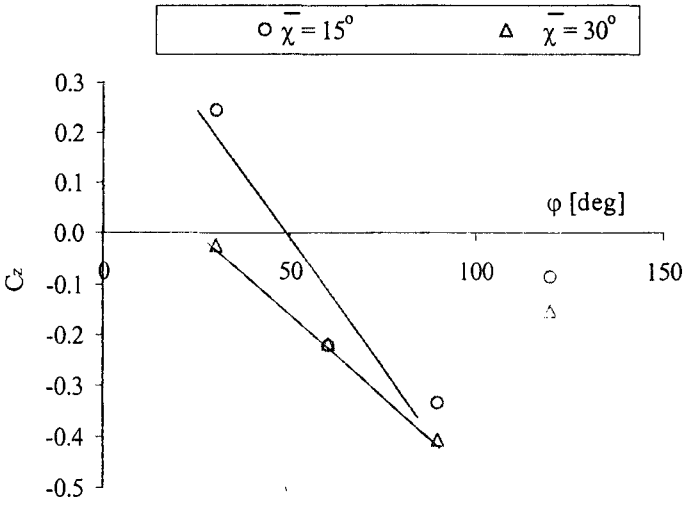

Fig 4.19 Variation of Force Coefficient C_z with Flap-Pitch Phase φ

4.3.3.2.2 Force Direction

The angle β^* is plotted against φ in Fig 4.20 for both the mean pitch angles of 15° and 30°. A linear trend, similar to that seen in the zero mean pitch cases, can be observed. Again, the stroke plane tilt and phase change combination may possibly be employed for vehicle control.

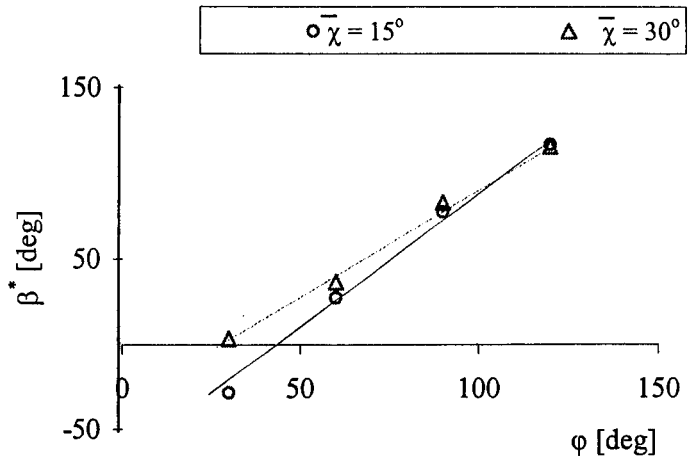

Fig 4.20 Variation of Stroke Plane Attitude β^* with Pitch-Flap Phase φ

4.3.3.2.3 Aerodynamic Power

The specific aerodynamic power is plotted against φ in Fig 4.21 for mean pitch angles values of 15° and 30°. The data points at φ = 120°, which consistently caused a drastic increase in the specific power requirement, were ignored.

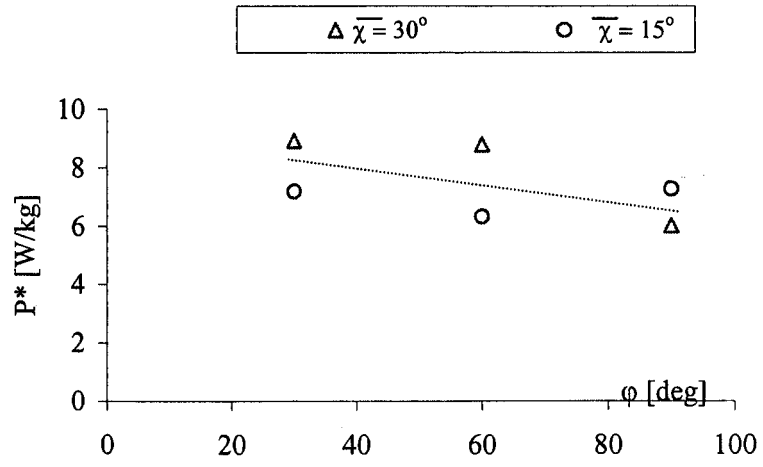

Fig 4.21 Variation of Specific Power P^* With Pitch-Flap Phase φ

It can be seen that P^* is lower in the cases where the mean pitch angles are non-zero. This is probably due to two reasons. Firstly, the 'feathered' wing generated less drag during the upstroke and the power required to overcome the flapping motion is hence reduced. Secondly, comparing the cases at $\varphi = 60°$, the resultant force coefficient C_v at non-zero mean pitch flapping was between 0.37 and 0.48 while that at zero mean pitch was found to be about 0.3. Since $P^* = P/F_v$, it follows that the specific power is lower for non-zero mean pitch flapping.

It appears that using wing drag as the main component to generate weight-supporting force would be a more efficient method. However, this finding is due to the fact that the angle of attack of the wing was consistently above 55° due to the design of the flapper. At this angle of attack, the wing would probably have seen separated flow and is inefficient in generating lift.

4.4 DISCUSSION OF RESULTS

The target weight of the micro air vehicle was required by DARPA to be around 50 grams. Since most insects weigh no more than a few grams and have flapping frequencies that are inversely proportional to their size and weight, even an exact reproduction of the mechanical insect may fall short of the target take-off weight.

Calculations by Ellington [1999] suggests that a 50-gram vehicle would require a flapping frequency of about 20 Hz if the root to tip dimension of each wing were to be 150 mm. Although the flap frequency lies around that of the hawk moth, the dimension of the wing and thus the Reynolds' number does not correspond to that experienced by the hawk moth wing.

Conversely, a vehicle modelled after the hawk moth with wing dimension of 48mm would require a flapping frequency of about 100 Hz to sustain the weight of 50 grams. This illustration shows that a simple mimicry of the design parameters of an insect would probably be unsuccessful in meeting the lift requirement. The wings of birds may be better suited to meet this lift requirement because most birds are heavier. Small birds like the European starling weighing about 80 grams and have a tip-to-tip wingspan of 39 cm. The flapping frequency is a couple of Hz.

The design of the flapping mechanism was aimed at achieving a flapping frequency of about 3 Hz. However, the uncertainty of component weights and motor performance led to the target frequency not being achieved. The first prototype achieved only 1.4 Hz with the model wing weighing 6 grams and the sting measuring 40 mm long from the face of the bearing. The forces in the P_BX_B axis cannot be sensibly measured with the JR3 force sensor. In order to achieve a better measurement, a few alternatives were explored or attempted. These included higher resolution sensors, increasing the flap frequency by a reduction in the moment of inertia as well as replacing the existing motors with more powerful ones.

The higher resolution sensors were costly and because of the resolution, a more stable platform for the flapper would be required. In view of the high investment cost, the procurement of such a system was not approved.

The cheaper option of reducing the inertia and increasing the driving torque of the motors was attempted. Excessive material in the bearing housing for the flapper was removed, the length of the sting was shortened and the pitch axis motor was replaced. Larger motors for the flap axis were also installed. The maximum frequency of 2.8 Hz was achieved.

However, the measurement was found to be corrupted by vibration of the support that was designed for the smaller motors. A strengthening of the support to cater for the increased motor weights would be required. However, due to the lack of time in the project and the restructuring of the laboratories, this option was not followed up.

Finally, a compromise of running the experiments with the highest possible flapping frequency of 1.86 Hz with the original flap motors without excessive vibration was accepted. The force sensor for measurement of forces in the P_BX_B axis was found to be marginal in most of the cases.

There is undoubtedly a difficulty in obtaining data of high accuracy in flapping tests under the present experimental conditions of low flapping frequencies and where the inertial forces are of the same magnitude as the aerodynamic forces.

The design of the flapping mechanism and the need to reduce the flap inertia in order to raise the flap frequency has resulted in the length of the sting being minimised. This has the consequence of limited amplitude in pitch for the wing. As was explained earlier, the angle of attack during the tests was thus above 45° throughout the flap cycle. This would mean that the lift would be generally very low. The sensitivity of the force balance is being compromised and could at best be marginal.

In addition, the aerodynamic force is obtained by subtraction of the calculated inertial forces from the measured forces with the model wing. It was found that although great care was taken to ensure that measurements are taken correctly, the force time histories, for some unknown reasons, seemed to be shifted vertically at times. Any shift would result in the magnitude of the forces be wrongly computed. This source of error was minimised by collecting data over several runs and comparing the forces at each run. Data sets with erratic shifts were discarded.

The experiments described in paragraph 4.3.3.1 have also shown that negative lift was generated near the end of the down stroke even though the angle of attack remained positive. Although this phenomenon was also observed if the data from the CFD model of Liu and Kawachi [1999] were transformed back to the appropriate axes system, it would not have changed the fact that the resolution of the force sensor is, at best, marginal in the lift axis under the test conditions.

On the other hand, the wing drag measurement was found to be consistent with expectation because the forces measured in this axis were larger. Because the aerodynamic power requirement is dependent on the drag and not the lift, its accuracy is also considered satisfactory.

CHAPTER 5

SIMULATION RESULTS WITH AERODYNAMICS

5.1 WING AERODYNAMIC MODEL

The aerodynamic data obtained from the experiments described in the previous chapter can be reproduced using Fourier series. It was found that the forces are well represented with the first five Fourier coefficients of each series. The force coefficients in the *k*-th direction and the *i*-th axis system are then given by

$$ {}^{i}C_k(\hat{t}) = \frac{\Delta F_k(\hat{t})}{\frac{1}{2}\rho(\overline{V}_{flap})^2 S_{wing}} \qquad \text{Eqn 5.1} $$

with the nominal flapping velocity given by V_{flap} in Eqn 4.4. In terms of the Fourier series this becomes

$$ F_k(\hat{t}) = a_{k0} + \sum_{j=1}^{n} \left\{ a_{kj}\cos(2\pi j\hat{t}) + b_{kj}\sin(2\pi j\hat{t}) \right\} \qquad \text{Eqn 5.2} $$

	i =	0	1	2	3	4	5
C_x	a_i	0.2052	-0.2659	-0.1769	-0.0138	0.0062	-0.0009
	b_i		0.08860	0.5679	-0.0008	-0.0046	0.0018
C_y	a_i	-0.0191	-0.1629	0.5111	-0.0066	-0.06923	0.0044
	b_i		0.0627	0.6813	0.0195	-0.0102	0.0065
C_z	a_i	0.0762	-0.3536	-0.2238	0.3068	0.0998	-0.0270
	b_i		-0.8769	0.1933	0.1194	0.0146	-0.0020

Table 5.1 Fourier Coefficients for Aerodynamic Force Coefficients for $\bar{\chi} = 0°$, $\varphi = 90°$

The above results show that the Fourier coefficients of the fourth and higher harmonics are generally an order of magnitude smaller than the first three harmonics.

The time-dependent aerodynamic force coefficients for the aerodynamic model ($\bar{\chi} = 0°$, $\varphi = 90°$) used in the simulation are given in the frame of reference $P_F x_F y_F z_F$ of the flapping mechanism, see Fig 4.5. They are listed in Table 5.1. The coefficients can then be converted to the fuselage frame of reference by the following transformation

$$^{I}C_k(\tau) = \mathbf{C}_{IF}\, ^{F}C_k(\tau) \qquad \text{Eqn 5.3}$$

where $\mathbf{C}_{IFp}$ for the port wing is given by

$$C_{IFp} = \begin{bmatrix} c_{\kappa_p} & s_{\kappa_p} s_{\bar{\delta}_p} & s_{\kappa_p} c_{\bar{\delta}_p} \\ 0 & c_{\bar{\delta}_p} & -s_{\bar{\delta}_p} \\ -s_{\kappa_p} & c_{\kappa_p} s_{\bar{\delta}_p} & c_{\kappa_p} c_{\bar{\delta}_p} \end{bmatrix} \qquad \text{Eqn 5.4}$$

and $\mathbf{C}_{IFs}$ for the starboard wing is given by

$$C_{IFs} = \begin{bmatrix} c_{\kappa_s} & -s_{\kappa_s} s_{\bar{\delta}_s} & s_{\kappa_s} c_{\bar{\delta}_s} \\ 0 & c_{\bar{\delta}_s} & s_{\bar{\delta}_s} \\ -s_{\kappa_s} & -c_{\kappa_s} s_{\bar{\delta}_s} & c_{\kappa_s} c_{\bar{\delta}_s} \end{bmatrix} \qquad \text{Eqn 5.5}$$

As the experimental data are given for the port wing, they can also be used for the starboard wing if the following corrections are made

$$\begin{aligned} ^{F}C_{xs} &= {}^{F}C_{xp} \\ ^{F}C_{ys} &= -\,{}^{F}C_{yp} \\ ^{F}C_{zs} &= {}^{F}C_{zp} \end{aligned} \qquad \text{Eqn 5.6}$$

Since no data about the aerodynamic moment is available, it is assumed in the first instance that the resultant aerodynamic force of each wing acts through a point that lies at 30% of the wingspan (root to tip) and at 25% local chord.

The aerodynamic moment generated by the resultant force $\mathbf{F}_{aero}$ is thus given by

$$\mathbf{M}_{aero} = \boldsymbol{l}_{cp}{}^{\times} \mathbf{F}_{aero} \qquad \text{Eqn 5.7}$$

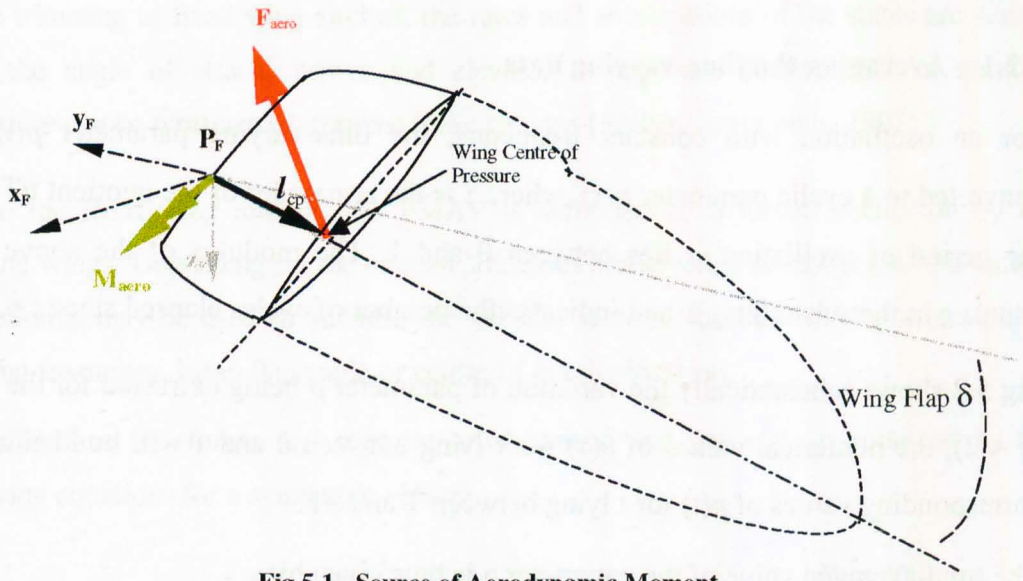

Fig 5.1 Source of Aerodynamic Moment

The aerodynamic model is then included in the simulation model as shown in Fig 3.1. With a flapping frequency of 40 Hz, a wingspan of 48.67 mm and flap amplitude of ±50° assumed for the MAV, the nominal flapping velocity is

$$\begin{aligned} V_{flap} &= 2n\hat{\delta}R \\ &= 6.8 \text{ ms}^{-1} \end{aligned} \qquad \text{Eqn 5.8}$$

At the hovering and low speed regime near the equilibrium position, the velocity and angular rate variations are not expected to be more than 0.4 ms^{-1} and 1 $rad.s^{-1}$ respectively. This is less than 6% of the mean flapping velocity. It is reasonable to assume that the small amplitude vehicle motion has negligible effects on the wing aerodynamics compared with the high frequency flapping. A change in stroke plane is accomplished, relative to the flapping frequency, slowly enough for its effects on the wing aerodynamics to be ignored.

5.2 TIME-VARYING AND TIME-AVERAGED DATA

The simulation results in Chapter 3 have shown that the entire vehicle is subject to forced oscillations by the wings as they flap. While the time-varying value of a parameter p, given by $p(t)$, gives much information about the system, it is certainly useful to also know the time-averaged value of the parameter within a flap cycle, ${}_c\overline{p}$ for the c-th cycle.

5.2.1 Averaging the time-varying data

For an oscillation with constant frequency, the time-varying parameter $p(t)$ can be converted to a cyclic parameter $p(\tau)$, where τ is the remainder of the quotient t/T, T being the period of oscillation. τ lies between 0 and 1. The modulus of the above quotient equals c in the subscript ${}_c\overline{p}$ and indicates the number of cycles elapsed since t = 0.

Fig 5.2 shows schematically the variation of parameter p being extracted for the 2nd cycle (c = 2), the numerical values of $p(\tau)$ for τ lying between 0 and 1 will be identical to the corresponding values of $p(t)$ for t lying between T and 2T.

The time-averaged value of the parameter p is thus given by

$$ {}_c\overline{p} = \int_{\tau=0}^{1} p(\tau)\,d\tau \qquad \text{Eqn 5.9} $$

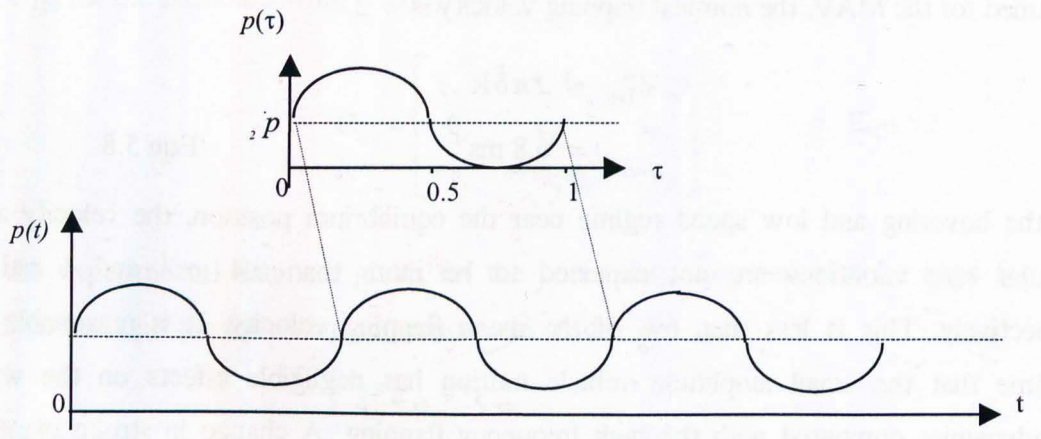

Fig 5.2 Averaging the Time-Varying Parameter p

5.3 TRIMMING THE MAV

In order to prevent aliaising of the signal of a sinusoidal motion, it is necessary to collect about 50 data points per cycle with constant time interval between them. For a flapping frequency of 40 Hz, this would mean that for each second of simulation time, a total of at least 200 steps are required and the simulation time step must be less than 5 milliseconds.

In the trimming of fixed wing aircraft, the rates and accelerations of the states are zeroed once the angle of attack, power and elevator settings are determined. An iterative procedure can be written to determine these settings [Stevens and Lewis, 1992].

Unlike the fixed wing aircraft, the FMAV is subjected to a forced oscillation by the flapping wings. Depending on the control strategies employed, a combination of a variety of measures may be used to stabilise the vehicle, such as variation of the stroke plane, flapping frequency, mean flap angle or centre of gravity location.

In equilibrium, the forces and moment are balanced and this state is reflected by the following equations for a symmetric vehicle,

$$\mathbf{d}_1^{\times}\mathbf{C}_{1E}m\mathbf{g}+\sum_{i=2}^{5}\mathbf{b}_i^{\times}\mathbf{C}_{1i}\mathbf{F}_i+\sum_{i=1}^{5}\mathbf{C}_{1i}\mathbf{M}_i=0 \qquad \text{Eqn 5.10}$$

$$\sum_{i=1}^{5}\mathbf{F}_{xi}=0 \qquad \text{Eqn 5.11}$$

$$\sum_{i=1}^{5}\mathbf{F}_{zi}=0 \qquad \text{Eqn 5.12}$$

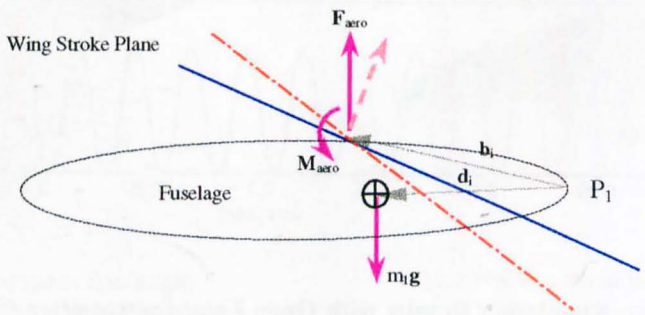

Fig 5.3 Effects of Stroke Plane Tilt

Varying the stroke plane angle directs the resultant force and thus affects the acceleration along longitudinal as well as vertical axes. It will also affect the pitch acceleration as the moment arm is changed as shown in Fig 5.3.

The flapping frequency directly affects the dynamic pressure experienced by the wing. Increasing it will increase the magnitude of the resultant force. If the force is directed vertically upwards, a change in the flapping frequency will only affect the vertical acceleration. If the flapping frequency is fixed, then the vertical acceleration will be affected by the weight of the MAV.

Shifting the mean position of the wings through variation of the mean flap angle can affect the moment balance just like a shift in the CG location.

5.3.1 Pitch Trim

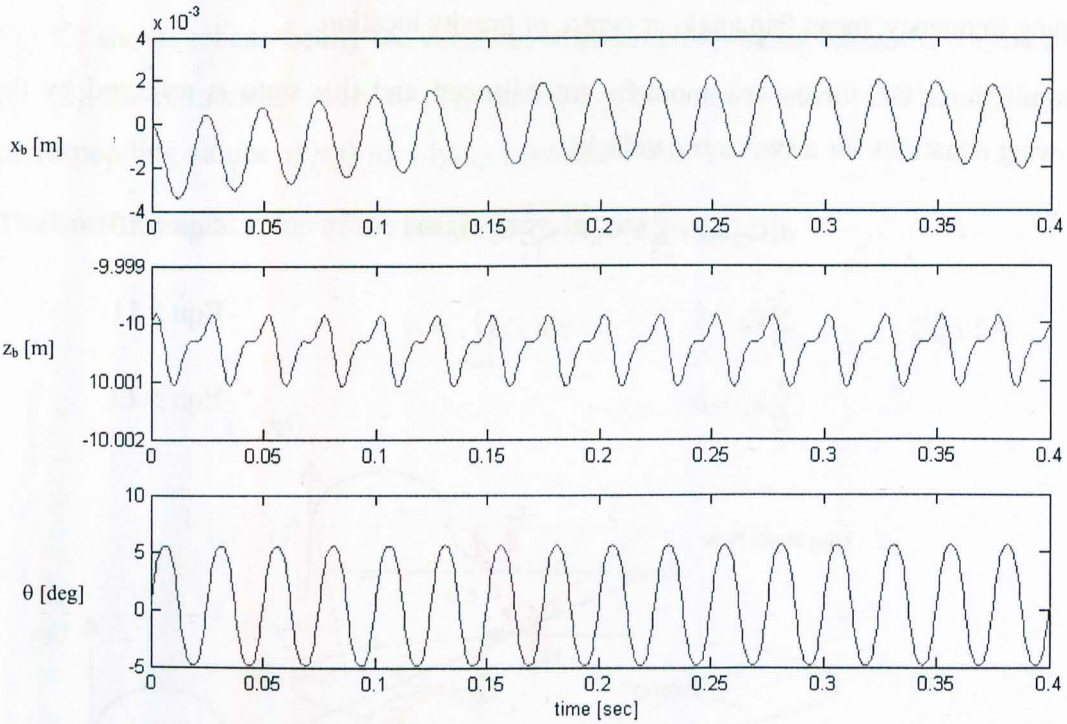

Fig 5.4 **Simulation Results with Open Loop System after CG location for Moment Balance was determined.**

Assuming the fuselage attitude is horizontal, $\theta = 0°$, the stroke plane angle κ for a vertical time-averaged resultant force can be calculated using Eqn 4.8 from the previous chapter. This would ensure that there was no horizontal acceleration ($\dot{u}_b$). The fuselage mass was varied to minimise vertical acceleration ($\dot{w}_b$), so that the flapping frequency remained constant at 40 Hz instead of letting the mass be constant and varying the flapping frequency. It was also necessary to find a centre of gravity location $\mathbf{d}_1$ from the origin P_1 of the fuselage reference frame for moment balance satisfying Eqn 5.10.

Fig 5.4 shows the simulation results lasting 0.4 sec. The pitch attitude was found to oscillate between ±5° and the vehicle hovers at a height of 10m above the ground with a variation of 1 mm due to the flapping of the wings. It was seen that the horizontal position of the vehicle varied about 2 mm. After this brief period of pitch stabilisation, the vehicle was found to drift due to the neutral stability of the vehicle at hover.

At the ideal hover, the time-averaged resultant force should be directed vertically upwards and be equal in magnitude to the weight of the vehicle for force balance. In the trim routine, although the time-averaged accelerations were minimised, they were numerically non-zero. These errors were integrated and caused the vehicle to drift. There was no restoring moment to return the vehicle to its trimmed state.

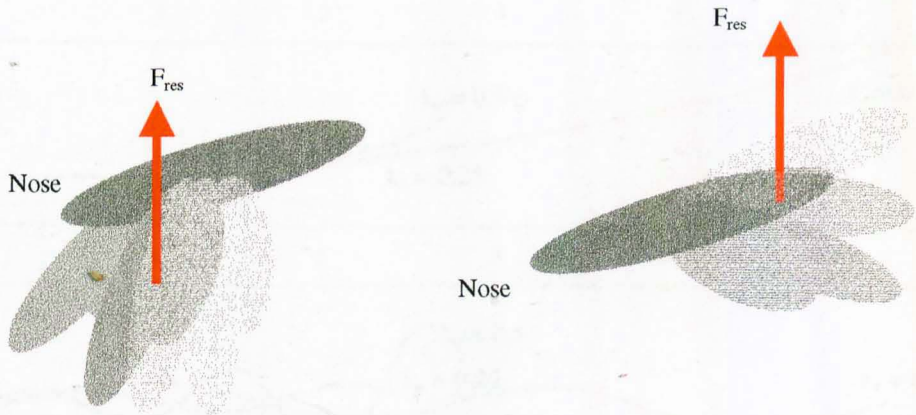

(a) Negative mean flap angle
Wings flap more forward
causing net nose-up pitching

(b) Positive mean flap angle
Wings flap more aft
causing net nose-down pitching

Fig 5.5 Effects of Mean Flap Angle

In order to actively correct this pitch attitude divergence, two methods observed in insects were attempted. Firstly, the mean flap angle can be used to correct the pitch attitude as shown in Fig 5.5. By shifting the flapping more forward (negative mean flap angle), a time-averaged nose up moment can be generated. It also causes a change in the moments due to inertial, centrifugal and Coriolis forces. Thus, adjusting the mean flap angle may serve as a means to stabilise pitch attitude.

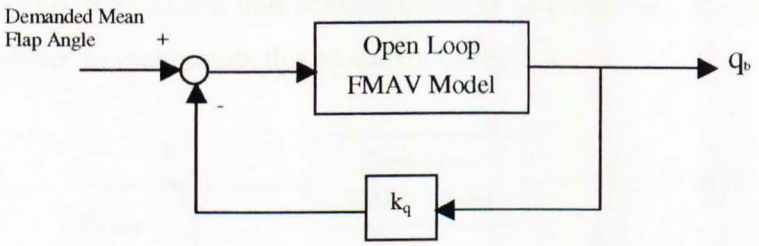

Fig 5.6 Active Stabilisation of Pitch Attitude through feedback of Pitch Rate to Mean Flap Angle

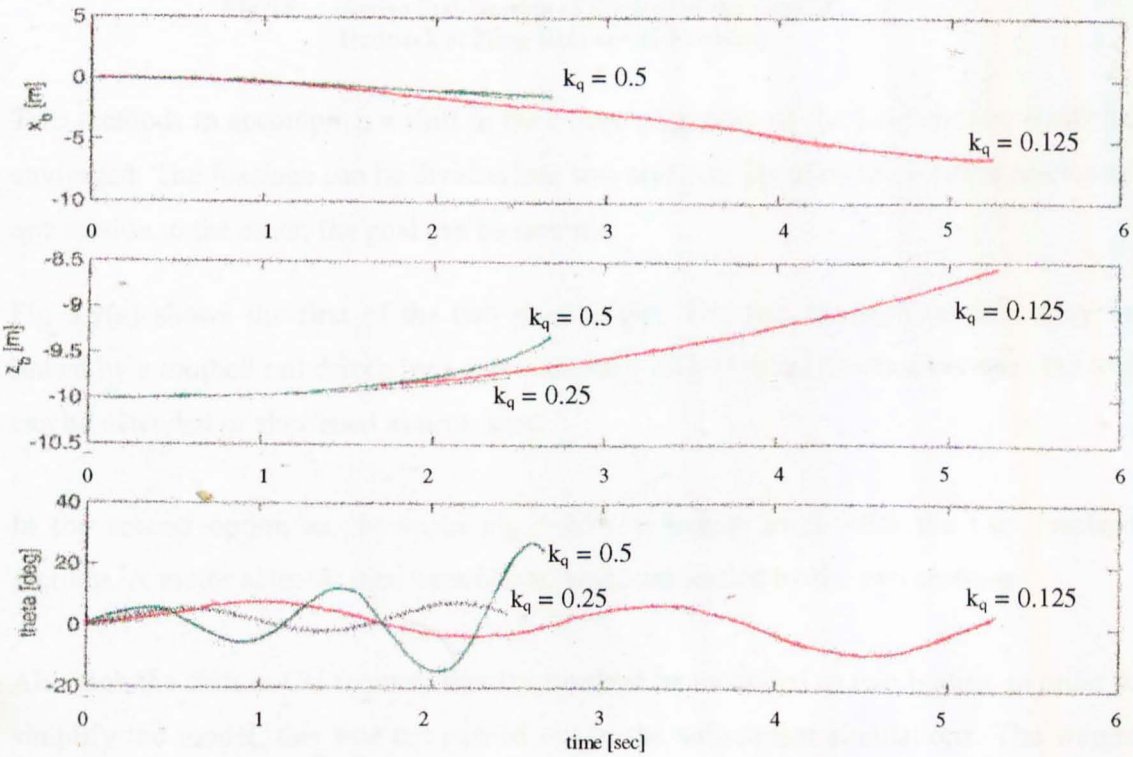

Fig 5.7 Variation of Fuselage Pitch Attitude and Position with feedback of Pitch Rate to Mean Flap Angle

The control system to achieve this is shown in Fig 5.6. However, as shown in Fig 5.7, it was found that feedback of the pitch rate or attitude to the mean flap angle causes the response to be changed from an exponential divergence (open loop) to an oscillatory divergence for the range of gains used (k_q = 0.125, 0.25, 0.5 were tested). The natural frequency of the oscillation is increased with an increase of the feedback gain.

The second method was to feedback the pitch rate to the centre of gravity location, $\mathbf{d}_1$. It can be seen that insects and birds hover with adjustments of their abdomen or tail, apparently to vary the CG and thus achieve moment equilibrium. The closed loop system was thus modified to incorporate this as shown in Fig 5.8.

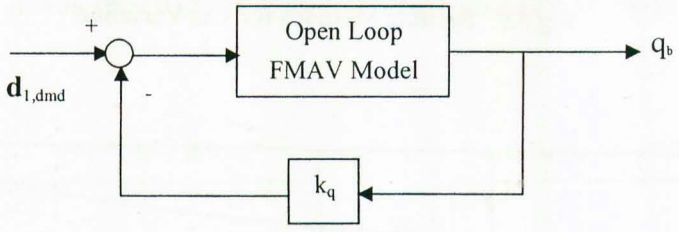

Fig 5.8 Active Stabilisation of Pitch Attitude through feedback of Pitch Rate to CG Location

Two methods to accomplish a shift in the centre of gravity of the fuselage can easily be envisaged. The fuselage can be divided into two sections. By allowing relative motion of one section to the other, the goal can be reached.

Fig 5.9(a) shows the first of the two possibilities. The two fuselage sections may be linked by a toothed rail driven by a servo-actuator such that the distance between the two can be extended or shortened as necessary.

In the second option as shown in Fig 5.9(b), a hinged joint links the two fuselage sections. A motor actuator then controls the angle subtended by the two sections.

Although the shift in CG requires that the fuselage be modelled as two bodies, in order to simplify the model, this was not carried out in the subsequent simulations. The weight shift mechanism is therefore assumed to be ideal with no lag.

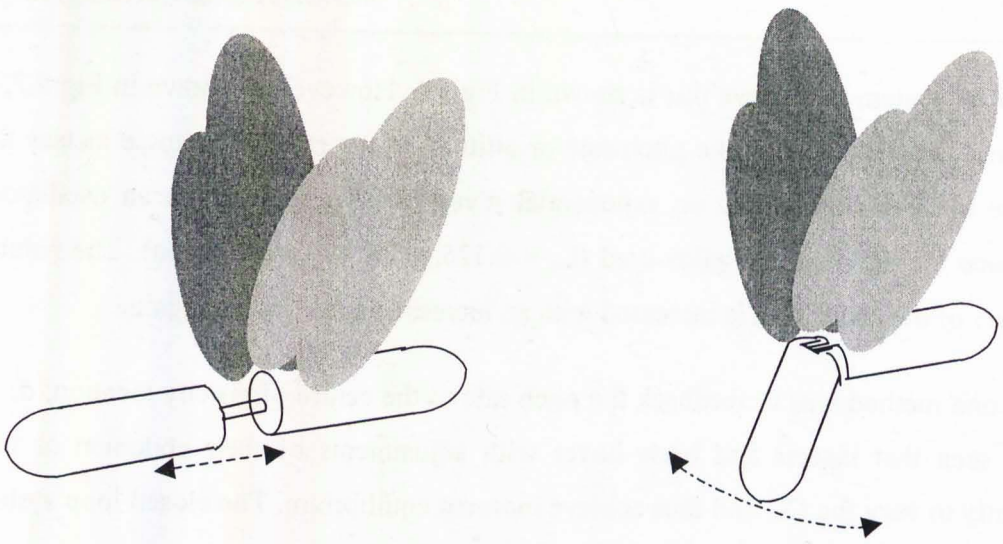

(a) CG Variation through 'sliding' fuselage (b) CG Variation through 'hinged' fuselage

Fig 5.9 Possible Methods for CG Variation

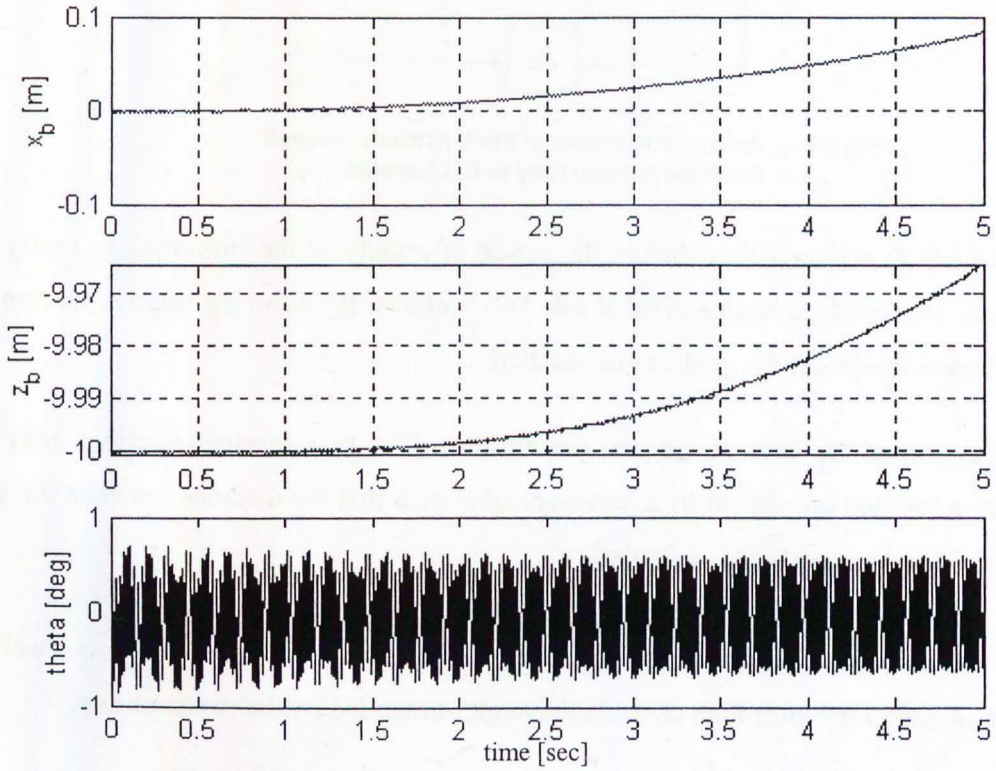

Fig 5.10 Simulation Results with feedback of Pitch Rate to CG Location, d_1

Fig 5.10 shows the simulation results and it can be seen that the vehicle pitch attitude can be stabilised using a unit gain. The fuselage pitch attitude now oscillates between approximately –0.75° and +0.5°, i.e. with a negative mean pitch. While the vehicle remained bound in pitch, the simulation also shows that there is a forward and downward drift. It was found that this might be due to the initial forward velocity, which couples with the negative mean fuselage pitch attitude resulting in a downward linear acceleration, forcing the vehicle downwards. Similarly, the downward velocity couples with the negative pitch resulting in longitudinal acceleration.

Fig 5.11 shows that by reducing the initial forward velocity and the fuselage mass, the accelerations along both the fuselage vertical and horizontal axes were reduced. The vehicle was able to find a trimmed state for more than 40 cycles. However, after the initial 40 cycles, it was seen to accelerate forward with a loss of height.

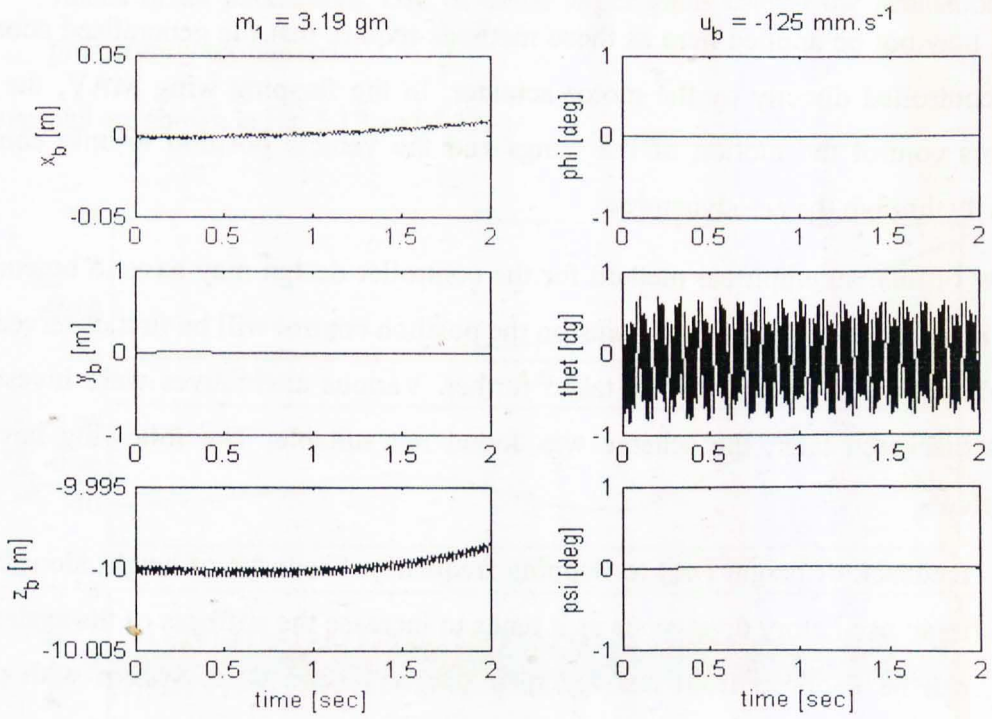

Fig 5.11 Simulation Results with feedback of Pitch Rate to CG Location, with initial velocity adjusted

The above results show that although it was able to stabilise the pitch attitude of the fuselage for a short duration, the system is neutrally stable and any perturbation from this state will lead to a divergence from the trimmed state.

Fig 5.11 has shown that the vehicle drifts from its trimmed state. A feedback control system has to be designed to enable the vehicle to maintain hover at a constant altitude and position.

5.3.2 Height Control

One possible means to control height is to modulate the flapping frequency. This modifies the magnitude of the force due to a change in the dynamic pressure experienced by the wing. The difficulty in the design of the controller at this stage is that there is no simplified linear model with which classical or modern control design technique can be applied. Control design methods for non-linear systems as described by Slotine and Li [1991] may not be applied here as those methods require that the generalised coordinate to be controlled directly by the motor actuator. In the flapping wing MAV, the motor actuators control the motion of the wings and the vehicle position is only controlled indirectly through the aerodynamics.

In view of this, an empirical method for the controller design may have to be embarked upon, in which the effects of the gains on the position control will be first observed and if found feasible, the design can be taken further. Various alternatives were investigated, but as discussed later, the scheme was found not suitable. The following have been attempted:

a. feedback of height ($-z_b$) to flapping frequency. Feedback of height alone resulted in an oscillatory divergence as it tends to increase the stiffness of the system. This can be deduced from analogy to a simple second order system with position feedback:

$$m\ddot{x} + c\dot{x} + (k + k_x)x = 0 \qquad \text{Eqn 5.13}$$

b. feedback of climb rate ($-w_b$) to flapping frequency. This caused the vehicle to diverge exponentially since the system minimises the climb rate only but not the position error.

c. feedback of a combination of both height and climb rate (P+D controller design). This resulted in oscillatory divergence and the period of oscillation of the mean values of all parameters depends on the feedback gain for the height since this alters the stiffness of the system as shown in Eqn 5.13.

d. and finally feedback of a combination of height, climb rate and vertical acceleration ($-\dot{w}_b$) in a PID controller design. Again, the system diverged either exponentially or exhibited oscillatory divergence for the range of gains tried. Increasing the gains led to reduction in the period of oscillation of the mean values of all parameters. Use of much larger gains caused the simulation to be prematurely terminated.

The results are shown in Fig 5.12 and 5.13.

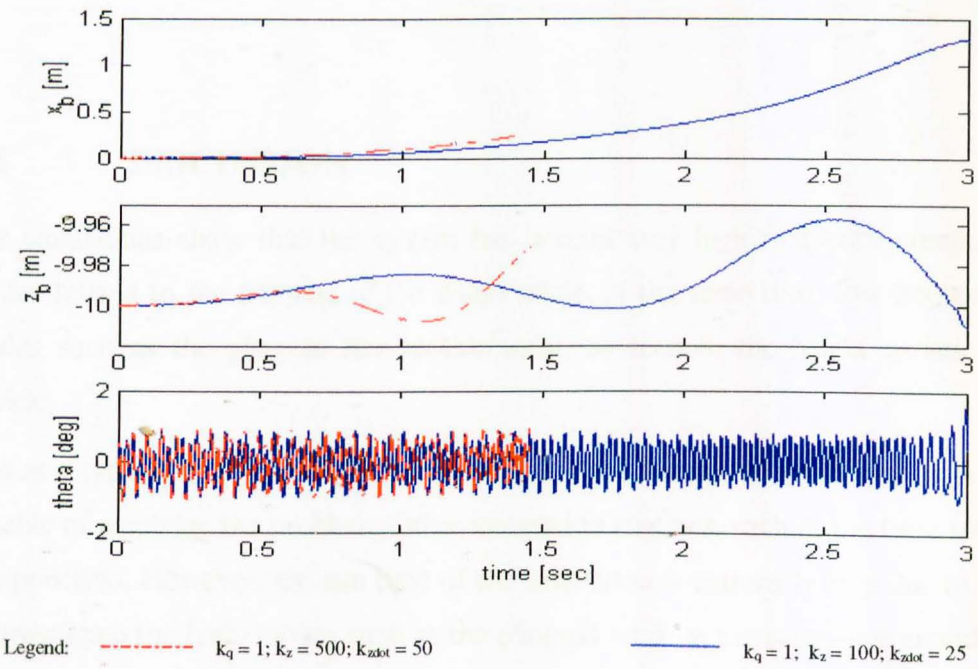

Fig 5.12 Simulation Results with P+D Controller : feedback of Climb Rate and Height to Flapping Frequency

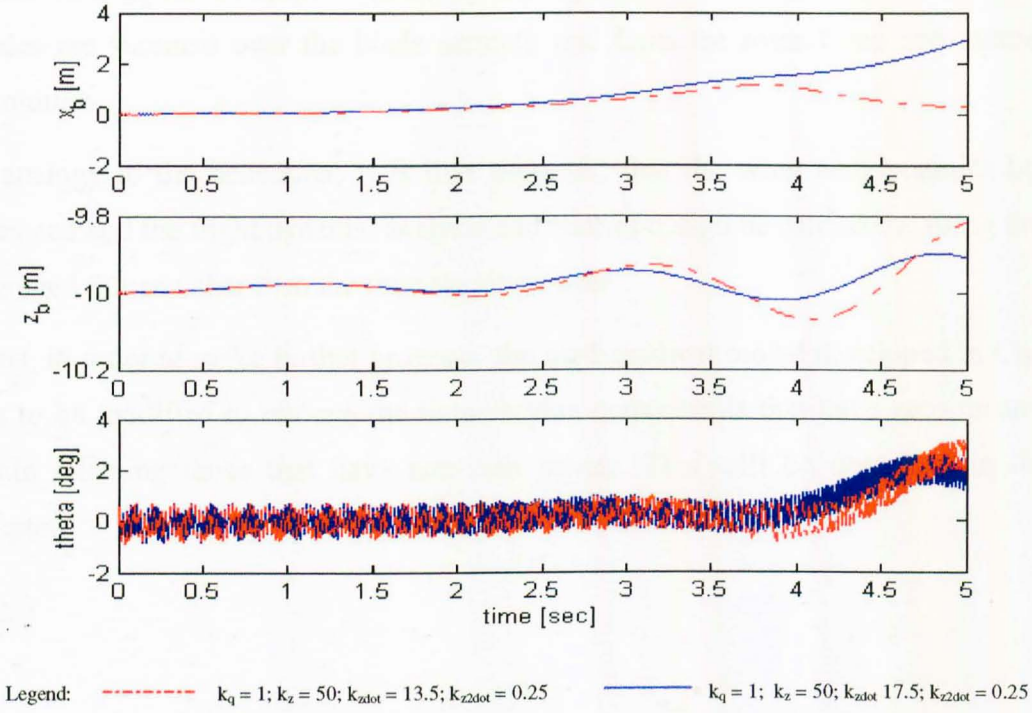

Fig 5.13 **Simulation Results with PID Controller : feedback of Vertical Acceleration, Climb Rate and Height to Flapping Frequency**

5.4 DISCUSSION

The simulations show that the system has several very high frequency components or modes related to the flapping of the wings while, at the same time, low frequency body modes such as the phugoid like motion exist, as seen in the height variation of the vehicle.

This is a typical case of a stiff system and the Runge-Kutta integration routine was not capable of resolving the problem. Other integration routines, such as the Gear solver may be applicable. However, the run time of the simulation is extremely long due to the need to investigate the body modes such as the phugoid while at the same time anti-aliaising is required.

While the time-varying data is important in vibration and ride-comfort studies in helicopters, for example, flight dynamics analysis often makes use of time-averaged data. In the case of the helicopter again, the aerodynamic forces and moments of the rotor blades are summed over the blade azimuth and form the rotor force and moment per revolution.

In analogy to the helicopter, it is thus proposed that the wing aerodynamics be time-averaged and the flight dynamic analysis and control design be carried out using the time-averaged forces rather than the time-varying forces.

Thus, in order to make further progress, the mathematical model developed in Chapter 2 has to be modified to remove the time-varying components that have zero mean values while retaining those that have non-zero means. This will be described in the next chapter.

CHAPTER 6

ORDER REDUCTION OF MATHEMATICAL MODEL

6.1 OBSERVATIONS OF SIMULATION RESULTS OF FULL-ORDER NON-LINEAR MODEL

It was seen in Chapter 5 that the solution of the full-order non-linear model of the multi-body representation of the MAV is not only time-consuming due to the small time steps required, it also encountered the problem of a typical stiff system where the time constants of the system are spread over a wide range. It was seen that the flapping frequency of 40 Hz results in very small time constants while the phugoid-like response of the vehicle has time constants of a few seconds.

One way of overcoming this problem is to reduce the order of the non-linear model by noting that the flapping of the wings is cyclical. It is then reasoned that the instantaneous force vector can be averaged over a cycle, known in this context as time averaging, and the time-averaged force vector would then be the resultant force generated within the flap cycle.

The above reasoning has been successfully applied to the forces on the rotor of the helicopter in stability and control analyses. The instantaneous force experienced by each blade of the rotor, which is dependent on the blade pitch, flap angle and azimuth, is summed over the cycle. The resultant is then applied at the rotor hub, taking into account the moment generated by the resultant force.

By applying the above reasoning, the flapping and pitching of the wings can then be eliminated. In the process, some of the forces cancel out and can be ignored. For example, as the wing flaps up and down, the vertical component of the inertial force due to the acceleration of the wing centre of gravity during the upstroke is equal and opposite in direction to that experienced during the down stroke, if the flapping is symmetrical about a zero mean flap angle. This means that the vertical component of the resultant of this force is zero.

Nonetheless, there are other forces, some of which are non-zero over a flap cycle. Examples of these are the centrifugal force and the aerodynamic forces.

In order to develop the time averaged flapping wing MAV model from the full order model developed in Chapter 2, the following observations based on the simulation results with the full order model have been made:

Observation 1: *An oscillatory term with zero mean value generally cancels out over a flap cycle*

Observation 2: *For* $i = 4$ *and* 5, ω_{pix} *and* ω_{piy} *have zero means while* ω_{piz} *are relatively small and may be ignored.*

Observation 3: *The predominant forces transmitted from the wings to the fuselage are the aerodynamic and centrifugal forces. The centrifugal forces due to the flapping are generally unaffected by the cyclic pitching of the wing.*

The effect of wing pitching on the dynamic forces depends on the perpendicular distance between the CG of the wing and its pitch axis. If it is assumed that the centre of gravity of the wing lies on or close to its pitch axis, this effect will be negligible.

Although ω_{pix} and ω_{piy} have effectively zero mean values, the sum of even powers of their instantaneous values will be non-zero and are the source of forces such as the centrifugal forces.

Based on the above assumptions, Eqns 2.35 to 2.39 can be re-examined and odd-powered terms of ω_{p4} and ω_{p5} will be removed. *Observation 3* above means that the pitching of the wing can be omitted and thus in the modified equations, even-powered terms of ω_{p4} and ω_{p5} will be replaced by the time-averaged value of

$$\overline{\boldsymbol{\omega}}_{pi} = \begin{bmatrix} 0 \\ 2\hat{\delta}_i n_i \\ 0 \end{bmatrix} \qquad \text{Eqn 6.1}$$

6.2 EQUATIONS OF MOTION

In the time-averaged model of the FMAV, the instantaneous orientation of the wing is of no interest. Only the mean attitude of the wing is of relevance. Hence, ω_{p4} and ω_{p5} can be removed from the state vector **V**, the derivative of which is given by Eqn 2.36. The state vector **V** can therefore be reduced to

$$\mathbf{V} = [\mathbf{v}_1 \;\; \boldsymbol{\omega}_1 \;\; \omega_{p2} \;\; \omega_{p3}]^T \qquad \text{Eqn 6.2}$$

Removing the rows and columns of the mass matrix **M** in Eqn 2.39 related to ω_{p4} and ω_{p5}, it can be rewritten as

$$\mathbf{M} = \begin{bmatrix} \mathbf{m} & -\mathbf{c}^{\times} & -\{\mathbf{C}_{12}(\mathbf{m}_2\mathbf{b}_4^{\times} + \mathbf{c}_2^{\times}) + \mathbf{C}_{14}\mathbf{c}_4^{\times}\mathbf{C}_{42}\} & -\{\mathbf{C}_{13}(\mathbf{m}_3\mathbf{b}_5^{\times} + \mathbf{c}_3^{\times}) + \mathbf{C}_{15}\mathbf{c}_5^{\times}\mathbf{C}_{53}\} \\ \mathbf{c}^{\times} & \mathbf{J} & (\mathbf{J}_{12} + \mathbf{J}_{142}) & (\mathbf{J}_{13} + \mathbf{J}_{153}) \\ \mathbf{c}_2^{\times}\mathbf{C}_{21} + \mathbf{m}_2\mathbf{b}_4^{\times}\mathbf{C}_{21} & \mathbf{J}_{21}\mathbf{C}_{21} - \mathbf{m}_4\mathbf{b}_4^{\times}\mathbf{C}_{21}\mathbf{b}_2^{\times} - \mathbf{b}_4^{\times}\mathbf{C}_{24}\mathbf{c}_4^{\times}\mathbf{C}_{41} & \mathbf{J}_2 - \mathbf{b}_4^{\times}\mathbf{C}_{24}\mathbf{c}_4^{\times}\mathbf{C}_{42} & \mathbf{0} \\ \mathbf{c}_3^{\times}\mathbf{C}_{31} + \mathbf{m}_3\mathbf{b}_5^{\times}\mathbf{C}_{31} & \mathbf{J}_{31}\mathbf{C}_{31} - \mathbf{m}_5\mathbf{b}_5^{\times}\mathbf{C}_{31}\mathbf{b}_3^{\times} - \mathbf{b}_5^{\times}\mathbf{C}_{35}\mathbf{c}_5^{\times}\mathbf{C}_{51} & \mathbf{0} & \mathbf{J}_3 - \mathbf{b}_5^{\times}\mathbf{C}_{35}\mathbf{c}_5^{\times}\mathbf{C}_{53} \end{bmatrix}$$

Eqn 6.3

6.2.1 FORCE VECTOR F

For the force vector **F** given by Eqn 2.37, the sources of the elements are aerodynamics, gravity, friction, motor and constraint of movement. As the flapping and pitching of the wing are assumed to move through equal half-amplitude in the up- and down stroke, the frictional and constraint forces and moments will cancel out in the two half strokes and can therefore be removed. Time varying aerodynamic forces and moments are replaced by their time-averaged expressions. Forces and moments due to gravity depend on their mean orientation in inertial space.

Eqn 2.37 can therefore be rephrased as follows:

$$\bar{\mathbf{F}} = \begin{bmatrix} \sum_{i=1}^{5} \mathbf{C}_{1i}\bar{\mathbf{f}}_i \\ \sum_{i=1}^{5} \mathbf{C}_{1i}\bar{\mathbf{g}}_i + \sum_{i=1}^{5}\left(\mathbf{C}_{1g}\mathbf{b}_h^{\times}\mathbf{C}_{1i} + \mathbf{C}_{1h}\mathbf{b}_i^{\times}\mathbf{C}_{hi}\right)\bar{\mathbf{f}}_i \\ \bar{\mathbf{g}}_2 + \bar{\mathbf{g}}_{p2} - \mathbf{C}_{24}\bar{\mathbf{g}}_{pmotor,4} + \mathbf{b}_4^{\times}\mathbf{C}_{24}\bar{\mathbf{f}}_4 \\ \bar{\mathbf{g}}_3 + \bar{\mathbf{g}}_{p3} - \mathbf{C}_{35}\bar{\mathbf{g}}_{pmotor,5} + \mathbf{b}_5^{\times}\mathbf{C}_{35}\bar{\mathbf{f}}_5 \end{bmatrix} \qquad \text{Eqn 6.4}$$

The motor torque $\mathbf{g}_{pmotor,j}$ (j = 4,5) in the third and fourth rows on the right hand side of Eqn 6.4 is equal and opposite to the moments generated by the aerodynamics and dynamics of the wings. Hence, the motor torque transmitted to the stroke plane actuator is

$$\mathbf{g}_{pmotor,j} = \mathbf{F}_{dyn,Rj} \qquad \text{Eqn 6.5}$$

where $\mathbf{F}_{dyn,Rj}$ is the time-averaged dynamic force vector for the wings R_j. Its components shall be examined later in section 6.2.2.4.

6.2.2 FORCE VECTOR $\mathbf{F}_{dyn}$

Finally, the dynamic force vector $\mathbf{F}_{dyn}$, given in Eqn 2.38, comprises of forces and moments arising from the motion of the masses and inertia of the vehicle.

$$\mathbf{F}_{dyn} = \begin{bmatrix} -\omega_1^{\times}\mathbf{p} + \mathbf{BB} \\ -\omega_1^{\times}\mathbf{h}_{P_1} - \mathbf{v}_1^{\times}\mathbf{p} - \dot{\mathbf{c}}^{\times}\mathbf{v}_1 - \dot{\mathbf{J}}\omega_1 - \left(\dot{\mathbf{J}}_{12} + \dot{\mathbf{J}}_{142}\right)\mathbf{C}_{12}\omega_{p2} - \left(\dot{\mathbf{J}}_{13} + \dot{\mathbf{J}}_{153}\right)\mathbf{C}_{13}\omega_{p3} - \dot{\mathbf{J}}_{14}\mathbf{C}_{14}\omega_{p4} - \dot{\mathbf{J}}_{15}\mathbf{C}_{15}\omega \\ \left\{\mathbf{h}_2^{\times} + \mathbf{C}_{21}\left(\mathbf{v}_1 + \omega_1^{\times}\mathbf{b}_2\right)^{\times}\mathbf{C}_{12}\mathbf{c}_4^{\times}\right\}\left(\mathbf{C}_{21}\omega_1 + \omega_{p2}\right) - \mathbf{b}_4^{\times}\mathbf{C}_{21}\omega_1^{\times}\mathbf{C}_{14}\mathbf{p}_4 - \mathbf{A}_{1,2} - \mathbf{A}_{2,2} \\ \left\{\mathbf{h}_3^{\times} + \mathbf{C}_{31}\left(\mathbf{v}_1 + \omega_1^{\times}\mathbf{b}_3\right)^{\times}\mathbf{C}_{13}\mathbf{c}_5^{\times}\right\}\left(\mathbf{C}_{31}\omega_1 + \omega_{p3}\right) - \mathbf{b}_5^{\times}\mathbf{C}_{31}\omega_1^{\times}\mathbf{C}_{15}\mathbf{p}_5 - \mathbf{A}_{1,3} - \mathbf{A}_{2,3} \\ \left\{\mathbf{h}_4^{\times} + \left[\mathbf{C}_{41}\left(\mathbf{v}_1 + \omega_1^{\times}\mathbf{b}_2 + \omega_1^{\times}\mathbf{C}_{12}\mathbf{b}_4\right)^{\times}\mathbf{C}_{14} + \mathbf{C}_{42}\left(\omega_{p2}^{\times}\mathbf{b}_4\right)^{\times}\mathbf{C}_{24}\right]\mathbf{c}_4^{\times}\right\}\left(\mathbf{C}_{41}\omega_1 + \mathbf{C}_{42}\omega_{p2} + \omega_{p4}\right) + \mathbf{A} \\ \left\{\mathbf{h}_5^{\times} + \left[\mathbf{C}_{51}\left(\mathbf{v}_1 + \omega_1^{\times}\mathbf{b}_3 + \omega_1^{\times}\mathbf{C}_{13}\mathbf{b}_5\right)^{\times}\mathbf{C}_{15} + \mathbf{C}_{53}\left(\omega_{p3}^{\times}\mathbf{b}_5\right)^{\times}\mathbf{C}_{25}\right]\mathbf{c}_5^{\times}\right\}\left(\mathbf{C}_{51}\omega_1 + \mathbf{C}_{53}\omega_{p3} + \omega_{p5}\right) + \mathbf{A}_3 \end{bmatrix}$$

Eqn 2.38

The following sections shall examine the effects of time averaging over the flap cycle on the expression of its components.

6.2.2.1 Forces On Fuselage $\mathbf{R}_1$

The dynamic forces acting on the fuselage as expressed in the first row of $\mathbf{F}_{dyn}$ is summarised as two terms $-\omega^{\times}\mathbf{p}$ and **BB**. Removing terms containing odd powers of ω_{p4} and ω_{p5} from Eqn 2.16 and writing it in scalar form, it can be reduced to

$$\overline{\mathbf{p}} = m\mathbf{v}_1 - \mathbf{c}^{\times}\omega_1 - \sum_{i=2}^{3}\left(\mathbf{C}_{1i}\mathbf{c}_i^{\times} + \mathbf{C}_{1j}\mathbf{c}_j^{\times}\mathbf{C}_{ji} + m_j\mathbf{C}_{1i}\mathbf{b}_j^{\times}\right)\omega_{pi} \qquad \text{Eqn 6.6}$$

The other term **BB** comprises the centrifugal forces of the system. It is given by Eqn 2.28 and can be rewritten (with the subscript n = i for i = 4,5) as

$$\begin{aligned} \overline{\mathbf{BB}} = &\sum_{i=1}^{3}\left[\left(\mathbf{C}_{1m}\omega_{pm} + \mathbf{C}_{1n}\omega_{pn}\right)^{\times}\mathbf{C}_{1i}\mathbf{c}_i\right]^{\times}\left(\omega_1 + \mathbf{C}_{1h}\omega_{ph} + \mathbf{C}_{1i}\omega_{pi}\right) \\ &+ \sum_{i=4}^{5}\left[\left(\mathbf{C}_{1m}\omega_{pm}\right)^{\times}\mathbf{C}_{1i}\mathbf{c}_i\right]^{\times}\left(\omega_1 + \mathbf{C}_{1h}\omega_{ph}\right) \qquad \text{Eqn 6.7} \\ &+ \sum_{i=4}^{5}\left[\left(\mathbf{C}_{1n}\overline{\omega}_{pn}\right)^{\times}\mathbf{C}_{1i}\mathbf{c}_i\right]^{\times}\mathbf{C}_{1i}\overline{\omega}_{pi} - \sum_{i=1}^{5}m_i\left(\omega_1 + \mathbf{C}_{1h}\omega_{ph}\right)^{\times}\mathbf{C}_{1h}\omega_{ph}^{\times}\mathbf{b}_i \end{aligned}$$

6.2.2.2 Moments Acting On Fuselage R_1

The moments acting on the fuselage are given in Eqn 2.38 as the second row in the vector $\mathbf{F}_{dyn}$.

$$F_{dyn,R_1} = -\omega_1^{\times}\mathbf{h}_{P_1} - \mathbf{v}_1^{\times}\mathbf{p} - \dot{\mathbf{c}}^{\times}\mathbf{v}_1 - \dot{\mathbf{J}}\omega_1 - (\dot{\mathbf{J}}_{12} + \dot{\mathbf{J}}_{142})\mathbf{C}_{12}\omega_{p2} - (\dot{\mathbf{J}}_{13} + \dot{\mathbf{J}}_{153})\mathbf{C}_{13}\omega_{p3} - \dot{\mathbf{J}}_{14}\mathbf{C}_{14}\omega_{p4} - \dot{\mathbf{J}}_{15}\mathbf{C}_{15}\omega_{p5}$$

Eqn 6.8

As explained earlier, the odd-powered terms of ω_{p4} and ω_{p5} must be removed.

The system angular momentum $\mathbf{h}_{P1}$ as given by Eqn 2.19 can be rewritten by omitting ω_{p4} and ω_{p5} as follows in scalar form

$$\bar{\mathbf{h}}_{P_1} = \mathbf{c}^{\times}\mathbf{v}_1 + \mathbf{J}\omega_1 + \sum_{i=4}^{5}(\mathbf{J}_{1h} + \mathbf{J}_{1ih})\mathbf{C}_{1h}\omega_{ph} \qquad \text{Eqn 6.9}$$

Next, the time derivative of the first moment of inertia of the system **c** is obtained from the Eqn C.58 of Appendix C, but is now reduced to

$$\begin{aligned}\dot{\bar{\mathbf{c}}}^{\times} = &-\sum_{i=2}^{5}\mathbf{C}_{1i}\left[\mathbf{c}_i^{\times}\left(\mathbf{C}_{im}\omega_{pm} + \mathbf{C}_{in}\omega_{pn}\right)\right]^{\times}\mathbf{C}_{i1} \\ &+\sum_{i=4}^{5}\left\{\mathbf{C}_{1i}\left[\mathbf{c}_i^{\times}\left(\mathbf{C}_{im}\omega_{pm}\right)\right]^{\times}\mathbf{C}_{i1} - \mathbf{m}_i\mathbf{C}_{1m}\left(\mathbf{b}_i^{\times}\omega_{pm}\right)^{\times}\mathbf{C}_{m1}\right\}\end{aligned} \qquad \text{Eqn 6.10}$$

The time derivative of the system inertia tensor **J**, which is found in the fourth term of Eqn 6.8, is given by Eqn E.27 in Appendix E.5 as

$$\begin{aligned}\dot{\mathbf{J}} = &\left[\sum_{i=2}^{5}\mathbf{C}_{1i}\dot{\mathbf{J}}_{i1}\mathbf{C}_{i1} + \sum_{i=2}^{5}\left(\dot{\mathbf{J}}_{1i} - \dot{\mathbf{J}}_i\right)\right] + \sum_{i=4}^{5}\mathbf{m}_i\mathbf{C}_{1h}\left\{\boldsymbol{\varpi}_{ph}^{T}\left[\mathbf{b}_i^{\times}\left(\mathbf{C}_{h1}\mathbf{b}_h + \mathbf{b}_i\right)\right]\mathbf{I} - \left(\mathbf{C}_{h1}\mathbf{b}_h + \mathbf{b}_i\right)\left(\boldsymbol{\varpi}_{ph}^{\times}\mathbf{b}_i\right)^{T}\right\}\mathbf{C}_{h1} \\ &+\sum_{i=4}^{5}\mathbf{m}_i\mathbf{C}_{1h}\left(\mathbf{C}_{h1}\mathbf{b}_h + \mathbf{b}_i\right)^{\times}\left[\boldsymbol{\varpi}_{ph}\mathbf{b}_i^{T} - \mathbf{b}_i\boldsymbol{\varpi}_{ph}^{T}\right]\mathbf{C}_{h1}\end{aligned}$$

Eqn 6.11

Only the terms within the first square parenthesis on the right hand side of Eqn 6.11 need to be examined, as the other two summations do not form a product with either ω_{p4} or ω_{p5}. First, the time derivative of $\mathbf{J}_i$ for i = 4,5. This is given by Eqn E.15 in Appendix E.

$$\dot{\mathbf{J}}_i = -m_i \mathbf{d}_i \left[\boldsymbol{\omega}_{i*}^{\times} \mathbf{d}_i\right]^T + m_i \mathbf{d}_i^{\times} \left[\boldsymbol{\omega}_{i*} \mathbf{d}_i^T - \mathbf{d}_i \boldsymbol{\omega}_{i*}^T\right] + \mathbf{D} \qquad \text{Eqn 6.12}$$

In Appendix E, ω_{i*} was defined as $\omega_{i*} = \mathbf{C}_{ih}\omega_{ph} + \omega_{pi}$. Since $\overline{\omega}_{pi}$ has a zero mean over a cycle, ω_{i*} would have to be replaced by $\mathbf{C}_{ih}\omega_{ph}$. Hence,

$$\overline{\dot{\mathbf{J}}}_i = -m_i \mathbf{d}_i \left[\left(\mathbf{C}_{ih}\boldsymbol{\varpi}_{ph}\right)^{\times} \mathbf{d}_i\right]^T + m_i \mathbf{d}_i^{\times} \left[\left(\mathbf{C}_{ih}\boldsymbol{\varpi}_{ph}\right)\mathbf{d}_i^T - \mathbf{d}_i \left(\mathbf{C}_{ih}\boldsymbol{\varpi}_{ph}\right)^T\right] + \overline{\mathbf{D}} \qquad \text{Eqn 6.13}$$

where $\overline{\mathbf{D}} = \left(\mathbf{C}_{ih}\boldsymbol{\omega}_{ph}\right)^{\times} \mathbf{J}_{Gi} - \mathbf{J}_{Gi}\left(\mathbf{C}_{ih}\boldsymbol{\omega}_{ph}\right)^{\times}$.

Next, consider the time derivative of $\mathbf{J}_{il}$ given in Eqn E.18 for the original model as

$$\begin{aligned}\dot{\mathbf{J}}_{il} = m_i \Big\{ &\boldsymbol{\omega}_{i*}^T \left[\mathbf{d}_i^{\times}\left(\mathbf{C}_{il}\mathbf{b}_h + \mathbf{C}_{ih}\mathbf{b}_i\right)\right]\mathbf{I} - \left(\mathbf{C}_{il}\mathbf{b}_h + \mathbf{C}_{ih}\mathbf{b}_i + \mathbf{d}_i\right)\left[\boldsymbol{\omega}_{i*}^{\times}\mathbf{d}_i\right]^T \Big\} \\ &+ m_i \mathbf{d}_i^{\times} \mathbf{C}_{ih}\left(\boldsymbol{\omega}_{ph}\mathbf{b}_i^T - \mathbf{b}_i\boldsymbol{\omega}_{ph}^T\right) + m_i \mathbf{d}_i^{\times}\left[\boldsymbol{\omega}_{i*}\mathbf{d}_i^T - \mathbf{d}_i\boldsymbol{\omega}_{i*}^T\right] + \mathbf{D}\end{aligned} \qquad \text{Eqn 6.14}$$

It can be readily seen again that there are no even powered ω_{p4} and ω_{p5} terms and the above equation can be rewritten by replacing ω_{i*} with $\mathbf{C}_{ih}\omega_{ph}$ for i = 4,5:

$$\begin{aligned}\overline{\dot{\mathbf{J}}}_{il} = m_i \Big\{ &\left(\mathbf{C}_{ih}\boldsymbol{\omega}_{ph}\right)^T \left[\mathbf{d}_i^{\times}\left(\mathbf{C}_{il}\mathbf{b}_h + \mathbf{C}_{ih}\mathbf{b}_i\right)\right]\mathbf{I} - \left(\mathbf{C}_{il}\mathbf{b}_h + \mathbf{C}_{ih}\mathbf{b}_i + \mathbf{d}_i\right)\left[\left(\mathbf{C}_{ih}\boldsymbol{\omega}_{ph}\right)^{\times}\mathbf{d}_i\right]^T \Big\} \\ &+ m_i \mathbf{d}_i^{\times} \mathbf{C}_{ih}\left(\boldsymbol{\omega}_{ph}\mathbf{b}_i^T - \mathbf{b}_i\boldsymbol{\varpi}_{ph}^T\right) + m_i \mathbf{d}_i^{\times}\left[\left(\mathbf{C}_{ih}\boldsymbol{\omega}_{ph}\right)\mathbf{d}_i^T - \mathbf{d}_i\left(\mathbf{C}_{ih}\boldsymbol{\omega}_{ph}\right)^T\right] + \overline{\mathbf{D}}\end{aligned} \qquad \text{Eqn 6.15}$$

Similarly, looking at the time derivative of $\mathbf{J}_{1i}$, given in Eqn E.16 for the original model, it can be deduced that none of the terms will yield even powered terms for ω_{p4} and ω_{p5}. The time-averaged time derivative of $\mathbf{J}_{1i}$ for i = 4,5 is therefore given by

$$\begin{aligned}\overline{\dot{\mathbf{J}}}_{1i} = m_i \Big\{ &\left(\mathbf{C}_{1h}\boldsymbol{\varpi}_{ph}\right)^T \left[\left(\mathbf{C}_{1h}\mathbf{b}_i\right)^{\times}\left(\mathbf{C}_{1i}\mathbf{d}_i\right)\right]\mathbf{I} - \left(\mathbf{C}_{1i}\mathbf{d}_i\right)\left(\mathbf{C}_{1h}\boldsymbol{\varpi}_{ph}^{\times}\mathbf{b}_i\right)^T \Big\} \\ &+ m_i\left(\mathbf{C}_{1h}\mathbf{b}_i + \mathbf{b}_h\right)^{\times}\left[\left(\mathbf{C}_{1h}\boldsymbol{\varpi}_{ph}\right)\left(\mathbf{C}_{1i}\mathbf{d}_i\right)^T - \left(\mathbf{C}_{1i}\mathbf{d}_i\right)\left(\mathbf{C}_{1h}\boldsymbol{\varpi}_{ph}\right)^T\right] \\ &+ \mathbf{C}_{1i}\left\{m_i\mathbf{d}_i^{\times}\left[\left(\mathbf{C}_{ih}\boldsymbol{\varpi}_{ph}\right)\mathbf{d}_i^T - \mathbf{d}_i\left(\mathbf{C}_{ih}\boldsymbol{\varpi}_{ph}\right)^T\right] - m_i\mathbf{d}_i\left[\left(\mathbf{C}_{ih}\boldsymbol{\varpi}_{ph}\right)^{\times}\mathbf{d}_i\right]^T + \overline{\mathbf{D}}\right\}\mathbf{C}_{1i}\end{aligned} \qquad \text{Eqn 6.16}$$

With the time averaged derivatives of $\mathbf{J}_i$, $\mathbf{J}_{i1}$ and $\mathbf{J}_{1i}$ given by Eqns 6.13, 6.15 and 6.16 respectively, Eqn 6.11 can be written for i = 4,5 as follows

$$\begin{aligned}\dot{\mathbf{J}} = &\left[\sum_{i=2}^{3}\mathbf{C}_{1i}\dot{\mathbf{J}}_{i1}\mathbf{C}_{i1} + \left(\dot{\mathbf{J}}_{1i} - \dot{\mathbf{J}}_i\right)\right] + \left[\sum_{i=4}^{5}\mathbf{C}_{1i}\bar{\dot{\mathbf{J}}}_{i1}\mathbf{C}_{i1} + \left(\bar{\dot{\mathbf{J}}}_{1i} - \bar{\dot{\mathbf{J}}}_i\right)\right] \\ &+ \sum_{i=4}^{5} m_i \mathbf{C}_{1h}\left\{\boldsymbol{\varpi}_{ph}^T\left[\mathbf{b}_i^{\times}\left(\mathbf{C}_{h1}\mathbf{b}_h + \mathbf{b}_i\right)\right]\mathbf{I} - \left(\mathbf{C}_{h1}\mathbf{b}_h + \mathbf{b}_i\right)\left(\boldsymbol{\varpi}_{ph}^{\times}\mathbf{b}_i\right)^T\right\}\mathbf{C}_{h1} \\ &+ \sum_{i=4}^{5} m_i \mathbf{C}_{1h}\left(\mathbf{C}_{h1}\mathbf{b}_h + \mathbf{b}_i\right)^{\times}\left[\boldsymbol{\varpi}_{ph}\mathbf{b}_i^T - \mathbf{b}_i\boldsymbol{\varpi}_{ph}^T\right]\mathbf{C}_{h1}\end{aligned} \qquad \text{Eqn 6.17}$$

The fifth and sixth terms of Eqn 6.8 can be written as $-\sum_{i=4}^{5}\left(\dot{\mathbf{J}}_{1h} + \dot{\mathbf{J}}_{1ih}\right)\mathbf{C}_{1h}\boldsymbol{\omega}_{ph}$. The first term within the parenthesis is given by Eqn E.16, which also shows that it is independent of ω_{pi}. Eqn E.24 shows that the second term contains the time derivatives of $\mathbf{J}_{1i}$, $\mathbf{J}_i$ and $\mathbf{J}_{ih}$.

It was seen earlier in Eqns 6.13 and 6.16 that the assessment of $\bar{\dot{\mathbf{J}}}_i$ and $\bar{\dot{\mathbf{J}}}_{1i}$ yield only odd powered terms of ω_{pi}. This is also true for the time average of the derivative of J_{ih} when Eqn E.20 is analysed, giving

$$\begin{aligned}\bar{\dot{\mathbf{J}}}_{ih} = &\, m_i\left\{\left(\mathbf{C}_{ih}\boldsymbol{\omega}_{ph}\right)^T\left(\mathbf{d}_i^{\times}\mathbf{C}_{ih}\mathbf{b}_i\right)\mathbf{I} - \left(\mathbf{C}_{ih}\mathbf{b}_i + \mathbf{d}_i\right)\left[\left(\mathbf{C}_{ih}\boldsymbol{\omega}_{ph}\right)^{\times}\mathbf{d}_i\right]^T\right\} \\ &+ m_i\mathbf{d}_i^{\times}\mathbf{C}_{ih}\left(\boldsymbol{\omega}_{ph}\mathbf{b}_i^T - \mathbf{b}_i\boldsymbol{\omega}_{ph}^T\right) + m_i\mathbf{d}_i^{\times}\left[\left(\mathbf{C}_{ih}\boldsymbol{\omega}_{ph}\right)\mathbf{d}_i^T - \mathbf{d}_i\left(\mathbf{C}_{ih}\boldsymbol{\omega}_{ph}\right)^T\right] + \bar{\mathbf{D}}\end{aligned} \qquad \text{Eqn 6.18}$$

Thus, reassessing Eqn E.24 for the time average of the derivative of J_{1ih} results in

$$\bar{\dot{\mathbf{J}}}_{1ih} = \bar{\dot{\mathbf{J}}}_{1i} - \bar{\dot{\mathbf{J}}}_i + \mathbf{C}_{1i}\bar{\dot{\mathbf{J}}}_{ih}\mathbf{C}_{i1} - m_i\mathbf{C}_{1h}\mathbf{b}_i^{\times}\boldsymbol{\varpi}_{ph}^{\times}\mathbf{b}_i + \left(\mathbf{b}_h + \mathbf{C}_{1h}\mathbf{b}_i\right)^{\times}\left(\boldsymbol{\varpi}_{ph}\mathbf{b}_i^T - \mathbf{b}_i\boldsymbol{\varpi}_{ph}^T\right) \qquad \text{Eqn 6.19}$$

Finally, in the last two terms of Eqn 6.8, although the time derivative of $\mathbf{J}_{1i}$ yields only odd powered terms of ω_{pi}, it is multiplied with ω_{pi}, thus resulting in even powered terms of ω_{pi}. They shall therefore be replaced by $\sum_{i=4}^{5} \dot{\bar{\bar{\mathbf{J}}}}_{1i} \mathbf{C}_{1i} \bar{\boldsymbol{\omega}}_{pi}$ where

$$\begin{aligned} \dot{\bar{\bar{\mathbf{J}}}}_{1i} = m_i (\mathbf{C}_{1h}\mathbf{b}_i + \mathbf{b}_h)^{\times} \left[(\mathbf{C}_{1i}\bar{\boldsymbol{\omega}}_{pi})(\mathbf{C}_{1i}\mathbf{d}_i)^T - (\mathbf{C}_{1i}\mathbf{d}_i)(\mathbf{C}_{1i}\bar{\boldsymbol{\omega}}_{pi})^T \right] \\ + \mathbf{C}_{1i} \left\{ m_i \mathbf{d}_i^{\times} \left[\bar{\boldsymbol{\omega}}_{i*} \mathbf{d}_i^T - \mathbf{d}_i \bar{\boldsymbol{\omega}}_{i*}^T \right] - m_i \mathbf{d}_i \left[\bar{\boldsymbol{\omega}}_{i*}^{\times} \mathbf{d}_i \right]^T + \bar{\bar{\mathbf{D}}} \right\} \mathbf{C}_{i1} \end{aligned} \qquad \text{Eqn 6.20}$$

and

$$\bar{\bar{\mathbf{D}}} = \bar{\boldsymbol{\omega}}_{i*}^{\times} \mathbf{J}_{Gi} - \mathbf{J}_{Gi} \bar{\boldsymbol{\omega}}_{i*}^{\times} \qquad \text{Eqn 6.21}$$

In Eqn 6.22, $\bar{\boldsymbol{\omega}}_{i*}$ is derived from $\boldsymbol{\omega}_{i*} = \mathbf{C}_{ih}\boldsymbol{\omega}_{ph} + \bar{\boldsymbol{\omega}}_{pi}$ in Appendix E. However, $\mathbf{C}_{ih}\boldsymbol{\omega}_{ph}$ when multiplied with $\bar{\boldsymbol{\omega}}_{pi}$ in the operation $\sum_{i=4}^{5} \dot{\bar{\bar{\mathbf{J}}}}_{1i} \mathbf{C}_{1i} \bar{\boldsymbol{\omega}}_{pi}$ will result in a zero-mean and thus be removed. Hence

$$\bar{\boldsymbol{\omega}}_{i*} = \bar{\boldsymbol{\omega}}_{pi} \qquad \text{Eqn 6.22}$$

6.2.2.3 Moments Acting On Stroke Plane Actuators R_2 and R_3

The third and fourth rows of the generalised force vector $\mathbf{F}_{dyn}$ represent the moments acting on R_2 and R_3 respectively, and is shown here in general form for convenience

$$\mathbf{F}_{dyn,R_i} = \left\{ \mathbf{h}_i^{\times} + \mathbf{C}_{il} (\mathbf{v}_1 + \boldsymbol{\omega}_1^{\times} \mathbf{b}_i)^{\times} \mathbf{C}_{1i} \mathbf{c}_h^{\times} \right\} (\mathbf{C}_{il}\boldsymbol{\omega}_1 + \boldsymbol{\omega}_{pi}) - \mathbf{b}_j^{\times} \mathbf{C}_{il} \boldsymbol{\omega}_1^{\times} \mathbf{C}_{1j} \mathbf{p}_j - \mathbf{A}_1 - \mathbf{A}_2$$

Eqn 6.23

For the time-averaged model, only the last three terms need to be modified.

Note that index i represents the stroke plane actuators

index j represents the wings and

index h represents the fuselage.

Eqn B.3 gives the general form of the linear momentum of the body R_i. Writing with respect to the stroke plane angles (i = 2,3), the linear momentum of the wings $\mathbf{p}_j$ (j = 4,5) in $\mathcal{F}_i$, after omission of the odd-powers of $\overline{\omega}_{pj}$, shall be

$$\overline{\mathbf{p}}_j = m_j\left[\mathbf{C}_{j1}\left(\mathbf{v}_0 - \mathbf{b}_i^{\times}\boldsymbol{\omega}_1\right) - \mathbf{C}_{ji}\mathbf{b}_j^{\times}\left(\mathbf{C}_{ij}\boldsymbol{\omega}_1 + \boldsymbol{\omega}_{pi}\right)\right] - \mathbf{c}_j^{\times}\left(\mathbf{C}_{j1}\boldsymbol{\omega}_1 + \mathbf{C}_{ji}\boldsymbol{\omega}_{pi}\right) \qquad \text{Eqn 6.24}$$

The term $\mathbf{A}_1$ in the moment equation for R_2 and R_3 is given by Eqn 2.31. Ignoring odd powered terms of $\overline{\omega}_{pj}$, it can be reduced to the following expression

$$\begin{aligned}\overline{\mathbf{A}}_1 = {} & m_j\mathbf{b}_j^{\times}\left(\mathbf{C}_{i1}\boldsymbol{\omega}_1 + \boldsymbol{\omega}_{pi}\right)^{\times}\left(\boldsymbol{\omega}_{pi}^{\times}\mathbf{b}_j\right) \\ & - \mathbf{b}_j^{\times}\mathbf{C}_{i1}\left[\left\{\left(\boldsymbol{\omega}_1^{\times}\mathbf{C}_{1j} + \mathbf{C}_{1i}\boldsymbol{\omega}_{pi}^{\times}\mathbf{C}_{ij}\right)\mathbf{c}_j\right\}^{\times}\mathbf{C}_{jm}\boldsymbol{\omega}_{pm} + \left(\mathbf{C}_{1j}\overline{\boldsymbol{\omega}}_{pj}^{\times}\mathbf{c}_j\right)^{\times}\mathbf{C}_{jn}\overline{\boldsymbol{\omega}}_{pn}\right]\end{aligned} \qquad \text{Eqn 6.25}$$

Note that the index n = j and m = i.

$\mathbf{A}_2$ as given by Eqn 2.32 does not contain any $\overline{\omega}_{pj}$ term and hence will remain unchanged. The expression for the angular momentum of the stroke plane actuators h_i for i = 2,3 as shown in the Appendix also remains unchanged.

6.2.2.4 Moments Acting On The Wing Joint

The last two rows of $\mathbf{F}_{dyn}$ represent the dynamic moments acting on the wing joints.

$$\mathbf{F}_{dyn,R_i} = \left\{\mathbf{h}_i^{\times} + \left[\mathbf{C}_{i1}\left(\mathbf{v}_1 + \boldsymbol{\omega}_1^{\times}\mathbf{b}_h + \boldsymbol{\omega}_1^{\times}\mathbf{C}_{1h}\mathbf{b}_i\right)^{\times}\mathbf{C}_{1i} + \mathbf{C}_{ih}\left(\boldsymbol{\omega}_{ph}^{\times}\mathbf{b}_i\right)^{\times}\mathbf{C}_{hi}\right]\mathbf{c}_i^{\times}\right\}\left(\mathbf{C}_{i1}\boldsymbol{\omega}_1 + \mathbf{C}_{ih}\boldsymbol{\omega}_{ph} + \boldsymbol{\omega}_{pi}\right) + \mathbf{A}_3$$

Eqn 6.26

These are the moments that the torque of the actuator motor has to overcome in order to follow the prescribed motion. Note that the index i now represents wings and the index h represents the stroke plane actuators.

The expression for the angular momentum of the wing, h_i for i = 4,5, given in Eqn 2.18 as a vector form, will now be replaced in $\mathcal{F}_i$ by

$$\mathbf{h}_i = \mathbf{c}_i^{\times}\mathbf{C}_{il}\mathbf{v}_1 + \mathbf{J}_{il}\mathbf{C}_{il}\boldsymbol{\omega}_1 + \mathbf{J}_{ih}\mathbf{C}_{ih}\boldsymbol{\omega}_{ph} \qquad \text{Eqn 6.27}$$

Inspecting the terms in the expression and omitting odd powered terms of $\overline{\omega}_{pi}$, results in the following expression for the dynamic moments of the wing

$$\mathbf{F}_{dyn,R_i} = \left\{ \mathbf{h}_i^{\times} + \left[\mathbf{C}_{il}\left(\mathbf{v}_1 + \boldsymbol{\omega}_1^{\times}\mathbf{b}_h + \boldsymbol{\omega}_1^{\times}\mathbf{C}_{1h}\mathbf{b}_i\right)^{\times}\mathbf{C}_{li} + \mathbf{C}_{ih}\left(\boldsymbol{\omega}_{ph}^{\times}\mathbf{b}_i\right)^{\times}\mathbf{C}_{hi}\right]\mathbf{c}_i^{\times}\right\}\left(\mathbf{C}_{il}\boldsymbol{\omega}_1 + \mathbf{C}_{ih}\boldsymbol{\omega}_{ph}\right) + \overline{\mathbf{A}}_3$$

Eqn 6.28

where $\overline{\mathbf{A}}_3$ is obtained by removing odd powered terms of $\overline{\omega}_{pi}$ from Eqn 2.34

$$\overline{\mathbf{A}}_3 = \mathbf{c}_i^{\times}\left[\left(\mathbf{C}_{im}\boldsymbol{\omega}_{pm}\right)^{\times}\mathbf{C}_{il}\mathbf{v}_1\right] - \overset{+}{\mathbf{J}}_{il}\mathbf{C}_{il}\boldsymbol{\omega}_1 - \mathbf{J}_{il}\left(\mathbf{C}_{il}\boldsymbol{\omega}_1\right)^{\times}\mathbf{C}_{im}\boldsymbol{\omega}_{pm} \qquad \text{Eqn 6.29}$$

and $\overset{+}{\mathbf{J}}_{il}$, obtained from Eqn D.31, becomes after removing odd powered terms of $\overline{\omega}_{pi}$

$$\overset{+}{\mathbf{J}}_{il} = -m_i\mathbf{d}_i^{\times}\left[\left(\mathbf{C}_{im}\boldsymbol{\omega}_{pm}\right)\left(\mathbf{C}_{il}\mathbf{b}_h\right)^{T} - \left(\mathbf{C}_{il}\mathbf{b}_h\right)\left(\mathbf{C}_{im}\boldsymbol{\omega}_{pm}\right)^{T}\right] \qquad \text{Eqn 6.30}$$

6.2.2.5 Time Averaged Dynamic Force Vector

Finally, the time averaged dynamic force vector can now be assembled using equations derived in sections 6.2.2.1 to 6.2.2.4 as follows:

$$\overline{\mathbf{F}}_{dyn} = \begin{bmatrix} -\boldsymbol{\omega}_1^{\times}\overline{\mathbf{p}} + \overline{\mathbf{BB}} \\ -\boldsymbol{\omega}_1^{\times}\overline{\mathbf{h}}_{P_1} - \mathbf{v}_0^{\times}\overline{\mathbf{p}} - \overline{\mathbf{c}}^{\times}\mathbf{v}_1 - \overline{\mathbf{J}}\boldsymbol{\omega}_1 - \left(\mathbf{J}_{12} + \overline{\mathbf{J}}_{142}\right)\mathbf{C}_{12}\boldsymbol{\omega}_{p2} - \left(\mathbf{J}_{13} + \overline{\mathbf{J}}_{153}\right)\mathbf{C}_{13}\boldsymbol{\omega}_{p3} - \overline{\overline{\mathbf{J}}}_{14}\mathbf{C}_{14}\overline{\boldsymbol{\omega}}_{p4} - \overline{\overline{\mathbf{J}}}_{15}\mathbf{C}_{15}\overline{\boldsymbol{\omega}}_{p5} \\ \left\{\mathbf{h}_2^{\times} + \mathbf{C}_{21}\left(\mathbf{v}_1 + \boldsymbol{\omega}_1^{\times}\mathbf{b}_2\right)^{\times}\mathbf{C}_{12}\mathbf{c}_4^{\times}\right\}\left(\mathbf{C}_{21}\boldsymbol{\omega}_1 + \boldsymbol{\omega}_{p2}\right) - \mathbf{b}_4^{\times}\mathbf{C}_{21}\boldsymbol{\omega}_1^{\times}\mathbf{C}_{14}\overline{\mathbf{p}}_4 - \overline{\mathbf{A}}_{1,2} - \overline{\mathbf{A}}_{2,2} \\ \left\{\mathbf{h}_3^{\times} + \mathbf{C}_{31}\left(\mathbf{v}_1 + \boldsymbol{\omega}_1^{\times}\mathbf{b}_3\right)^{\times}\mathbf{C}_{13}\mathbf{c}_5^{\times}\right\}\left(\mathbf{C}_{31}\boldsymbol{\omega}_1 + \boldsymbol{\omega}_{p3}\right) - \mathbf{b}_5^{\times}\mathbf{C}_{31}\boldsymbol{\omega}_1^{\times}\mathbf{C}_{15}\overline{\mathbf{p}}_5 - \overline{\mathbf{A}}_{1,3} - \overline{\mathbf{A}}_{2,3} \end{bmatrix}$$

Eqn 6.31

6.3 SUMMARY

The time averaged equations of motion for the micro air vehicle have been derived from the set of equations in Chapter 2 by removing the odd-powered terms of ω_{p4} and ω_{p4}. Furthermore, the degrees of freedom related to the wings have also been removed. This reduced the order of the equations from 18 to 12. The equations are summarised as follows:

$$\dot{\mathbf{V}} = \mathbf{M}^{-1}\left(\overline{\mathbf{F}} + \overline{\mathbf{F}}_{dyn}\right) \qquad \text{Eqn 6.32}$$

with

$$\mathbf{V} = [v_1 \;\; \omega_1 \;\; \omega_{p2} \;\; \omega_{p3}]^T \qquad \text{Eqn 6.2}$$

$$\mathbf{M} = \begin{bmatrix} m & -c^{\times} & -\left\{C_{12}\left(m_2 b_4^{\times} + c_2^{\times}\right) + C_{14} c_4^{\times} C_{42}\right\} & -\left\{C_{13}\left(m_3 b_5^{\times} + c_3^{\times}\right) + C_{15} c_5^{\times} C_{53}\right\} \\ c^{\times} & J & (J_{12} + J_{142}) & (J_{13} + J_{153}) \\ c_2^{\times} C_{21} + m_2 b_4^{\times} C_{21} & J_{21} C_{21} - m_4 b_4^{\times} C_{21} b_2^{\times} - b_4^{\times} C_{24} c_4^{\times} C_{41} & J_2 - b_4^{\times} C_{24} c_4^{\times} C_{42} & 0 \\ c_3^{\times} C_{31} + m_3 b_5^{\times} C_{31} & J_{31} C_{31} - m_5 b_5^{\times} C_{31} b_3^{\times} - b_5^{\times} C_{35} c_5^{\times} C_{51} & 0 & J_3 - b_5^{\times} C_{35} c_5^{\times} C_{53} \end{bmatrix}$$

Eqn 6.3

$$\overline{\mathbf{F}} = \begin{bmatrix} \sum_{i=1}^{5} C_{1i} \overline{f}_i \\ \sum_{i=1}^{5} C_{1i} \overline{g}_i + \sum_{i=1}^{5} \left(C_{1g} b_h^{\times} C_{1i} + C_{1h} b_i^{\times} C_{hi}\right) \overline{f}_i \\ \overline{g}_2 + \overline{g}_{p2} - C_{24} \overline{g}_{pmotor,4} + b_4^{\times} C_{24} \overline{f}_4 \\ \overline{g}_3 + \overline{g}_{p3} - C_{35} \overline{g}_{pmotor,5} + b_5^{\times} C_{35} \overline{f}_5 \end{bmatrix} \qquad \text{Eqn 6.4}$$

$$\overline{\mathbf{F}}_{dyn} = \begin{bmatrix} -\omega_1^{\times} \overline{p} + \overline{BB} \\ -\omega_1^{\times} \overline{h}_{p_1} - v_1^{\times} \overline{p} - \overline{c}^{\times} v_1 - \overline{J} \omega_1 - \left(\dot{J}_{12} + \overline{J}_{142}\right) C_{12} \omega_{p2} - \left(\dot{J}_{13} + \overline{J}_{153}\right) C_{13} \omega_{p3} - \overline{\dot{J}}_{14} C_{14} \overline{\omega}_{p4} - \overline{\dot{J}}_{15} C_{15} \overline{\omega}_{p5} \\ \left\{h_2^{\times} + C_{21}\left(v_1 + \omega_1^{\times} b_2\right)^{\times} C_{12} c_4^{\times}\right\}\left(C_{21} \omega_1 + \omega_{p2}\right) - b_4^{\times} C_{21} \omega_1^{\times} C_{14} \overline{p}_4 - \overline{A}_{1,2} - \overline{A}_{2,2} \\ \left\{h_3^{\times} + C_{31}\left(v_1 + \omega_1^{\times} b_3\right)^{\times} C_{13} c_5^{\times}\right\}\left(C_{31} \omega_1 + \omega_{p3}\right) - b_5^{\times} C_{31} \omega_1^{\times} C_{15} \overline{p}_5 - \overline{A}_{1,3} - \overline{A}_{2,3} \end{bmatrix}$$

Eqn 6.31

The time-averaged linear and angular momenta of the system are given by

$$\bar{\mathbf{p}} = m\mathbf{v}_1 - \mathbf{c}^{\times}\boldsymbol{\omega}_1 - \sum_{i=2}^{3}\left(\mathbf{C}_{1i}\mathbf{c}_i^{\times} + \mathbf{C}_{1j}\mathbf{c}_j^{\times}\mathbf{C}_{ji} + m_j\mathbf{C}_{1i}\mathbf{b}_j^{\times}\right)\boldsymbol{\omega}_{pi} \qquad \text{Eqn 6.6}$$

and

$$\bar{\mathbf{h}}_{P_1} = \mathbf{c}^{\times}\mathbf{v}_1 + \mathbf{J}\boldsymbol{\omega}_1 + \sum_{i=4}^{5}\left(\mathbf{J}_{1h} + \mathbf{J}_{1ih}\right)\mathbf{C}_{1h}\boldsymbol{\omega}_{ph} \qquad \text{Eqn 6.9}$$

The term $\overline{\mathbf{BB}}$ is given by Eqn 6.7

$$\begin{aligned}\overline{\mathbf{BB}} = &\sum_{i=1}^{3}\left[\left(\mathbf{C}_{1m}\boldsymbol{\omega}_{pm} + \mathbf{C}_{1n}\boldsymbol{\omega}_{pn}\right)^{\times}\mathbf{C}_{1i}\mathbf{c}_i\right]^{\times}\left(\boldsymbol{\omega}_1 + \mathbf{C}_{1h}\boldsymbol{\omega}_{ph} + \mathbf{C}_{1i}\boldsymbol{\omega}_{pi}\right)\\ &+\sum_{i=4}^{5}\left[\left(\mathbf{C}_{1m}\boldsymbol{\omega}_{pm}\right)^{\times}\mathbf{C}_{1i}\mathbf{c}_i\right]^{\times}\left(\boldsymbol{\omega}_1 + \mathbf{C}_{1h}\boldsymbol{\omega}_{ph}\right)\\ &+\sum_{i=4}^{5}\left[\left(\mathbf{C}_{1n}\bar{\boldsymbol{\omega}}_{pn}\right)^{\times}\mathbf{C}_{1i}\mathbf{c}_i\right]^{\times}\mathbf{C}_{1i}\bar{\boldsymbol{\omega}}_{pi} - \sum_{i=1}^{5}m_i\left(\boldsymbol{\omega}_1 + \mathbf{C}_{1h}\boldsymbol{\omega}_{ph}\right)^{\times}\mathbf{C}_{1h}\boldsymbol{\omega}_{ph}^{\times}\mathbf{b}_i\end{aligned} \qquad \text{Eqn 6.7}$$

and the time derivative of the first moment of inertia for the system is

$$\begin{aligned}\dot{\bar{\mathbf{c}}}^{\times} = &-\sum_{i=2}^{5}\mathbf{C}_{1i}\left[\mathbf{c}_i^{\times}\left(\mathbf{C}_{im}\boldsymbol{\omega}_{pm} + \mathbf{C}_{in}\boldsymbol{\omega}_{pn}\right)\right]^{\times}\mathbf{C}_{i1}\\ &+\sum_{i=4}^{5}\left\{\mathbf{C}_{1i}\left[\mathbf{c}_i^{\times}\left(\mathbf{C}_{im}\boldsymbol{\omega}_{pm}\right)\right]^{\times}\mathbf{C}_{i1} - m_i\mathbf{C}_{1m}\left(\mathbf{b}_i^{\times}\boldsymbol{\omega}_{pm}\right)^{\times}\mathbf{C}_{m1}\right\}\end{aligned} \qquad \text{Eqn 6.10}$$

Also, the time-derivatives of the second moments of inertia are given by Eqns 6.11, 6.19 and 6.20. The terms $\mathbf{A}_1$ is given by Eqn 6.25 while $\mathbf{A}_2$ is unchanged and given by Eqn 2.32.

CHAPTER 7

RESULTS WITH TIME-AVERAGED SIMULATION MODEL

7.1 INTRODUCTION

In Chapter 5, the trimming of the MAV using the full-order non-linear simulation model was described. It was seen that although the MAV was trimmed for a short duration, it quickly drifted away from this trim point due to the neutral stability of the vehicle. It was also seen that the need to compute a large number of steps within a single flap cycle in order to prevent aliaising meant that small time steps and hence a long computational time are necessary. Furthermore, the high frequency flapping and the low frequency body modes, such as the phugoid, resulted in a stiff system and the need for a stiff solver of the equations of motion. All the above led to an inefficient solution of the equations of motion, which can be avoided by simplifying the mathematical model through time-averaging the dynamics as described in Chapter 6.

7.2 TIME-AVERAGED AERODYNAMIC MODEL

The aerodynamic model was revised to deliver the time-averaged force and moment coefficients for the new simulation. Time averaging the aerodynamic force coefficients was carried out along the same scheme as described in Chapter 5.2.1.

The time-dependent aerodynamic moment vector was then calculated, assuming that it is due only to the aerodynamic forces and the moment arm l_{cp} between the point of action of the resultant aerodynamic force (assumed to be the centre of pressure) and the shoulder joint at P_i (i = 4,5), refer to Fig 5.1

The aerodynamic moment vector is thus

$$\mathbf{M}_{aero}(\tau) = \boldsymbol{l}_{cp}{}^{\times}\, \mathbf{F}_{aero}(\tau) \qquad \text{Eqn 7.1}$$

where

$$\mathbf{F}_{aero}(\tau) = \frac{1}{2}\rho\left(\overline{V}_{flap}\right)^2 S_{wing} \begin{bmatrix} C_{x_F}(\tau) \\ C_{y_F}(\tau) \\ C_{z_F}(\tau) \end{bmatrix} \qquad \text{Eqn 7.2}$$

Once the time-dependent force and moment vectors are known, they can be averaged over a flap cycle in the manner as described in Chapter 5.2. The time-averaged moment coefficients for (i = 4,5) are then found with the wingspan b_{wing} as reference length :

$$\mathbf{C}_{i,\overline{M}} = \frac{\overline{\mathbf{M}}_{i,aero}}{\frac{1}{2}\rho\left(\overline{V}_{flap}\right)^2 S_{wing} b_{wing}} \qquad \text{Eqn 7.3}$$

The time-averaged force coefficient (i = 4,5) vector is

$$\mathbf{C}_{i,\overline{F}} = \frac{\overline{\mathbf{F}}_{i,aero}}{\frac{1}{2}\rho\left(\overline{V}_{flap}\right)^2 S_{wing}} \qquad \text{Eqn 7.4}$$

The time-averaged aerodynamic data for $\overline{\chi} = 0°$ as a function of the phase φ between the pitch and flap degrees of freedom is curve-fitted and presented in Table 7.1.

	Fitted Curve
$\overline{C}_x$	$-0.1066\varphi + 0.37$
$\overline{C}_y$	$\pm (0.00757\varphi + 0.0045)$
$\overline{C}_z$	$0.1449\varphi - 0.309$
$\overline{C}_l$	$\pm (0.0386\varphi - 0.0688)$
$\overline{C}_m$	$-0.2062\varphi^4 + 0.9147\varphi^3 - 1.4412\varphi^2 + \varphi - 0.1796$
$\overline{C}_n$	$\pm (0.0518\varphi - 0.1562)$

Table 7.1 Time-averaged aerodynamic coefficients

7.3 TRIMMING THE MAV

Although MATLAB has a trimming function, the result returned by this function was not satisfactory. Numerical values for each of the states were found for the 'trim', but use of these numerical values to run the non-linear time-averaged simulation resulted in an untrimmed condition. The reason for this was not determined.

Hence, instead of using this MATLAB trimming function, the equations for the forces and moment balance given in Eqns 5.10 to 5.12 were used instead, these equations being applicable for the time-averaged model as well if the time-dependent forces, moments and DCMs are replaced by their time-averaged counterparts.

A trim routine was written for the iterative solution of the equations. Beginning with estimated initial values, the longitudinal acceleration $\ddot{x}$ was determined for the MAV using the simulation. The stroke plane angle κ can be adjusted iteratively using an

appropriate value for the gain k_κ in Eqn 7.5 until the longitudinal acceleration falls within the pre-set tolerance:

$$\kappa = \kappa_o + \Delta\kappa = \kappa_o + k_\kappa \ddot{x} \qquad \text{Eqn 7.5}$$

where $\kappa_o = \tan^{-1}\dfrac{C_{x,aero}}{|C_{z,aero}|}$ is the initial stroke plane angle and $C_{x,aero}$ and $C_{z,aero}$ are the appropriate aerodynamic force coefficients for the wing beat kinematics in use.

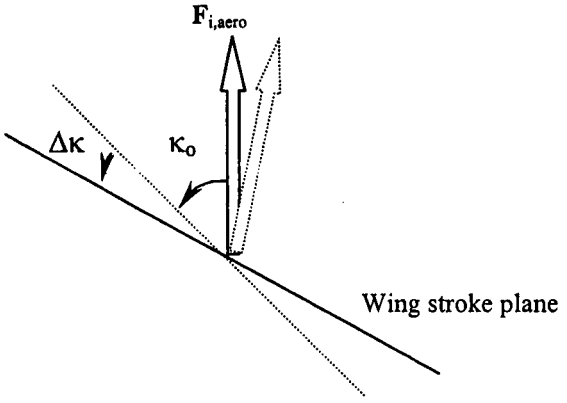

Fig 7. 1 Force balance in longitudinal axis

By maintaining the flap frequency at a constant 40 Hz, m_l (fuselage mass) and $\mathbf{d}_l$ (location of the centre of gravity of the fuselage from the origin of the fuselage axes system $P_l x_l y_l z_l$) are varied iteratively until the force and moment balance given by Eqns 5.10 to 5.12 are fulfilled. It is to be noted that $d_{ly} = 0$ for a symmetrical fuselage, which is assumed for simplicity. For the same reason, d_{lz} is also assumed to be zero. Hence, m_l and d_{lx} can be adjusted as follows:

$$m_l = m_{l,o} + k_m . \ddot{z} \qquad \text{Eqn 7.6}$$

$$d_{lx} = d_{lx,o} + k_d . \ddot{q}_b \qquad \text{Eqn 7.7}$$

The gains k_m and k_d can be appropriately selected. The trim values for three conditions lasting 1 second each were obtained as shown in Table 7.2 below, with the wing mass assumed to be 0.1 gram per wing

	m_l [grams]	d_{lx} [mm]	Mean Pitch	κ_o [°]	φ [°]
Trim 1	3.8090	-6.36235	0	76	90
Trim 2	4.3730	6.025	0	58.7	60
Trim 3	5.9557	-3.1462	30	7.45	90

Table 7.2 Trim Parameters for MAV

If the simulation continues for a longer period using the above trim parameters, it is found that the vehicle tends to drift away from the trim condition slowly as shown in Fig 7.1 for Trim 3.

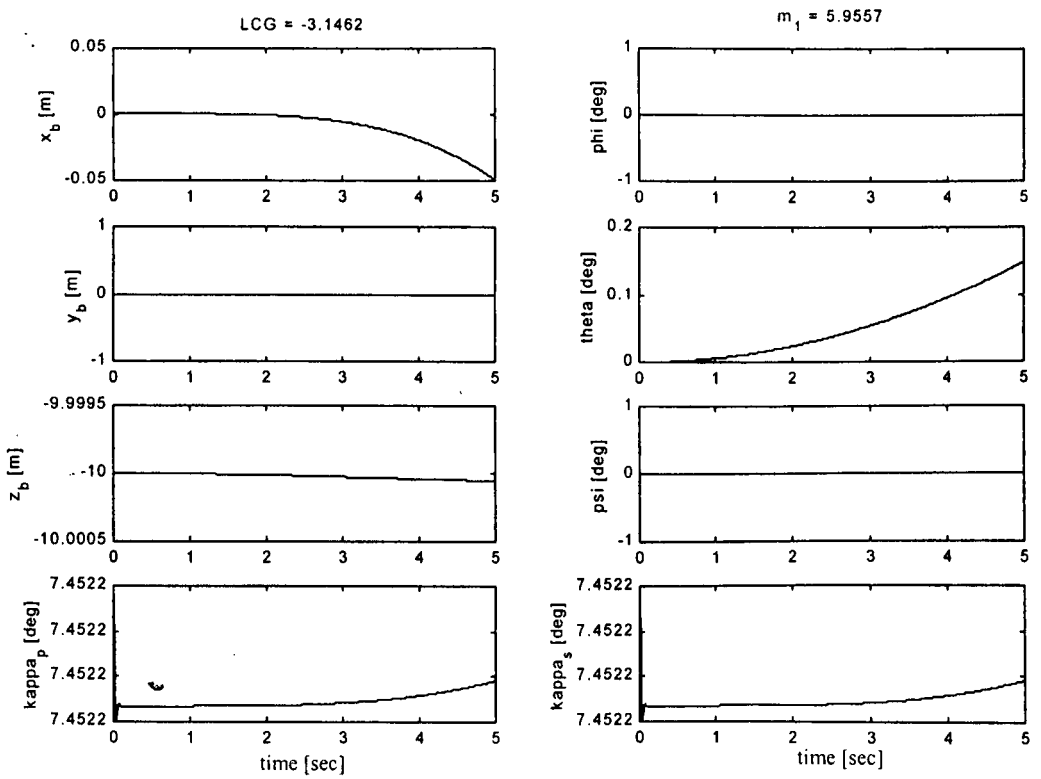

Fig 7.2 Drift from trim evident after prolonged simulation

This is a manifestation of both the trim routine as well as the vehicle dynamics. The longitudinal, vertical as well as angular accelerations were reduced iteratively but were still non-zero. This caused the vehicle to accelerate very slowly. Added to this, the vehicle is neutrally stable because the resultant force vector needs to point vertically in order to maintain hover. Any tilt in this vector causes the vehicle to accelerate forward, lose altitude and pitch. There is no restoring moment or force in the open loop to return the vehicle to the trim condition.

Fig 7.2 shows that the vehicle drifted away very slowly from the trimmed point and in the 5 seconds of simulation, the vehicle tilted nose up causing the force vector to point backwards. Hence, the vehicle drifts backwards for 50 mm behind the starting point.

7.4 OPEN LOOP LINEARISED DYNAMICS

7.4.1 LINEARISED DYNAMIC MODEL

The SIMULINK model is a non-linear model of the flapping wing MAV. MATLAB has a function that allows the linearised dynamic model to be extracted numerically and represented in state-space form with the matrices **A**, **B**, **C** and **D** such that

$$\dot{\mathbf{x}} = \mathbf{A}\mathbf{x} + \mathbf{B}\mathbf{u} \qquad \text{Eqn 7.8}$$

and

$$\mathbf{y} = \mathbf{C}\mathbf{x} + \mathbf{D}\mathbf{u} \qquad \text{Eqn 7.9}$$

The column vector **x** has 20 elements

$$\mathbf{x} = [u_b\ v_b\ w_b\ p_b\ q_b\ r_b\ \omega_{p2x}\ \omega_{p2y}\ \omega_{p2z}\ \omega_{p3x}\ \omega_{p3y}\ \omega_{p3z}\ x_b\ y_b\ z_b\ \phi\ \theta\ \psi\ \kappa_p\ \kappa_s]^T.$$

It is unlike the usual state vector because it includes the output of the simulation model. In fact, the first 12 being the states of the system of fuselage and the stroke plane actuator motors. The other 8 are the position of the fuselage and its orientation and the stroke plane angles κ_p and κ_s, being the output of the simulation model. This is a peculiarity of MATLAB and it is not the author's choice.

The output vector **y** is a 6×1 vector,

$$\mathbf{y} = [u_b\ w_b\ q_b\ x_b\ z_b\ \theta]^T.$$

The system inputs are, in general, the stroke plane angles (κ_p and κ_s), the actual centre of gravity location of the fuselage, the phase angle φ and the flapping frequency n. The use of mean pitch angle as a control variable was not investigated here. For the analyses in the longitudinal plane, the port and starboard kinematics are to be identical and hence only one value each of κ, n and φ needs to be defined. The control vector **u** is thus given by

The matrix **A** is a 20×20 matrix, **B** is a 20×4 matrix, **C** is a 6×20 matrix and **D** is a 6×4 matrix. For clarity, the **A**, **B** and **C** matrices are reproduced below for the case of Trim 2 with the phase φ being constant at 90°. The matrix **D** is a zero-matrix.

A =

0	0	0	0	0	0	0	0	0	0	0	0	0	0	0	0	-9.81	0	0	0
0	0	0	0	0	0	0	0	0	0	0	0	0	0	0	9.81	0	0	0	0
0	0	0	0	0	0	0	0	0	23.5	0	0	0	0	0	0	0	0	0	0
0	0	0	0	0	0	0	0	0	0	0	0	0	0	0	0	0	0	0	0
0	0	0	0	0	0	23.5	0	0	-23.5	0	0	0	0	0	0	0	0	2675	2675
0	0	0	0	0	0	0	0	0	0	0	0	0	0	0	0	0	0	0	0
0	0	0	0	0	0	-243.5	0	0	0	0	0	0	0	0	0	0	0	-2675	-27675
0	0	0	0	0	0	0	0	0	-243.5	0	0	0	0	0	0	0	0	0	0
0	0	0	0	0	0	0	0	0	0	0	0	0	0	0	0	0	0	0	0
0	0	0	0	0	0	-23.5	0	0	0	0	0	0	0	0	0	0	0	-27675	-2675
0	0	0	0	0	0	0	0	0	0	0	0	0	0	0	0	0	0	0	0
0	0	0	0	0	0	0	0	0	0	0	0	0	0	0	0	0	0	0	0
1	0	0	0	0	0	0	0	0	0	0	0	0	0	0	0	0	0	0	0
0	1	0	0	0	0	0	0	0	0	0	0	0	0	0	0	0	0	0	0
0	0	1	0	0	0	0	0	0	0	0	0	0	0	0	0	0	0	0	0
0	0	0	1	0	0	0	0	0	0	0	0	0	0	0	0	0	0	0	0
0	0	0	0	1	0	0	0	0	0	0	0	0	0	0	0	0	0	0	0
0	0	0	0	0	1	0	0	0	0	0	0	0	0	0	0	0	0	0	0
0	0	0	0	0	0	0	0	0	1	0	0	0	0	0	0	0	0	0	0
0	0	0	0	0	0	1	0	0	0	0	0	0	0	0	0	0	0	0	0

B =

0	0	0	0
0	0	0	0
0	0	0	0
-5350	0	-3006	0
0	0	0	0
30350	0	3006	0
0	0	0	0
0	0	0	0
30350	0	3006	0
0	0	0	0
0	0	0	0
0	0	0	0
0	0	0	0
0	0	0	0
0	0	0	0
0	0	0	0
0	0	0	0
0	0	0	0

C =

1	0	0	0	0	0	0	0	0	0	0	0	0	0	0	0	0	0	0	0
0	0	1	0	0	0	0	0	0	0	0	0	0	0	0	0	0	0	0	0
0	0	0	0	1	0	0	0	0	0	0	0	0	0	0	0	0	0	0	0
0	0	0	0	0	0	0	0	0	0	0	0	0	0	0	0	1	0	0	0
0	0	0	0	0	0	0	0	0	0	0	0	1	0	0	0	0	0	0	0
0	0	0	0	0	0	0	0	0	0	0	0	0	0	1	0	0	0	0	0

7.4.2 OPEN LOOP EIGENVALUES AND EIGENVECTORS

The solution of the characteristic equation $s\mathbf{I} - \mathbf{A} = 0$ leads to twenty roots, s_1 to s_{20}. Sixteen of these are real roots at the origin, $s_i = 0$ for $i = 1..16$. The other four form two conjugate pairs. For the case of Trim 2, one pair has a natural frequency of 158 rad/sec and a damping ratio of 0.7, corresponding to those specified for the stroke plane actuator motors ($s_{17,18} = -110 \pm 114i$). The other pair has a natural frequency of 174 rad/sec and a damping ratio of 0.77 ($s_{19,20} = -134 \pm 112i$). This is the short period mode of the fuselage and changing the fuselage pitch inertia can be shown to affect the natural frequency.

The corresponding eigenvectors can also be extracted numerically from the linearised dynamic model described above. These are shown below for the matrices **A** and **B** of Trim 2 given in the previous section. Each of the twenty eigenvectors (λ_1 to λ_{20}) has twenty elements corresponding to the twenty elements of the vector **x**. For all the above trim cases, most of the eigenvectors have elements that are zero except in the dominant degrees of freedom, which identifies the mode.

For example, the solution of the characteristic equation $s_1 = 0$ has an eigenvector λ_1 with all its elements being zero except for the 13th being one, corresponding to x_b, indicating that the mode is a forward surge mode.

Going through the twenty eigenvectors, it can be seen that the vehicle motion at hover can be characterised as 4 forward surge modes, 2 heave modes, 8 lateral modes that can be excited through asymmetrical wing kinematics, 2 heading modes, all being neutrally stable. In addition, it has two oscillatory modes corresponding to the stroke plane actuator motion in terms of κ and the short period pitch oscillation.

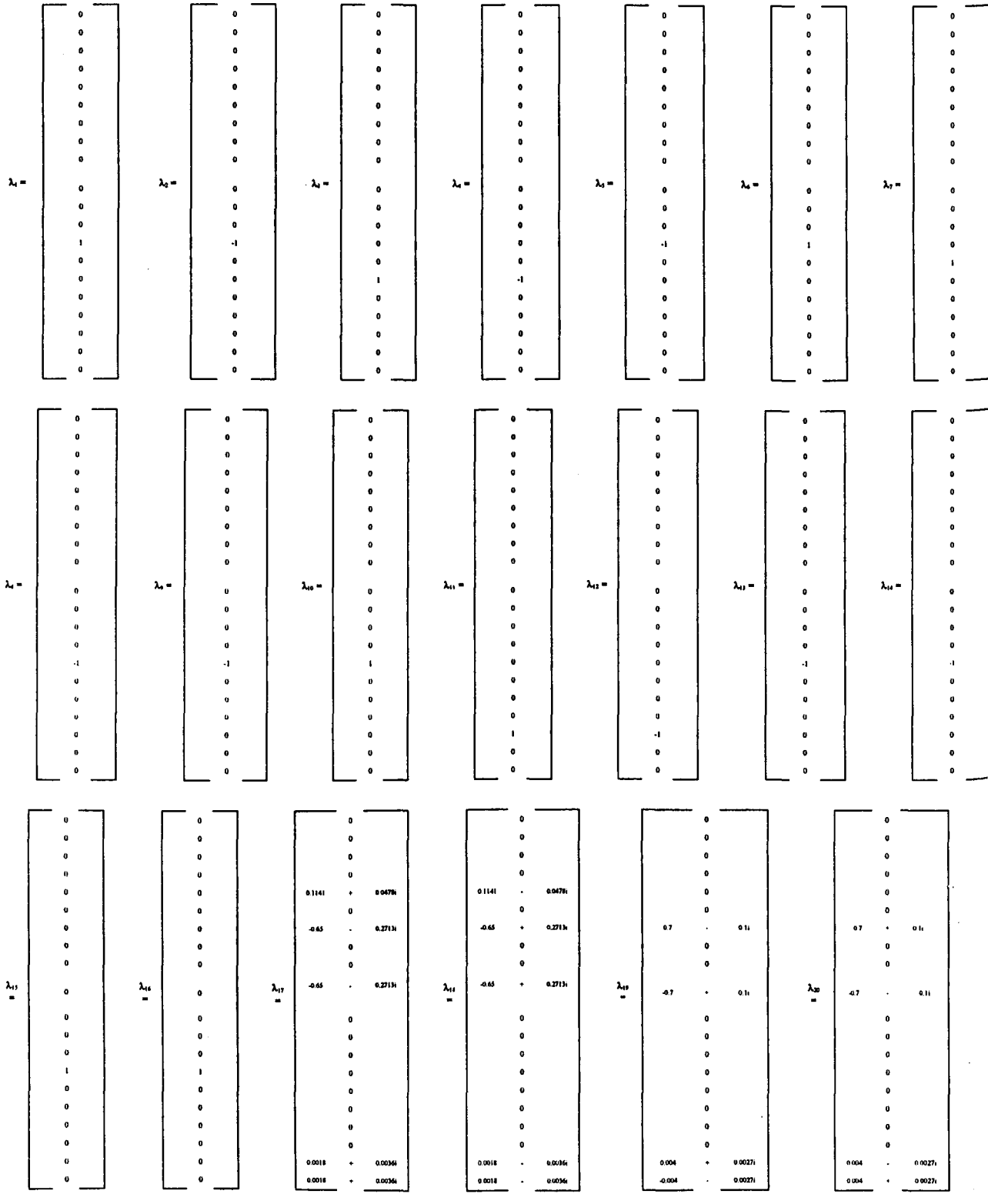

7.4 STABILISING THE PITCH MODE

The eigenvectors λ_{17} and λ_{18} correspond to the oscillatory pitching mode of the fuselage as it can be seen that the dominant degrees of motion are q_b, ω_{2x}, ω_{3x}, κ_p and κ_s. It is evident that feedback of the fuselage pitch rate to one of three possible mechanisms (control effectors) can be used to stabilise the motion. The three control effectors can be the stroke plane angle κ, flap frequency n or the CG location of the fuselage d_{1x}. The use of phase φ as a control effector shall not be investigated yet until a better grasp of the vehicle dynamics is first obtained.

In the control system design for the MAV, it is required that each of the three degrees of freedom x_B, z_B and θ (called controlled variables) be controlled directly with a separate control effector. Since κ affects the direction of the resultant force, it may be used to control the pitching moment because the moment arm will be affected by a change in κ. However, as it affects the force direction as well and therefore the longitudinal acceleration directly, it shall be reserved for the longitudinal (fore-aft) motion.

The dynamic pressure is proportional to the square of the flap frequency n. Changes in n will thus affect the force magnitude. Since this can be used to effectively control the vertical acceleration, it will be reserved as a control effector for the vertical motion.

The CG location affects the moment arm and hence the pitching moment directly. It is thus possible to feedback the fuselage pitch rate to the centre of gravity location $\mathbf{d}_1$ and in particular its longitudinal component d_{1x} in order to stabilise the pitch degree of freedom.

The linear transfer function for the pitch rate response due to a small perturbation Δd_{1x} obtained numerically from MATLAB for the case Trim 2 is given by

$$\frac{q_b(s)}{\Delta d_{1x}(s)} = G(s) = \frac{-3006.3(s+110-113.58i)(s+110+113.58i)}{s(s+133.5-111.9i)(s+133.5+111.9i)} \qquad \text{Eqn 7.10}$$

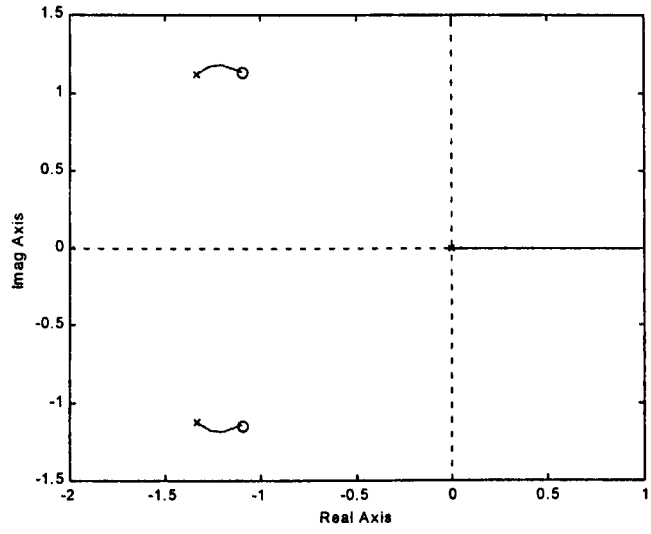

Fig 7.3 Root Locus for Negative Feedback of Pitch Rate q_b to CG Location d_{1x}

The root locus for negative feedback of pitch rate to the CG location is shown above in Fig 7.3 and it can be seen that the pole at the origin moves into the positive s-plane indicating an unstable system for any feedback gain.

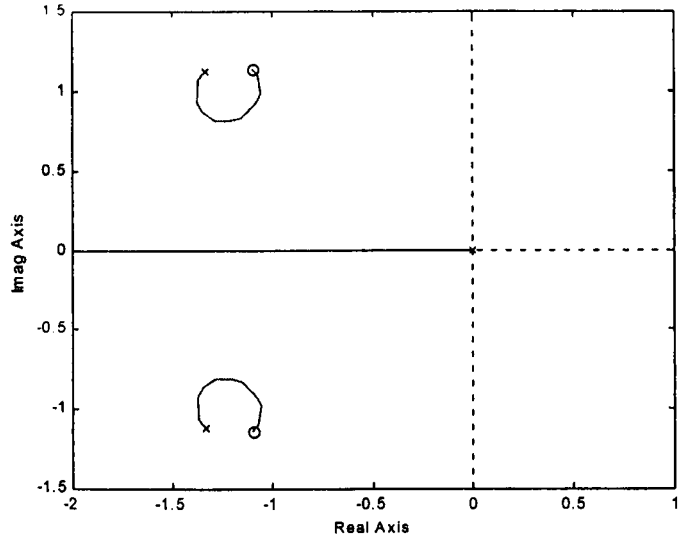

Fig 7.4 Root Locus for Positive Feedback of Pitch Rate q_b to CG Location d_{1x}

Fig 7.4 shows the root locus of the system for positive feedback of pitch rate to CG location. Here, it can be seen that the pole at the origin now tends towards -∞, signifying a stable system. Physically, this means that a positive (nose-up) pitching requires that the CG be shifted in the positive sense (forward) to increase the moment arm so that the upward lift force would generate a negative moment about the centre of gravity to restore the fuselage attitude.

A positive feedback with positive gain with the root locus shown in Fig 7.5 can be implemented as a negative feedback system with negative gain. For consistency, this shall be adopted and the closed loop system is shown in Fig 7.6.

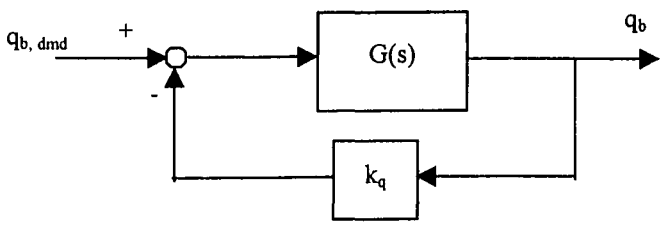

Fig 7.5 Pitch Stability through Feedback of Pitch Rate q_b to CG Location d_{1x}

For the open loop system with transfer function G(s) given by Eqn 7.10, the closed loop characteristic equation for negative feedback is given by $\Delta(s) = 1+kG(s)$ or

$$s^3 + (267+k)s^2 + (30350+220k)s + 25000k = 0 \qquad \text{Eqn 7.11}$$

This closed loop characteristic equation has a pair of conjugate roots and a real root whose position determines the exponential rate of decay. The more negative the real root, the faster the decay. If s = -40 is empirically chosen, k is found to be 48 using the root locus function of MATLAB, and Eqn 7.11 becomes

$$s^3 + 315s^2 + 40910s + 1.2e^6 = 0 \qquad \text{Eqn 7.12}$$

The closed loop roots of which being s = -40.2, -137.4 ± 105i. It is to be noted that the gain k in MATLAB refers to $K_{ss}.k_q$, where K_{ss} = -3006.3, the steady state gain for the open loop transfer function G(s). Hence k = $-3006.3k_q$ and thus k_q = -0.016 m.s.rad^{-1}.

The pitch stabilisation loop shown in Fig 7.5 is implemented with the pitch rate gain selected to be k_q = -0.016 m.s.rad^{-1}. Fig 7.6 shows the response of the pitch-stabilised system compared to the open loop system. It can be seen that the fuselage pitch remains horizontal throughout the simulation when it previously diverged. More importantly, the vehicle remained around the initial position when it previously drifted backwards due to the positive drift in pitch of the fuselage.

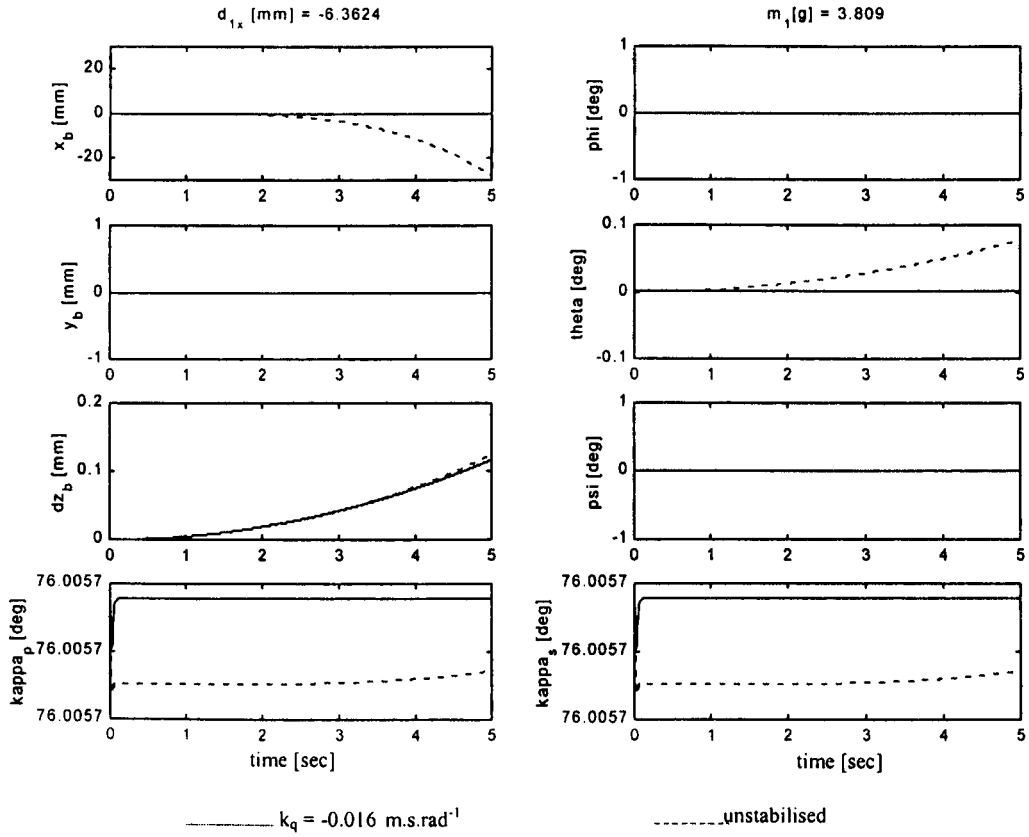

Fig 7.6 Comparison of Response for Pitch-stabilised and Unstabilised System (k_q = -0.016 m.s.rad^{-1})

CHAPTER 8

FLIGHT CONTROL SYSTEM DESIGN FOR LONGITUDINAL AXES

8.1 INTRODUCTION

The previous chapter has shown that the vehicle is neutrally stable in hover and will drift very slowly from the trimmed point due to any slight tilt of the resultant force vector from the vertical. This tilt was the result of the difficulty in obtaining a perfect numerical moment balance in the simulation and the fuselage thus has non-zero pitch acceleration. It was seen in Fig 7.6 that in the open loop the vehicle pitched up only 0.1° within 5 seconds but it was pushed 30 mm backwards.

It was also shown in the same figure that it was possible to stabilise the vehicle in pitch by feeding the pitch rate back to the centre of gravity location. In the pitch-stabilised system of Fig 7.5, with k_q = -0.016 m.s.rad^{-1}, it was shown in Fig 7.6 that the pitch attitude remained horizontal at all times and there was no drift in the horizontal position of the vehicle.

It was also shown that the vehicle loses height gradually, due to the tilt of the force vector away from the vertical and also because the dynamic pressure was not sufficient to sustain the vehicle. It was necessary to reduce the vehicle mass further. This can be achieved by reducing the tolerance of the trim routine further. An alternative would be to form a closed loop system in order to drive the error between the demanded and actual position to zero.

Ellington [1999] has suggested a number of ways insects deal with their stability and control. Change of stroke plane angle, the mean flap angle of the wings, wing angles of attack during the flapping cycle or deflecting the abdomen are some of these mechanisms that can be employed singularly or in combination.

The experimental determination of the wing aerodynamics described in Chapter 4 examined the effects of phase shifts between the wing pitch and flap angles. Changes in wing pitch affects the wing angle of attack directly. Hence, changes in phase φ can be treated as one of the many possible ways in which the angle of attack of the wing is controlled.

8.2 THE CONTROL CONCEPTS

To control the vehicle, besides a moment balance, the force magnitude and direction must be controllable. In the studies described in this chapter, three different combinations of some of the mechanisms employed in the insect world were assessed in maintaining the stability and control of the MAV. These permutations are listed in Table 8.1 below. Due to time constraint, the effects of mean flap angle were not investigated.

Control Concept	Pitch Moment Balance	Force Direction	Force Magnitude
1	CG location d_{1x}	Stroke plane tilt	Flap frequency
2		Stroke plane tilt	Phase Variation
3		Fuselage tilt through Δd_{1x}	Phase Variation

Table 8.1 Definition of the Control Concepts assessed in the study

8.2.1 Control Concept 1

In Control Concept 1, the force magnitude is controlled by variation of the flapping frequency which changes the dynamic pressure. The stroke plane angle is free to tilt. This tilt controls the direction of the aerodynamic force with respect to the vertical.

8.2.2 Control Concept 2

In Control Concept 2, the force magnitude is controlled by variation of the phase φ between the flap and pitch attitudes of the wing. This changes the angle of attack of the wing and thus affects the magnitude. The direction of the aerodynamic force is also inherently affected by this change of phase.

The direction of the aerodynamic force is controlled by the stroke plane tilt as in Control Concept 1.

8.2.3 Control Concept 3

In Control Concept 3, the force magnitude is also controlled by a variation of the phase φ between the flap and pitch attitudes of the wing. As in Concept 2, the direction of the aerodynamic force is also inherently affected by this change of phase.

In this concept, the stroke plane angle is fixed with respect to the fuselage. The direction of the aerodynamic force is controlled by the tilt of the fuselage, effected by a shift in the fuselage CG. By moving the CG, the moment balance is changed causing the fuselage to tilt to the desired attitude and with the stroke plane fixed, the aerodynamic force is pointed to the required direction.

The advantage of Concept 3 is that there is no need for the stroke plane actuators in the design. The actuator motor required to shift the CG is a pre-requisite for moment balance for all three concepts. Thus, a weight reduction can be realised by this design. Fig 5.9 of Chapter 5.3 shows two possible means of achieving a CG shift.

In the following sections, the flight control systems for the three concepts are designed based on the Trim Case 2 of Table 7.2, with zero mean wing pitch.

8.3 CONTROL CONCEPT 1

The control system for this concept is shown in Fig 8.1.

It consists of

(a) a pitch stability loop with feedback of the pitch rate to the fuselage CG location. The feedback gain is k_q. This loop stabilises the vehicle in the pitch axis.

(b) a rate of climb control loop with feedback of the climb rate to the flap frequency.

(c) a height control loop with feedback of the vertical position z_b of the vehicle to a P+I controller. The output of this controller is connected to the rate of climb control loop by a summation block. The result determines the demanded flapping frequency.

(d) a CG compensation path that determines CG shift dependent on the demanded flap frequency to maintain moment balance about the pitch axis

(e) a speed control loop with feedback of the forward velocity of the vehicle to the stroke plane angle

(f) a horizontal position control loop with feedback of the vertical position x_b of the vehicle to a P+I controller. The output of this controller is connected to the speed control loop by a summation block. The result determines the demanded stroke plane angle.

The pitch stability loop has been described in Chapter 7 and will not be repeated here.

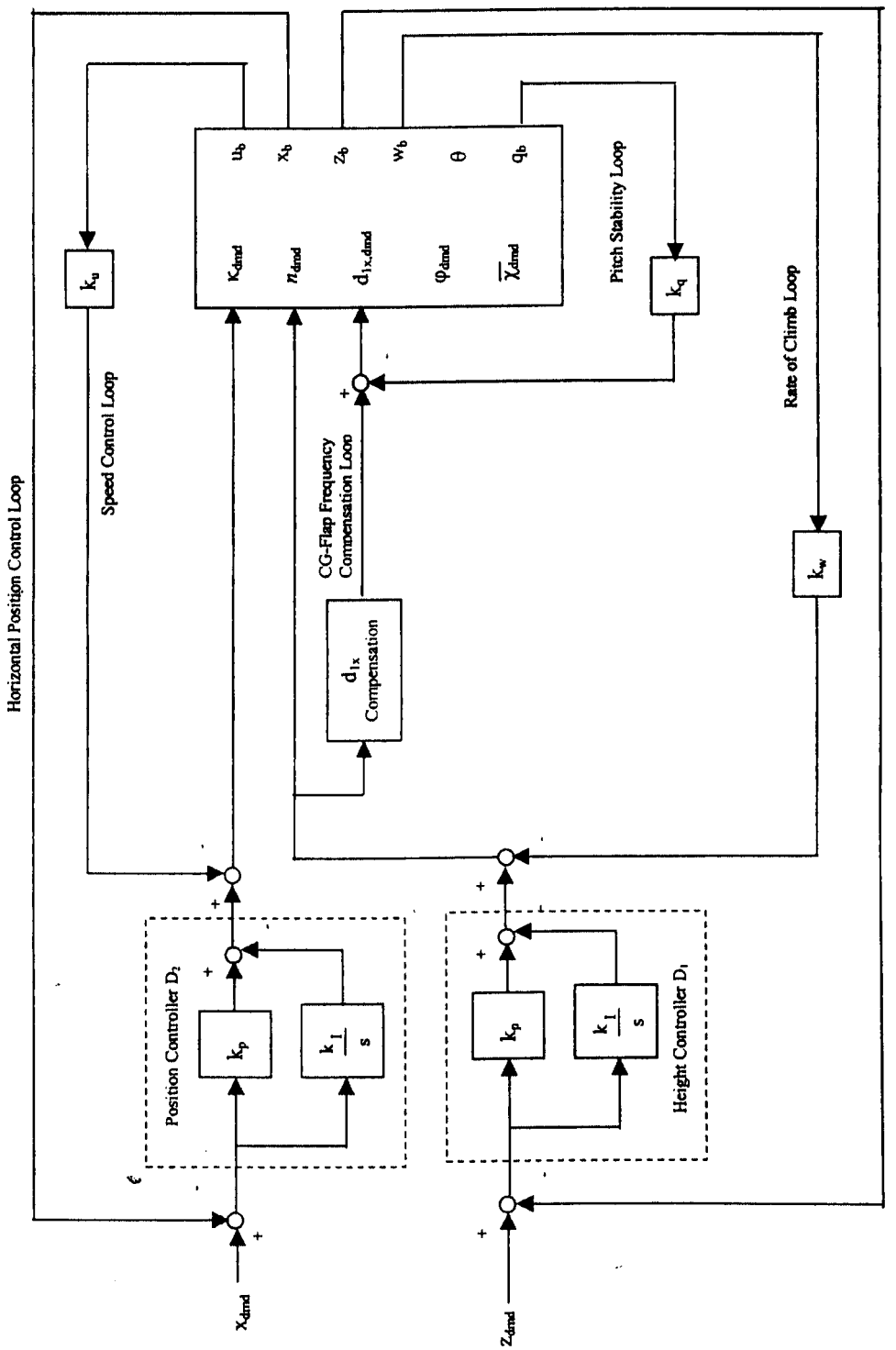

Fig 8.1 Flight Control System Block Diagram for Concept 1

8.3.1 DESIGN OF THE RATE OF CLIMB CONTROL LOOP

The dynamic pressure is proportional to the square of the flap frequency and by varying the flap frequency, the lift and therefore the vertical acceleration $\dot{w}_b$ for a given vehicle mass can be controlled.

However, the moment balance as shown in Eqn 5.10 indicates that with the wing attachment points fixed on the fuselage, i.e. b_i = constant, there will be a moment imbalance unless $\mathbf{d}_l$, and more specifically d_{lx}, is also varied accordingly. As the perturbation moment is aerodynamic in nature, it is proportional to the dynamic pressure or the square of flapping frequency. Hence, d_l must be varied inversely proportional to the ratio of the actual flapping frequency to the nominal flapping frequency.

$$\frac{d_{lx,dmd}}{d_{lx,nom}} = \left(\frac{n_{dmd}}{n_{nom}}\right)^2 \qquad \text{Eqn 8.1}$$

This scheme is shown simplified in Fig 8.2.

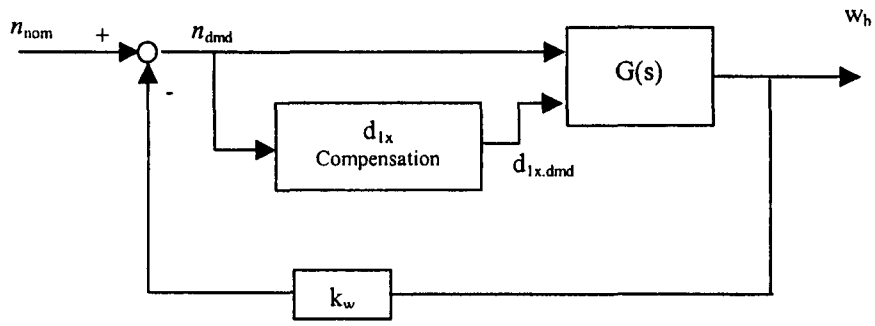

Fig 8.2 Rate of Climb Control Loop

G(s) is the transfer function of the response of vertical speed to a perturbation in the flap frequency for the pitch-stabilised system. G(s) is given by Eqn 8.2 after all the common terms are removed from the numerator and denominator

$$\frac{w_b(s)}{n_{dmd}(s)} = G(s) = \frac{K_{fw}}{s} \qquad \text{Eqn 8.2}$$

Eqn 8.2 implies that the vertical acceleration $\dot{w}_b$ is proportional to the flapping frequency. The constant of proportionality K_{fw} is the gradient with which w_b increases with time for a unit step input of n_{dmd}. K_{fw} is given in the linearised model as $-2.1e^{-8}$. This is an exceptionally small number. In the non-linear simulation, a step input in the flapping frequency to the system (Fig 8.2) results in the response shown in Fig 8.3. The rate of climb w_b shows a constant increase to -2.5 ms^{-1} over a period of 5 seconds, corresponding to a K_{fw} of -0.5 ms^{-2} Hz^{-1}.

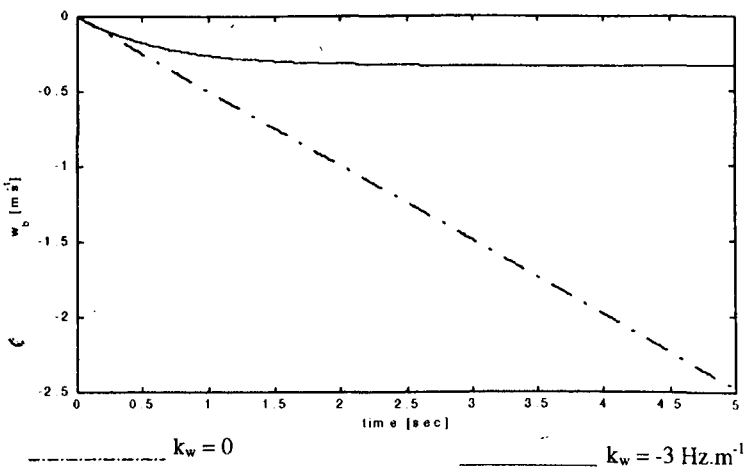

Fig 8.3 Response to a step input in flapping frequency of 1 Hz with and without climb rate stabilisation in pitch-stabilised system

The closed loop transfer function of the negative feedback system (Fig 8.1) is given by

$$G_2(s) = \frac{w_b(s)}{n_{dmd}(s)} = \frac{G(s)}{1 + k_w G(s)} \qquad \text{Eqn 8.3}$$

The closed loop characteristic equation is thus

$$s + k_w K_{fw} = 0 \qquad \text{Eqn 8.4}$$

with a single real pole at $s = - k_w K_{fw}$. The choice of this pole is arbitrary noting that the more negative it is, i.e. $k_w K_{fw}$ positive, the faster would be the response. Assuming the pole is to be located at s = -1.5, then $k_w = -3$ Hz.m^{-1}.s since $K_{fw} = -0.5$ ms^{-2} Hz^{-1}.

Fig 8.3 also shows the response of w_b to a unit step input in n_{dmd} with w_b feedback. The steady state value of w_b in the case with feedback is –0.333 ms^{-1}. The closed loop transfer function of the system, Eqn 8.3, can also be written as

$$\frac{w_b(s)}{n_{dmd}(s)} = G_2(s) = \frac{K_{fw}}{s + k_w K_{fw}} \qquad \text{Eqn 8.5}$$

Applying the final value theorem ($s \to 0$ when $t \to \infty$), the steady state value of w_b is given by

$$w_{b(t=\infty)} = \lim_{s \to 0} \left(\frac{K_{fw}}{s + k_w K_{fw}} \right) = \frac{1}{k_w} \qquad \text{Eqn 8.6}$$

corresponding to the w_b seen in the simulation.

8.3.2 DESIGN OF THE HEIGHT CONTROL LOOP

Integrating the output of the control system depicted in Fig 8.2 results in the vertical position z_b of the vehicle. If the error signal from the demanded position of the vehicle and the actual position is obtained and passed to a controller with the transfer function $D_1(s)$, the resulting system would be as shown in the following design

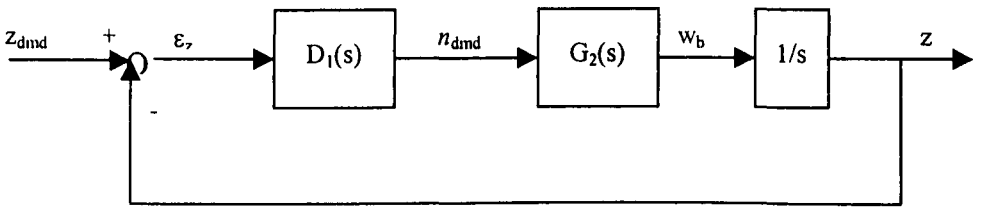

Fig 8.4 Height Control Loop

where $G_2(s)$ is the closed loop transfer function of the vertical speed stability system of Eqn 8.5. The effects of different controller transfer function $D_1(s)$ for the system can be studied.

8.3.2.1 Proportional Controller

In a proportional control system, $D_1(s) = k_p$, the proportional gain. The open loop transfer function for the position due to an input for the demanded position is given by

$$\frac{z_b(s)}{z_{b,dmd}(s)} = G_3(s) = D_1(s)G_2(s)\frac{1}{s} = \frac{k_p K_{fw}}{s(s + k_w K_{fw})} \qquad \text{Eqn 8.7}$$

The closed loop transfer function for the system is hence

$$\frac{z_b(s)}{z_{b,dmd}(s)} = G_4(s) = \frac{k_p K_{fw}}{s(s + k_w K_{fw}) + k_p K_{fw}} = \frac{k_p K_{fw}}{s^2 + ks + k_p K_{fw}} \qquad \text{Eqn 8.8}$$

Comparing the above closed loop transfer function of the system and the standard second order differential equation, $k = k_w.K_{fw} = 2\zeta\omega_n = 1.5$. Hence, if the response is to have a damping ratio of 0.7, then clearly ω_n must be 1.07 rad/sec. This results in $k_pK_{fw} = \omega_n^2 = 1.07^2 = 1.1449$ or $k_p = -2.29$ Hz.m^{-1}.s.

Fig 8.5 shows the response of z_b to a step input for z_{dmd} of –10 mm in the height control system with proportional feedback from both the linear transfer function of Eqn 8.8 and the non-linear time-averaged simulation model of Fig 8.4. There is a slight difference in the initial few seconds where the linear transfer function shows slightly higher overshoot and faster response. The demanded position is reached after about 7 seconds.

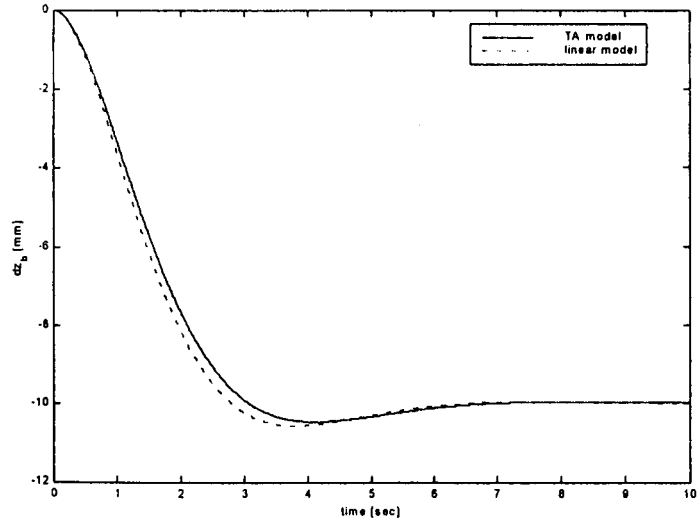

Fig 8.5 Response of z_b to a Step Input of Magnitude –10mm in Height Control with Proportional Controller [k_w = -3 Hz.m^{-1}.s, k_p = -2.49 Hz.m^{-1}]

In order to have a faster response, ω_n was set to 20 rads^{-1} and the damping ratio ζ at 0.7. This results in k_w = -56 Hz.m^{-1}.s and k_p = -800 Hz.m^{-1} and the corresponding responses from both the linear and time-averaged models are shown in Fig 8.6. There is a better correlation between the two models. The demanded position is reached after about 0.4 seconds.

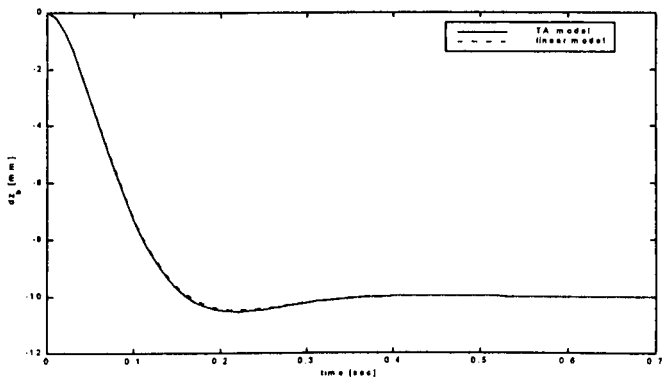

Fig 8.6 Response of z_b to a Step Input of Magnitude –10mm in Height Control with Proportional Controller [k_w = -56 Hz.m^{-1}.s, k_p = -800 Hz.m^{-1}]

The response to a ramp input of gradient –10 mms^{-1} is shown in Fig 8.6 for the above system. It shows that the response lags behind the input ramp for this system and has poor tracking behaviour because the system is of Type I.

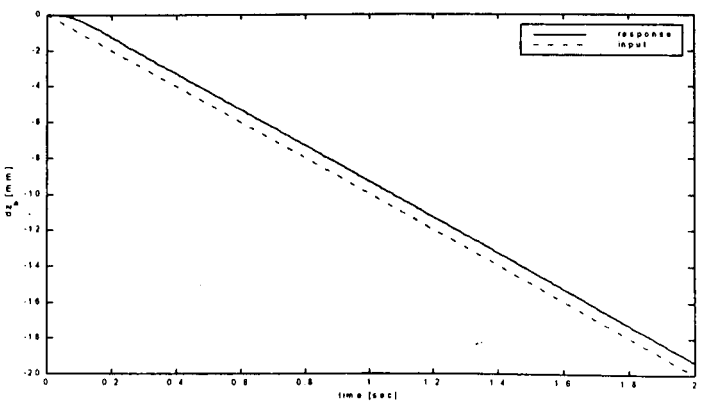

Fig 8.7 Response of z_b to a Ramp Input of Gradient –10 mms^{-1} in Height Control with Proportional Controller [k_w = -56 Hz.m^{-1}.s, k_p = -800 Hz.m^{-1}]

8.3.2.2 Proportional plus Integral Controller

The proportional controller described in the previous section results in a tracking error for ramp inputs and can be corrected using a proportional plus integral controller with the standard transfer function

$$D_1(s) = k_p\left(1+\frac{1}{T_I s}\right) = \frac{k_p(T_I s+1)}{T_I s} = \frac{k_p s + k_I}{s} \qquad \text{Eqn 8.9}$$

where $k_I = \frac{k_p}{T_I}$.

Ziegler and Nichols [1942] suggested a method to 'tune' the controller. First, the ultimate gain k_{ult}, which is the value of k_p at which the system is marginally stable, and the period of oscillation P_{ult} are to be determined. The gains are then set, with $k_p = 0.45k_{ult}$ and $T_I = 0.833P_{ult}$. Following this suggestion, it was found that $k_{ult} = 2500$ Hz.m^{-1} and $P_{ult} = 0.33$ second. This would have resulted in $k_p = 1125$ Hz.m^{-1} and $T_I = 0.58$ sec. This suggestion was not feasible as the proportional gain was much too high. Besides, the response was also found to be poorly damped. Alternatively, the characteristic equation of the system can be examined and the control gains determined analytically.

The open loop transfer function for the position due to an input for the demanded position is given by

$$\frac{z_b(s)}{z_{b,dmd}(s)} = G_5(s) = D_1(s)G_2(s)\frac{1}{s} = \frac{(k_p s + k_I)K_{fw}}{s^2(s+k_w K_{fw})} \qquad \text{Eqn 8.10}$$

The closed loop transfer function for the height control system with this controller is then

$$\frac{z_b(s)}{z_{b,dmd}(s)} = G_6(s) = \frac{(k_p s + k_I)K_{fw}}{s^2(s + k_w K_{fw}) + (k_p s + k_I)K_{fw}}$$

Eqn 8.11

$$= \frac{(K_{fw}k_p s + K_{fw}k_I)}{(s^3 + k_w K_{fw} s^2 + k_p K_{fw} s + k_I K_{fw})}$$

The closed loop characteristic equation of the response in Eqn 8.11 is of order 3. If it is to have a real root and a conjugate pair, it is found that the response lags behind the demand by a magnitude determined by the real root. A small negative real pole (large integral time constant T_I) results in a large tracking error while a large negative real pole (small integral time constant) results in a 'hangover' in the step response. Fig 8.8 shows the responses to a ramp input for $T_I = 1$ sec and $T_I = 100$ sec, when the roots of the conjugate pair are set for $\zeta = 0.7$ and $\omega_n = 10$ rad/s (i.e. at -7±7.14i)

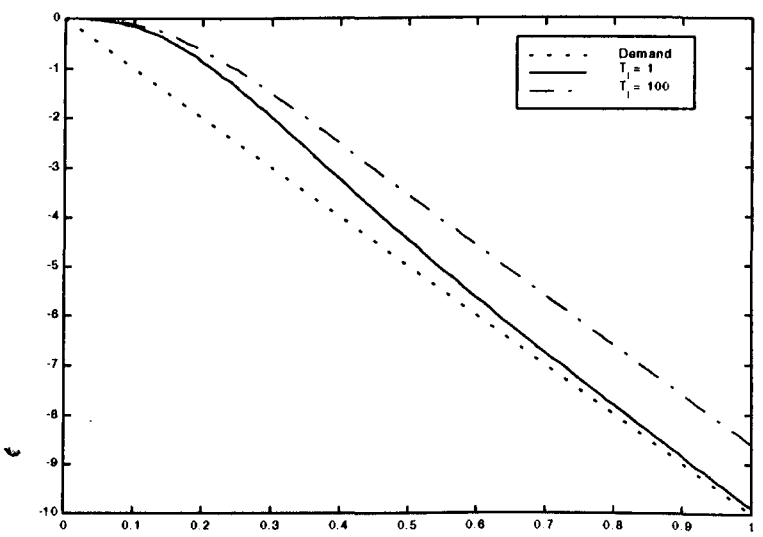

Fig 8.8 Effect of T_I on Response to Ramp Input

With the conjugate pair is selected with $\zeta = 0.7$ and $\omega_n = 10$ rad/s ($s = -7 \pm 7.14i$), and the real pole is placed at $s = -3$, the response is fast and tracking performance is good without degrading the step response too much.

The characteristic equation is thus $s^3 + 17s^2 + 142s + 300$. By comparing this with the denominator of Eqn 8.11, the gains are found to be $k_w = -34$ Hz.m^{-1}.s, $k_p = -284$ Hz.m^{-1}, $k_I = -600$ Hz.m^{-1}.s^{-1} (or $T_I = 0.473$ sec) when $K_{fw} = -0.5$ m.s^{-2}.Hz^{-1}. The step and ramp responses with this controller are shown in Fig 8.9 and the closed loop transfer function for this system is represented by

$$\frac{z_b(s)}{z_{b,dmd}(s)} = \frac{142(s+2.13)}{(s+3)(s^2+14s+100)} \qquad \text{Eqn 8.12}$$

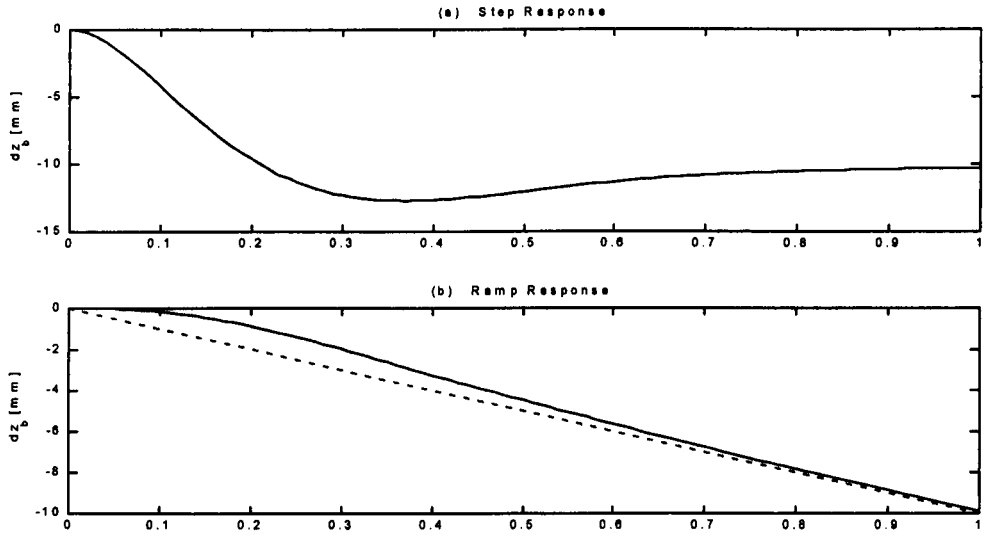

Fig 8.9 Response of z_b to (a) a Step Input of –10mm and (b) a Ramp Input of –10 mms^{-1} for the Height Control with P+I Controller. [$k_q = -0.016$ m.s.rad^{-1}, $k_w = -34$ Hz.m^{-1}.s, $k_p = -284$ Hz.m^{-1}, $T_I = 0.473$ s]

8.3.3 DESIGN OF THE SPEED CONTROL LOOP

In this control concept, the vehicle horizontal velocity u_b will be controlled by the tilt of the wing stroke plane, which effectively tilts the resultant force vector either forward or rearwards, as shown previously in Fig 5.2. Once tilted, the vertical component of the resultant force is reduced and the vehicle will not be able to maintain height without the height control loop designed in the previous section.

In the pitch stabilised system designed in Chapter 7.4, Eqn 8.13 gives the transfer function for the response of axial speed ub as a function of the stroke plane after the common terms in the numerator and denominator are removed.

$$\frac{u_b(s)}{\kappa(s)} = G_7(s) = \frac{K_{\kappa u}}{s} \qquad \text{Eqn 8.13}$$

Again, the linearised value of $K_{\kappa u}$ was given by MATLAB to be $5.76e^{-8}$. It does not correspond to the response to a step input of magnitude –0.01745 rad (or 1°) as shown in Fig 8.10. The calculated response is $-9.7783\ ms^{-1}rad^{-1}$.

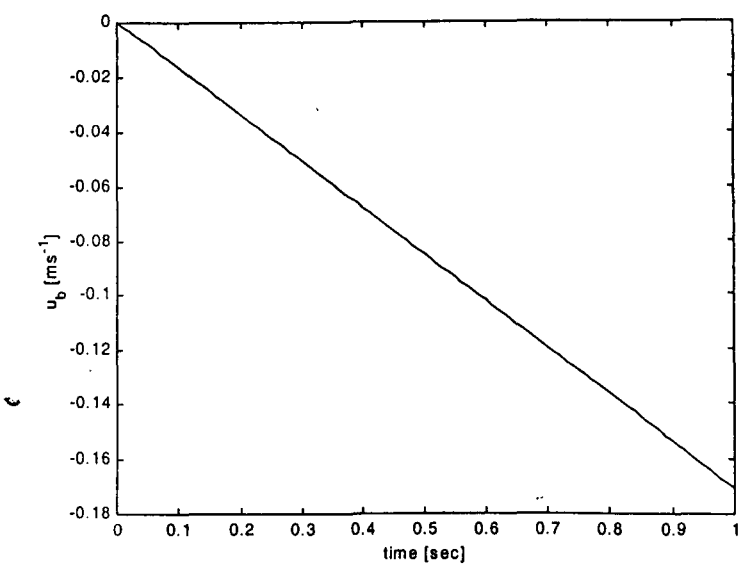

Fig 8.10 Response of u_b to a Step Input in κ of Magnitude 1°

If the horizontal velocity is now fed back to form an error signal $\varepsilon_\kappa = \kappa + k_u.u_b$ as shown in Fig 8.11, it is possible to stabilise the horizontal velocity of the vehicle.

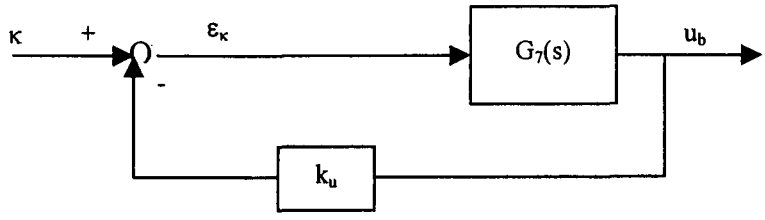

Fig 8.11 Horizontal Velocity Stability Loop

Fig 8.12 shows the response of the above system to a step input of 1° change in the stroke plane angle κ with unity feedback, or $k_u = -1$ rad.m^{-1}.s. The response in the linear model is superimposed. There is a good correlation between the two models.

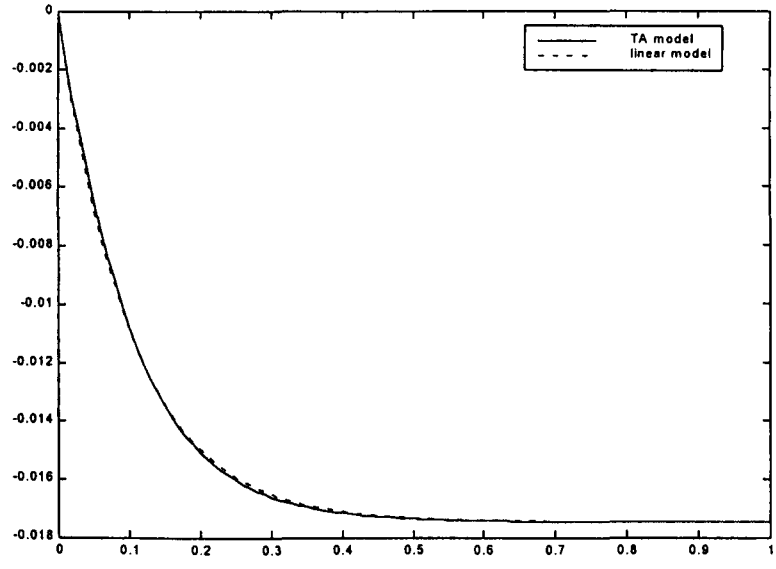

Fig 8.12 Response of u_b to a Step Input of Magnitude of 1° in κ with $k_u = -1$ rad.m^{-1}.s

The closed loop transfer function for the horizontal velocity control loop is given by

$$G_8(s) = \frac{K_{ku}}{s + k_u K_{ku}} \qquad \text{Eqn 8.14}$$

with $k_u = -1$ rad.m^{-1}.s.

8.3.4 DESIGN OF THE HORIZONTAL POSITION CONTROL LOOP

As in the case of height control, integrating the horizontal velocity output from the system in Fig 8.11 results in the horizontal position x_b of the vehicle, since the fuselage pitch (θ) is near zero and the roll (ϕ) and yaw (ψ) angles are practically zero. The error signal ε_x, being the difference between the demanded position of the vehicle x_{dmd} and the actual position x_b, serves as input to a controller with the transfer function $D_2(s)$, resulting in the following design shown in Fig 8.13

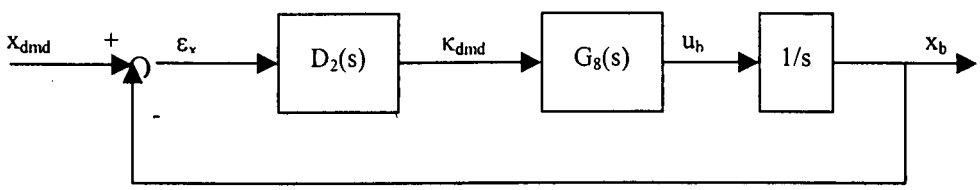

Fig 8.13 Horizontal Position control loop

where $G_8(s)$ is the closed loop transfer function of the horizontal velocity stability system given in Eqn 8.14. The effects of different controller transfer function $D_2(s)$ for the system shall be analysed in the following sections.

8.3.4.1 Proportional Controller

In a proportional control system, $D_2(s) = k_p$, the proportional gain. The open loop transfer function for the position due to an input for the demanded position is given by

$$\frac{x_b(s)}{x_{b,dmd}(s)} = G_9(s) = D_2(s)G_8(s)\frac{1}{s} = \frac{k_p K_{\kappa u}}{s(s + k_u K_{fw})} \qquad \text{Eqn 8.15}$$

The closed loop transfer function for the system is hence

$$\frac{x_b(s)}{x_{b,dmd}(s)} = G_9(s) = \frac{k_p K_{\kappa u}}{s(s + k_u K_{\kappa u}) + k_p K_{\kappa u}} = \frac{k_p K_{\kappa u}}{s^2 + ks + k_p K_{\kappa u}} \qquad \text{Eqn 8.16}$$

Comparing the closed loop characteristic equation of the above system and that of the standard second order differential equation, it can be seen that if k_u = -1 rad.m^{-1}.s (as selected previously in Chapter 8.3.3) and $K_{\kappa u}$ = -9.7783 m.s^{-2}.rad^{-1}, then $k = 2\zeta\omega_n = -K_{\kappa u}$. Hence if a response with a damping ratio of 0.7 is desired, then ω_n must be 6.98 rad.s^{-1}. This results in $k_p K_{\kappa u} = \omega_n^2$ or k_p = -4.98 rad.m^{-1}.

Fig 8.14 shows the responses of the time-averaged model and the linear model to a step input of $x_{b,dmd}$ of magnitude 10 mm. Again, there is a very good match between the two models. The demanded position is reached in slightly over 1 second.

In order to improve the performance, ω_n was set to 10 rad.s^{-1} and ζ = 0.7. This results in the characteristic equation being s^2 + 14s + 100 with k_u = -1.43 rad.m^{-1}.s and k_p = -10.2 rad.m^{-1}. The corresponding response from the linearised and the time-averaged models are shown in Fig 8.15. The demanded position is reached after about 0.6 seconds in the time-averaged model.

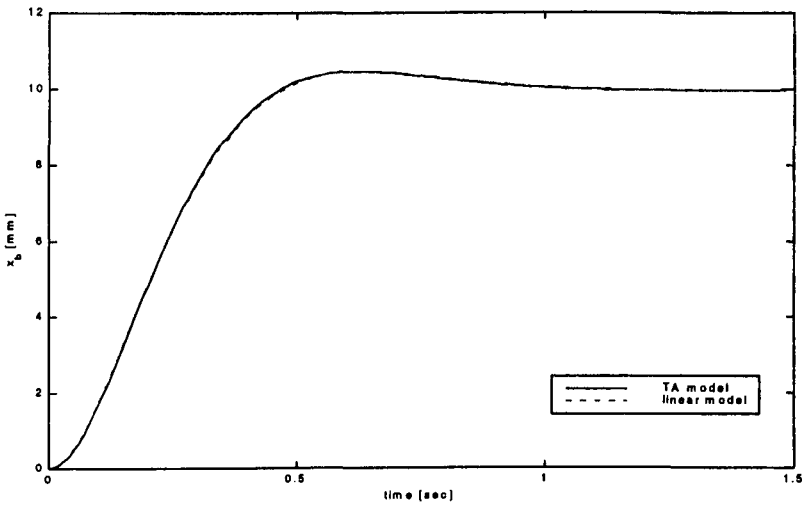

Fig 8.14 Response of x_b to a Step Input in x_{dmd} of Magnitude 10 mm [k_q = -0.016 m.rad^{-1}.s, k_u = -1 rad. m^{-1}.s, k_p = -4.98 rad. m^{-1}]

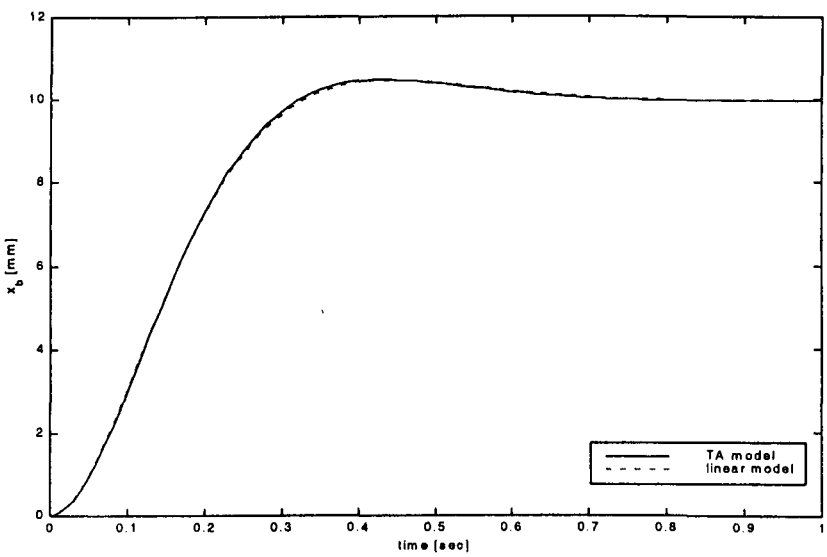

Fig 8.15 Response of x_b to a Step Input in x_{dmd} of Magnitude 10 mm [k_q = -0.016 m.rad^{-1}.s, k_u = -1.43 rad. m^{-1}.s, k_p = -10.2 rad. m^{-1}]

The response to a ramp input of gradient -10 mm.s^{-1} is shown in Fig 8.16 for the above system. It shows that the response lags behind the input ramp for this system and has poor tracking behaviour because the system is of Type I.

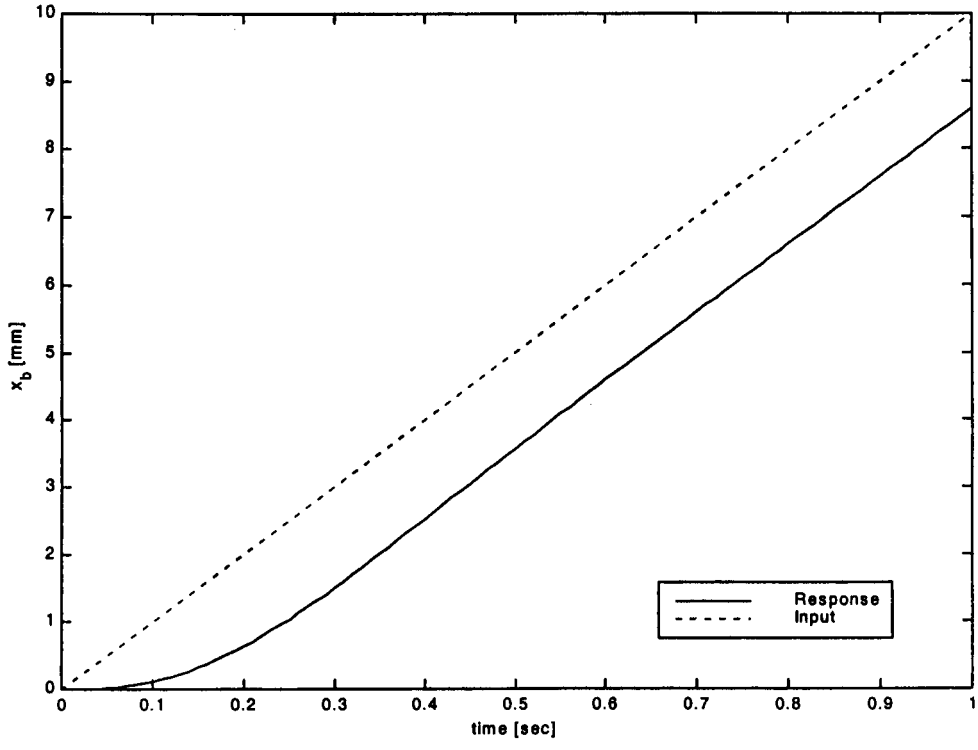

Fig 8.16 Response of x_b to a Ramp Input in x_{dmd} of Magnitude 10 mm.s^{-1} [k_q = -0.016 m.rad^{-1}.s, k_u = -1.43 rad. m^{-1}.s, k_p = -10.2 rad. m^{-1}]

8.3.4.2 Proportional plus Integral Controller

The proportional controller described in the previous section results in a tracking error for ramp inputs and this can be corrected using a proportional plus integral (P+I) with transfer function

$$D_2(s) = k_p\left(1+\frac{1}{T_I s}\right) = \frac{(k_p s + k_I)}{s} \qquad \text{Eqn 8.17}$$

The open loop transfer function for the position due to an input for the demanded position is given by

$$\frac{x_b(s)}{x_{b,dmd}(s)} = G_{10}(s) = D_2(s)G_8(s)\frac{1}{s} = \frac{k_p(T_I s+1)K_{ku}}{T_I s^2(s+k_u K_{ku})} \qquad \text{Eqn 8.18}$$

The closed loop transfer function for the horizontal position control system with the P+I controller is then

$$\frac{x_b(s)}{x_{b,dmd}(s)} = G_{10}(s) = \frac{(k_p s+k_I)K_{ku}}{s^2(s+k_u K_{ku})+(k_p s+k_I)K_{ku}}$$

$$= \frac{(k_p s+k_I)K_{ku}}{(s^3+k_u K_{ku}s^2+k_p K_{ku}s+k_I K_{ku})} \qquad \text{Eqn 8.19}$$

$$= \frac{(K_{ku}k_p s+K_{ku}k_I)}{(s^3+k_u K_{ku}s^2+k_p K_{ku}s+k_I K_{ku})}$$

The characteristic equation given by the denominator of Eqn 8.19 is of order 3. If it is to have a real root and two conjugate roots, and if the natural frequency of the conjugate pair is 10 rad/sec with damping ratio of 0.7, then $s_{1,2} = -7 \pm 7.14i$.

In the design of the height controller, it was noted that the choice of the real root determines the tracking response of the system. In line with that design, the real root was chosen to be at $s_3 = -5$, the characteristic equation shall be $s^3 + 19s^2 + 170s + 500$. Comparing this with the denominator of Eqn 8.19, it can be shown that k_u=-1.94rad.m^{-1}.s, k_p = -17.4 rad.m^{-1} and k_I = -51.1 rad.m^{-1}.s^{-1} (or T_I = 0.34 sec) The step and ramp responses with this controller are shown in Fig 8.17(a) and (b) respectively. The step response obtained from the linear model is also shown in Fig 8.17(a). There is a good

correlation between the linear and non-linear model. The tracking performance of the system is acceptable.

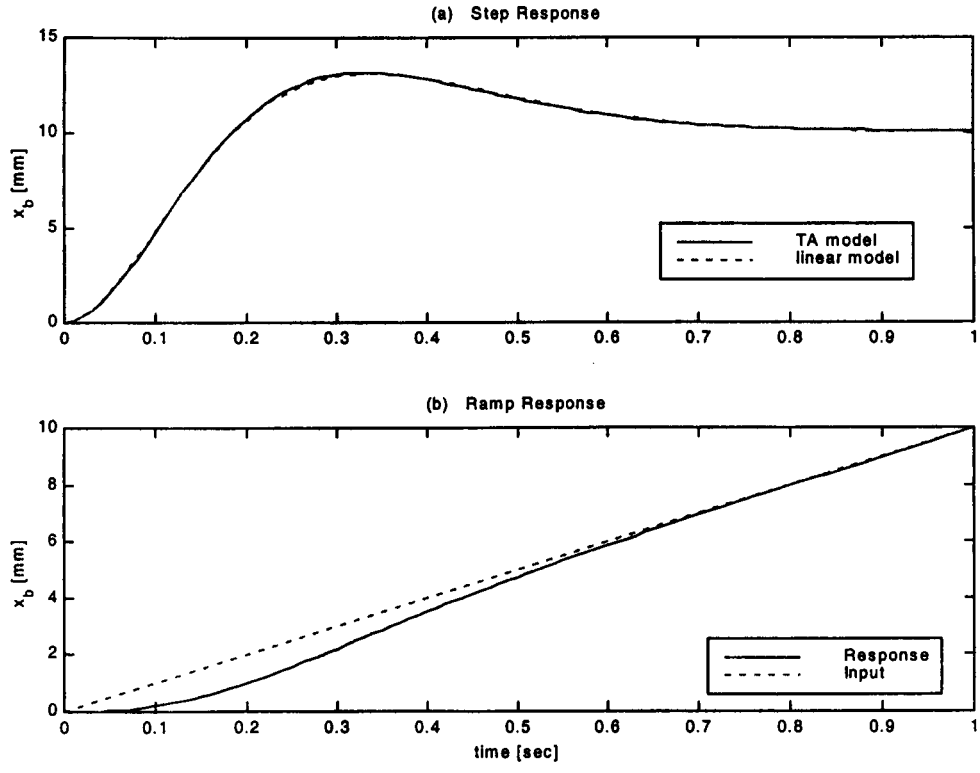

Fig 8.17 Response of x_b to (a) a Step Input of 10 mm and (b) a Ramp Input of –10 mms^{-1} for the Horizontal Position Control with P+I Controller [k_q = -0.016 $m.rad^{-1}.s$, k_u =-1.94 $rad.m^{-1}.s$, k_p = -17.4 $rad.m^{-1}$, T_I = 0.34 s]

This closed loop transfer function for the system is given by

$$\frac{x_b(s)}{x_{b,dmd}(s)} = \frac{170.3(s+2.94)}{(s+5)(s^2+14s+100)} \qquad \text{Eqn 8.20}$$

8.3.5 SYSTEM PERFORMANCE: CONTROL CONCEPT 1

The flight control system employing variation of flap frequency and stroke plane angle and named Control Concept 1 have been designed in the previous sections. The block diagram representation of the system is shown in Fig 8.1 and Table 8.2 summarises the control gains for the design.

Control Concept 1			
x_b-Channel	k_u = -1.94 radm^{-1}s	k_p = -17.4 radm^{-1}	T_I = 0.34 s
z_b-Channel	k_w = -34 Hz.m^{-1}.s	k_p = -284 Hz.m^{-1}	T_I = 0.473 s
q_b-Channel	k_q = -0.016 m.rad^{-1}s		

Table 8.2 Control Gains for Concept 1 Flight Control System Design

Simultaneous steps of magnitude 10 mm in both $x_{b,dmd}$ and $z_{b,dmd}$ were input to the above system. Fig 8.18 shows the longitudinal parameters of the MAV in this simulation. It can be seen that the vehicle responded immediately by tilting the stroke plane by about 8° forward to accelerate the vehicle while at the same time increasing the flap frequency to 42.5 Hz.

The fuselage pitched nose up in response to the change in stroke plane angle due to the conservation of angular momentum about this axis. As the vehicle reaches its demanded position, the parameters returned steadily to their trim values. During the entire manoeuvre, the d_{1x} varied between +23.2 mm and –5.1 mm, the nominal value at trim being 6.025mm.

Fig 8.19 shows a similar simulation except that the magnitudes are now 50 mm instead of 10 mm. It can be seen that the variations on the flapping frequency and the CG travel are much larger now.

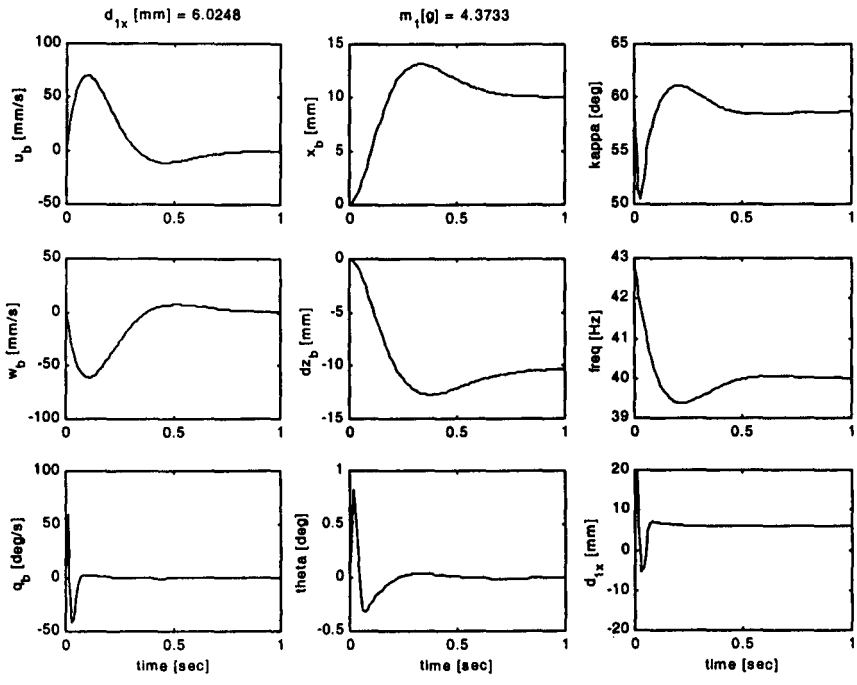

Fig 8.18 Response to Simultaneous Step Inputs in $x_{b,dmd}$ and $z_{b,dmd}$ of Magnitude 10 mm

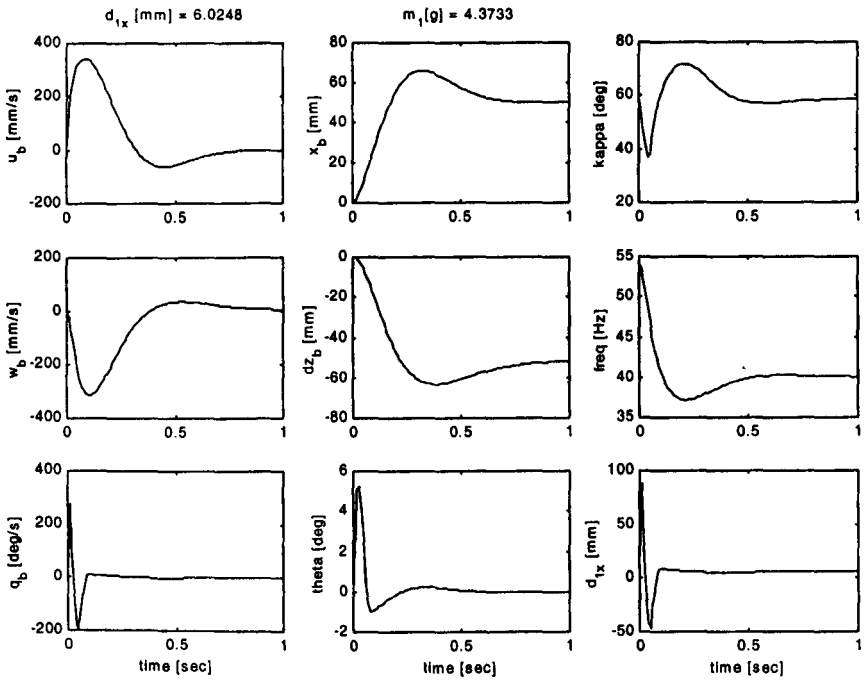

Fig 8.19 Response to Simultaneous Step Inputs in $x_{b,dmd}$ and $z_{b,dmd}$ of Magnitude 50 mm

Step inputs represent abrupt demands on the control system. Simultaneous step inputs are generally the most severe demands placed upon the control system. Larger magnitude inputs may place an excessive demand on the control system. This usually results in a requirement for a large variation in the CG position. If the CG is limited, the vehicle may not be controllable. Hence, large magnitude abrupt inputs should be avoided when possible.

More detailed assessment of the control system performance shall be described in Chapter 9 where the various control concepts are being compared.

8.4 CONTROL CONCEPT 2

The control system for this concept (force magnitude control by variation of phase φ and force orientation control by stroke plane tilt) is shown in Fig 8.20. It consists of

(a) *a pitch stability loop* through the feedback of the fuselage pitch rate to the fuselage CG location

(b) *a rate of climb control loop* with feedback of the rate of climb to the demanded phase φ_{dmd}

(c) *a height control loop* which builds an error between the demanded height $z_{b,dmd}$ and the actual height z_b of the vehicle. This error is then input to a PID controller which together with feedback of the rate of climb in the rate of climb control loop determines the demanded phase φ_{dmd}.

(d) *a speed control loop* with feedback of the forward velocity u_b to the demanded stroke plane angle κ_{dmd}

(e) *a horizontal position control loop* which builds an error between the demanded position $x_{b,dmd}$ and the actual position x_b of the vehicle. This error is then input to a P+I controller which together with feedback of the forward velocity in the forward velocity control loop determines the demanded phase κ_{dmd}.

The vehicle can be stabilised in pitch as described in Chapter 7.4 with the gain $k_q = -0.05$ $m.rad^{-1}.s$.

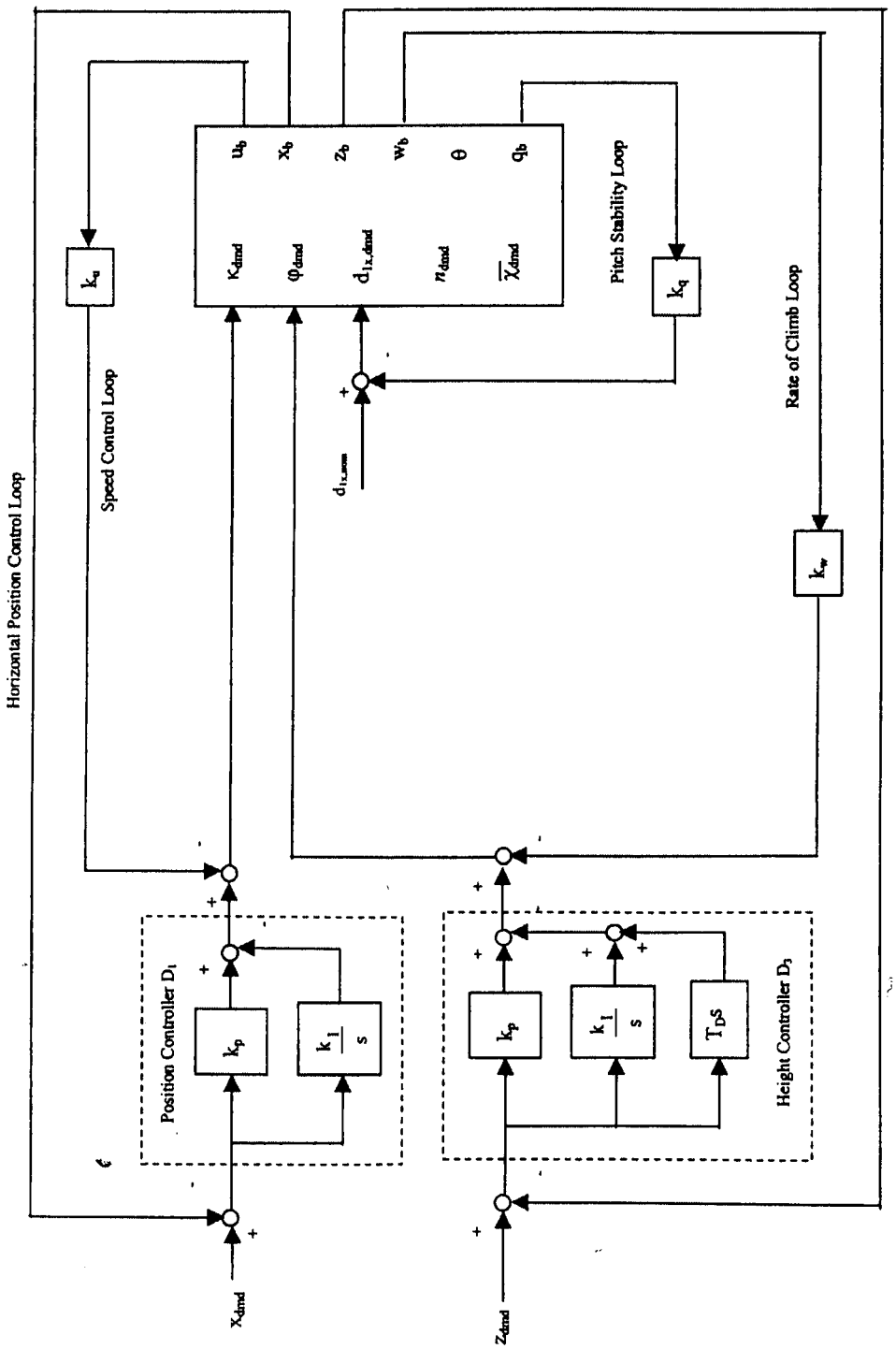

Fig 8.20 Flight Control System Block Diagram for Concept 2

8.4.1 DESIGN OF THE RATE OF CLIMB CONTROL LOOP

The transfer function of w_b in response to a perturbation in the phase angle φ is obtained numerically from the linearised MATLAB model as

$$\frac{w_b(s)}{\varphi_{dmd}(s)} = G_{11}(s) = \frac{K_{\varphi w}}{s} \qquad \text{Eqn 8.21}$$

The gain $K_{\varphi w}$ was obtained from the open loop simulation in a similar fashion as described previously in Chapter 8.3.1 by a step input of 0.0873 rad (5°) from the nominal phase φ of 1.0472 rad (or 60°) and was found to be 5.439 $ms^{-2}rad^{-1}$.

Fig 8.21 shows the rate of climb control system. As a simple relation between the trim CG and the phase does not exist as was previously the case. A CG compensation will not be included in the system.

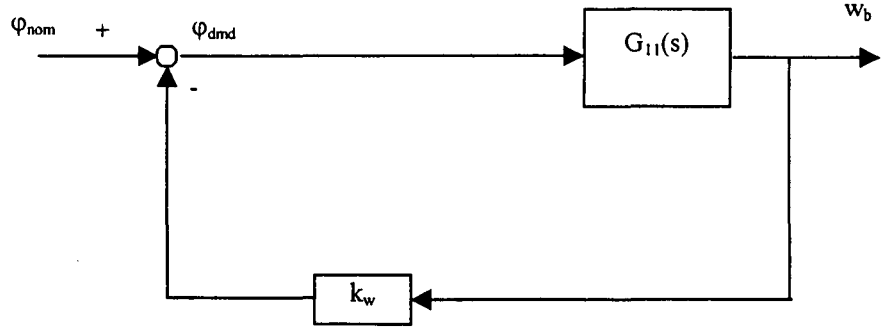

Fig 8.21 Rate of Climb Control Loop

The closed loop transfer function of the linear model of the above system is

$$\frac{w_b(s)}{\varphi_{dmd}(s)} = G_{12}(s) = \frac{K_{\varphi w}}{s + k_w K_{\varphi w}} \qquad \text{Eqn 8.22}$$

The closed loop characteristic equation of the system with negative feedback is

$$s + k_w.K_{\varphi w} = 0 \qquad \text{Eqn 8.23}$$

It has a single real pole whose location determines the speed of response. If the pole is selected to be similar to that in Concept 1 at s = -1.5, then $k_w = 0.2739$ rad.s.m^{-1}.

Fig 8.22 shows the response of w_b to a unit step input in the demanded phase φ_{dmd} simulated with the time-averaged model of the vehicle, with q_b and w_b feedback.

The figure shows that the match between the time-averaged model and the linearised model is extremely good.

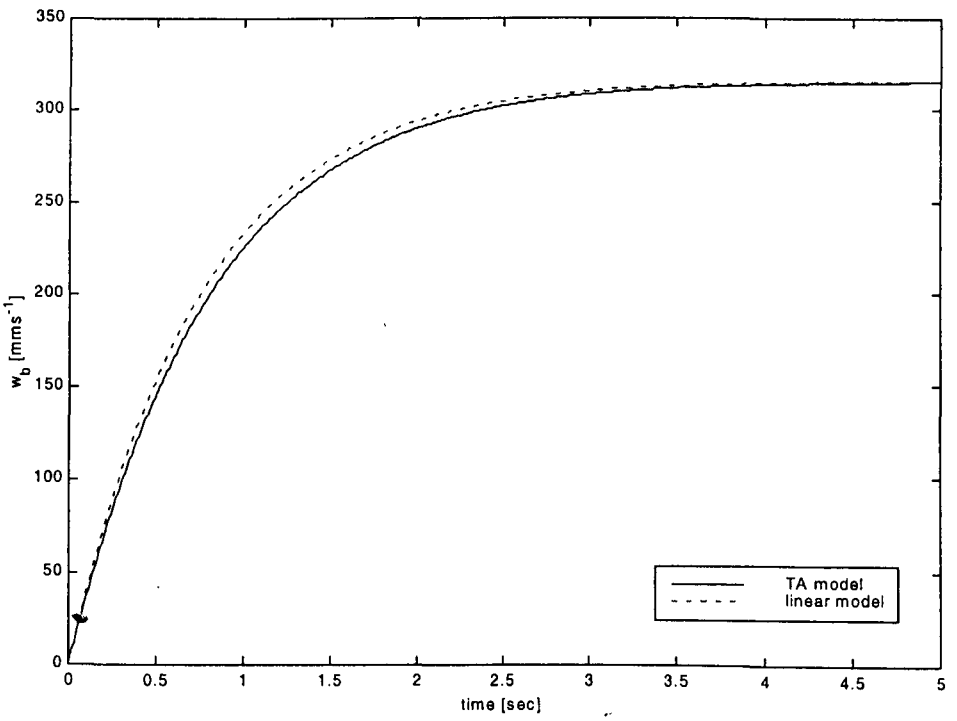

Fig 8.22 **Response to a step input in Phase φ of 5° in pitch-stabilised system [k_q = -0.05m.rad^{-1}.s, k_w = 0.2739 rad. m^{-1}.s]**

8.4.2 DESIGN OF THE HEIGHT CONTROL LOOP

The vehicle height is obtained by integrating the output of the rate of climb control system shown in Fig 8.23. The position error $\varepsilon_z = z_{b,dmd} - z_b$ serves as input to the controller with the transfer function $D_3(s)$ in the following control system design.

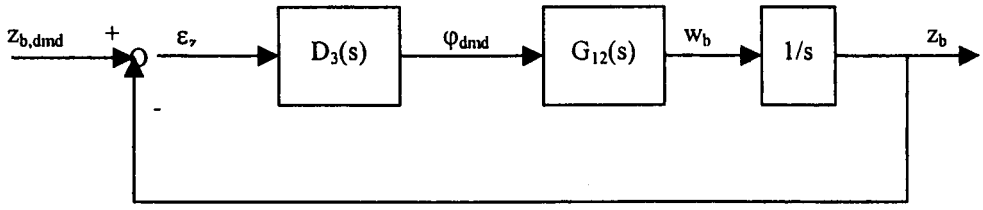

Fig 8.23 Height Control Loop

$G_{12}(s)$ is the closed loop transfer function of the vertical speed stability system from the previous section. The effects of different controller transfer function $D_3(s)$ for the system can be studied. As the tracking performance of a proportional controller was shown in Chapter 8.3.2.1 to be unsatisfactory, the study of its effects is omitted.

8.4.2.1 Proportional plus Integral Control

The transfer function for a proportional plus integral controller is given by

$$D_3(s) = k_p\left(1+\frac{1}{T_I s}\right) = \frac{k_p s + k_I}{s} \qquad \text{Eqn 8.24}$$

where $k_I = \frac{k_p}{T_I}$. The open loop transfer function for the position due to an input for the demanded position is given by

$$\frac{z_b(s)}{z_{b,dmd}(s)} = G_{13}(s) = D_3(s)G_{12}(s)\frac{1}{s} = \frac{(k_p s + k_I)K_{\varphi w}}{s^2(s + k_w K_{\varphi w})} \qquad \text{Eqn 8.25}$$

resulting in the following closed loop transfer function for the height control system

$$\frac{z_b(s)}{z_{b,dmd}(s)} = G_{13}(s) = \frac{(K_{\varphi w}k_p s + K_{\varphi w}k_I)}{(s^3 + k_w K_{\varphi w}s^2 + k_p K_{\varphi w}s + k_I K_{\varphi w})} \qquad \text{Eqn 8.26}$$

Eqn 8.26 can be rewritten in the form

$$G_{13}(s) = \frac{K_a(s + a)}{(s + b)(s^2 + 2\zeta\omega_n s + \omega_n^2)} \qquad \text{Eqn 8.27}$$

where $K_a = K_{\varphi w}k_p$ and $b = \frac{k_I}{k_p} = \frac{1}{T_I}$. In order to have second order like response, the real pole can be selected to cancel out the real zero, i.e. $b \approx a$. As seen in Concept 1, the choice of the real pole affects the tracking response. A small negative real pole (large integral time constant T_I) results in a large tracking error while a large negative real pole (small integral time constant) results in a 'hangover' in the step response. Given a second order like response, e.g. ω_n was set at 20 rad.s^{-1} and the damping ratio ζ is 0.7, the effect of the real pole is shown in Figs 8.24 (T_I = 100 sec) and 8.25 (T_I = 1 sec).

The closed loop characteristic equation is given by

$$\Delta(s) = (s + b)(s^2 + 2\zeta\omega_n s + \omega_n^2) = s^3 + (2\zeta\omega_n + b)s^2 + (2b\zeta\omega_n + \omega_n^2)s + b\omega_n^2 = 0$$

Eqn 8.28

With $K_{\varphi w} = 5.439\ m.s^{-2}.rad^{-1}$, substituting the desired numerical values of b, ω_n and ζ into Eqn 8.28 and comparing the result with the denominator of Eqn 8.26, the gains can be deduced for the system with the larger time constant ($T_I = 100$ sec, ie $b = 0.01\ s^{-1}$):

For $T_I = 100$ sec, $\omega_n = 20\ rad.s^{-1}$ and $\zeta = 0.7$, the gains are found to be $k_w = 5.148\ rad.m^{-1}.s$, $k_p = 73.54\ rad.m^{-1}$ and $k_I = 0.7354\ rad.m^{-1}.s^{-1}$. The closed loop transfer function is given by

$$\frac{z_b(s)}{z_{b,dmd}(s)} = \frac{400(s + 0.01)}{(s + 0.01)(s^2 + 28s + 400)}$$

Eqn 8.29

For $T_I = 1$ sec, $\omega_n = 20\ rad.s^{-1}$ and $\zeta = 0.7$, the gains are found to be $k_w = 5.3\ rad.m^{-1}.s$, $k_p = 78.69\ rad.m^{-1}$ and $k_I = 73.54\ rad.m^{-1}.s^{-1}$. The closed loop transfer function is given by

$$\frac{z_b(s)}{z_{b,dmd}(s)} = \frac{42(s + 0.9346)}{(s + 1)(s^2 + 28s + 400)}$$

Eqn 8.30

It is seen that the zero cancels the real pole in Eqn 8.23, leaving a second order like response, which is shown in Fig 8.24.

Fig 8.24(a) shows the comparison of the response to a step input of –10 mm obtained from the time-averaged model and the linear model in Eqn 8.29. Good correlation between the response from the linear transfer function and the non-linear time-averaged model can still be observed. The response to a ramp input of –10 mm/sec is shown in Fig 8.24(b). The response lags the demand by about 8% in the above design. This was undesirable.

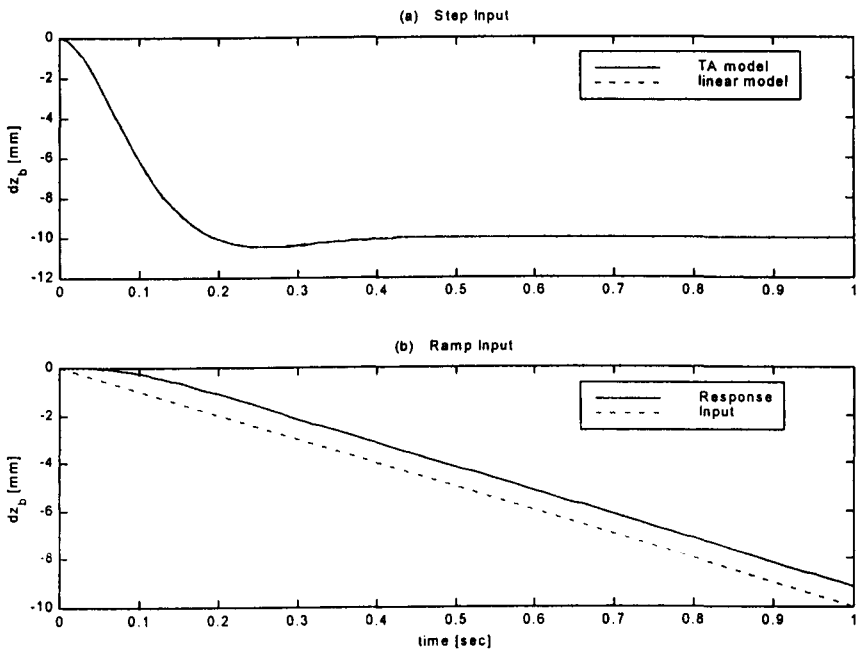

Fig 8.24 Response of z_b to (a) a Step Input of zb,dmd of Magnitude of –10mm and (b) a Ramp Input of $z_{b,dmd}$ of Magnitude of –10mms^{-1}.
[k_q = -0.05 m.rad^{-1}.s, k_w = 5.148 rad.m^{-1}.s, k_p = 73.549 rad.m^{-1}, T_I = 100 s]

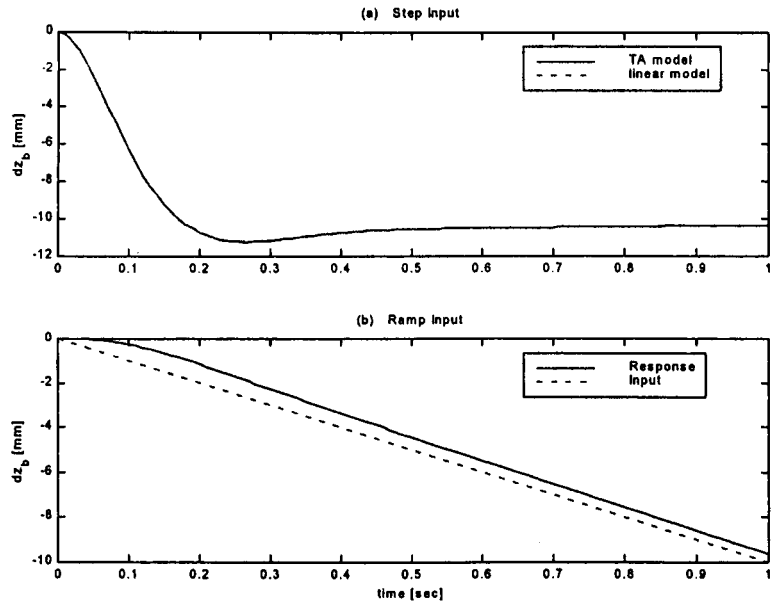

Fig 8.25 Response of z_b to (a) a Step Input of zb,dmd of Magnitude of –10mm and (b) a Ramp Input of $z_{b,dmd}$ of Magnitude of –10mms^{-1}. [k_q = -0.05 m.rad^{-1}.s, k_w = 5.33 rad.m^{-1}.s, k_p = 78.7 rad.s^{-1}, T_I = 1 sec]

By reducing T_I to 1 second, it was found that the steady state error to the ramp input was reduced to 3.15% but resulted in the 'overhang' in the response to a step input, as shown in Fig 8.25.

The large integral gain k_I = 73.54 rad.m^{-1}.s^{-1} in Fig 8.25 resulted in a 'hangover' where the position error tends slowly to zero. If the proportional gain k_p was increased instead to 100 rad.m^{-1}, while maintaining k_I at 0.7354 rad.m^{-1}.s^{-1} (or T_I = 136 sec) the response to the step input was seen to settle faster, reaching the demanded value after 0.5 seconds as shown in Fig 8.26(a). The ramp response still lagged the input by 4% after 1 second.

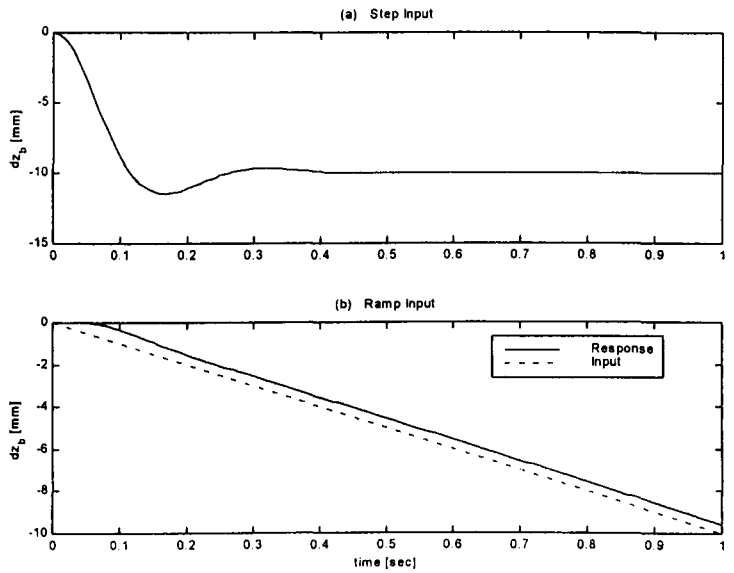

Fig 8.26 Response of z_b to (a) a Step Input of zb,dmd of Magnitude of –10mm and (b) a Ramp Input of $z_{b,dmd}$ of Magnitude of $-10mms^{-1}$. [$k_q = -0.05\ m.rad^{-1}.s$, $k_w = 5.148\ rad.m^{-1}.s$, $k_p = 100\ rad.s^{-1}$, $T_I = 136\ sec$]

The dependence of the real and complex poles of the closed loop transfer function as given in Eqn 8.26 on the gains can be found analytically [Bartsch 1982, pp 66-67]. The rather complicated mathematical manipulations can be avoided by observations of the response during the gain variations which are:

a. an increase in k_I (or a reduction in T_I with constant k_p) improves the tracking performance but results in a 'hangover' in the step response,

b. an increase in k_p does not produce a 'hangover' in the step response, but tracking performance was not as good as when k_I was increased

c. a reduction in k_w results in lower damping in both the step and ramp response but tracking performance was improved significantly.

With $k_p = 100\ rad.m^{-1}$, $k_I = 1\ rad.m^{-1}.s^{-1}$ (or $T_I = 100$ sec) and k_w at $2\ rad.m^{-1}.s^{-1}$, the position error for a ramp input at the end of 1 second was reduced to 2%, the reduction in damping can be compensated for using a PID controller, Fig 8.27.

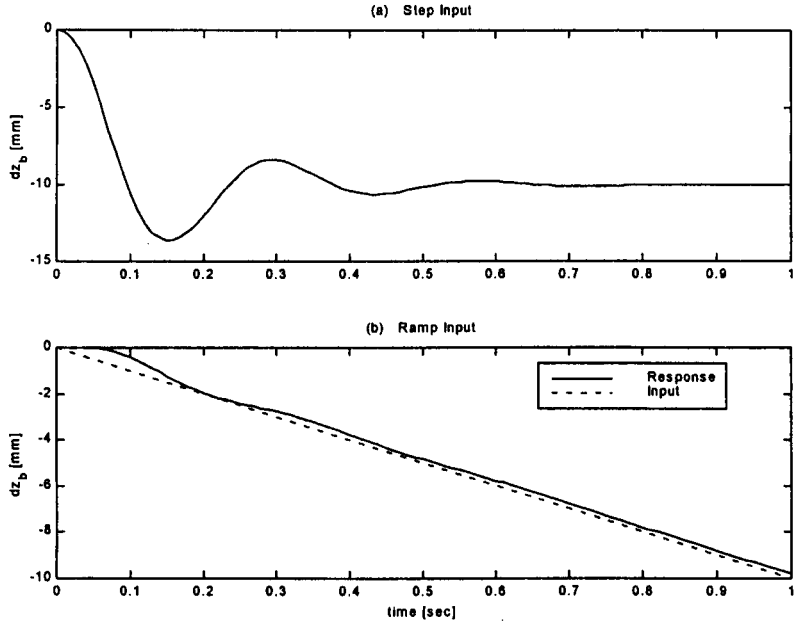

Fig 8.27 Response of z_b to (a) a Step Input of $z_{b,dmd}$ of Magnitude of –10mm and (b) a Ramp Input of $z_{b,dmd}$ of Magnitude of $-10mms^{-1}$.
[$k_q = -0.05\ m.rad^{-1}.s$, $k_w = 2\ rad.m^{-1}.s$, $k_p = 100\ rad.s^{-1}$, $T_I = 100\ sec$]

8.4.2.2 PID Control

In order to improve the damping of the P+I controller, a PID controller was selected with similar gains as those found in the previous section. The value of T_d was then determined for a satisfactory damping.

The controller transfer function is given by

$$D_3(s) = k_p\left(1+\frac{1}{T_I s}+T_d s\right) = k_p + \frac{k_p}{T_I s} + k_p T_d s$$

$$= \frac{k_p\left(T_d T_I s^2 + T_I s + 1\right)}{T_I s} \qquad \text{Eqn 8.31}$$

The closed loop transfer function for the PID controlled height loop is thus

$$\frac{z_b(s)}{z_{dmd}(s)} = \frac{k_p K_{\varphi w}\left(T_d T_I s^2 + T_I s + 1\right)}{T_I s^2\left(s + k_w K_{\varphi w}\right) + k_p K_{\varphi w}\left(T_d T_I s^2 + T_I s + 1\right)}$$

$$= \frac{k_p K_{\varphi w}\left(T_d T_I s^2 + T_I s + 1\right)}{T_I s^3 + K_{\varphi w} T_I\left(k_w + k_p T_d\right)s^2 + k_p K_{\varphi w} T_I s + k_p K_{\varphi w}} \qquad \text{Eqn 8.32}$$

with the gains being $K_{\varphi w} = 5.439\ \text{m.s}^{-2}.\text{rad}^{-1}$, $k_p = 100\ \text{rad.m}^{-1}$, $k_I = \frac{k_p}{T_I} = 1\ \text{rad.m}^{-1}.\text{s}^{-1}$ (or $T_I = 100$ sec). The closed loop characteristic equation $\Delta(s)$ given by the denominator of Eqn 8.32 can be rewritten in the form $1 + kG(s)$ as follows:

$$\Delta(s) = 100s^3 + 543.9\left(2 + 100T_d\right)s^2 + 54390s + 543.9 = 0$$

$$\Rightarrow 1 + T_d \frac{543.9s^2}{s^3 + 10.878s^2 + 543.9s + 5.439} \qquad \text{Eqn 8.33}$$

where $k = T_d$ and

$$G(s) = \frac{543.9s^2}{s^3 + 10.878s^2 + 543.9s + 5.439} \qquad \text{Eqn 8.34}$$

The gain $k = T_d$ can then be varied and the root locus plotted as shown in Fig 8.28.

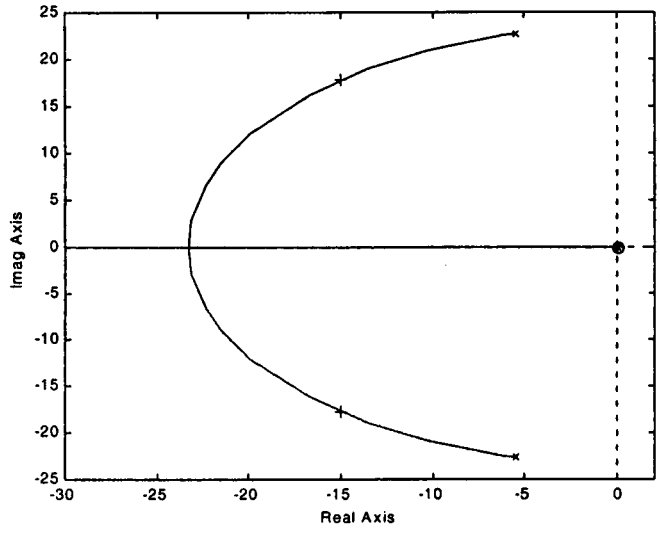

Fig 8.28 Root Locus for Variation of T_d
[$K_{\varphi w} = 5.439\ m.s^{-2}.rad^{-1}$, $k_p = 100\ rad.m^{-1}$, $T_I = 100\ s$]

If a damping ratio of about 0.7 is desired, T_d is found to be 0.04 sec. The closed loop transfer function for the PID controlled height loop is given as

$$\frac{z_b(s)}{z_{b,dmd}(s)} = \frac{21.76(s + 23.96)(s + 1.044)}{(s^2 + 31.6s + 510.3)(s + 1.066)} \qquad \text{Eqn 8.35}$$

One of the poles roughly cancels one of the zeros, leaving the linear transfer function second order like with a damping ratio of 0.7 and natural frequency of 22.6 $rads^{-1}$. However, Fig 8.29(a) seems to suggest that the response can no longer be represented by this linear transfer function.

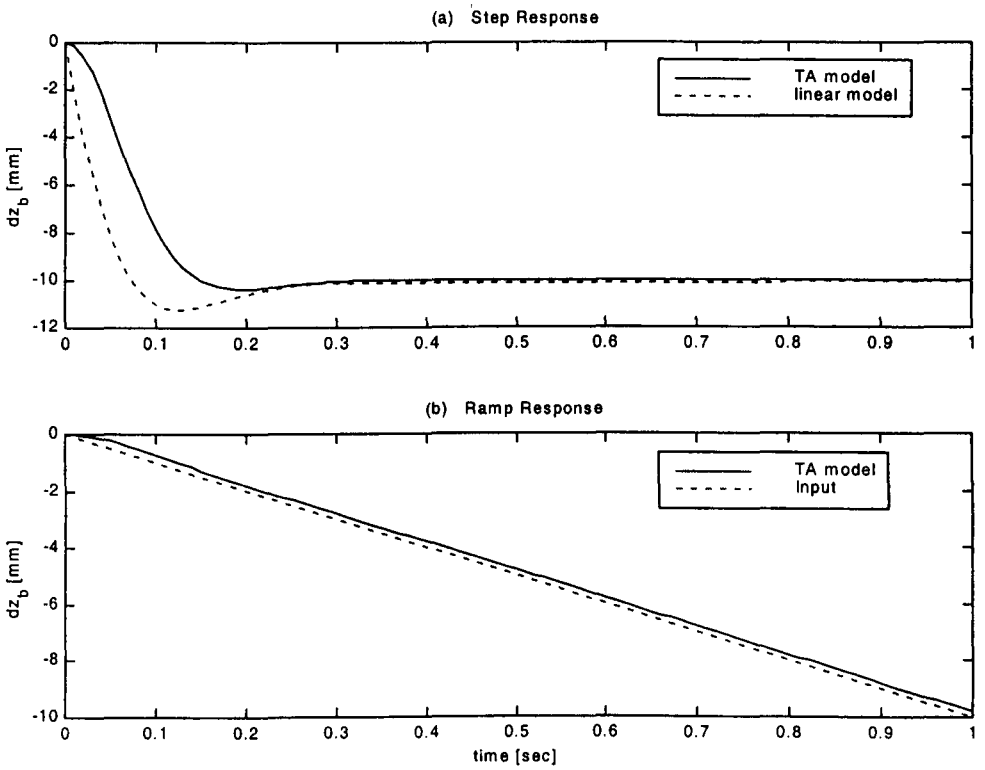

Fig 8.29 Response of z_b to (a) a Step Input of $z_{b,dmd}$ of Magnitude of –10mm and (b) a Ramp Input of $z_{b,dmd}$ of Magnitude of –10mm.s^{-1} [k_q = -0.05 m.rad^{-1}.s, k_w = 2 rad.m^{-1}.s, k_p = 100 rad.m^{-1}, T_f = 100 s, T_d = 0.04 s]

The ramp response still lagged behind the input by about 2% after 1 second as in the system with P+I controller. However, the damping of the response has been improved significantly by the introduction of the differential component of the PID controller.

8.4.3 DESIGN OF THE HORIZONTAL POSITION CONTROL LOOP

The open loop response of the horizontal speed of the vehicle to perturbation in the stroke plane angle will be similar to Eqn 8.13, but $K_{\kappa u}$ may take on a different value due to a change in the resultant force at the point of linearisation.

$$\frac{u_b(s)}{\kappa(s)} = G_{14}(s) = \frac{K_{\kappa u}}{s} \qquad \text{Eqn 8.36}$$

$K_{\kappa u}$ was found here, in a similar manner as described in Chapter 8.3.3, from the simulation to be $-9.777\ m.s^{-1}.rad^{-1}$. It is practically unchanged and when compared to the value for the vehicle investigated in Chapter 8.3. The horizontal position control system designed for Concept 1 was found to be still be applicable to the vehicle here if the gains of the final design of the control loop with P+I controller as shown in Table 8.2 are used ($k_u = -1.94\ rad.m^{-1}.s$, $k_p = -17.4\ rad.m^{-1}$ and $T_I = 0.34$ sec). The response to a step input is shown in Fig 8.30.

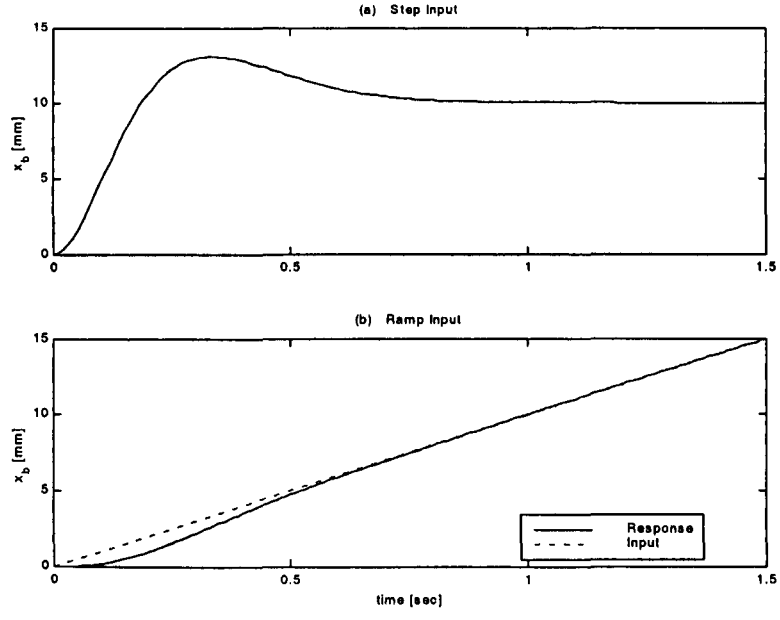

Fig 8.30 Response of x_b to (a) a Step Response in $x_{b,dmd}$ of Magnitude of 10 mm and (b) a Ramp Response in $x_{b,dmd}$ of Magnitude of 10 $mm.s^{-1}$
[$k_q = -0.05\ m.rad^{-1}.s$, $k_u = -1.94\ rad.m^{-1}.s$, $kp = -17.4\ rad.m^{-1}$, $T_I = 0.34$ s]

The response of the system to both the step and ramp inputs in $x_{b,dmd}$ is acceptable and hence there is no change in the horizontal control loop design of Chapter 8.3.3.

8.4.4 SYSTEM PERFORMANCE: CONTROL CONCEPT 2

The flight control system for the MAV that employs a variation in the phase between pitch and flap of the wings and stroke plane angle have been designed. The block diagram representation of the system is shown in Fig 8.20. A P+I controller was required in the horizontal axis while a PID controller was necessary to improve the damping of the system. Table 8.3 summarises the control gains for the design.

Control Concept 2				
x_b-Channel	$k_u = -1.94\ radm^{-1}s$	$k_p = -17.4\ radm^{-1}$	$T_I = 0.34$ s	
z_b-Channel	$k_w = 2\ rad.m^{-1}.s$	$k_p = 100\ rad.m^{-1}$	$T_I = 100$ s	$T_d = 0.04$ sec
q_b-Channel	$k_{\dot{q}} = -0.05\ m.rad^{-1}.s$			

Table 8.3 Control Gains for Concept 2 Flight Control System Design

Simultaneous steps of magnitude 10 mm in both $x_{b,dmd}$ and $z_{b,dmd}$ were input to the above system. Fig 8.31 shows the longitudinal parameters of the MAV in this simulation. It can be seen that the vehicle responded immediately by tilting the stroke plane forward, i.e. negative κ, to accelerate the vehicle while at the same time reducing the phase to about 30°.

The tendency of the fuselage to pitch up initially in response to a forward tilt of the stroke was again evident here. The CG location d_{1x} varied between +7mm and –33mm during the entire manoeuvre with the nominal position being at +6mm. The CG travel of a total of 40 mm is slightly higher than that in a similar manoeuvre with Concept 1, where 29 mm was registered.

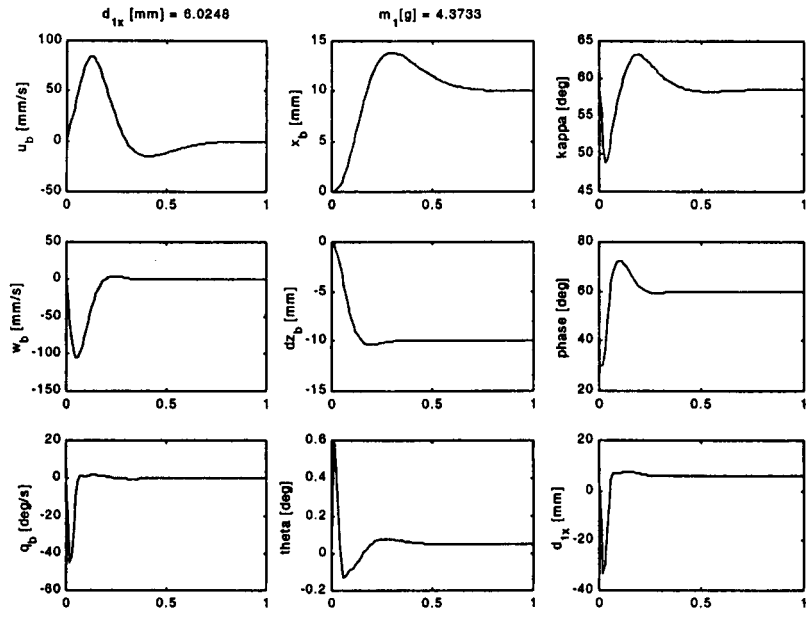

Fig 8.31 Response to Step Inputs in $x_{b,dmd}$ and $z_{b,dmd}$ of Magnitude 10 mm

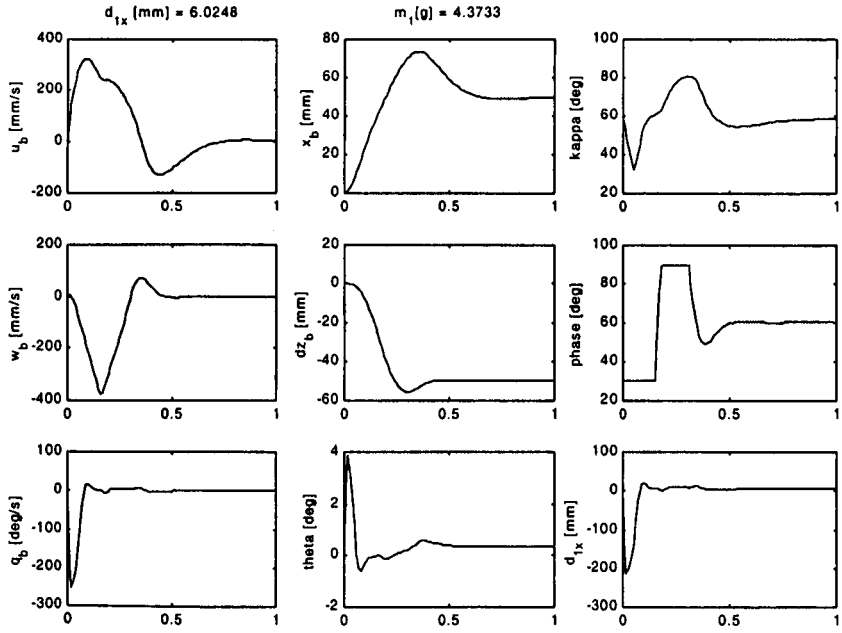

Fig 8.32 Response to Step Inputs in $x_{b,dmd}$ and $z_{b,dmd}$ of Magnitude 50 mm

Fig 8.32 shows the response of the system to a 50 mm input to both axes. It is seen now that the phase reaches both the upper and lower limits of 90° and 30° respectively in the initial 0.4 second of the manoeuvre. Also, the CG travel was about 200 mm, a value clearly unacceptable for a vehicle of this scale.

It is shown here again that abrupt inputs with larger magnitude push the control system to the limit. If the CG travel were limited, the vehicle might lose control and depart. It is therefore necessary to limit the input magnitude if these were to be abrupt.

8.5 CONTROL CONCEPT 3

In the two control concepts previously analysed, the resultant force was made to point in the direction of advance of the vehicle by tilting in the stroke plane accordingly. This has the advantage that, together with the control of the centre of gravity of the fuselage, the pitch attitude remained more or less horizontal. As a result, the onboard camera would not require additional stabilisation if the stability of the fuselage is sufficient. The camera can then be panned "care-free" from the attitude of the fuselage when a change in the field of view is required.

However, the tilt of the stroke plane with the wings flapping requires the motor actuators controlling the stroke plane to overcome the large inertia of the wings. These would have to be correspondingly sized, increasing the basic empty weight of the vehicle.

An alternative to point the resultant force would be to fix the stroke plane and tilt the fuselage by controlling the CG location. This removes the requirement of the stroke plane actuator motors and thereby reducing the all-up weight of the vehicle.

In such a control strategy, the rate of climb and height control loops designed in Chapter 8.4 will not be affected. In order to control the horizontal velocity and position of the vehicle, the fuselage pitch attitude must first be controlled. Its attitude will then determine the thrust vectoring of the resultant force.

8.5.1 CONTROL SYSTEM DESIGN

The control system for this concept is shown in Fig 8.33.

It consists of

(a) *a pitch stability loop* with feedback of the pitch rate to the fuselage CG location. The feedback gain is k_q. This loop stabilises the vehicle in the pitch axis.

(b) *a pitch attitude control loop* that forms an error from the demanded pitch attitude and the actual pitch attitude. This error is amplified with gain $k_{p\theta}$ added to the pitch rate feedback from the pitch stability loop and the nominal CG location, resulting in the demanded CG location $d_{1x,dmd}$.

(c) *a speed control loop* that forms an error from the demanded forward velocity $u_{b,dmd}$ and the actual velocity u_b of the vehicle. This error is amplified with the gain k_u and serves as input θ_{dmd} to the pitch attitude control loop.

(d) *a horizontal position control loop* that forms an error from the demanded position $x_{b,dmd}$ and the actual position x_b of the vehicle. This error is then passed through a P+I controller. The output from the controller is the demanded position x_{dmd} for the forward velocity control loop

(e) *a rate of climb control loop* with feedback of the climb rate to the phase φ.

(d) *a height control loop* that forms an error from the demanded height $z_{b,dmd}$ and the actual height z_b of the vehicle. This error is then passed through a PID controller. The output from the controller is the demanded height z_{dmd} for the rate of climb control loop

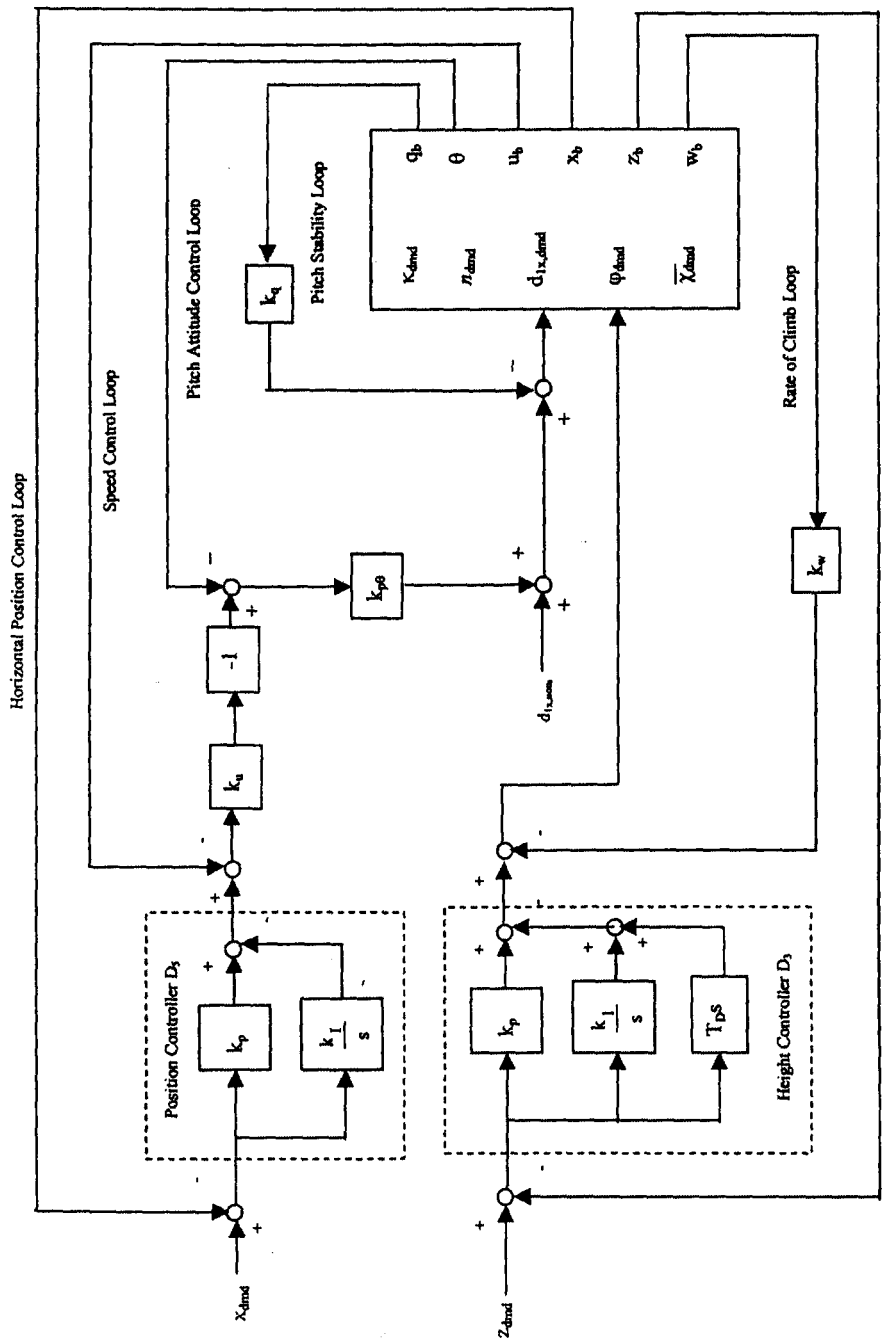

Fig 8.33 Flight Control System Block Diagram for Concept 3

8.5.2 PITCH AXIS CONTROL LOOP

The open loop transfer function for the pitch rate response due to a small perturbation Δd_{1x} is given by Eqn 7.10.

$$\frac{q_b(s)}{\Delta d_{1x}(s)} = G(s) = \frac{-3006.3(s+110-113.58i)(s+110+113.58i)}{s(s+133.5-111.9i)(s+133.5+111.9i)} \qquad \text{Eqn 7.10}$$

The closed loop transfer function with q_b feedback to Δd_{1x} as shown in Fig 7.5 is

$$\frac{q_b(s)}{q_{b,dmd}(s)} = \frac{-4290(s^2+220s+25000)}{s^3+(267-4290k_q)s^2+(30344-943800k_q)s-1.0725e^6k_q} \qquad \text{Eqn 8.37}$$

The value of the feedback gain k_q was found to be –0.05 $m.rad^{-1}.s$. Integrating the pitch rate results in the pitch attitude of the fuselage. Hence, if the error between the demanded and actual pitch attitude is passed to a controller with a transfer function $D_4(s)$, the closed loop control system as shown in Fig 8.34 can be used to control the pitch attitude, with $G_{15}(s)$ being the transfer function in Eqn 8.37.

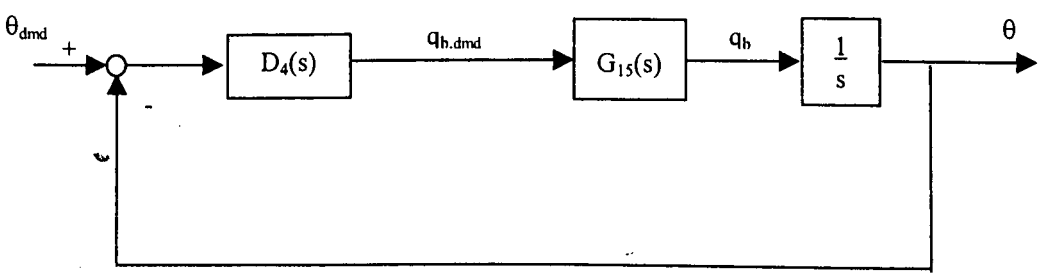

Fig 8.34 Pitch Attitude Control Loop for Concept 3

If a proportional controller is used, then $D_4(s) = k_{p\theta}$ and the closed loop transfer function for the system is given by

$$\frac{\theta(s)}{\theta_{dmd}(s)} = \frac{k_{p\theta}G_{15}(s)}{1+k_{p\theta}G_{15}(s)}\cdot\frac{1}{s} = G_{16}(s)$$

$$= \frac{-4290k_{p\theta}\left(s^2+220s+25000\right)}{s^4+\left(267-4290k_q\right)s^3+\left(30344-4290\left[k_{p\theta}+220k_q\right]\right)s^2-943800\left[k_{p\theta}+113.64k_q\right]s-1.0725e^8k_{p\theta}}$$

Eqn 8.38

The gains k_q and $k_{p\theta}$ can be selected by the choice of the closed loop poles. If the pitch stability feedback gain k_q was selected to be -0.05 $m.rad^{-1}.s$ as in Concept 2, the denominator of the above equation can be rearranged as

$$\Delta(s) = s^4+481.5s^3+\left(77534-4290k_{p\theta}\right)s^2-943800\left[k_{p\theta}-5.682\right]s-1.0725e^8k_{p\theta}$$

$$= s^4+481.5s^3+77534s^2+5.36e^6s-4290k_{p\theta}\left(s^2+220s+25000\right)$$

Eqn 8.39

Eqn 8.39 represents the characteristic equation of the pitch attitude control loop of Fig 8.34. It can be written in the form $1 + k_{p\theta}G_{17}(s) = 0$ as follows:

$$\Delta(s) = s^4+481.5s^3+77534s^2+5.36e^6s-4290k_{p\theta}\left(s^2+220s+25000\right)=0$$

Eqn 8.40

$$\Rightarrow 1+k_{p\theta}\frac{-4290\left(s^2+220s+25000\right)}{s^4+481.5s^3+77534s^2+5.36e^6s}=0$$

where

$$G_{17}(s) = \frac{-4290\left(s^2+220s+25000\right)}{s\left(s^3+481.5s^2+77534s+5.36e^6\right)}$$

Eqn 8.41

The poles are at s = 265.5 and 108 ± 92.3i while the zeros are at s = 110 ± 113.6i for the equivalent open loop system $G_{17}(s)$. Because the steady state gain for $G_{17}(s)$ is negative, a

positive feedback with a positive gain is equivalent to a negative feedback with a negative gain. The root locus for the system with negative feedback and negative gain is shown in Fig 8.35

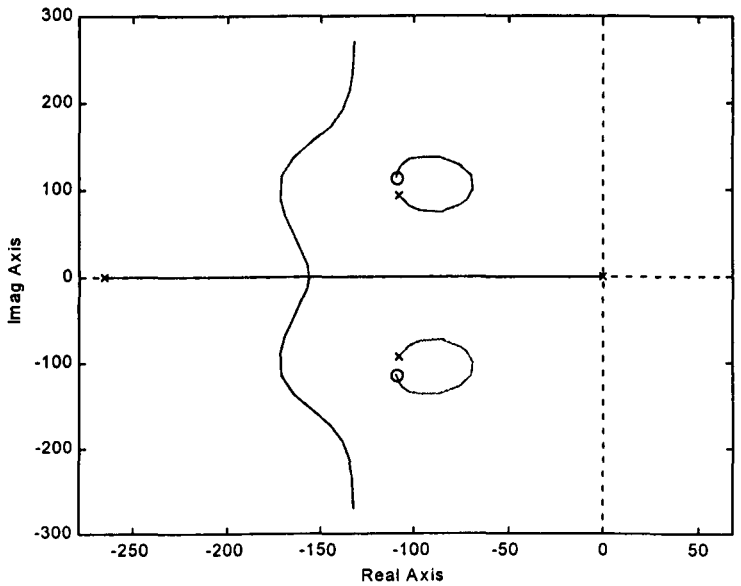

Fig 8.35 Root Locus for Pitch Attitude Control with Variation of Proportional Control Gain $k_{p\theta}$, with k_q=-0.05m.rad^{-1}.s

From the root locus above, a $k_{p\theta}$ = -1 m.rad^{-1} is required for a damping ratio of $\zeta \approx 0.7$. Substituting this gain back to Eqn 8.38, together with k_q = -0.05m.rad^{-1}.s, results in the closed loop transfer function for the pitch attitude control loop

$$G_{16}(s) = \frac{\theta(s)}{\theta_{dmd}(s)} = \frac{4290(s^2 + 220s + 25000)}{(s+23)(s+245.7)(s^2 + 212s + 18989)} \qquad \text{Eqn 8.42}$$

The oscillatory mode has a natural frequency ω_n = 137.8 rad.s^{-1} and a ζ = 0.77. The responses of the linear model together with that of the time-averaged model are plotted in Fig 8.36. It can be seen that the demanded pitch attitude is achieved within 0.25 second.

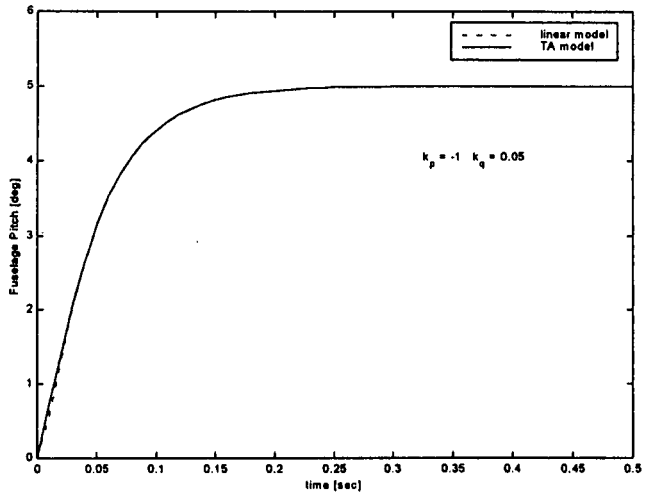

Fig 8.36 Response to a step input in $q_{b,dmd}$ of 5° [k_q = -0.05m.rad^{-1}.s, $k_{p\theta}$ = -1 m.rad^{-1}]

8.5.3 DESIGN OF THE HORIZONTAL POSITION CONTROL LOOP

8.5.3.1 Speed Response Transfer Function

In order to obtain the transfer function of u_b as a response to a perturbation in θ_{dmd}, the non-linear time-averaged model was linearised using the MATLAB linearisation command *linmod*. However, the transfer function so obtained shows that there are unstable roots in the characteristic equation, which is not evident in the system.

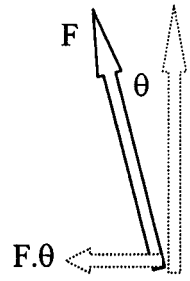

Fig 8.37 Effect of Tilt of Force Vector

A physical model for the u_b response is now derived with reference to Fig 8.37. The horizontal component of the resultant force is given by $F.\sin\theta \approx F.\theta$, for a small perturbation in θ. This results in an acceleration in the horizontal axis:

$$\dot{u}(t) = -\frac{F}{m}\theta(t) \qquad \text{Eqn 8.43}$$

In the s-plane, this can be written as

$$s \cdot u(s) = K_{u\theta}\theta(s) \Rightarrow \frac{u(s)}{\theta(s)} = \frac{F}{m}\cdot\frac{1}{s} = \frac{K_{u\theta}}{s} = G_{18}(s) \qquad \text{Eqn 8.44}$$

where $K_{u\theta} = -g\ m.s^{-2}$, the acceleration due to gravity, since F is the force to support the weight of the vehicle in trim.

With $G_{16}(s)$ being the closed loop pitch attitude control system shown in Fig 8.34, the horizontal velocity control path is shown in Fig 8.38.

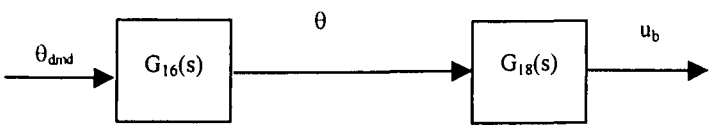

Fig 8.38 Linear Model of u_b path

The transfer function for the speed response to a perturbation in θ is given by

$$\frac{u_b(s)}{\theta(s)} = G_{16}(s)\cdot G_{18}(s) = G_{19}(s)$$
$$= \frac{42170k_p\left(s^2 + 220s + 25000\right)}{s\left(s^4 + as^3 + bs^2 + cs + d\right)} \qquad \text{Eqn 8.45}$$

where $G_{16}(s)$ is given by Eqn 8.42 and $G_{18}(s)$ is given by Eqn 8.44. The coefficients a = 481.5, b = 81824, c =$6.306e^6$ and d = $1.0725e^8$ are obtained by expanding the denominator of Eqn 8.42.

Fig 8.39 shows the response of θ and u_b to a step input in θ_{dmd} of 5° from both the non-linear time-averaged model and the linear transfer functions of Eqn 8.45. There is a good match between the responses from the linear model and the non-linear time-averaged model for both u_b and θ. It is seen that u_b is increased linearly after an initial build-up phase lasting about 0.3 second, corresponding to the build-up of the fuselage pitch attitude θ.

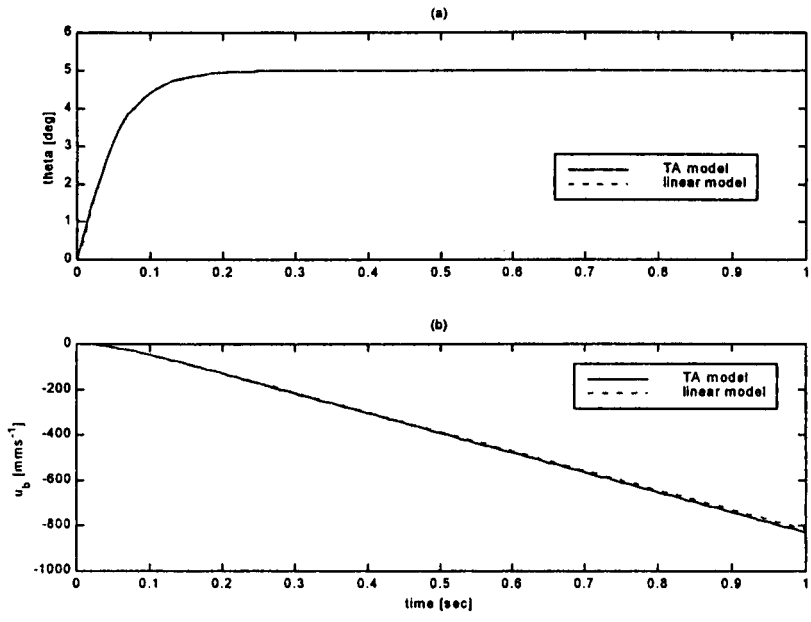

Fig 8.39 Response of (a) fuselage pitch attitude θ and (b) u_b due to a Step Input in θ_{dmd} of 5° [k_q = -0.05 m.rad^{-1}.s, $k_{p\theta}$ = -1 m.rad^{-1}]

8.5.3.2 Horizontal Velocity Control Loop

Fig 8.40 shows the speed stability and control loop for u_b. The stability gain k_u is in the forward path so that a steady state unity gain between the output u_b and the input $u_{b,dmd}$ is achieved. Also, a gain of –1 is included since a positive increase in horizontal speed requires a negative (nose-down) tilt of the fuselage.

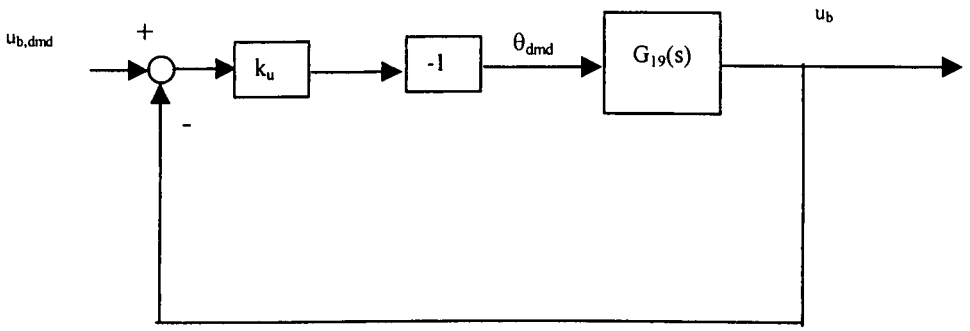

Fig 8.40 Horizontal Speed Control Loop

The closed loop transfer function for the system with k_q = -0.05 m.s.rad^{-1} and $k_{p\theta}$ = -1 m.rad^{-1} is given by

$$G_{20}(s) = \frac{u_b(s)}{u_{b,dmd}(s)} = \frac{-k_u G_{19}(s)}{1 - k_u G_{19}(s)}$$

$$= \frac{-42170 k_u k_{p\theta}\left(s^2 + 220s + 25000\right)}{s^5 + as^4 + bs^3 + \left(c - 42170 k_u k_{p\theta}\right)s^2 + \left(d - 9.28e^6 k_u k_{p\theta}\right)s - 1.054e^9 k_u k_{p\theta}}$$

Eqn 8.46

where a, b, c and d have already been determined for Eqn 8.45 previously.

Similar to the treatment of the pitch attitude control, the denominator of Eqn 8.46 can be rewritten as

$$1 - k_u \frac{42170\left(s^2 + 220s + 25000\right)}{s\left(s^4 + as^3 + bs^2 + cs + d\right)} = 0 \qquad \text{Eqn 8.47}$$

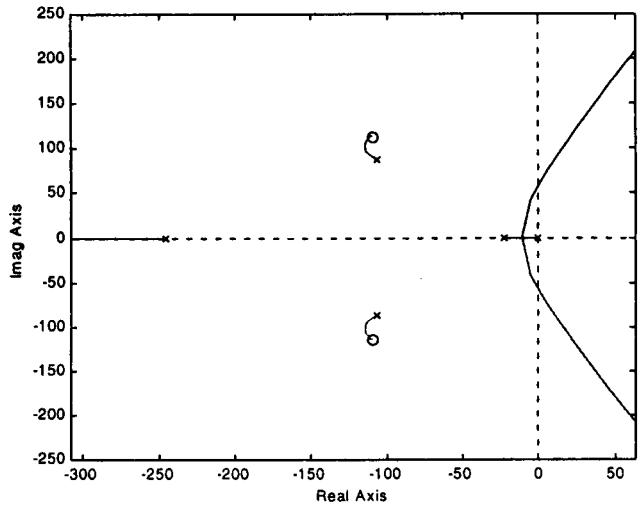

Fig 8.41 Root Locus for Horizontal Velocity Control with Variation of Proportional Control Gain k_u, with k_q = -0.05m.rad-1.s, $k_{p\theta}$ = -1 m.rad^{-1}

The root locus is shown in Fig 8.41 and the gain k_u = 1.0 rad.m^{-1}.s was determined using the root locus method for a damping ratio of about 0.7. However, the system damping is expected to be degraded when the system order is increased. In order to have sufficient damping, a k_u = 2.0 rad.m^{-1}.s was selected. The closed loop transfer of the speed control loop with k_q = -0.05 m.s.rad^{-1} and $k_{p\theta}$ = -1 m.rad^{-1} is found by substituting the numerical values into Eqn 8.46

$$G_{20}(s) = \frac{u_b(s)}{u_{b,dmd}(s)} = \frac{84340\left(s^2 + 220s + 25000\right)}{(s + 240)\left(s^2 + 219s + 18769\right)\left(s^2 + 20.3s + 462\right)} \qquad \text{Eqn 8.48}$$

The two oscillatory modes have damping ratio of 0.8 and 0.47 with natural frequencies of 137 rad/sec and 21.5 rad/sec respectively.

The results for both linear and time-averaged models are shown in Fig 8.42.

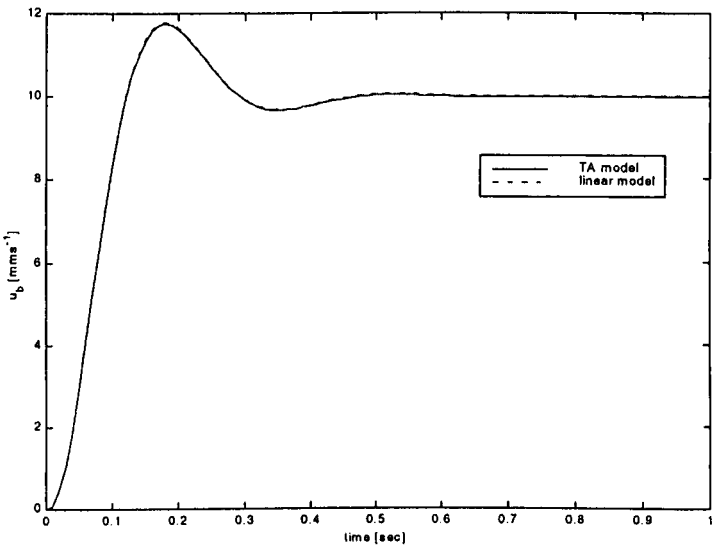

Fig 8.42 Response of u_b to a Step Input in $u_{b,dmd}$ of 10 mms^{-1} [k_u = 2 $rad.s.m^{-1}$, k_q = -0.05 $m.s.rad^{-1}$, $k_{p\theta}$ = -1 $m.rad^{-1}$]

8.5.3.3 Horizontal Position Control Loop

Fig 8.40 shows the horizontal velocity control loop. If this is then represented as $G_{20}(s)$, integrating the output u_b from the system in results the position of the vehicle. The position control loop can be represented by Fig 8.43 below

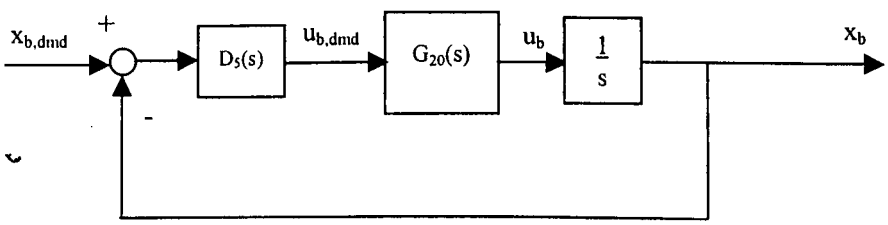

Fig 8.43 Horizontal Position Control Loop

The previous designs have shown that the tracking performance of the system was not satisfactory if $D_5(s)$ were a simple proportional controller. A P+I or PID controller would be required.

The method proposed by Ziegler and Nichols [1942], which although did not provide good results for the height control loop of Concept 1, proved successful in tuning the controller this time. The controller gains k_{px} and T_{Ix} for the P+I controller was determined by first finding the gain k_{ult}, for which the response is marginally stable. The period of oscillation P_{ult} is also determined. The proportional gain was set as

$$k_{px} = 0.45k_{ult} \qquad \text{Eqn 8.49(a)}$$

$$T_{Ix} = 0.833P_{ult} \qquad \text{Eqn 8.49(b)}$$

The ultimate gain k_{ult} and period of oscillation P_{ult} were found to be 17.5 s^{-1} and 0.35 second respectively. Hence, the proportional and integral gains k_{px} and T_{Ix} were selected as 7.9 s^{-1} and 0.29 second respectively. Fig 8.44(a) shows the step response of the system with marginal stability (k_{px} = -17.5 s^{-1}) and the 'tuned' system (k_{px} =-7.9 s^{-1} and T_{Ix} = 0.29 sec).

The response to a ramp input of $x_{b,dmd}$ of magnitude 10 mm.s^{-1} is shown in Fig 8.44(b). It can be seen that the tracking response is satisfactory and the vehicle had zero position error after only 0.75 second.

The closed loop transfer function for the system is given by

$$\frac{x_b(s)}{x_{b,dmd}(s)} = \frac{D_5(s)G_{20}(s)\frac{1}{s}}{1 + D_5(s)G_{20}(s)\frac{1}{s}} \qquad \text{Eqn 8.50}$$

where $G_{20}(s)$ is the closed loop transfer function for the horizontal speed as given by Eqn 8.47.

$D_5(s)$ is the transfer function for a P+I controller.

$$D_5(s) = \frac{k_{px}(T_I s + 1)}{T_I s} = k_{px} + \frac{k_I}{s} \qquad \text{Eqn 8.50}$$

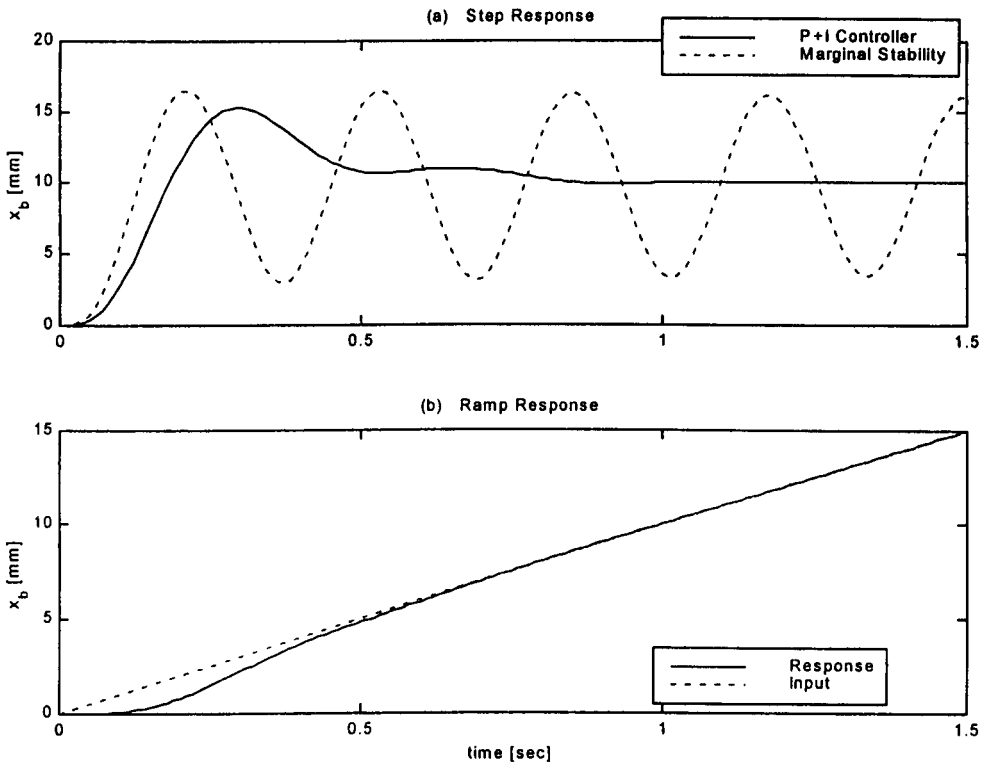

Fig 8.44 **(a)** **Step response in a marginally stable system and with a 'tuned' P+I controller**

(b) **Response to a Ramp Input of $x_{b,dmd}$ of 10 mms^{-1} with a 'tuned' P+I controller**

[k_u= 2 $rad.s.m^{-1}$, k_q= -0.05 $m.s.rad^{-1}$, $k_{p\theta}$= -1 $m.rad^{-1}$, k_{px}= 7.9 s^{-1}, T_{Ix}= 0.29sec]

Substituting the gains k_q = -0.05 $m.s.rad^{-1}$, k_u = 2 $rad.s.m^{-1}$, $k_{p\theta}$ = -1 $m.rad^{-1}$, k_{px} = 7.9 s^{-1} and T_{Ix} = 0.29 sec into the Eqn 8.51, it can be shown that

$$\frac{x_b(s)}{x_{b,dmd}(s)} = \frac{666286(s+3.44)(s^2+220s+25000)}{(s+240)(s^2+10.9s+43.4)(s^2+9.7s+292.4)(s^2+220s+18769)} \qquad \text{Eqn 8.52}$$

The above linear transfer function shows that the response has a convergent exponential mode with a time constant of about 4 millisecond, and three oscillatory modes with natural frequencies of 137 rad.s^{-1} (ζ = 0.8), 17.1 rad.s^{-1} (ζ = 0.28) and 6.6 rad.s^{-1} (ζ = 0.83).

The comparison of the responses to the linear and the non-linear time-averaged models are shown in Fig 8.45 for the P+I controlled system.

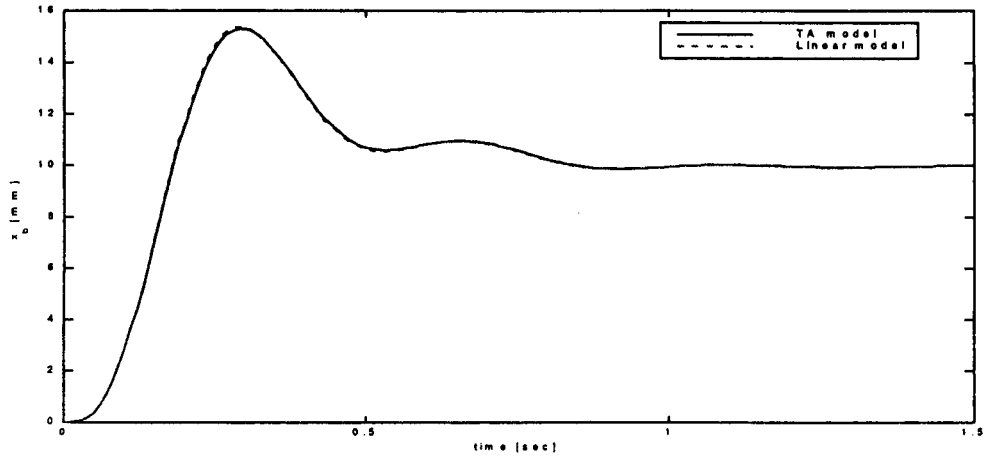

Fig 8.45 **Comparison of Response of x_b to a Step Input of $x_{b,dmd}$ of 10 mm in the Non-linear Time-Averaged Model and Linear Model**
[k_u= 2 rad.s.m^{-1}, k_q= -0.05 m.s.rad^{-1}, $k_{p\theta}$= -1 m.rad^{-1}, k_{px}= 7.9 s^{-1}, T_{Ix}= 0.29sec]

8.5.4 SYSTEM PERFORMANCE: CONTROL CONCEPT 3

In Concept 3, the flight control system employs a variation in the phase between pitch and flap of the wings for z-axis control and fuselage tilt through CG variation for the x-axis control. The block diagram representation of the system is shown in Fig 8.33. A P+I controller was designed for the x-axis while the PID controller designed in Chapter 8.4.2.2 for Concept 2 was adopted without change for the z-axis. Table 8.4 summarises the control gains for the design.

Control Concept 3				
x_b-Channel	$k_u = 2$ radm^{-1}s	$k_{p\theta} = -1$ m.rad^{-1}	$k_{px} = 7.9$ s^{-1}	$T_{Ix} = 0.29$ sec
z_b-Channel	$k_w = 2$ rad.m^{-1}s	$k_p = 100$ s^{-1} rad^{-1}	$T_I = 100$ s	$T_d = 0.04$ sec
q_b-Channel	$k_q = -0.05$ m.rad^{-1}s			

Table 8.4 Control Gains for Concept 3 Flight Control System Design

Simultaneous steps of magnitude 10 mm in both $x_{b,dmd}$ and $z_{b,dmd}$ were input to the above system. Fig 8.46 shows the longitudinal parameters of the MAV in this simulation.

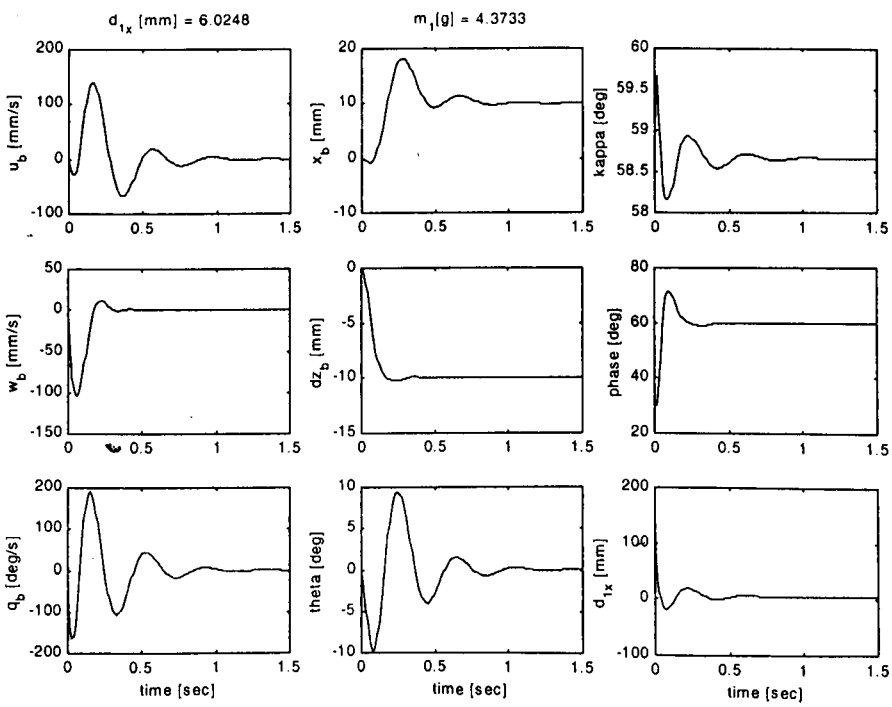

Fig 8.46 Response to Step Inputs in $x_{b,dmd}$ and $z_{b,dmd}$ of Magnitude 10 mm

It can be seen that the stroke plane is relatively constant and the fuselage tilted nose-down to accelerate forward. In so doing, the CG of the vehicle has to traverse a range of more than 170 mm. This CG movement is apparently not feasible for the vehicle of the scale being studied. The response of the vehicle in the x-axis took more than 1 second to settle at the desired position. Although care was taken to provide sufficient damping in the control design, the high order of the system has obviously degraded the damping.

Although this current control concept has its advantages as previously discussed, the large CG movement required to effect the fuselage tilt has made it unfeasible without any modification of the control system. One such modification, which can also be applied to the other concepts, is to include a filter in the system to smooth the input. Fig 8.47 shows the modification being made to the horizontal axis only.

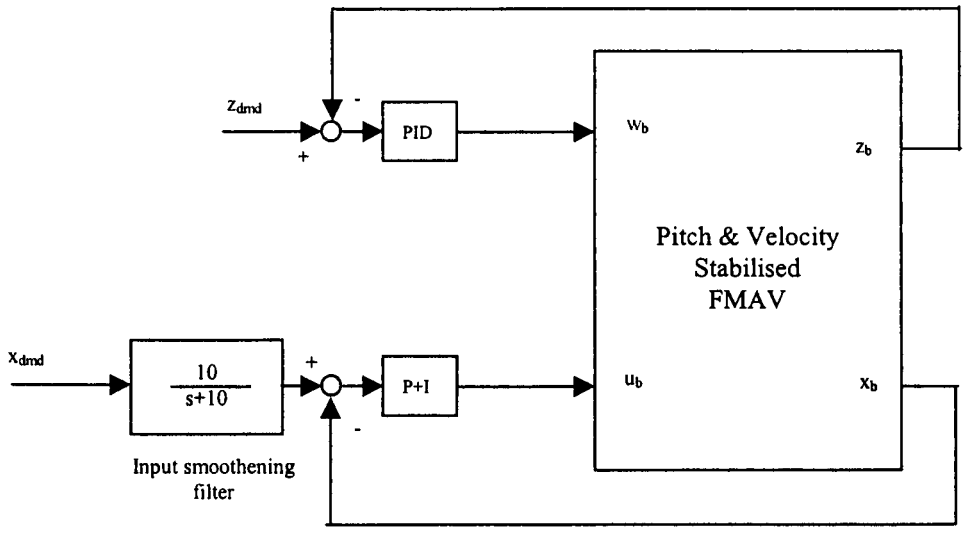

Fig 8.47 Input smoothing for x-axis of Pitch and Velocity stabilised FMAV

Fig 8.48 shows the response of the vehicle when simultaneous inputs to both axes of magnitude 10 mm are demanded. It can be seen now that the CG movement is being significantly reduced to between +21mm and –9mm, the nominal location being +6mm. The overshoot in fuselage position x_b was also reduced.

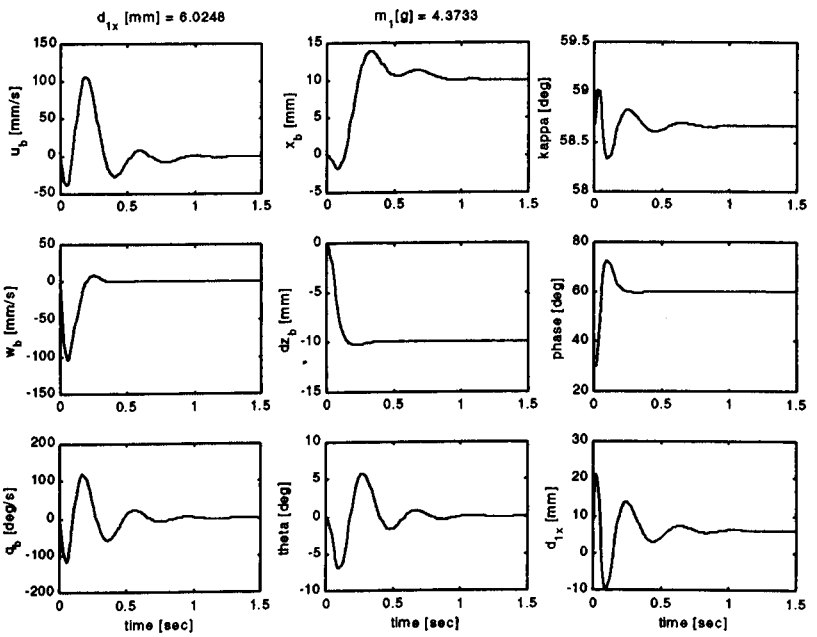

Fig 8.48 **Response to Step Inputs in $x_{b,dmd}$ and $z_{b,dmd}$ of Magnitude 10 mm with Input Smoothening**

Fig 8.49 shows the comparison of the relative CG travel from its nominal position, i.e. $d_{1x,actual} - d_{1x,nom}$, for the three control concepts. Simultaneous step inputs of 50 mm were demanded and the same input smoothing filter has been applied during the simulations. As can be seen, the demand on CG movement for Concept 3 was still excessive for such large amplitude abrupt inputs into both axes simultaneously.

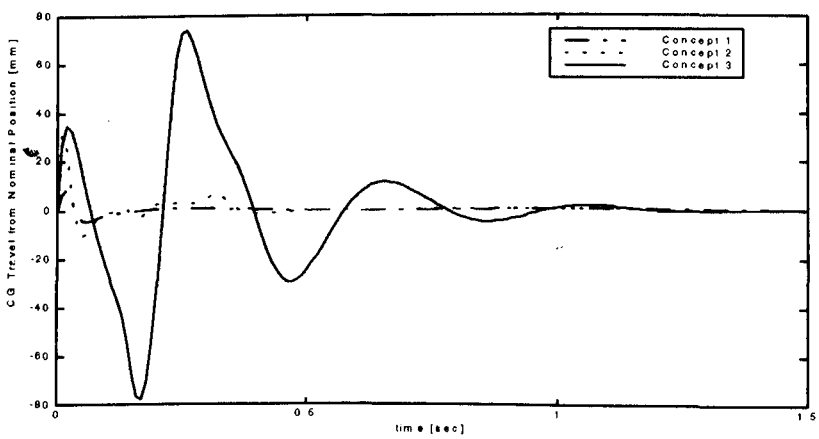

Fig 8.49 **Relative CG Travel from Nominal Position during Step Inputs in $x_{b,dmd}$ and $z_{b,dmd}$ of Magnitude 50 mm with Input Smoothening**

8.6 CONTROL ROBUSTNESS – EFFECTS OF AERODYNAMIC UNCERTAINTY

The flight control systems based on the three concepts described in Chapter 8.2 have been designed using the aerodynamic data obtained in the experiments described in Chapter 4. However, as explained earlier, there is a concern on the validity of the aerodynamic data in the x_B-axis (wing lift) because the forces lie in the vicinity of the measurement resolution threshold.

It is necessary now to assess the effectiveness of the designs in view of the uncertainty of the aerodynamic data by repeating the simulations for each of the three designs with the wing lift and its contribution to the aerodynamic moments being omitted.

	Unmodified Data	**Modified Data**
$\overline{C}_x$	$-0.1066\varphi + 0.37$	0
$\overline{C}_y$	$\pm (0.00757\varphi + 0.0045)$	$\pm (0.00757\varphi + 0.0045)$
$\overline{C}_z$	$0.1449\varphi - 0.309$	$0.1449\varphi - 0.309$
$\overline{C}_l$	$\pm (0.0386\varphi - 0.0688)$	$\pm (0.0386\varphi - 0.0688)$
$\overline{C}_m$	$-0.2062\varphi^4 + 0.9147\varphi^3 - 1.4412\varphi^2 + \varphi - 0.1796$	0
$\overline{C}_n$	$\pm (0.0518\varphi - 0.1562)$	$\pm (0.028\varphi - 0.56)$

Table 8.5 Modification of Aerodynamic Force and Moment Coefficients at Wing Root due to Omission of Wing Lift Forces

Table 8.5 shows the modified aerodynamic data. As the wing lift contributes to a certain extent to the aerodynamic pitch and yaw moments acting on the fuselage, these are also affected.

As the wing lift no longer contributes to the weight support, a higher flap frequency of 55.5 Hz was necessary to support the same fuselage mass. Also, the stroke plane is now

expected to be vertical, i.e. $\kappa = 0°$. There is also no need to trim the vehicle now as the flight control systems should stabilise the vehicle.

Repeating the simulations in the previous chapters with the modified aerodynamic model revealed that the vehicle with Control Concept 1 control system was not able to achieve the demanded x-position due to excessive pitching as shown in Fig 8.50. This is because the pitch loop in the control system designs only attempts to stabilise the pitch rate and not control the pitch attitude.

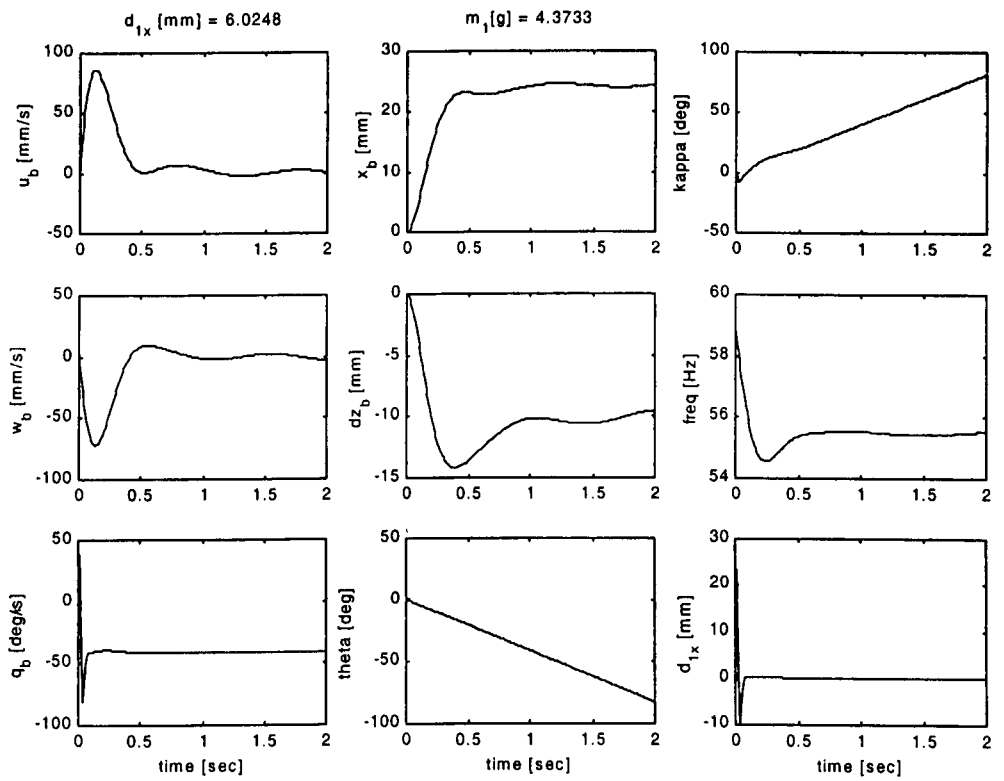

Fig 8.50 Vehicle Response to Simultaneous Step Inputs of 10 mm in $x_{b,dmd}$ and $z_{b,dmd}$ with unmodified Control Concept 1 and Wing Lift Omitted

With Concept 2, the vehicle was, to a certain extent, still able to achieve the demanded position as shown in Fig 8.51. However, the fuselage continued to pitch nose down at a rate of about 7.5° per second.

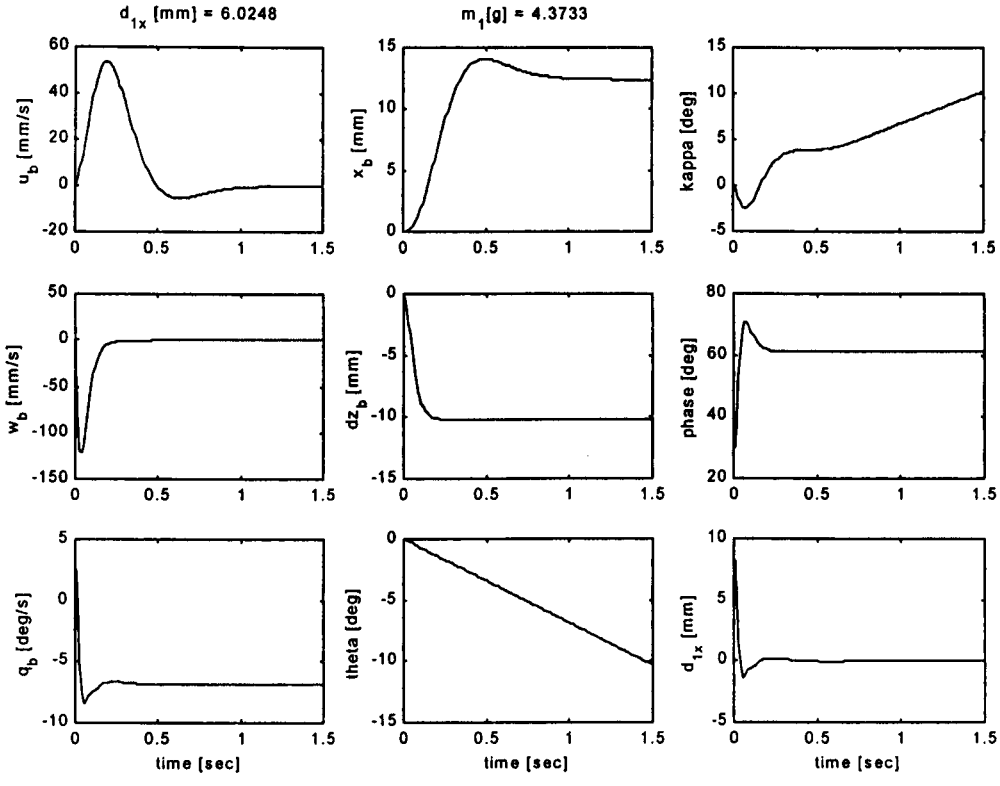

Fig 8.51 Vehicle Response to Simultaneous Step Inputs of 10 mm in $x_{b,dmd}$ and $z_{b,dmd}$ with unmodified Control Concept 2 and Wing Lift Omitted

The vehicle employing the Concept 3 system departed quickly from controlled flight when the modified data was used. The difference between this concept and that of Concept 2 is the use of CG variation to control the fuselage tilt for horizontal axis control. It is possible that the gains used in the design were not sufficient to maintain stability.

The design processes in Chapters 8.3 to 8.4 were repeated. Besides having to modify the gains, the fuselage attitude has to be maintained horizontal for Concepts 1 and 2. An additional pitch control loop has to be included as shown in Fig 8.52.

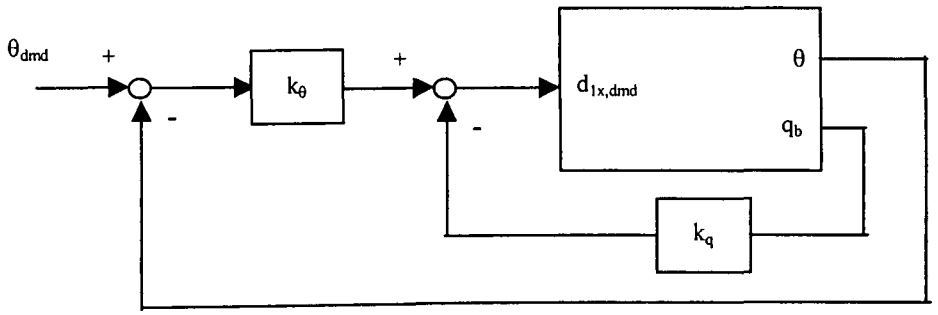

Fig 8.52 Pitch Attitude Control and Stabilisation Loop

Figs 8.53 to 8.55 show the responses of the vehicles after the modifications were made to the flight control systems for the three concepts. Table 8.6 shows the gains being used in the modified control systems.

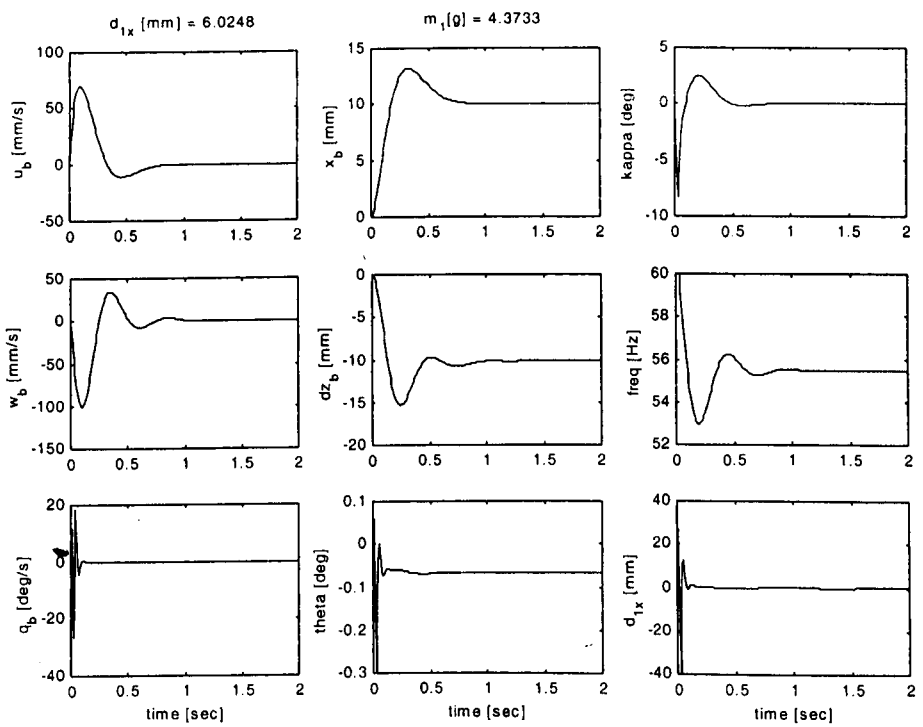

Fig 8.53 Vehicle Response to Simultaneous Step Inputs to $x_{b,dmd}$ and $z_{b,dmd}$ (Control Concept 1 with Pitch Control and Stabilisation Loop and Modified Aerodynamics and Control Gains)

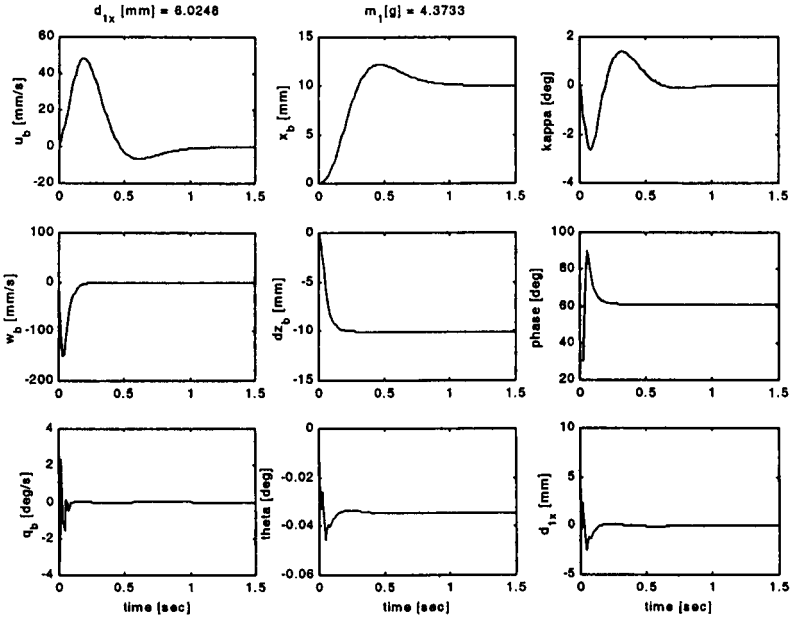

Fig 8.54 Vehicle Response to Simultaneous Step Inputs to $x_{b,dmd}$ and $z_{b,dmd}$ (Control Concept 2 with Pitch Control and Stabilisation Loop and Modified Aerodynamics and Control Gains)

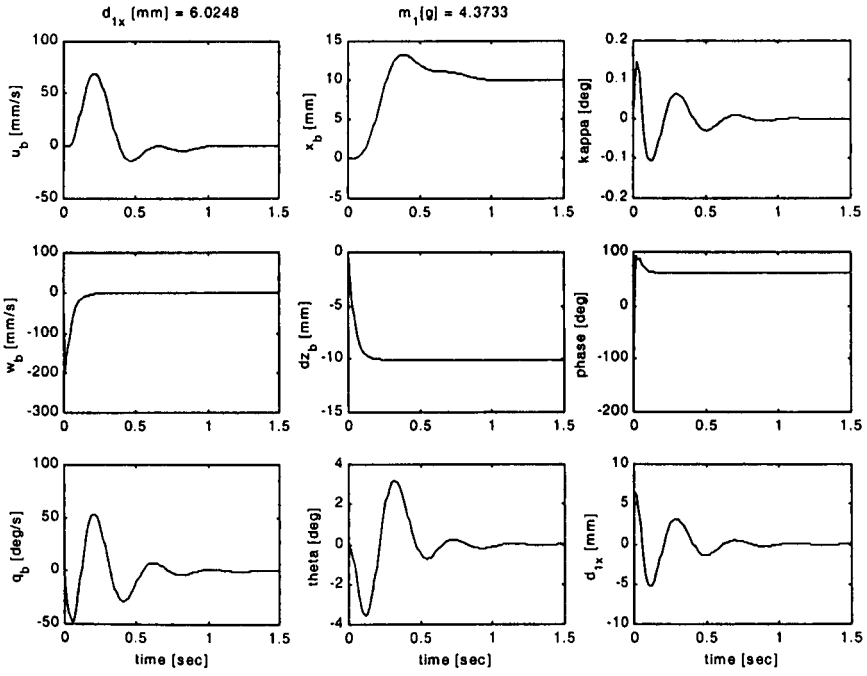

Fig 8.55 Vehicle Response to Simultaneous Step Inputs to $x_{b,dmd}$ and $z_{b,dmd}$ (Control Concept 3 with Modified Aerodynamics and Control Gains)

Control Concept 1				
x_b-Channel	k_u = -1.94 rad.m^{-1}.s	k_{px} = -17.4 rad.m^{-1}	T_{Ix} = 0.34 sec	
z_b-Channel	k_w = -34 Hz.m^{-1}.s	k_{pz} = -284	T_{Iz} = 0.47 sec	
q_b-Channel	k_q = -0.016 m.rad^{-1}.s	k_θ = -1 m.rad^{-1}		

Control Concept 2				
x_b-Channel	k_u = -1.94 rad.m^{-1}.s	k_{px} = -17.4 rad.m^{-1}	T_{Ix} = 0.34 sec	
z_b-Channel	k_w = 12 rad.m^{-1}.s	k_{pz} = 600 rad^{-1}.s^{-1}	T_{Iz} = 600 sec	T_{dz} = 0.24 sec
q_b-Channel	k_q = -0.05 m.rad^{-1}.s	k_θ = -10 m.rad^{-1}		

Control Concept 3				
x_b-Channel	k_u = 2 rad.m^{-1}.s	$k_{p\theta}$ = -1 m.rad^{-1}	k_{px} = 7.9 rad.m^{-1}	T_{Ix} = 0.29 sec
z_b-Channel	k_w = 2 rad.m^{-1}.s	k_{pz} = 400 rad^{-1}.s^{-1}	T_{Iz} = 4 sec	T_{dz} = 0.16 sec
q_b-Channel	k_q = -0.05 m.rad^{-1}.s			

Table 8.6 Modified Control Gains for Flight Control Systems

8.7 SUMMARY

The MAV was stabilised in the pitch axis with a feedback of the pitch rate to the centre of gravity location of the fuselage. It is assumed that a mechanism to achieve this, either by 'lengthening' or 'bending' the fuselage as shown in Fig 5.9 (a) and (b) respectively, is feasible. Two different values for the gain were determined, depending on whether the frequency was varied or fixed.

Once stabilised in the pitch axis, three different concepts for position and velocity control were then explored. In Control Concept 1, the flapping frequency and the stroke plane angle were used as control effectors. In both axes, the velocity stability loop requires that the velocities (u_b and w_b) to be fed back. Negative gains were required as the gain K_{ku} and K_{fw} are both negative. P+I position controllers for both the vertical and horizontal axes were used for good tracking performance.

In Control Concept 2, the phase difference between wing pitch and flap was used to control the vertical axis while the stroke plane angle remained as the horizontal axis control effector. As $K_{\varphi w}$ is now positive, the gains in the vertical axis are all positive. Similarly, since $K_{\kappa u}$ is still negative, gains in the horizontal axis are all negative. A P+I controller was sufficient for the horizontal axis but a PID controller was necessary to increase the damping and tracking performance in the vertical axis.

The vertical axis control in Control Concept 3 is adopted unchanged from Concept 2. In order to point the resultant force in the direction or advance, the fuselage was tilted by a change in the centre of gravity location. A pitch attitude control loop was included since the fuselage pitch attitude is important in this concept. This is achieved by feeding back the pitch attitude to the centre of gravity location

Finally, due to the experimental uncertainty presented by the accuracy of the wing lift, the effects of its omission were also studied. It was found that the control concepts were still valid, provided some modifications were included in the control system designs. These included variation of the gains to account for the difference in the aerodynamics and also the inclusion of the pitch attitude control loop in the Concepts 1 and 2.

In conclusion, the findings so far have shown that for the systems being investigated

a. the flapping wing MAV can be stabilised using appropriate feedback to the selected control effectors.

b. the flight control designs with appropriately selected controllers were able to provide precise position control at hover and low speed flight

c. although there is aerodynamic uncertainty, the control concepts investigated are effective provided proper gain scheduling is implemented.

d. vehicle performance can be improved by including a pitch attitude control loop.

CHAPTER 9

PERFORMANCE COMPARISON OF THE FLIGHT CONTROL CONCEPTS

9.1 INTRODUCTION

Three different control concepts for the flapping wing MAV have been described in Chapter 8. These are

a. Concept 1: Variation of flapping frequency to control force magnitude and tilt of stroke plane for force vectoring. The phase angle between wing pitch and wing flap was fixed. This can be referred to as control by flap frequency and stroke plane tilt.

b. Concept 2: The flapping frequency is fixed and the phase angle between wing pitch and wing flap was varied to control force magnitude. Tilt of stroke plane angle vectors the force. This can be referred to as control by pitch phase and stroke plane tilt.

c. Concept 3: The flapping frequency is fixed and the phase angle between wing pitch and wing flap was varied to control force magnitude, as in Concept 2. The stroke plane angle was also fixed. For force direction control, the centre of gravity location of the fuselage with respect to wing attachment was varied. This results in a change in the pitch attitude of the fuselage, indirectly vectoring the resultant wing force. This can be referred to as control by pitch phase and CG shift.

Each of the control systems designed for the above concepts has three command channels (q_b, x_b and z_b). It was found that although there is no need for a pitch attitude control loop when the vehicle is in trim, the inclusion of such a loop is beneficial when the vehicle is off trim. As such, a pitch attitude control loop was included for all three concepts in the subsequent simulations.

Each of the above channels has an inner stability loop with simple rate feedback and an outer position control loop with a controller in the forward path. The controller may be

a. a simple proportional controller for the case of the pitch attitude control for all three concepts

b. a P+I controller in the cases of the x_b and z_b channels of Concept 1 and the x_b channels of Concept 2 and Concept 3.

c. a PID controller as in the cases of the z_b channel of Concept 2.

The control laws, block diagrams and gains of the final design for each of the three concepts are shown in Figs 9.1 to 9.3.

Although an input filter in the x_b-channel was seen to reduce the range of travel in the fuselage CG, it will be shown later that it affects the response to a ramp input. This is not shown in the figures.

CONTROL CONCEPT 1

Control Laws:

$$\kappa_{dmd} = \left(k_{px} + \frac{k_{Ix}}{s} \right)(x_{dmd} - x) - k_u u_b$$

$$n_{dmd} = \left(k_{pz} + \frac{k_{Iz}}{s} \right)(z_{dmd} - z) - k_w w_b$$

$$d_{1x,dmd} = \left(1 + \frac{n_{dmd}}{n_{nom}} \right)^2 d_{1x,nom} + k_\theta (\theta_{dmd} - \theta) - k_q q_b$$

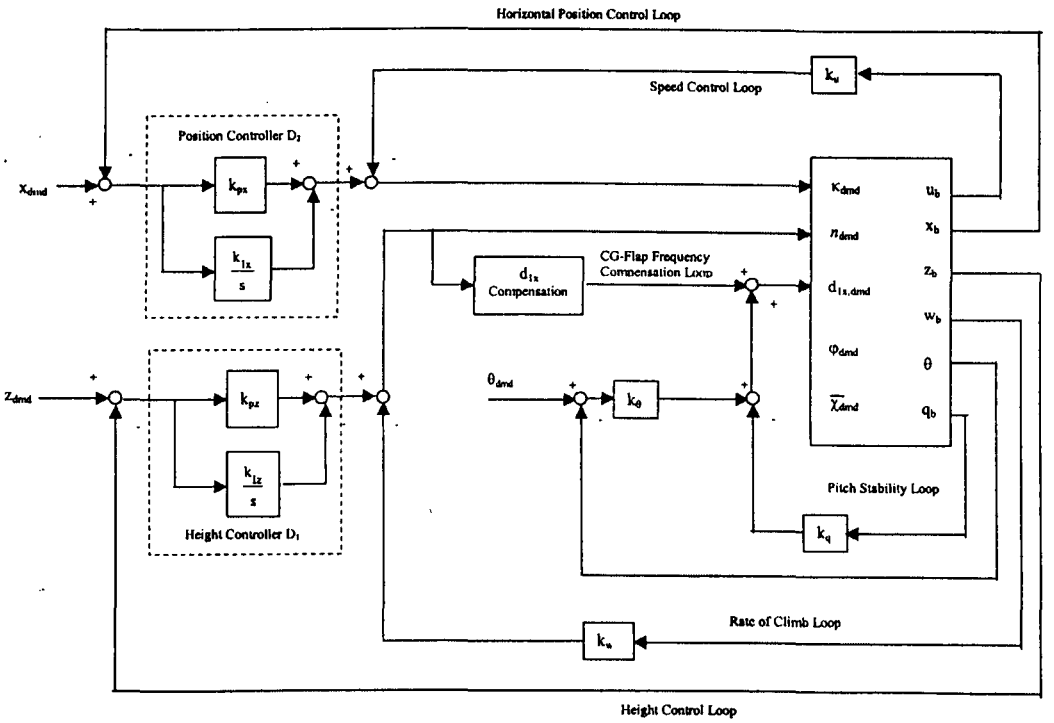

Control Concept 1			
x_b-Channel	k_u = -1.94 rad.m^{-1}1.s	k_{px} = -17.4 rad.m^{-1}	k_{Ix} = -51.18 rad.m^{-1}.s^{-1}
z_b-Channel	k_w = -34 Hz.m^{-1}1.s	k_{pz} = -284 Hz.m^{-1}	k_{Iz} = 600 Hz.m^{-1}s^{-1}
q_b-Channel	k_q = -0.016 m.rad^{-1}s	k_θ = 1 m.rad^{-1}	

Fig 9.1 Final Design of Flight Control System for Concept 1

CONTROL CONCEPT 2

Control Laws:

$$\kappa_{dmd} = \left(k_{px} + \frac{k_{Ix}}{s} \right)(x_{dmd} - x) - k_u u_b$$

$$\varphi_{dmd} = \left(k_{pz} + \frac{k_{Iz}}{s} + T_{Dz} s \right)(z_{dmd} - z) - k_w w_b \qquad \text{where } T_{Dz} = k_{pz} T_d$$

$$d_{1x,dmd} = d_{1x,nom} + k_\theta(\theta_{dmd} - \theta) - k_q q_b$$

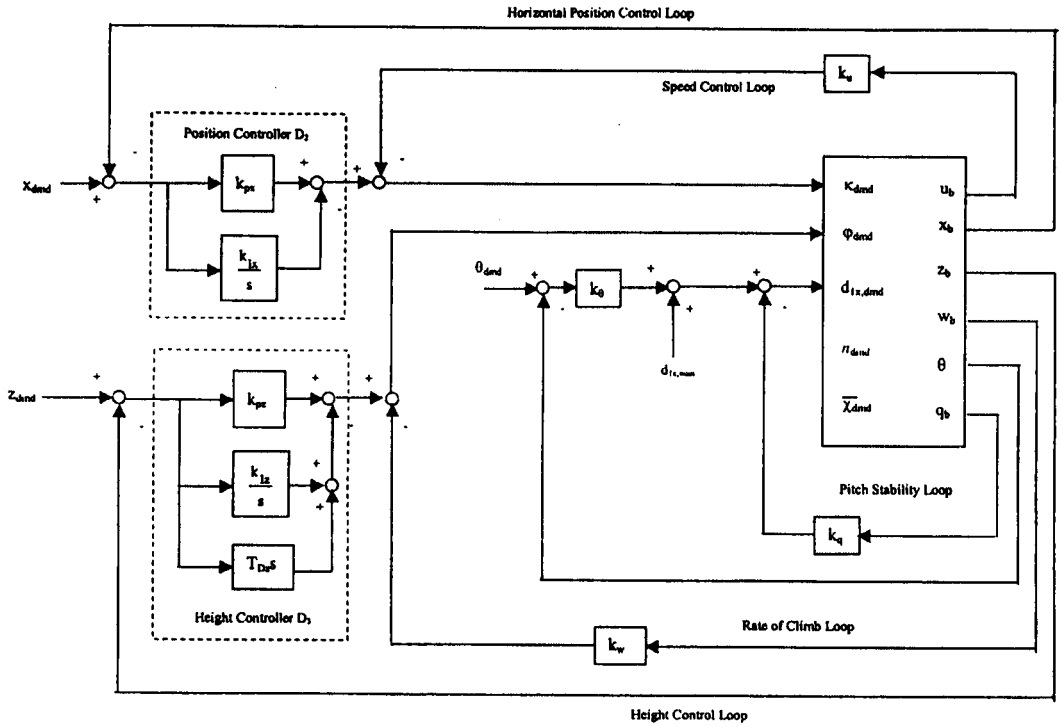

Control Concept 2				
x_b-Channel	k_u = -1.94 rad.m^{-1}1.s	k_{px} = -17.4 rad.m^{-1}	k_{Ix} = -51.18 rad.m^{-1}.s^{-1}	
z_b-Channel	k_w = 2 rad.m^{-1}s	k_{pz} = 100 rad.m^{-1}	k_{Iz} = 1 rad.m^{-1}.s^{-1}	T_{Dz} = 4 rad.m^{-1}
q_b-Channel	k_q = -0.05 m.rad^{-1}s	k_θ = 1 m.rad^{-1}		

Fig 9.2 Final Design of Flight Control System for Concept 2

CONTROL CONCEPT 3

Control Laws:

$$\varphi_{dmd} = \left(k_{pz} + \frac{k_{Iz}}{s} + T_{Dz}s\right)(z_{dmd} - z) - k_w w_b \qquad \text{where } T_{Dz} = k_{pz} T_d$$

$$d_{1x,dmd} = d_{1x,nom} - k_{p\theta}\left\{k_u\left[k_{px}\left(1 + \frac{1}{T_{Ix}s}\right)(x_{dmd} - x) - u_b\right] + \theta\right\} - k_q q_b$$

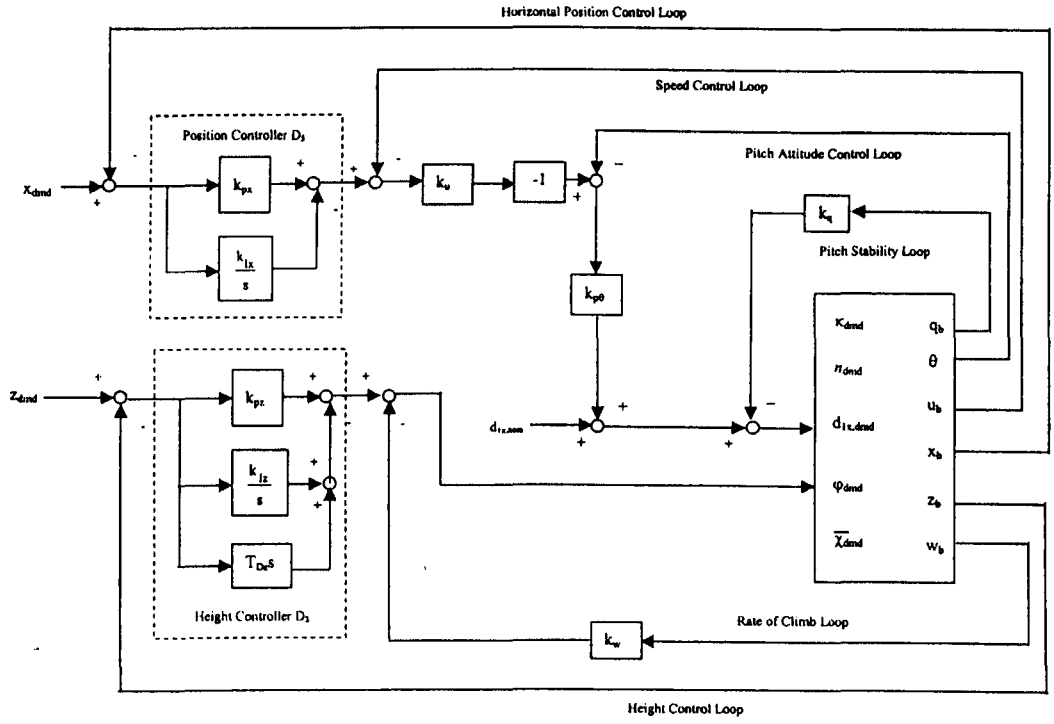

Control Concept 3				
x_b-Channel	$k_u = 2$ radm^{-1}s	$k_{p\theta} = -1$ m.rad^{-1}	$k_{px} = 7.9$ s^{-1}	$k_{Ix} = 27.24$ s^{-2}
z_b-Channel	$k_w = 2$ rad.m^{-1}s	$k_{pz} = 100$ rad.m^{-1}	$k_{Iz} = 1$ rad.m^{-1}.s^{-1}	$T_{Dz} = 4$ rad.m^{-1}.s
q_b-Channel	$k_q = -0.05$ m.rad^{-1}s			

Fig 9.3 Final Design of Flight Control System for Concept 3

While it can be seen that omitting the contribution of the wing lift to the resultant aerodynamic force required some modifications to the control gains in order to improve the response of the vehicle, the simulations in this chapter are carried out with the assumption that the wing lift aerodynamics are accurate and its contribution to the total resultant force has been included.

The three control concepts are compared in this chapter for their respective merits and shortcomings. Six reference manoeuvres are defined to which the three concepts are subjected. These are

a. step input in x_{dmd} only,

b. step input in z_{dmd} only,

c. step input simultaneously in both x_{dmd} and z_{dmd}

d. ramp input in the x_b-channel only

e. ramp input in the z_b-channel only

f. ramp input simultaneously in both x_b- and z_b-channels

9.2 SIMULATION RESULTS

9.2.1 PRESENTATION OF RESULTS

The response of the vehicle in terms of its position (x_b and z_b), the control inputs for the vertical axis (flapping frequency n or phase φ) and for the horizontal axis (stroke plane angle κ and fuselage pitch attitude θ) as well as the centre of gravity shift d_{1x} shall form the basis of comparison for the different concepts.

The variable η_x denotes the control input for the horizontal axis, i.e. $d\eta_x = \Delta\kappa = \kappa - \kappa_o$ for Concept 1 and Concept 2 and $d\eta_x = \Delta\theta = \theta - \theta_o$ for Concept 3. For the vertical axis, η_z denotes the control input, i.e. $\eta_z = \Delta n = n - n_o$ Concept 1 and $\eta_z = \Delta\varphi = \varphi - \varphi_o$ Concept 2 and Concept 3.

The response of the vehicle to each set of manoeuvres will be described by a set of 5 charts. Referring to Fig 9.4, the charts on the left column represent the horizontal and vertical position of the vehicle. On the right column, the relative range for the control input for the horizontal axis will be depicted. For the vertical axis, this will be represented as a percentage change since different units are used for the different concepts, 100% being the nominal input or trim value. Finally, the bottom left chart of the set depicts the CG travel.

9.2.2 STEP INPUTS

9.2.2.1 Step Inputs in $x_{b,dmd}$

A step input of 10 mm magnitude is demanded. The responses are shown in Fig 9.4. It can be seen that both Concept 1 and Concept 2 has very similar response while Concept 3 shows slightly higher overshoot in x_b.

As soon as the there is a deflection in the horizontal axis control η_x, the vehicle begins to lose some height. However, this loss is quite insignificant, amounting to slightly more than 0.05 mm in the worst case in Concept 3. It took Concept 1 the longest time to recover to the initial height.

The variations in vertical axis control input for all the designs from the nominal values were negligible. It is to be noted that an in-depth comparison between change in frequency and change in phase in the other concepts may not meaningful.

Concept 1 also has the smallest variation in the centre of gravity location, not exceeding ±3mm from the nominal position while the other two concepts experienced CG variation of close to ±5 mm.

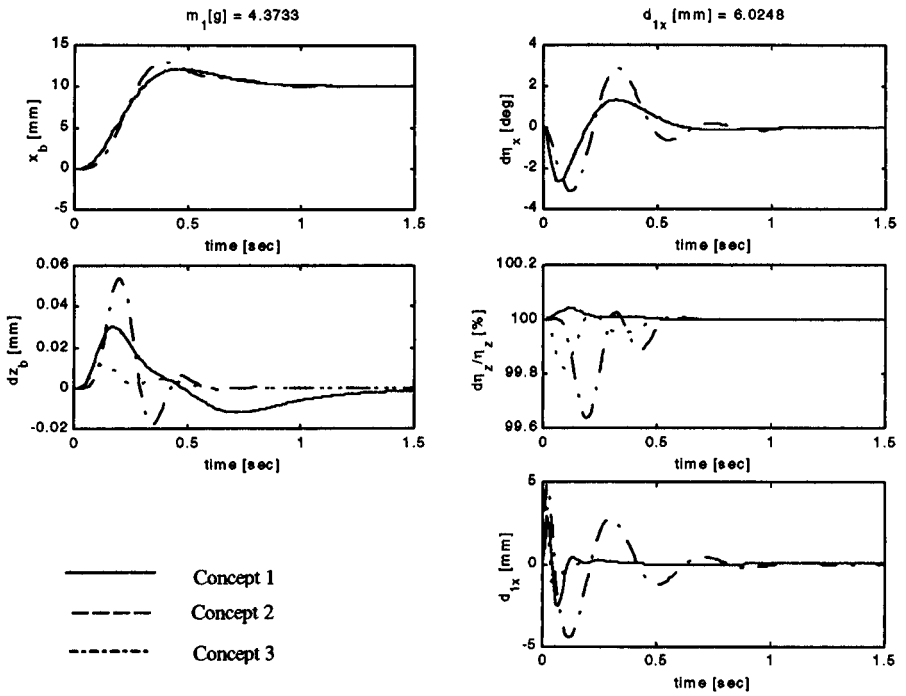

Fig 9.4 Response to Step Input in $x_{b,dmd}$

9.2.2.2 Step Input in $z_{b,dmd}$

Fig 9.5 shows the response of the vehicle to a step input of -10 mm in $z_{b,dmd}$. It can be seen that the response of Concept 1 was the slowest amongst the three, taking more than 1 second to reach the demanded height. However, there was no forward or aft motion accompanying this transition, unlike that seen in the other two Concepts. This is because the effect of an increase in flapping frequency on the pitch attitude was properly taken care of by the d_{1x} compensation. The resultant force is still pointed vertically upwards and the vehicle climbs without being thrusted forward.

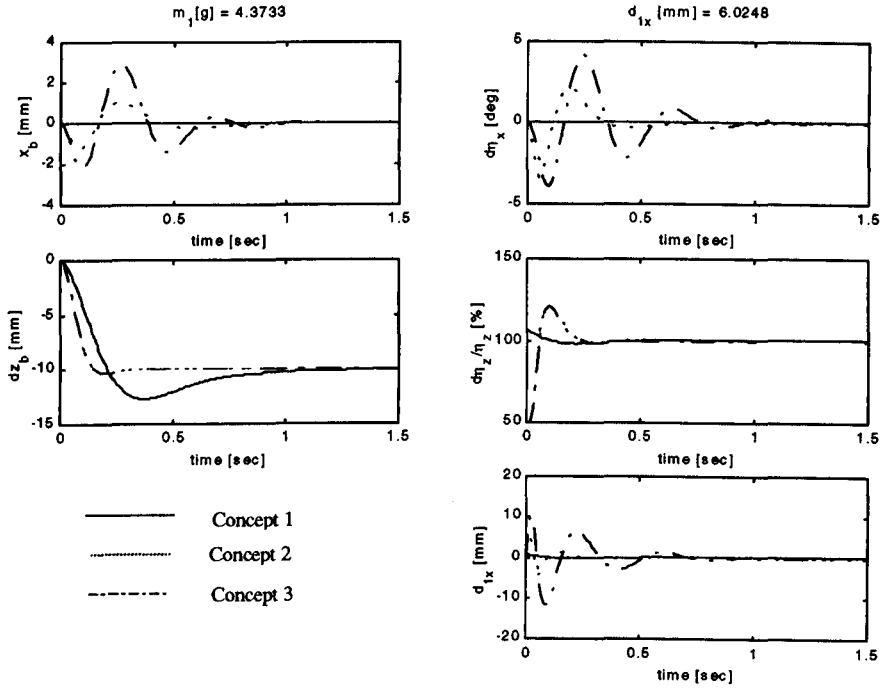

Fig 9.5 Response to Step Input in $z_{b,dmd}$

In the other two control concepts, note that $d\eta_z / \eta_z$ was reduced indicating that the phase φ has to be reduced in order to increase the force magnitude to initiate the climb. Accompanying the change in phase is a change in the direction of the resultant force. As a result, the vehicle will be accelerated backwards and forward initially and the horizontal control input has to counter this. This cross-axis response has a maximum of about 3 mm in Concept 3. This may still be acceptable but if larger magnitude input were demanded, the response may be undesirable, especially if the vehicle has to climb in confined spaces, e.g. if climbing up close behind but without colliding into the obstacle.

The maximum excursion in centre of gravity is observed in Concept 3, where it exceeds ±10 mm. It also takes the longest to settle, the damping ratio being the lowest amongst the three concepts. This is also observed in the oscillation of the horizontal axis control input η_x.

9.2.2.3 Simultaneous Step Inputs in $x_{b,dmd}$ and $z_{b,dmd}$

Fig 9.6 shows the vehicle response to simultaneous step inputs to both horizontal and vertical axes of magnitude 10 mm.

It can be seen that the vehicle controlled by Concept 1 took the longest time to reach the demanded height again. Its response in the horizontal axis is, however, the best amongst the three. It is observed to transit immediately in the demanded direction, i.e. forward, unlike the vehicles controlled by the other concepts where they were thrusted backwards before moving forward. Both the horizontal control deflection η_x and vertical control input η_z were also minimum when compared to the other two concepts.

Concept 3 again shows maximum centre of gravity travel, as much as –15mm from its nominal position. Furthermore, its damping in the horizontal axis is worse off than the other two concepts, due to the high pitching inertia of the vehicle as a whole.

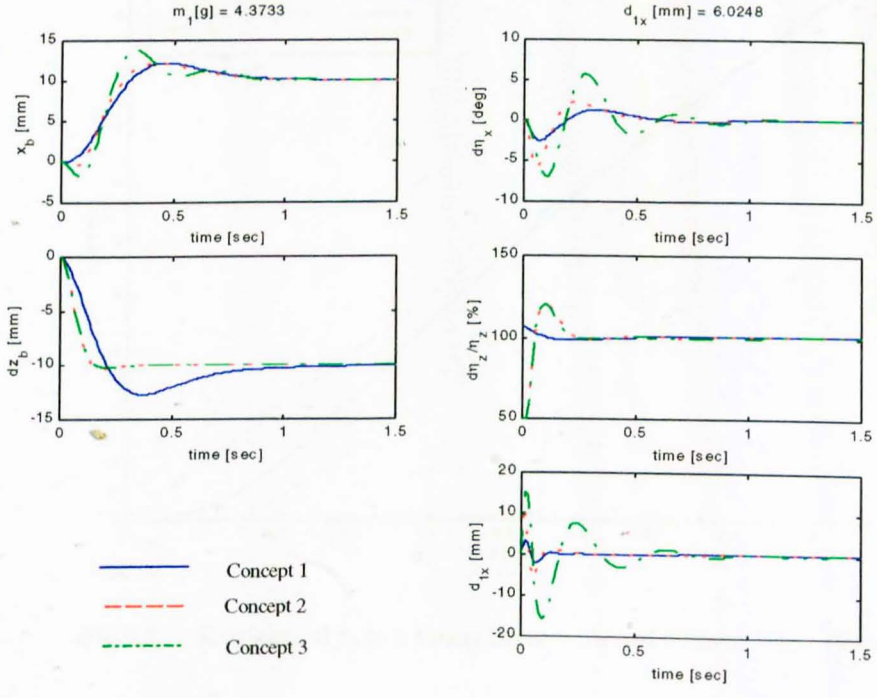

Fig 9.6 Response to Simultaneous Step Input in $x_{b,dmd}$ and $z_{b,dmd}$

9.2.3 RAMP INPUTS

9.2.3.1 Effects of Input Filter

It was seen in Chapter 8 that when abrupt inputs of large magnitude, as is with step inputs, are demanded, the centre of gravity excursion may be excessive. In order to alleviate this, an input-smoothing filter was suggested as shown in Fig 8.47. This resulted in much smaller CG excursion during step demands as seen in the simulations in Chapter 9.2.2.

Fig 9.7 shows the tracking performance of Concept 1 with and without the input smoothening filter for a ramp input in $x_{b,dmd}$ of 10 mm.s^{-1}. It can be seen, however, the input-smoothing filter leads to a degradation of the tracking performance. A 10% position error was recorded at the end one second.

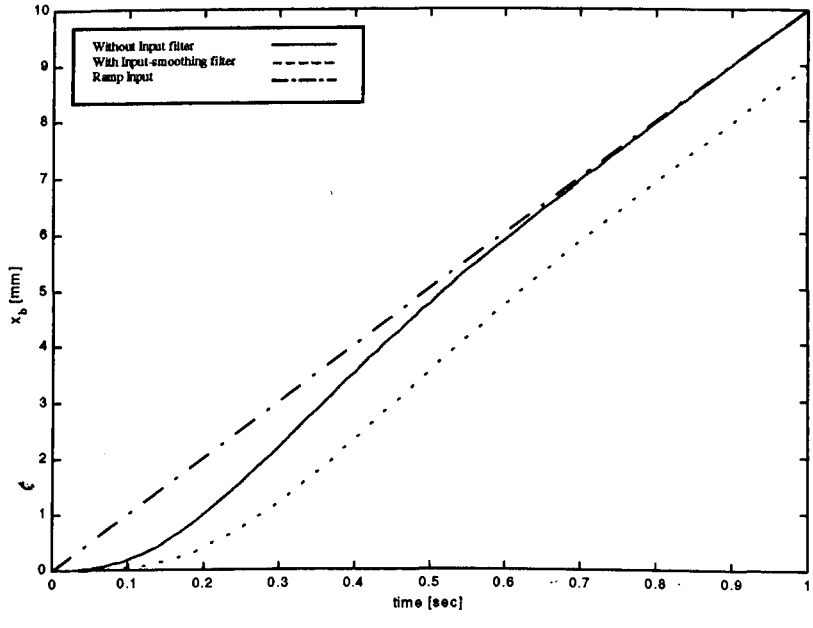

Fig 9.7 Response of x_b to a Ramp Input with and without Input Filter

The steady state rate of increase of x_b was still 10 mm.s^{-1} as demanded. It would be thinkable in the control system design, that a switch be put in place that triggers the inclusion of the smoothening filter only when the rate of change of input exceeds a given threshold so that the tracking performance will not be degraded during low gradient ramp inputs.

In order to compare the tracking performance properly, the input smoothening filter will be removed from the simulations with ramp input for the present comparisons of ramp responses of the difference concepts.

9.2.3.2 Ramp Input in $x_{b,dmd}$

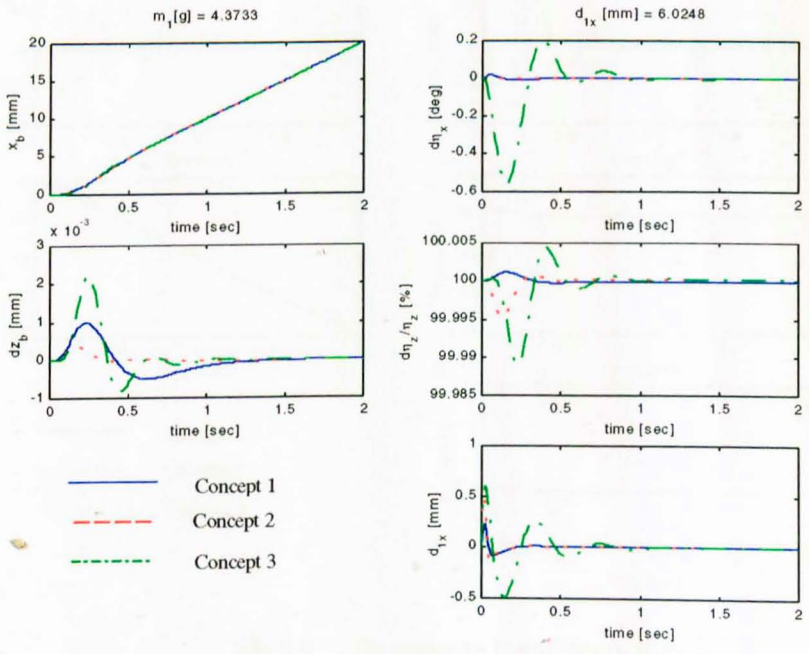

Fig 9.8 Response to Ramp Input in $x_{b,dmd}$

A ramp input of magnitude 10 mm.s^{-1} is demanded. The responses are shown in Fig 9.8. It is seen that there is no discernible difference in the tracking response of x_b while the height

loss due to the tilt of the resultant force vector is negligible. Although the changes in both horizontal and vertical control inputs as well as the centre of gravity excursion are highest in Concept 3, these variations are small compared to the cases of step inputs.

9.2.3.3 Ramp Input in $z_{b,dmd}$

A ramp input of magnitude -10 $mm.s^{-1}$ is demanded. The responses are shown in Fig 9.8. There is little difference between the tracking performance of Concepts 2 and 3, which are better than that of Concept 1.

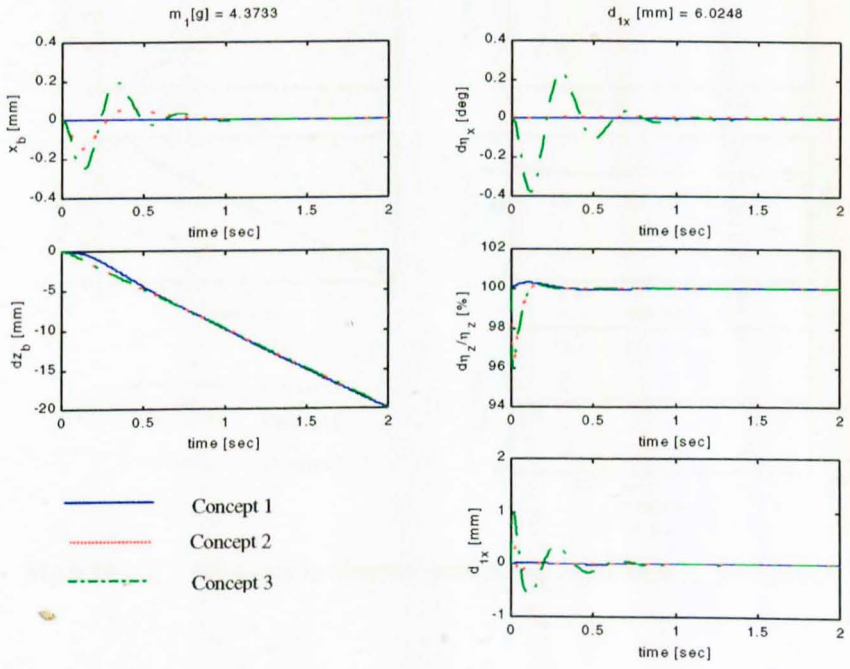

Fig 9.9 Response to Ramp Input in $z_{b,dmd}$

There is practically no cross-axis response in Concept 1 while the other two concepts result in some fore-aft motion of the vehicle. Again, the control inputs were minimal when compared to the step demands of the previous sections.

9.2.3.4 Simultaneous Ramp Input in $x_{b,dmd}$ and $z_{b,dmd}$

A simultaneous ramp input of magnitude 10 mm.s^{-1} are placed on $x_{b,dmd}$ and $z_{b,dmd}$. The response of the three systems is shown in Fig 9.10. There is no discernible difference in the tracking of $x_{b,dmd}$ while Concept 1 shows slightly poorer performance than the other two concepts in the tracking of $z_{b,dmd}$.

The biggest variation of control inputs is evident in Concept 3, but the variations are all minimal when compared with step inputs.

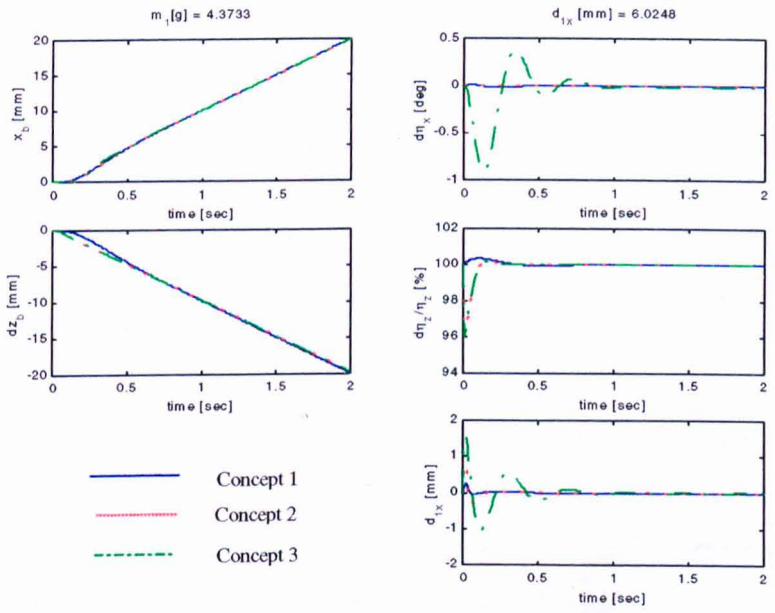

Fig 9.10 Response to Simultaneous Ramp Input in $x_{b,dmd}$ and $z_{b,dmd}$

9.2.4 LARGE MAGNITUDE ABRUPT INPUTS

It was seen in the previous sections that ramp inputs of magnitude 10 $mm.s^{-1}$ generate relatively mild demands on the pertinent control parameters such as the centre of gravity variation, flap frequency or phase variation, stroke plane or fuselage tilt. The maximum centre of gravity travel was only ±1.5 mm from the nominal position for Concept 3. In view of this, larger magnitude ramp inputs are not expected to pose a problem.

On the other hand, step inputs place higher demands on the control parameters even when input smoothening filters were in place. The centre of gravity travel for step inputs of magnitude 10 mm was found to be in excess of ±10 mm from the nominal position for Concept 3, and close to 10 mm for Concept 2. Without the use of the input smoothing filter, the centre of gravity travel for Concept 3 was seen to exceed 100 mm as shown in Fig 8.42.

From the previous simulations, the most severe of the six manoeuvres studied is when step inputs were simultaneously demanded for $x_{b,dmd}$ and $z_{b,dmd}$. When the magnitudes are increased, the flight control systems may experience saturation and the vehicle may possibly depart from controlled flight.

Fig 9.11 shows the comparison of the vehicle response and control parameters for the three flight control concepts when simultaneous steps of magnitude 50 mm were demanded. It can be seen that Concept 1 shows the best overall performance because the demanded position is achieved without much oscillation, although the height was achieved about 0.8 second later than in Concept 2 and Concept 3. More importantly, the centre of gravity travel was much lower at about ±10mm compared to the ±75 mm of Concept 3. The disadvantage of Concept 1 was the need to increase flap frequency by 35% from 40 Hz to 54 Hz. This demand would put a high demand on energy to overcome the effects of inertia.

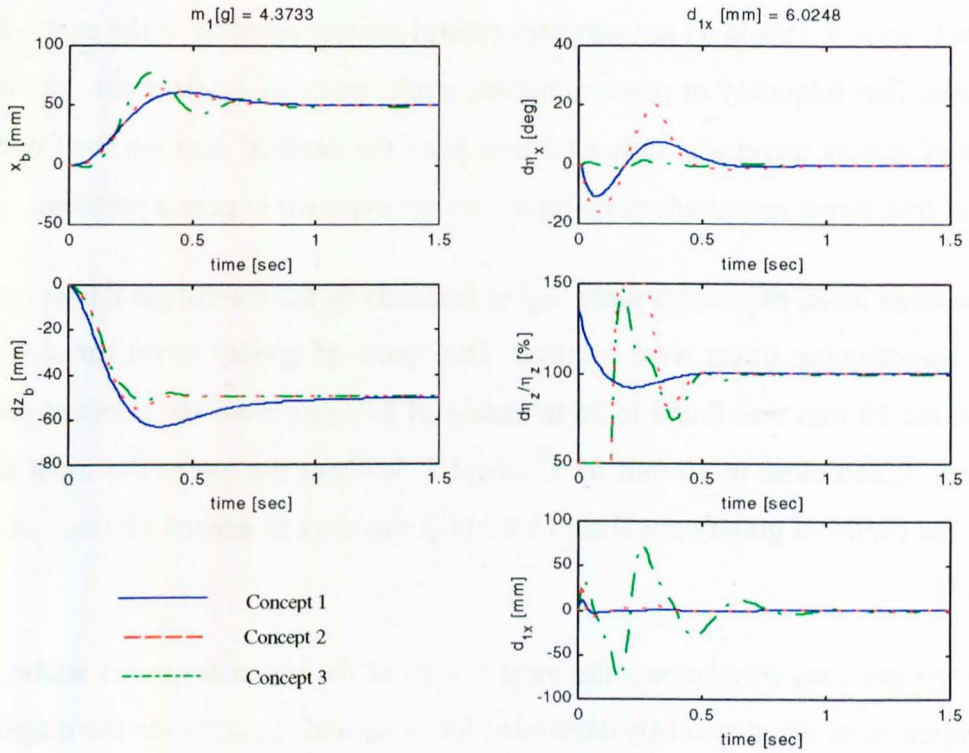

Fig 9.11 Response to Simultaneous Step Input of 50 mm with Input Smoothing Filters

9.3 DISCUSSION

The foregoing studies have revealed both the advantages and disadvantages of the three different flight control concepts. Important factors affecting the feasibility of each control strategy are as follows:

a. the range travel of the centre of gravity

b. the cross-axis response or the effect of input on one axis on the response of the other axis.

c. speed and damping of response

d. vehicle empty weight

e. energy usage

9.3.1 CENTRE OF GRAVITY TRAVEL

The centre of gravity travel was shown in the previous sections to be more significant for some control concepts than for others. In particular, Concept 3 faired worst in this aspect with the range exceeding ±15mm from the nominal position for a 10 mm simultaneous step input to both axes. For larger magnitude inputs, the range will be higher even with an input smoothing filter.

The Concept 1 flight control system performed best here. Even for a 50 mm simultaneous step input to both axes, the travel was limited to ±12.5 mm from the nominal position. This is because an increase in force magnitude is demanded during an initiation to climb, the moment imbalance is much lower if effected by an increase in the flapping frequency than if effected by a change in phase. In the latter, the accompany change in force direction adds to the moment imbalance.

For the pitch stabilisation through centre of gravity shift to be feasible, the travel must be kept at a minimum. The addition of the input smoothening filter has clearly helped in reducing the range of travel. Avoiding abrupt, large magnitude inputs may help further.

9.3.2 CROSS-AXIS RESPONSE

This is defined as the response of the motion parameters along one axis due to the input in another axis. Hence, if a step input is demanded of the z-axis, the cross-axis response would be that in the x_b-axis and vice-versa. This criterion is important if the vehicle has to make a vertical climb or accelerate forward close to obstacles without hitting them.

It was seen in the preceding sections that Concept 1 performed best where the cross-axis response was significant. Fig 9.5 shows that during a step demand of 10 mm on z_b alone, the vehicle response in x_b-axis was practically zero, unlike that of the other two where the vehicle oscillated between ±2.5 mm for Concept 3 and ±1 mm for Concept 1, which is up to 25% of the demanded step. The reason for the exceptional performance of Concept 1 here is due to the fact that an change in flap frequency does not come with a change in the force direction with respect to the stroke plane as is the case with the change of phase.

During a step input in x_b, the cross axis response in the z_b-axis was negligible for all the three control concepts. Similarly, there was practically very little cross-axis response in the case for a ramp input in z_b.

During a ramp input in x_b in Fig 9.8, it can be seen the vehicle controlled by Concept 1 lost 1 mm in height in the initial 0.5 second. This is because the tilt in the stroke plane to accelerate the vehicle forward resulted in a reduced vertical component of the aerodynamic force. The vehicle with Concept 2 performed best with only 0.5 mm loss in height while the vehicle controlled by Concept 3 lost more than 2 mm.

9.3.3 SPEED AND DAMPING OF RESPONSE

From the time histories of Figs 9.4 to 9.10 as well as the linear transfer functions shown in Table 9.1, it can be seen that Concept 2 has the fastest response and best-damped system amongst the three.

	x_b-axis	z_b-axis
Concept 1	$\frac{x_b(s)}{x_{b,dmd}(s)} = \frac{170.3\ (s + 2.94)}{(s + 5)(s^2 + 14s + 100)}$ $\zeta = 0.7 \quad \omega_n = 10\ \text{rad.s}^{-1}$	$\frac{z_b(s)}{z_{b,dmd}(s)} = \frac{142\ (s + 2.13)}{(s + 3)(s^2 + 14\,s + 100)}$ $\zeta = 0.7 \quad \omega_n = 10\ \text{rad.s}^{-1}$
Concept 2	$\frac{x_b(s)}{x_{b,dmd}(s)} = \frac{170.3\ (s + 2.94)}{(s + 5)(s^2 + 14s + 100)}$ $\zeta = 0.7 \quad \omega_n = 10\ \text{rad.s}^{-1}$	$\frac{z_b(s)}{z_{b,dmd}(s)} = \frac{21.76\ (s + 23.96)(s + 1.044)}{(s^2 + 31.6s + 510.3)(s + 1.066)}$ $\zeta = 0.7 \quad \omega_n = 22.6\ \text{rad.s}^{-1}$
Concept 3	$\frac{x_b(s)}{x_{b,dmd}(s)} = \frac{66628(s+3.44)(s^2+220s+25000)}{(s+240)(s^2+10.9s+43.4)(s^2+9.7s+292.4)(s^2+220s+18769)}$ $\zeta = 0.27 \quad \omega_n = 16.3\ \text{rad.s}^{-1}$ $\zeta = 0.77 \quad \omega_n = 139\ \text{rad.s}^{-1}$ $\zeta = 0.8 \quad \omega_n = 6.6\ \text{rad.s}^{-1}$	$\frac{z_b(s)}{z_{b,dmd}(s)} = \frac{21.76\ (s + 23.96)(s + 1.044)}{(s^2 + 31.6s + 510.3)(s + 1.066)}$ $\zeta = 0.7 \quad \omega_n = 22.6\ \text{rad.s}^{-1}$

Table 9.1 Linear Transfer Functions, Damping and Natural Frequencies

The horizontal axis in Concept 3 has a total of four modes, three of which are oscillatory. Of these 3 oscillatory modes, one has a damping ratio of only 0.27. The poor damping results from the choice of control gains in the design process. A reduction of the proportional gain k_{px} to 6 s^{-1} from 7.9 s^{-1} results in an improvement to the overall damping of the system as shown in Fig 9.12. The integral time was affected because the integral gain $k_{Ix} = 27.25\ s^{-2}$ was unchanged.

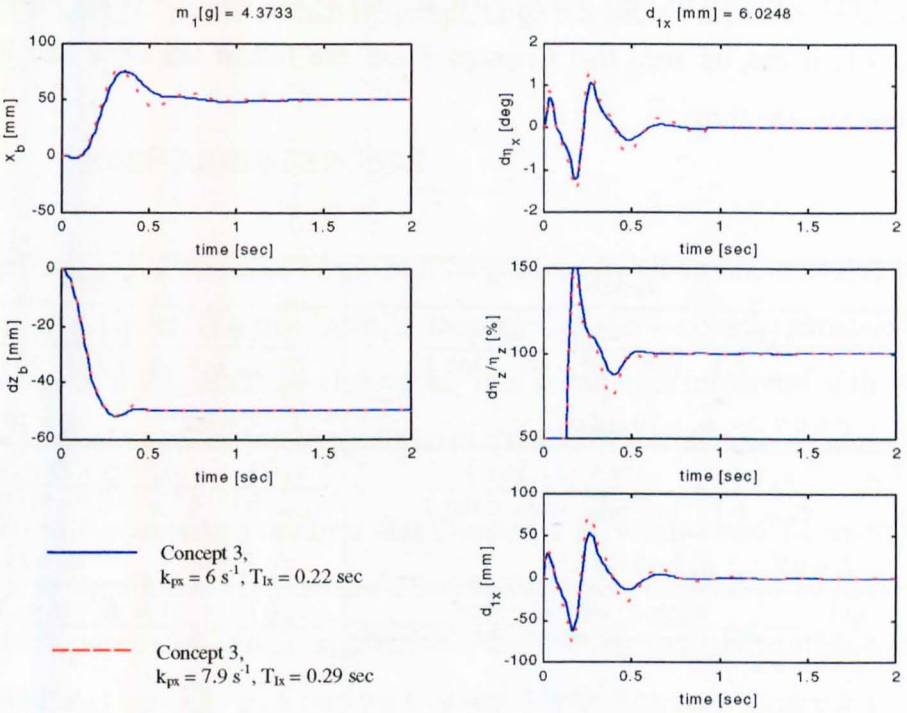

Fig 9.12 Effects of Reduction of Proportional Gain k_{px} in Concept 3 [k_u = 2 rad.m^{-1}, $k_{p\theta}$ = -17.4 rad.m^{-1}]

9.3.4 VEHICLE EMPTY WEIGHT

Only a qualitative assessment shall be attempted in this respect here. As mentioned earlier, Concept 3 has made the stroke plane actuator motors redundant since the stroke plane angle is to remain practically constant. This constitutes a weight reduction in the design of the vehicle. In order to tilt the fuselage, the centre of gravity is shifted accordingly. The mechanism to carry out this centre of gravity shift is already required for pitch stability and is not an additional requirement. Concept 3 thus has an edge over the other two designs.

9.3.5 ENERGY REQUIREMENT

The stroke plane actuator motors in Concept 1 and Concept 2 will have to overcome the high inertia of the wings flapping at a very high frequency in order to change the stroke plane angles. The energy required may be considerably higher than that required to extend the length of the fuselage or to bend it. This is, however, a qualitative assessment and further proof is required based on the actual design weights and inertia of the wings and fuselage.

Comparing phase variation with flap frequency variation for vertical axis control, it is to be noted that changing the phase between flap and pitch attitudes of the wing may require less energy than changing the flap frequency. Increasing the flap frequency would necessarily mean overcoming the moment of inertia about the flap axis while changing the phase would require overcoming the moment of inertia about the pitch axis, the latter being an order of magnitude smaller in most wings.

9.4 SUMMARY

Three different concepts to control a flapping wing micro air vehicle have been studied in the previous sections. These concepts combine two options for each of the two axes to be controlled, namely

a. vertical axis control : pitch phase or flap frequency

b. horizontal axis control : stroke plane or fuselage tilt

The corresponding flight control systems have also been designed and their performance were compared with each other based on six manoeuvres, the most severe of which is the simultaneous step inputs to both axes.

The requirement to shift the centre of gravity location of the fuselage in order to control and stabilise the pitch axis of the vehicle means that the fuselage has to be made up of two separate bodies, either hinged together or linked by an extending mechanical arm.

In the simulations described in this chapter, it was found that large amplitudes result in high demands on the control parameters, especially on the range of CG travel. Installing an input-smoothing filter can, to some extent, alleviate this problem.

The simulations have also shown that Concept 1 has the best cross-axis behaviour, especially during the vertical climb. The vehicle employing Concept 3 performs less desirably in this aspect, with the cross-axis response being 25% of the input magnitude.

In terms of vehicle empty weight, there is a clear advantage in Concept 3. Since the fuselage, instead of the stroke plane, is being tilted to direct the force for horizontal speed and position control, the stroke plane actuator motors have been made redundant with the result of weight savings.

Finally, the speed of the response and the damping ratio of a vehicle controlled by Concept 3 can readily be improved by an appropriate choice of gains to match those of the other two as shown in Fig 9.12.

A vehicle with Concept 3 flight controls can be built lighter, carry a higher payload and probably also have higher endurance. Mechanical wear and tear can also be optimised by design about a constant flap frequency. By limiting the amplitude of abrupt inputs, the range of CG travel can be made more manageable. With a better gain selection, the damping ratio and speed of the response has been shown to be comparable to those of the other two concepts. Its disadvantage lies in the less desirable cross-axis response, which can probably be made more acceptable by a better flight control system design. It is believed that this concept of flight control would prove to be better than the other two.

CHAPTER 10

CONCLUSION

A flight control system was successfully implemented for each of the three design concepts using classical control theory. Simple P+I and PID controllers were used with rate and position feedback for stability. Although there was a certain degree of uncertainty in the experimentally obtained aerodynamic data, the simulation results have shown that the flight control system designs were valid once the pitch attitude control loop has been included and appropriate adjustments to the feedback control gains have been implemented.

In the course of the research, it was recognized that the variation in the centre of gravity location of the fuselage with respect to the wing attachment point determines the pitch moment balance. As such, it could be used for pitch attitude control for the vehicle. At the same time, the fuselage pitch attitude could be used for force vectoring and hence as a means to control the horizontal axes.

Of the three control concepts analysed, it is believed that Concept 3 (force magnitude modulation by phase variation and force direction control through fuselage tilt / CG shift) would result in a vehicle with minimum empty weight due to the redundancy of the stroke plane actuator motors. It is also more energy efficient compared with the other two concepts.

The use of CG shift for moment balance also allows relatively slower actuators to be employed compared with the use of wing kinematics variation for the same purpose. In the latter, the fuselage response and the wing parameters have to be sampled and controlled at frequencies much higher than the flapping frequency.

It was found that large amplitude, abrupt demands placed on the vehicle lead to saturation in the system and control effectors. These types of inputs should be avoided. Alternatively, input-smoothing filters can help alleviate the problem, although this degrades the tracking response.

Although the vehicle employs large amplitude flapping to generate aerodynamic forces, the dynamics of the fuselage and stroke plane actuator motors can be quite adequately modelled with the linearised time-averaged dynamics. While the full-order equations of motion allow the exact vehicle dynamics to be modelled, it was found that this results in a stiff system and is computationally slow. The use of the time-averaged model allows the system to be simplified, while maintaining the essential dynamics of the flapping wings. This speeds up the simulation and avoids the problem associated with stiff systems.

By linearising the time-averaged model, it was possible to further simplify the mathematical representation of the vehicle. The vehicle was found to be adequately represented as a pure integrator in all the fuselage modes. It is neutrally stable in all axes and lacks any restoring forces and moments in the open loop. The control systems can generally be designed from this linearised model, although differences in response can be observed between the linear and non-linear models for some of the design cases.

generally be designed from this linearised model, although differences in response can be observed between the linear and non-linear models for some of the design cases.

The control of the speed and position of the vehicle using feedback of angular rates, velocities, position and attitude of the vehicle to the appropriate control effectors was successful. The controllers are either P+I or PID type in order to improve the tracking performance.

In the experiments conducted to measure the aerodynamic forces, it was found that wing drag was sufficiently accurately measured while wing lift measurements were less accurate due to its small magnitude at the elevated angles of attack. In this respect, improvement of test rig and the use of a force balance with better resolution will be necessary for better aerodynamic data.

RECOMMENDATIONS FOR FUTURE WORK

The work carried out in this thesis has shown that the aerodynamic data can be experimentally collected quite quickly when compared with CFD methods. It has also shown that the aerodynamic data can be quickly incorporated into a simulation model, with which flight control systems can be designed and analysed. Most importantly, it has shown that a flapping wing MAV can be controlled through means inspired by natural flyers such as birds, insects and bats. Nonetheless, as in all other initial works, the research in this area of flight can be extended in many directions.

The success of the experiments carried out in this thesis to obtain aerodynamic data of the wing is limited by the fact that the magnitude of the forces were such that the resolution of the force balance may be marginal. At the same time, any attempt to increase the magnitude is bound by the upper limit of the flapping frequency of the mechanical flapper considering the high moment of inertial about the flap axis. In view of this, the design of

the flapping mechanism can be improved such that more powerful motors can be catered to provide higher torque. Lighter materials than aluminium can be used to fabricate the flapping arm so that the moments of inertia are reduced. The support structure can also be made stiffer in order to improve the measurement of the forces. A force balance with better resolution to measure low magnitude forces can also help improve the quality of the data.

Currently, the measurement of moments has not been undertaken in the experiments. Measurements of aerodynamic moments can be looked into once the methods for the measurement of forces have been improved.

The experiments were also conducted in still air to simulate the hovering flight. Future measurements in a low speed wind tunnel can also be carried out for forward flight simulation.

The mathematical model currently depicts the fuselage as a single body although the use of CG shift requires it to be made up of two bodies moving relative to each other. This can be included in the future modelling of the vehicle.

Three control concepts have been studied here and considered for the design of the flight control system. Nature's flyers have many other control concepts that may prove to be better suited for hovering flight or for some other flight regime. One such control concept briefly discussed but not studied is the use of the mean flap attitude of the wings for pitch control rather than the use of centre of gravity location.

The current design of the flight control system employing Concept 3 can further be improved to reduce the cross-axis response, which is currently the main disadvantage of the design. One area is to study the feasibility of anticipating the cross-axis response for a given input with the intention of pre-emptive application of the necessary control effector inputs to counter this inherent, but undesired, motion.

The simulation and control design for the longitudinal plane can be extended to forward flight once the corresponding aerodynamic data is available.

Finally, the lateral-directional cases can also be analysed and the flight control system for this plane can also be designed.

References

Archer R.D., Sapuppo J., Betteridge D.S., 1979, '*Propulsion characteristics of flapping wings*', Aeronautical Journal, pp 355-371.

Anonymous, 1999, http://mems.engr.wisc.edu/research/linear.html accessed on 26 Oct 1999

Anonymous, 2000a, http://mems.engr.wisc.edu/partners/SSI/SSI3.gif accessed on 10 July 2000.

Anonymous, 2000b, '*Ready for the next big thing*', The Engineer, 10 Mar, pg 20-22.

Ashley S., 1998, '*Palm-size spy planes*', Mechanical Engineering, Vol 120, Issue 2, pg 74-78.

Bartsch H.J., 1982, '*Taschenbuch mathematischer Formeln*', Verlag Harri Deutsch, Thun-Frankfurt/M, ISBN 3 87144 239 9

Chanute O, 1976, 'Progress in Flying Machines', reprinted from the 1st Edition of 1894, Lorenz & Herweg, Publishers

DeLaurier J.D., 1993, '*An aerodynamic model for flapping wing flight*', Aeronautical Journal, Vol 97 No 964, pp 125-130.

DeLaurier J.D., 1994, '*An ornithopter wing design*', Canadian Aeronautics and Space Journal, Vol 40, No 1

DeLaurier J.D., 1999, '*The development of and testing of a full scale piloted ornithopter*', Canadian Aeronautics and Space Journal Vol 95 No 2

DeLaurier J.D. and Harris J.M., 1993 '*A study of mechanical flapping wing flight*', Aeronautical Journal, pp 277-286

Deng X, Schenato L, Sastry S, 2001, '*Hovering flight control of a micromechanical flying insect*', Proceedings of the 40th IEEE Conference on Decision and Control, Orlando, Florida USA.

Dickinson M, 1994, '*The effects of wing rotation on unsteady aerodynamic performance at low reynolds numbers*', Journal of Experimental Biology, 192: 179-206.

Dornheim M.A., 1999, '*Several micro air vehicles in flight test programs*', Aviation Week & Space Technology, pg 47-48.

Drake J., 1998, '*Micromachinery: Shirt button turbines*', Technology Review, Vol 100 No 9 pg 10-11.

Dudley R and Ellington C P, 1990, '*Mechanics of forward flight in bumble bees II: Quasi-steady lift and power requirements*', Journal of Experimental Biology, Vol 148, pp 53-58.

Ellington C.P., April 1999, '*The aerodynamics of insect based flying machines*', Paper 37, 14th International Conference of Unmanned Aerial Vehicles, Bristol UK

Fejtek I. and Nehera J., 1980, '*Experimental study of flapping wing lift and propulsion*', Aeronautical Journal, Vol 84, pp 28-33

Grasmeyer J M, Keennon M T, 2001, '*Development of the Black Widow micro air vehicle*', AIAA-2001-0127

Grundy T, Keefe G, Lowson MV, 2000, '*Aerofoil performance variability at low Reynolds number*', Paper 34, 15th International Conference of Unmanned Air Vehicle Systems, Bristol UK, Apr

Hall K.C. and Pigott S.A., 1998, '*Power requirements for large amplitude flapping flight*', Journal of Aircraft, Vol 35 No 3.

Hughes P C, 1986, '*Space craft attitude dynamics*', New York, J Wiley

Katzmayr R, 1922, '*Effects of periodic changes of angle of attack on behaviour of airfoils*', NACA Report No 147, Oct 1922 (translated from Zeitshrift für Flugtechnik und Motorluftshiffahrt, Mar 31, pp 80-82 and Apr 13, pp 95-101)

K.D.Jones and M.F.Platzer, 1999, '*An experimental and numerical investigation of flapping wing propulsion*', AIAA 99-0995, 37th AIAA Aerospace Sciences Meeting and Exhibit, Reno, NV

Lehmann F.O. and Dickinson M.H., 1998, '*The control of wing kinematics and flight forces in fruit flies (Drosophila spp.)*', Journal of Experimental Biology, Vol 201, pp 385-401.

Lippisch A.M., 1960, '*Man powered flight in 1929*', Journal of the Royal Aeronautical Society, Vol 64, pp 395-398.

Liu H., Ellington C.P., Kawachi K., van den Berg C. and Willmott A.P., 1998, '*A computational fluid dynamic study of hawkmoth hovering*', Journal of Experimental Biology, Vol 201, pp 461-477.

Liu H, Kawachi K, 1999, '*A numerical study of insect flight*', Journal of Computational Physics (146), 124-156, Article No CP986019

McFarland M.W., 1953, '*The papers of Wilbur and Orville Wright – Volume one 1899-1905*', McGraw-Hill Book Co.

Michelson R.C., Reece S., 1998, '*Update on flapping wing micro air vehicle research*', RPVs 13th Int Conf, Bristol, UK

Mraz S.J., 1998, '*Honey, I shrunk the plane*', Machine Design, Vol 70, Issue 18, pg 35-37.

Nelson R.C., 1990, '*Flight stability and automatic control*', McGraw-Hill Book Company, Singapore, ISBN 0-07-100835-7.

Okamoto M., Yazuda K. and Azuma A., 1996, '*Aerodynamic characteristics of the wings and body of a dragonfly*', Journal of Experimental Biology, Vol 199, pp 281-294.

Phlips P.J., East R.A. and Pratt N.H., 1981, '*An unsteady lifting line theory of flapping wings with application to forward flight of birds*', Journal of Fluid Mechanics, Vol 112, pp 97-125.

Rashid T., 1995, '*The flight dynamics of a full-scale ornithopter*', M.A.Sc Thesis, University of Toronto Institute of Aerospace Studies.

Robertson R.M. and Johnson A.G., 1993, '*Collision avoidance of flying locusts: Steering torques and behaviour*', Journal of Experimental Biology, Vol 183, pp 35-60.

Sato M. and Azuma A., 1997, '*The flight performance of a damselfly Ceriagrion melanurum selys*', Journal of Experimental Biology, Vol 200, pp 1765-1779.

Schenato L, Deng X, Wu W C, Sastry S, 2001, '*Flight control system for a micromechanical flying insect: Architecture and implementation*', Proceedings of the 2001 IEEE Conference on Robotics & Automation, p1641-1646, Seoul, Korea

Schenato L, Deng X, Wu W C, Sastry S, 2001, '*Virtual insect flight simulator (VIFS): A software testbed for insect flight*', p3885-3892, Proceedings of the 2001 IEEE Conference on Robotics & Automation, Seoul, Korea

Slotine J-J. E, Li W, 1991, '*Applied nonlinear control*', Englewood Clibffs, NJ : Prentice Hall

Smith M.J.C., July 1996, '*Simulating moth wing aerodynamics: towards the development of flapping wing technology*', AIAA Journal Vol 34 No 7

Sunada S. Azuma A. et al, 1993, '*Performance of a butterfly in take-off flight*', Journal of Experimental Biology, Vol 183, pp 249-277.

Sunada S., Kawachi K., Watanabe I. and Azuma A., 1993b, '*Fundamental analysis of three-dimensional 'near fling"*', Journal of Experimental Biology, Vol 183, pp 217-248.

Taylor, M J H, 1989, 'The Aerospace Chronology', Tri-service Press Ltd, ISBN 1 85488-003-9

Tennekes H, 1997, '*The simple science of flight*', MIT Press

Tilston J.R., Cheung W.S., 2000, '*A novel propulsion system for micro air vehicle applications*', Paper 32, 15th International Conference of Unmanned Air Vehicle Systems, Bristol UK

Tobalske B.W., Peacock W.L. and Dial K.P., 1999, '*Kinematics of flap-bounding flight in the zebra finch over a wide range of speeds*', Journal of Experimental Biology, Vol 202, pp 1725-1739.

Ueha S., Tomikawa Y., 1993, '*Ultrasonic Motors: Theory and Application*', Clarendon Press, Oxford.

van den Berg C. and Ellington C.P., 1997, '*The three dimensional leading-edge vortex of a 'hovering' model hawkmoth*', Phil. Trans. R. Soc., London B, Vol 352, pp 329-340.

Vest M S, 1996, '*Unsteady aerodynamics and propulsive characteristics of flapping wings with applications to avian flight*', Doctoral dissertation, San Diego State University and University of California, San Diego.

Vest M.S. and Katz J., 1996, '*Unsteady aerodynamic model of flapping wings*', AIAA Journal Vol 34 No 7

Vest M.S. and Katz J., 1999, '*Aerodynamic study of a flapping wing micro-UAV*', AIAA 99-0994, Reno, NV

Wakeling J.M. and Ellington C.P., 1997a, '*Dragonfly Flight II: Velocities, accelerations and kinematics of flapping flight*', Journal of Experimental Biology, Vol 200, pp 557-582.

Wakeling J.M. and Ellington C.P., 1997b, '*Dragonfly Flight III: Lift and power requirements*', Journal of Experimental Biology, Vol 200, pp 583-600.

Warrick D.R. and Dial K.P., 1998, '*Kinematic, aerodynamic and anatomical mechanisms in the slow manoeuvring flight of pigeons*', Journal of Experimental Biology, Vol 201, pp 655-672.

Wilkin P.J. and Williams M.H., 1993, '*Comparison of the aerodynamic forces on a flying sphingid moth with those predicted by quasi-steady theory*', Journal of Physiol. Zool., Vol 66, pp 1015-1044.

Wilmot A.P. and Ellington C.P., 1997a, '*The mechanics of flight in the hawkmoth Manduca sexta I. Kinematics of hovering and forward flight*', Journal of Experimental Biology, Vol 200, pp 2705-2722.

Wilmot A.P. and Ellington C.P., 1997b, '*The mechanics of flight in the hawkmoth Manduca sexta II. Aerodynamic consequences of kinematic and morphological variation*', Journal of Experimental Biology, Vol 200, pp 2723-2745.

Wortmann M. and Zarnack W., 1993, '*Wing movements and lift requlation in the flight of desert locusts*', Journal of Experimental Biology, Vol 182, pp 57-69.

Zbikowski R., 1999, '*Flapping wing autonomous micro air vehicles: Research programme outline*', Paper 38, 14th International Conference, Unmanned Aerial Vehicles, Bristol, UK

Ziegler J.G. and Nichols N.N., 1942, '*Optimum settings for automatic controllers*', Trans ASME, Vol 64, pp 759-768

APPENDIX A VECTORS AND MATRICES PRELIMINARIES

This Appendix shall address, without going into the details of proving, the preliminaries about vector and matrix representation and operation required in the development of the equations of motion later. It also introduces the concept of vectrices or matrices whose elements are vectors. Proof of the various definitions can be found in advanced texts on the subject.

A.1 VECTORS AND FRAMES

A vector is a quantity possessing both magnitude and direction in three-dimensional space. It may be understood as a line joining two points, A and B. It is fully defined when the orientation and magnitude of the line is given. It is given the symbol $\vec{v}$.

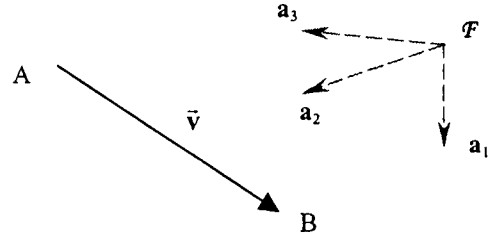

Fig A.1 Definition of Vectors and Frames

The orientation of the vector can be given only with respect to other reference vectors. The minimum number of reference vectors is three, and the orientation of any vector $\vec{v}$ is uniquely specified by the three direction cosines between $\vec{v}$ and these reference vectors. The reference vectors form the reference frame $\mathcal{F}$. The most common set of reference vectors is a dextral (i.e. right-handed) orthonormal (i.e. mutually perpendicular and of unit length) triad, and these are used exclusively.

If the reference vectors of frame $\mathcal{F}_a$ are denoted by $\vec{a}_1$, $\vec{a}_2$ and $\vec{a}_3$, then the vector $\vec{v}$ can be defined with respect to this frame as follows:

$$^a\vec{v} = v(c_1\vec{a}_1 + c_2\vec{a}_2 + c_3\vec{a}_3) \qquad \text{Eqn A.1}$$

where v is the length of the vector $\vec{v}$. The direction cosines of $\vec{v}$ with respect to $\mathcal{F}_a$ are given by $c_i = \cos\theta_i$, being the angle between $\vec{v}$ and $\vec{a}_i$, i = 1..3.

Defining $v_i = v.\cos\theta_i$, Eqn A.1 takes the form of

$$^a\vec{v} = v_1\vec{a}_1 + v_2\vec{a}_2 + v_3\vec{a}_3 \qquad \text{Eqn A.2}$$

The components of $\vec{v}$ in the frame of $\mathcal{F}_a$ are v_i, where i = 1..3, $\vec{v}$ may be represented as $[v_1\ v_2\ v_3]^T$. The frame $\mathcal{F}_a$ can be represented as $[\vec{a}_1\ \vec{a}_2\ \vec{a}_3]^T$, although not conventional since the elements are vectors. This form of matrices will be called vectrices. This allows a set of vectors to be operated in much the same way as matrices.

A compact form for Eqn A.2 may now be given as

$$^a\vec{v} \equiv \mathbf{v}^T\mathcal{F}_a \equiv \mathcal{F}_a^T\mathbf{v} \qquad \text{Eqn A.3}$$

A.2 DIRECTION COSINE MATRIX, DCM

Consider two reference frames, $\mathcal{F}_a$ and $\mathcal{F}_b$, and denote their vectrices by $[\vec{a}_1\ \vec{a}_2\ \vec{a}_3]^T$ and $[\vec{b}_1\ \vec{b}_2\ \vec{b}_3]^T$. A similar form as in Eqn A.1 can be written for each of the unit reference vectors of $\mathcal{F}_b$ with respect to the unit reference vectors of $\mathcal{F}_a$.

$$\begin{aligned}\vec{b}_1 &= c_{11}\vec{a}_1 + c_{12}\vec{a}_2 + c_{13}\vec{a}_3\\ \vec{b}_2 &= c_{21}\vec{a}_1 + c_{22}\vec{a}_2 + c_{23}\vec{a}_3\\ \vec{b}_3 &= c_{31}\vec{a}_1 + c_{32}\vec{a}_2 + c_{33}\vec{a}_3\end{aligned} \qquad \text{Eqn A.4}$$

where c_{ij} is the direction cosine between $\vec{b}_i$ and $\vec{a}_j$.

Eqn A.4 can be compactly expressed with the aid of vectrices as

$$\mathcal{F}_b = \mathbf{C}_{ba}\mathcal{F}_a \qquad \text{Eqn A.5}$$

where $C_{ba} = \{c_{ij}\}$ is known as the direction cosine matrix, DCM or transformation matrix, that transforms a vector from frame $\mathcal{F}_a$ to frame $\mathcal{F}_b$.

A.3 DYADICS

Two vectors $\vec{u}$ and $\vec{v}$ placed side by side together results in a dyadic $\tilde{W}$ as defined below:

$$\begin{aligned}\vec{u}\vec{v} = \mathcal{F}_a^T\mathbf{u}\mathbf{v}^T\mathcal{F}_a &= \mathcal{F}_a^T\begin{bmatrix}u_1\\u_2\\u_3\end{bmatrix}\begin{bmatrix}v_1 & v_2 & v_3\end{bmatrix}\mathcal{F}_a\\ &= \mathcal{F}_a^T\begin{bmatrix}u_1v_1 & u_1v_2 & u_3v_2\\ u_2v_1 & u_2v_2 & u_3v_2\\ u_3v_1 & u_3v_3 & u_3v_3\end{bmatrix}\mathcal{F}_a \qquad \text{Eqn A.6}\\ &= \mathcal{F}_a^T\mathbf{W}\mathcal{F}_a = \tilde{\mathbf{W}}\end{aligned}$$

Eqn A.6 can be rearranged as

$$\mathbf{W} = \mathcal{F}_a \cdot \tilde{\mathbf{W}} \cdot \mathcal{F}_a^T \qquad \text{Eqn A.7}$$

A.4 OPERATIONS WITH FRAMES

The dot product between a frame $\mathcal{F}_a$ and its transpose is defined as

$$\mathcal{F}_a \cdot \mathcal{F}_a^T = \begin{bmatrix} \vec{a}_2 \cdot \vec{a}_1 & \vec{a}_1 \cdot \vec{a}_2 & \vec{a}_1 \cdot \vec{a}_3 \\ \vec{a}_2 \cdot \vec{a}_1 & \vec{a}_2 \cdot \vec{a}_2 & \vec{a}_2 \cdot \vec{a}_3 \\ \vec{a}_3 \cdot \vec{a}_1 & \vec{a}_3 \cdot \vec{a}_2 & \vec{a}_3 \cdot \vec{a}_3 \end{bmatrix} = \begin{bmatrix} 1 & 0 & 0 \\ 0 & 1 & 0 \\ 0 & 0 & 1 \end{bmatrix} = \mathbf{I} \qquad \text{Eqn A.8}$$

I is known as the identity matrix.

Further, the following cross product between a frame $\mathcal{F}_a$ and its transpose is defined as

$$\begin{aligned} \mathcal{F}_a \times \mathcal{F}_a^T &= \begin{bmatrix} \vec{a}_1 \\ \vec{a}_2 \\ \vec{a}_3 \end{bmatrix} \times \begin{bmatrix} \vec{a}_1 & \vec{a}_2 & \vec{a}_3 \end{bmatrix} \\ &= \begin{bmatrix} \vec{a}_1 \times \vec{a}_1 & \vec{a}_1 \times \vec{a}_2 & \vec{a}_1 \times \vec{a}_3 \\ \vec{a}_2 \times \vec{a}_1 & \vec{a}_2 \times \vec{a}_2 & \vec{a}_2 \times \vec{a}_3 \\ \vec{a}_3 \times \vec{a}_1 & \vec{a}_3 \times \vec{a}_2 & \vec{a}_3 \times \vec{a}_3 \end{bmatrix} = \begin{bmatrix} 0 & \vec{a}_3 & -\vec{a}_2 \\ -\vec{a}_3 & 0 & \vec{a}_1 \\ \vec{a}_2 & -\vec{a}_1 & 0 \end{bmatrix} \end{aligned} \qquad \text{Eqn A.9}$$

The result of $\mathcal{F}_a \times \mathcal{F}_a^T$ is a skew-symmetric vectrix whose elements are the unit vectors of the frame $\mathcal{F}_a$.

Performing a dot product operation on Eqn A.5 with $\mathcal{F}_a^T$ allows the following to be written

$$\begin{aligned} \mathcal{F}_b \cdot \mathcal{F}_a^T &= \mathbf{C}_{ba} \mathcal{F}_a \cdot \mathcal{F}_a^T \\ &= \mathbf{C}_{ba} \mathbf{I} = \mathbf{C}_{ba} \end{aligned} \qquad \text{Eqn A.10}$$

Taking this a step further allows the following form

$$\mathcal{F}_b^T \cdot \mathcal{F}_b \cdot \mathcal{F}_a^T = \mathcal{F}_a^T = \mathcal{F}_b^T \cdot \mathbf{C}_{ba} \qquad \text{Eqn A.11}$$

A.4 VECTOR OPERATIONS

A.4.1 Vector Dot Product

The dot product or scalar product between two vectors, $\vec{\mathbf{u}}$ and $\vec{\mathbf{v}}$, expressed in two different frames $\mathcal{F}_a$ and $\mathcal{F}_b$ respectively, can be written in $\mathcal{F}_a$ as

$$\vec{\mathbf{u}} \cdot \vec{\mathbf{v}} = \mathbf{u}^T \mathcal{F}_a \cdot \mathcal{F}_b^T \mathbf{v} = \mathbf{u}^T \mathbf{C}_{ab} \mathbf{v} \qquad \text{Eqn A.12}$$

A.4.2 Vector Cross Product

The cross product between two vectors, $\vec{\mathbf{u}}$ and $\vec{\mathbf{v}}$, expressed in two different frames $\mathcal{F}_a$ and $\mathcal{F}_b$ respectively, can be written in $\mathcal{F}_a$ as

$$\vec{\mathbf{u}} \times \vec{\mathbf{v}} = \mathbf{u}^T \mathcal{F}_a \times \mathcal{F}_b^T \mathbf{v} = \mathbf{u}^T \mathcal{F}_a \times \mathcal{F}_a^T \mathbf{C}_{ab} \mathbf{v} \qquad \text{Eqn A.13}$$

Let $\mathbf{w} = \mathbf{C}_{ab}\mathbf{v}$ and substituting into Eqn A.13 results in

$$\vec{\mathbf{u}} \times \vec{\mathbf{v}} = \mathbf{u}^T \mathcal{F}_a \times \mathcal{F}_a^T \mathbf{w} = \mathbf{u}^T \begin{bmatrix} 0 & \vec{\mathbf{a}}_3 & -\vec{\mathbf{a}}_2 \\ -\vec{\mathbf{a}}_3 & 0 & \vec{\mathbf{a}}_1 \\ \vec{\mathbf{a}}_2 & -\vec{\mathbf{a}}_1 & 0 \end{bmatrix} \begin{bmatrix} w_1 \\ w_2 \\ w_3 \end{bmatrix}$$

$$= \begin{bmatrix} u_1 & u_2 & u_3 \end{bmatrix} \begin{bmatrix} \vec{\mathbf{a}}_3 w_2 - \vec{\mathbf{a}}_2 w_3 \\ \vec{\mathbf{a}}_1 w_3 - \vec{\mathbf{a}}_3 w_1 \\ \vec{\mathbf{a}}_2 w_1 - \vec{\mathbf{a}}_1 w_2 \end{bmatrix} = \mathcal{F}_a^T \begin{bmatrix} u_2 w_3 - u_3 w_2 \\ u_3 w_1 - u_1 w_3 \\ u_1 w_2 - u_2 w_1 \end{bmatrix} \qquad \text{Eqn A.14}$$

$$= \mathcal{F}_a^T \mathbf{u}^\times \mathbf{w} = \mathcal{F}_a^T \mathbf{u}^\times \mathbf{C}_{ab} \mathbf{v}$$

with $\mathbf{u}^\times \doteq \begin{bmatrix} 0 & u_3 & -u_2 \\ -u_3 & 0 & u_1 \\ u_2 & -u_1 & 0 \end{bmatrix}$

A.4.3 Multiple Vector Product

The following identities are given without proof:

$$\vec{\mathbf{a}}\times\left(\vec{\mathbf{b}}\times\vec{\mathbf{c}}\right)=\left(\vec{\mathbf{c}}\cdot\vec{\mathbf{a}}\tilde{\mathbf{I}}-\vec{\mathbf{c}}\vec{\mathbf{a}}\right)\cdot\vec{\mathbf{b}} \qquad \text{Eqn A.15}$$

$$\left(\vec{\mathbf{a}}\times\vec{\mathbf{b}}\right)\times\vec{\mathbf{c}}=\left(\vec{\mathbf{a}}\cdot\vec{\mathbf{c}}\tilde{\mathbf{I}}-\vec{\mathbf{a}}\vec{\mathbf{c}}\right)\cdot\vec{\mathbf{b}} \qquad \text{Eqn A.16}$$

$$\vec{\mathbf{d}}\times\left[\vec{\mathbf{a}}\times\left(\vec{\mathbf{b}}\times\vec{\mathbf{c}}\right)\right]=\left[\vec{\mathbf{d}}\times\left(\vec{\mathbf{c}}\cdot\vec{\mathbf{a}}\tilde{\mathbf{I}}-\vec{\mathbf{c}}\vec{\mathbf{a}}\right)\right]\cdot\vec{\mathbf{b}} \qquad \text{Eqn A.17}$$

$$\begin{aligned}\left(\vec{\mathbf{a}}\times\vec{\mathbf{b}}\right)\times\left(\vec{\mathbf{c}}\times\vec{\mathbf{d}}\right)&=\left[\vec{\mathbf{a}}\cdot\left(\vec{\mathbf{b}}\times\vec{\mathbf{d}}\right)\right]\vec{\mathbf{c}}-\left[\left(\vec{\mathbf{a}}\times\vec{\mathbf{b}}\right)\cdot\vec{\mathbf{c}}\right]\vec{\mathbf{d}}\\&=\left[\vec{\mathbf{a}}\cdot\left(\vec{\mathbf{b}}\times\vec{\mathbf{d}}\right)\right]\tilde{\mathbf{I}}\cdot\vec{\mathbf{c}}-\left[\vec{\mathbf{d}}\left(\vec{\mathbf{a}}\times\vec{\mathbf{b}}\right)\right]\cdot\vec{\mathbf{c}}\\&=\left[\vec{\mathbf{a}}\cdot\left(\vec{\mathbf{b}}\times\vec{\mathbf{d}}\right)\tilde{\mathbf{I}}-\vec{\mathbf{d}}\left(\vec{\mathbf{a}}\times\vec{\mathbf{b}}\right)\right]\cdot\vec{\mathbf{c}}\end{aligned} \qquad \text{Eqn A.18}$$

where $\tilde{\mathbf{I}}$ is the identity dyad and has properties similar to the identity matrix.

A.4.3.1 Multiple Vector Product in Scalar Form

The above identities can be expressed in scalar form as follows. Let the vector $\vec{\mathbf{a}}$, $\vec{\mathbf{b}}$, $\vec{\mathbf{c}}$ and $\vec{\mathbf{d}}$ be expressed in $\mathcal{F}_a$, $\mathcal{F}_b$, $\mathcal{F}_c$ and $\mathcal{F}_d$ respectively.

In Eqn A.6, it was shown that $\tilde{\mathbf{W}}=\mathcal{F}_a^T\mathbf{W}\mathcal{F}_a$ and $\mathcal{F}_a\cdot\vec{\mathbf{u}}\vec{\mathbf{v}}=\mathbf{u}\mathbf{v}^T\mathcal{F}_a$. Making use of these relations and Eqn A.12, the Eqn A.15 can be rewritten in $\mathcal{F}_a$ as follows

$$\begin{aligned}\left[\left(\vec{\mathbf{a}}\times\vec{\mathbf{b}}\right)\times\vec{\mathbf{c}}\right]&=\left[\mathbf{a}^T\cdot\left(\mathbf{C}_{ac}\mathbf{c}\right)\mathcal{F}_a^T\mathbf{I}\mathcal{F}_a-\mathcal{F}_a^T\mathbf{a}\left(\mathbf{C}_{ac}\mathbf{c}\right)^T\mathcal{F}_a\right]\cdot\mathcal{F}_a^T\mathbf{C}_{ab}\mathbf{b}\\&=\mathcal{F}_a^T\left[\mathbf{a}^T\cdot\left(\mathbf{C}_{ac}\mathbf{c}\right)\mathbf{I}-\mathbf{a}\left(\mathbf{C}_{ac}\mathbf{c}\right)^T\right]\mathcal{F}_a\cdot\mathcal{F}_a^T\mathbf{C}_{ab}\mathbf{b}\\&=\mathcal{F}_a^T\left[\mathbf{a}^T\cdot\left(\mathbf{C}_{ac}\mathbf{c}\right)\mathbf{I}-\mathbf{a}\left(\mathbf{C}_{ac}\mathbf{c}\right)^T\right]\mathbf{C}_{ab}\mathbf{b}\end{aligned} \qquad \text{Eqn A.19}$$

Similarly, Eqn A.16 will be given in $\mathcal{F}_a$ as follows

$$\left[(\vec{\mathbf{a}}\times\vec{\mathbf{b}})\times\vec{\mathbf{c}}\right] = \mathcal{F}_a^T\left[\mathbf{a}^T(\mathbf{C}_{ac}\mathbf{c})\mathbf{I} - \mathbf{a}(\mathbf{C}_{ac}\mathbf{c})^T\right]\mathbf{C}_{ab}\vec{\mathbf{b}} \qquad \text{Eqn A.20}$$

Eqn A.17 can be rewritten in $\mathcal{F}_a$, making use of the vector cross product in Eqn A.14, as

$$\begin{aligned}\left\{\vec{\mathbf{d}}\times\left[\vec{\mathbf{a}}\times(\vec{\mathbf{b}}\times\vec{\mathbf{c}})\right]\right\} &= \left\{\mathbf{d}^T\mathcal{F}_d\times\mathcal{F}_a^T\left[(\mathbf{C}_{ac}\mathbf{c})^T\mathbf{a}\mathbf{I} - (\mathbf{C}_{ac}\mathbf{c})\mathbf{a}^T\right]\mathcal{F}_a\cdot\mathcal{F}_a^T\mathbf{C}_{ab}\mathbf{b}\right\} \\ &= \left\{(\mathbf{C}_{ad}\mathbf{d})^T\mathcal{F}_a\times\mathcal{F}_a^T\left[(\mathbf{C}_{ac}\mathbf{c})^T\mathbf{a}\mathbf{I} - (\mathbf{C}_{ac}\mathbf{c})\mathbf{a}^T\right]\mathbf{C}_{ab}\mathbf{b}\right\} \\ &= \mathcal{F}_a^T(\mathbf{C}_{ad}\mathbf{d})^\times\left[(\mathbf{C}_{ac}\mathbf{c})^T\mathbf{a}\mathbf{I} - (\mathbf{C}_{ac}\mathbf{c})\mathbf{a}^T\right]\mathbf{C}_{ab}\mathbf{b}\end{aligned} \qquad \text{Eqn A.21}$$

Finally, Eqn A.18 can be given in $\mathcal{F}_a$ as

$$\left[(\vec{\mathbf{a}}\times\vec{\mathbf{b}})\times(\vec{\mathbf{c}}\times\vec{\mathbf{d}})\right] = \mathcal{F}_a^T\left[\mathbf{a}^T(\mathbf{C}_{ab}\mathbf{b})^\times(\mathbf{C}_{ad}\mathbf{d})\mathbf{I} - (\mathbf{C}_{ad}\mathbf{d})(\mathbf{C}_{ab}\mathbf{b})^T\right]\cdot\mathbf{C}_{ac}\mathbf{c} \qquad \text{Eqn A.22}$$

A.5 Kinematics of Vectrices

Let the time derivative as observed in frame $\mathcal{F}_a$ is denoted by an overdot $(\dot{})$ and an overcircle $(\mathring{})$ when observed in frame $\mathcal{F}_b$. Then $\dot{\mathcal{F}}_a = \mathbf{0}$ and $\mathring{\mathcal{F}}_b = \mathbf{0}$. If $\mathcal{F}_a$ and $\mathcal{F}_b$ rotate with absolute angular velocities $\vec{\omega}_a$ and $\vec{\omega}_b$ respectively, then

$$\dot{\mathcal{F}}_b = (\vec{\omega}_b - \vec{\omega}_a)\times\mathcal{F}_b = \vec{\omega}_{ba}\times\mathcal{F}_b \qquad \text{Eqn A.23}$$

The time derivative of a vector $\vec{\mathbf{v}}$ observed in $\mathcal{F}_a$ and $\mathcal{F}_b$ is related by the following expression

$$\dot{\vec{\mathbf{v}}} = \mathring{\vec{\mathbf{v}}} + \vec{\omega}_{ba}\times\vec{\mathbf{v}} \qquad \text{Eqn A.24}$$

APPENDIX B MASS AND INERTIA PROPERTIES AND DIMENSIONS OF MICRO AIR VEHICLE

The following are assumed for the micro air vehicle in this study:

$n_{nom} = 40$ Hz nominal wing flap frequency

Fuselage

The dimensions and mass for the fuselage are

$m_1 = 4.37$ mass of fuselage in grams

$\mathbf{d}_1 = [6.025 \quad 0 \quad 0]^T$ position vector of fuselage centre of gravity from origin of $\mathcal{F}_1$ in mm, given in $\mathcal{F}_1$.

The moment of inertia for the fuselage is estimated by assuming the following mass distribution

	Mass m [g]	CG Location x [mm]	Moment mx	I_{YY} Contribution $m(x-x_{CG})^2$
Power and Transmission unit	1.8	100	180	2602.4
Fuel or battery	0.5	70	35	32.2
Flight Control Computer	0.2	30	6	204.5
Stroke Plane Actuator Motors	0.2	68	13.6	6.9
Fuselage	0.5	50	25	71.7
Receiver and Transmitter	0.1	25	2.5	136.7
Payload	1	5	5	3246.3
	4.3		267.1	**6301.0**
		$x_{CG}=$	**62.1**	

The contribution to the second moment of inertia I_{YY} due to the parallel axes theorem is 6300 g.mm^2. The fuselage itself is cylindrical and has a contribution given by

$$I_{XX} = \frac{m\left(r_o^2 + r_i^2\right)}{2} \qquad \text{Eqn B.1}$$

$$I_{YY} = \frac{m\left(r_o^2 + r_i^2 + \frac{h^2}{3}\right)}{4} \qquad \text{Eqn B.2}$$

where m = 0.6 g, r_o = 5 mm, r_i = 4 mm and h = 120 mm are the mass of the fuselage (without the components), outer radius, inner radius and length of the hollow cylinder respectively.

Substituting the values results in I_{XX} = 12 g.mm^2 and I_{YY}=I_{ZZ}=1450 g.mm^2.

The total I_{YY} is therefore I_{YY} = 1450 + 6301 = 7550 gmm^2. Hence,

$I_{XX,1}$ = 12 g.mm^2	fuselage roll moment of inertia at the CG position
$I_{YY,1}$ = 7550 g.mm^2	fuselage pitch moment of inertia at the CG position
$I_{ZZ,1}$ = 7550 g.mm^2	fuselage yaw moment of inertia at the CG position

Stroke Plane Actuators

The mass of the stroke plane actuators have already been accounted for in the fuselage mass and will be assumed to be of zero mass. It is fixed in location with respect to the fuselage and hence does not influence the dynamics. Its dimension data are being assumed for the stroke plane actuators.

$m_2 = 0$	mass of port stroke plane actuator in grams
$m_3 = 0$	mass of starboard stroke plane actuator in grams
$\mathbf{b}_2 = [0 \quad 2.5 \quad 0]^T$	position vector of port stroke plane actuator attachment point from origin of $\mathcal{F}_1$ in mm, given in $\mathcal{F}_1$.
$\mathbf{b}_3 = [0 \quad -2.5 \quad 0]^T$	position vector of starboard stroke plane actuator attachment point from origin of $\mathcal{F}_1$ in mm, given in $\mathcal{F}_1$.
$\mathbf{d}_2 = [0 \quad 0 \quad 0]^T$	position vector of centre of gravity of port stroke plane actuator from origin of $\mathcal{F}_2$ in mm, given in $\mathcal{F}_2$.
$\mathbf{d}_3 = [0 \quad 0 \quad 0]^T$	position vector of centre of gravity of starboard stroke plane actuator from origin of $\mathcal{F}_3$ in mm, given in $\mathcal{F}_3$.

The moments of inertia of the stroke plane actuators are being arbitrary chosen as follows:

$I_{XX,2} = I_{XX,3} = 1$ g.mm^2	second moment of inertia of stroke plane actuator at the CG position about its P_iX_i axis (i = 2,3)
$I_{YY,2} = I_{YY,3} = 10$ g.mm^2	second moment of inertia of stroke plane actuator at the CG position about its P_iy_i axis (i = 2,3)
$I_{ZZ,2} = I_{ZZ,3} = 10$ g.mm^2	second moment of inertia of stroke plane actuator at the CG position about its P_iz_i axis (i = 2,3)

Wings

The wings are assumed to weigh 0.1 gram each.

$m_4 = 0.1$	mass of port wing in grams
$m_5 = 0.1$	mass of starboard wing in grams

The dimensions are as follows:

$b_{wing} = 48.7$ mm	wing measurement from root to tip
$S_{wing} = 808.53$ mm^2	wing reference area
$\mathbf{b}_4 = [0 \quad 0 \quad 0]^T$	position vector of port wing attachment point from origin of $\mathcal{F}_2$ in mm, given in $\mathcal{F}_2$.
$\mathbf{b}_5 = [0 \quad 0 \quad 0]^T$	position vector of starboard wing attachment point from origin of $\mathcal{F}_3$ in mm, given in $\mathcal{F}_3$.
$\mathbf{d}_4 = [-20 \quad 0 \quad 0]^T$	position vector of centre of gravity of port wing from origin of $\mathcal{F}_4$ in mm, given in $\mathcal{F}_4$.
$\mathbf{d}_5 = [20 \quad 0 \quad 0]^T$	position vector of centre of gravity of starboard wing from origin of $\mathcal{F}_5$ in mm, given in $\mathcal{F}_5$.
$\boldsymbol{l}_{cp,p} = [-20 \quad 0 \quad 0]^T$	position vector of port wing centre of pressure from origin of $\mathcal{F}_4$ in mm, given in $\mathcal{F}_4$
$\boldsymbol{l}_{cp,s} = [20 \quad 0 \quad 0]^T$	position vector of starboard wing centre of pressure from origin of $\mathcal{F}_5$ in mm, given in $\mathcal{F}_5$.

The mass moments of inertia about the P_4y_4 and P_4z_4 axes due to the contribution of the parallel axes theorem are estimated to be

$$I_{YY} \approx I_{YY} = 0.1 \times 20^2 = 40 \text{ g.mm}^2$$

The contribution to the moment of inertia about the P_4x_4 axis is given by

$$I_{XX} = \frac{m\bar{c}^2}{12} \qquad \text{Eqn B.3}$$

where $\bar{c} \approx 20$ mm is the mean chord of the wing. Hence $I_{xx} = 3.3$ g.mm^2.

$I_{XX,4} = I_{XX,5} = 3$ g.mm^2 — second moment of inertia of stroke plane actuator at the CG position about its P_ix_i axis (i = 2,3)

$I_{YY,4} = I_{YY,5} = 40$ g.mm^2 — second moment of inertia of stroke plane actuator at the CG position about its P_iy_i axis (i = 2,3)

$I_{ZZ,4} = I_{ZZ,5} = 40$ g.mm^2 — second moment of inertia of stroke plane actuator at the CG position about its P_iz_i axis (i = 2,3)

APPENDIX C DEVELOPMENT OF EQUATIONS OF MOTION

This Appendix describes the development of the equations of motion for the multi-body system representing the flapping wing micro air vehicle based on a method adapted from Hughes [1986]. The steps of which can be summarised as follows:

a. The kinematics of the individual bodies and then of the system are first established.

b. The linear momenta of the individual bodies making up the system are derived.

c. The linear momentum of the system is then found by summing up the individual linear momenta.

d. The time derivative of the linear momentum of the system is equated to the forces applied to the system, forming the force equations of motion.

e. The time derivative of the individual linear momentum will also be equated to the forces applied to the said body to obtain the force equations of motion of the body.

f. The angular momenta of the individual bodies making up the system are derived.

g. The angular momentum of the system is then found by summing up the individual linear momenta.

h. The time derivative of the angular momentum of the system is equated to the moments applied to the system, forming the moment equations of motion.

i. The time derivative of the individual angular momentum will also be equated to the moments applied to the said body to obtain the moments equations of motion of the body.

j. The equations are then transformed to the body frame.

k. These are then expressed in scalar form.

C.1 SYSTEM DESCRIPTION

As shown in Fig C.1, the vehicle is modelled as 5 rigid bodies, namely R_1 (fuselage), R_2 (port stroke plane actuator), R_3 (starboard stroke plane actuator), R_4 (port wing) and R_5 (starboard wing). The fuselage is allowed 6 degrees of freedom (D.O.F.), namely the 3 translational and 3 rotational D.O.F.

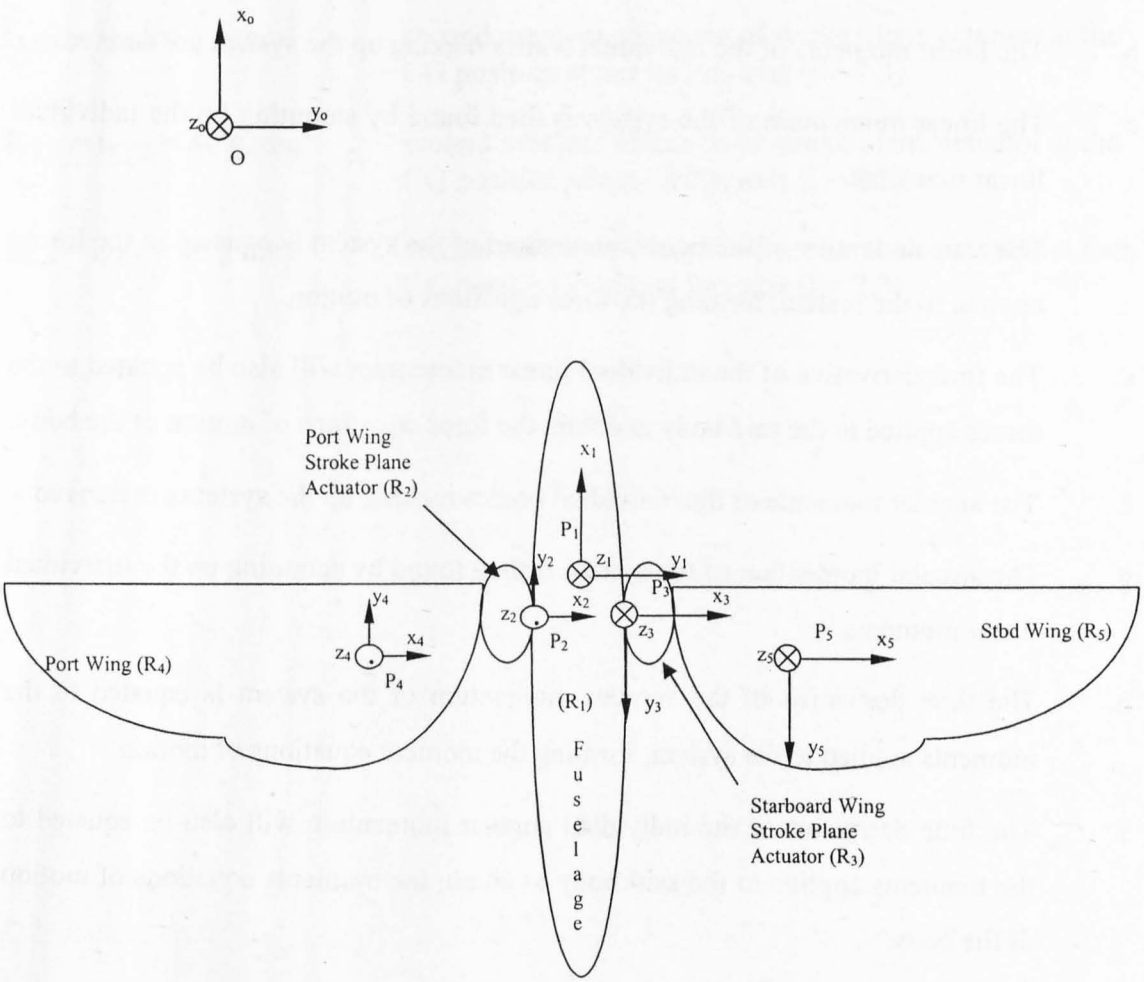

Fig C.1 Definition of Coordinate Systems for the MAV Model

The wings (R_4 and R_5) are attached to the fuselage via the stroke plane actuators (R_2 and R_3 respectively). Each stroke plane actuator can be rotated about a single axis so that the stroke plane angle can be adjusted with respect to the fuselage axes system $P_1x_1y_1z_1$ or $\mathcal{F}_1$. Each wing is allowed two D.O.F., namely the flap and pitch as shown in Fig C.2.

Fig C.2 Illustration of Wing Degrees of Freedom

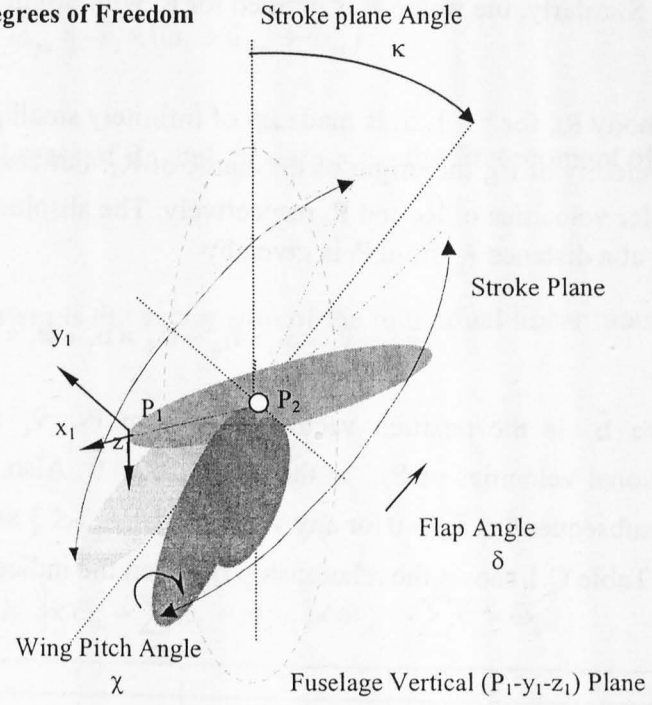

C.2 KINEMATICS

The bodies are represented schematically by an open chain with each body linked to a maximum of two other bodies, Fig C.3 shows three of the five bodies.

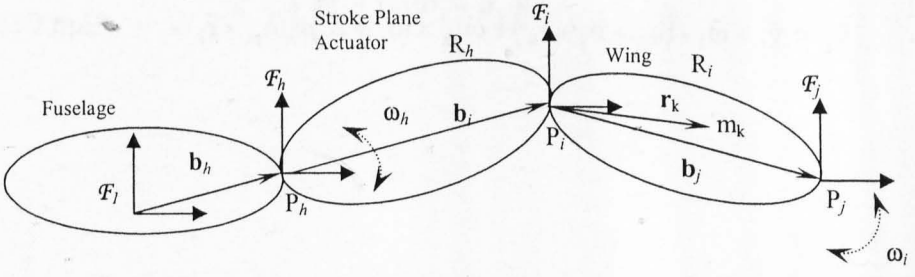

Fig C.3 Schematic Representation of the MAV

The stroke plane actuators R_2 and R_3 are each linked to the fuselage R_1 at the inboard joint and a wing at the outboard joint. For any body R_i, a body lying just outboard of it will have a higher index and will be denoted as R_j. The joint between R_i and R_j will be named P_j. The body lying just inboard of R_i will be denoted R_h and the joint will be P_i. A right handed orthogonal body fixed axes system or frame $\mathcal{F}_i$ is defined for R_i with origin at P_i. Similarly, the frame $\mathcal{F}_j$ is defined for R_j with origin at P_j.

The body R_i, for i = 1..5, is made up of infinitely small particles of mass Δm_k. Let $\vec{v}_0$ be the velocity of P_1, the origin of the frame of R_1. Let also $\vec{\omega}_h$ and $\vec{\omega}_i$ denote the absolute angular velocities of R_h and R_i respectively. The absolute linear velocity of a particle Δm_i in R_i at a distance $\vec{r}_k$ from P_i is given by

$$\vec{v}_k = \vec{v}_i + \vec{\omega}_1 \times \vec{b}_h + \vec{\omega}_h \times \vec{b}_i + \vec{\omega}_i \times \vec{r}_k \qquad \text{Eqn C.1}$$

where $\vec{b}_i$ is the position vector of P_i from P_h, $\vec{v}_1$ and $\vec{\omega}_1$ are the translational and rotational velocities of P_1. In the model, $\vec{b}_1 = \vec{0}$. Also, in all the equations derived here and subsequently, $\vec{a}_h = \vec{0}$ for any vector $\vec{a}$ when $i \leq 3$ and $\vec{a}_j = \vec{0}$ for any vector $\vec{a}$ when $i \geq 4$. Table C.1 shows the relationship between the indices h, i and j.

i	1	2	3	4	5
h	-	1	1	2	3
j	2 or 3	4	5	-	-

Table C.1 Relationship between the indices h, i and j

With $\vec{\omega}_{pi} = \vec{\omega}_i - \vec{\omega}_h$ defined as the relative angular velocity of R_i with respect to the adjoining body R_h, Eqn C.1 can be rewritten as

$$\vec{v}_k = \vec{v}_1 + \vec{\omega}_1 \times \left(\vec{b}_h + \vec{b}_i + \vec{r}_k\right) + \vec{\omega}_{ph} \times \left(\vec{b}_i + \vec{r}_k\right) + \vec{\omega}_{pi} \times \vec{r}_k \qquad \text{Eqn C.2}$$

C.3 LINEAR MOMENTUM

The linear momentum $\vec{p}_i$ of each individual body R_i, for i = 1..5, is given by the Eqn C.3

$$\vec{p}_i = \int \vec{v}_k dm_k = \int \left[\vec{v}_1 + \vec{\omega}_1 \times \left(\vec{b}_h + \vec{b}_i + \vec{r}_k\right) + \vec{\omega}_{ph} \times \left(\vec{b}_i + \vec{r}_k\right) + \vec{\omega}_{pi} \times \vec{r}_k\right] dm_k$$

$$= m_i\left[\vec{v}_1 - \vec{b}_h \times \vec{\omega}_1 - \vec{b}_i \times \left(\vec{\omega}_1 + \vec{\omega}_{ph}\right)\right] - \int \vec{r}_k dm_k \times \left(\vec{\omega}_1 + \vec{\omega}_{ph} + \vec{\omega}_{pi}\right) \qquad \text{Eqn C.3}$$

$$= m_i\left[\vec{v}_1 - \vec{b}_h \times \vec{\omega}_1 - \vec{b}_i \times \left(\vec{\omega}_1 + \vec{\omega}_{ph}\right)\right] - \vec{c}_i \times \left(\vec{\omega}_1 + \vec{\omega}_{ph} + \vec{\omega}_{pi}\right)$$

noting that $\int dm_k = m_i$, the total mass of R_i, and $\int r_k dm_k = \vec{c}_i$, the first moment of inertia of R_i.

The linear momentum of the system is the vector sum of the individual linear momenta given by

$$\vec{p} = \sum \vec{p}_i$$

$$= \sum_{i=1}^{5} m_i \vec{v}_1 - \sum_{i=1}^{5} \left[\vec{c}_i + m_i\left(\vec{b}_h + \vec{b}_i\right)\right] \times \vec{\omega}_1 - \sum_{i=4}^{5} \left(\vec{c}_i + m_i \vec{b}_i\right) \times \vec{\omega}_{ph} - \sum_{i=2}^{5} \vec{c}_i \times \vec{\omega}_{pi}$$

$$= \sum_{i=1}^{5} m_i \vec{v}_1 - \vec{c} \times \vec{\omega}_1 - \sum_{i=2}^{5} \left(\vec{c}_i + \vec{c}_j + m_i \vec{b}_j\right) \times \vec{\omega}_{pi}$$

Eqn C.4

where

$$\vec{c} = \sum_{i=1}^{5} \left[\vec{c}_i + m_i\left(\vec{b}_i + \vec{b}_h\right)\right] \qquad \text{Eqn C.5}$$

C.4 ANGULAR MOMENTUM

The angular momentum $\vec{\mathbf{h}}_i$ of the body R_i (i = 1..5), referenced at the origin of its frame $\mathcal{F}_i$, is given by the following equation:

$$\vec{\mathbf{h}}_i = \int \vec{\mathbf{r}}_k \times \vec{\mathbf{v}}_k \, dm_k \qquad \text{Eqn C.6}$$

which can be written by substituting Eqn C.1 as

$$\begin{aligned}\vec{\mathbf{h}}_i &= \int \vec{\mathbf{r}}_k \times \left[\vec{\mathbf{v}}_1 + \vec{\omega}_1 \times \left(\vec{\mathbf{b}}_h + \vec{\mathbf{b}}_i + \vec{\mathbf{r}}_k\right) + \vec{\omega}_{ph} \times \left(\vec{\mathbf{b}}_i + \vec{\mathbf{r}}_k\right) + \vec{\omega}_{pi} \times \vec{\mathbf{r}}_k\right] dm_k \\ &= \vec{\mathbf{c}}_i \times \vec{\mathbf{v}}_1 + \int \vec{\mathbf{r}}_k \times \vec{\omega}_1 \times \left(\vec{\mathbf{b}}_h + \vec{\mathbf{b}}_i + \vec{\mathbf{r}}_k\right) dm_k + \int \vec{\mathbf{r}}_k \times \vec{\omega}_{ph} \times \left(\vec{\mathbf{b}}_i + \vec{\mathbf{r}}_k\right) dm_k \\ &\quad + \int \vec{\mathbf{r}}_k \times \vec{\omega}_{pi} \times \vec{\mathbf{r}}_k \, dm_i \\ &= \vec{\mathbf{c}}_i \times \vec{\mathbf{v}}_1 + \tilde{\mathbf{J}}_{il} \cdot \vec{\omega}_1 + \tilde{\mathbf{J}}_{ih} \cdot \vec{\omega}_{ph} + \tilde{\mathbf{J}}_i \cdot \vec{\omega}_{pi}\end{aligned} \qquad \text{Eqn C.7}$$

whereby the following are being defined

$$\tilde{\mathbf{J}}_{il} \cdot \vec{\omega}_1 = \int \vec{\mathbf{r}}_k \times \vec{\omega}_1 \times \left(\vec{\mathbf{b}}_h + \vec{\mathbf{b}}_i + \vec{\mathbf{r}}_k\right) dm_k \qquad \text{Eqn C.8}$$

$$\tilde{\mathbf{J}}_{ih} \cdot \vec{\omega}_{ph} = \int \vec{\mathbf{r}}_k \times \vec{\omega}_{ph} \times \left(\vec{\mathbf{b}}_i + \vec{\mathbf{r}}_k\right) dm_k \qquad \text{Eqn C.9}$$

and

$$\tilde{\mathbf{J}}_i \cdot \vec{\omega}_{pi} = \int \vec{\mathbf{r}}_k \times \left(\vec{\omega}_{pi} \times \vec{\mathbf{r}}_k\right) dm_k \qquad \text{Eqn B.10}$$

For i = 1, Eqn C.10 takes the form of

$$\tilde{\mathbf{J}}_1 \cdot \vec{\omega}_1 = \int \vec{\mathbf{r}}_k \times \left(\vec{\omega}_1 \times \vec{\mathbf{r}}_k\right) dm_k \qquad \text{Eqn C.11}$$

The angular momentum of R_i (i = 2..5) referenced at P_1 is given by

$$\vec{\mathbf{h}}_{i,P_1} = \int\left[\left(\vec{\mathbf{b}}_h + \vec{\mathbf{b}}_i + \vec{\mathbf{r}}_k\right)\times \vec{\mathbf{v}}_k\right] dm_k$$

$$= \vec{\mathbf{h}}_i + \int\left[\left(\vec{\mathbf{b}}_h + \vec{\mathbf{b}}_i\right)\times \vec{\mathbf{v}}_k\right] dm_k \qquad \text{Eqn C.12}$$

For simplicity, the system angular momentum referred to at P_1 will be denoted as $\vec{\mathbf{h}}_{P_1}$. This is given by

$$\vec{\mathbf{h}}_{P_1} = \sum_{i=1}^{5} \vec{\mathbf{h}}_{i,P_1} + \sum_{i=2}^{5} \int_{R_i} \left[\left(\vec{\mathbf{b}}_h + \vec{\mathbf{b}}_i\right)\times \vec{\mathbf{v}}_k\right] dm_k \qquad \text{Eqn C.13}$$

The second term on the right hand side (RHS) or Eqn C.13 is evaluated for R_i, i = 2..5, as

$$\int\left[\left(\vec{\mathbf{b}}_h + \vec{\mathbf{b}}_i\right)\times \vec{\mathbf{v}}_k\right]dm_k = \left(\vec{\mathbf{b}}_h + \vec{\mathbf{b}}_i\right)\times \int\left[\vec{\mathbf{v}}_1 + \vec{\omega}_1 \times \left(\vec{\mathbf{b}}_h + \vec{\mathbf{b}}_i + \vec{\mathbf{r}}_k\right) + \vec{\omega}_{ph} \times \left(\vec{\mathbf{b}}_i + \vec{\mathbf{r}}_k\right) + \vec{\omega}_{pi} \times \vec{\mathbf{r}}_k\right]dm_k$$

$$= m_i\left(\vec{\mathbf{b}}_h + \vec{\mathbf{b}}_i\right)\times \vec{\mathbf{v}}_1 + \int\left(\vec{\mathbf{b}}_h + \vec{\mathbf{b}}_i\right)\times\left[\vec{\omega}_1 \times \left(\vec{\mathbf{b}}_h + \vec{\mathbf{b}}_i + \vec{\mathbf{r}}_k\right)\right]dm_k$$
$$+ \int\left(\vec{\mathbf{b}}_h + \vec{\mathbf{b}}_i\right)\times\left[\vec{\omega}_{ph} \times \left(\vec{\mathbf{b}}_i + \vec{\mathbf{r}}_k\right)\right]dm_k + \int\left(\vec{\mathbf{b}}_h + \vec{\mathbf{b}}_i\right)\times\left[\vec{\omega}_{pi} \times \vec{\mathbf{r}}_k\right]dm_k$$

Eqn C.14

The following relations shall be defined

$$\tilde{\mathbf{J}}_{1i} \cdot \vec{\omega}_{pi} = \int\left(\vec{\mathbf{b}}_h + \vec{\mathbf{b}}_i + \vec{\mathbf{r}}_k\right)\times\left(\vec{\omega}_{pi} \times \vec{\mathbf{r}}_k\right)dm_k$$
$$= \int\left(\vec{\mathbf{b}}_h + \vec{\mathbf{b}}_i\right)\times\left(\vec{\omega}_{pi} \times \vec{\mathbf{r}}_k\right)dm_k + \tilde{\mathbf{J}}_i \cdot \vec{\omega}_{pi} \qquad \text{Eqn C.15}$$

$$\tilde{\mathbf{J}} \cdot \vec{\omega}_1 = \int_{R_1} \left(\vec{\mathbf{r}}_k \times \vec{\omega}_1 \times \vec{\mathbf{r}}_k\right)dm_1 + \sum_{i=2}^{5} \int\left(\vec{\mathbf{b}}_h + \vec{\mathbf{b}}_i + \vec{\mathbf{r}}_k\right)\times \vec{\omega}_1 \times \left(\vec{\mathbf{b}}_h + \vec{\mathbf{b}}_i + \vec{\mathbf{r}}_k\right)dm_k$$
$$= \tilde{\mathbf{J}}_1 \cdot \vec{\omega}_1 + \sum_{i=2}^{5} \int \vec{\mathbf{r}}_k \times \vec{\omega}_1 \times \left(\vec{\mathbf{b}}_h + \vec{\mathbf{b}}_i + \vec{\mathbf{r}}_k\right)dm_k + \sum_{i=2}^{5} \int\left(\vec{\mathbf{b}}_h + \vec{\mathbf{b}}_i\right)\times \vec{\omega}_1 \times \left(\vec{\mathbf{b}}_h + \vec{\mathbf{b}}_i + \vec{\mathbf{r}}_k\right)dm_k$$
$$= \tilde{\mathbf{J}}_1 \cdot \vec{\omega}_1 + \sum_{i=2}^{5} \tilde{\mathbf{J}}_{i1} \cdot \vec{\omega}_1 + \sum_{i=2}^{5} \int\left(\vec{\mathbf{b}}_h + \vec{\mathbf{b}}_i\right)\times \vec{\omega}_1 \times \left(\vec{\mathbf{b}}_h + \vec{\mathbf{b}}_i + \vec{\mathbf{r}}_k\right)dm_k$$

Eqn C.16

and

$$\tilde{\mathbf{J}}_{1ih} \cdot \vec{\omega}_{ph} = \int (\vec{b}_h + \vec{b}_i) \times \vec{\omega}_{ph} \times (\vec{r}_k + \vec{b}_i) dm_k + \tilde{\mathbf{J}}_{ih} \cdot \vec{\omega}_{ph} \qquad \text{Eqn C.17}$$

Substituting Eqns C.14 to C.17 into Eqn C.13 and after some manipulation, results in the following expression for the system angular momentum about the point P_1

$$\vec{\mathbf{h}}_{P_1} = \vec{\mathbf{c}} \times \vec{\mathbf{v}}_1 + \tilde{\mathbf{J}} \cdot \vec{\omega}_1 + \sum_{i=4}^{5} (\tilde{\mathbf{J}}_{1h} + \tilde{\mathbf{J}}_{1ih}) \cdot \vec{\omega}_{ph} + \sum_{i=4}^{5} \tilde{\mathbf{J}}_{1i} \cdot \vec{\omega}_{pi} \qquad \text{Eqn C.18}$$

C.5 FORCES AND MOMENTS AT P_i

Fig C.4 shows the free-body diagram of the multi-body system. Let $\vec{\mathbf{f}}_i$ and $\vec{\mathbf{g}}_i$ be the external forces and moments applied to R_i. Further, let $\vec{\mathbf{f}}_{pl}$ and $\vec{\mathbf{g}}_{pl}$ (l = i, j) refer to the forces and moments acting on R_i at P_l due to the adjoining bodies, R_h or R_j, respectively.

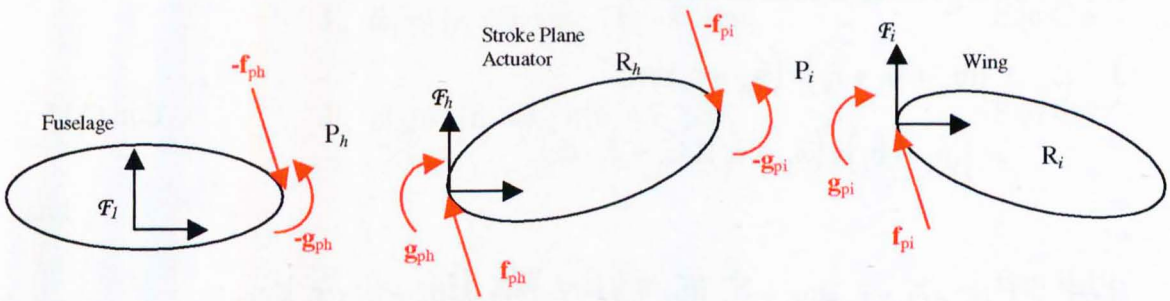

Fig C.4 Free-body Diagram

The time derivative of the vector $\vec{\mathbf{a}}$ shall be denoted

- in the inertial frame $\mathcal{F}_0$ by $\overset{*}{\vec{\mathbf{a}}}$
- in the frame of R_1, $\mathcal{F}_1$, by $\dot{\vec{\mathbf{a}}}$
- in the frame of R_2 or R_3, $\mathcal{F}_2$ or $\mathcal{F}_3$, by $\overset{o}{\vec{\mathbf{a}}}$
- in the frame of R_4 or R_5, $\mathcal{F}_4$ or $\mathcal{F}_5$, by $\overset{+}{\vec{\mathbf{a}}}$

C.6 FORCE EQUATIONS

Applying Newton's law of motion to each individual body, which states that the rate of change of the linear momentum is equal to the sum of applied forces, result in the following expression for R_1

$$\vec{\mathbf{p}}_1^{\,*} = \vec{\mathbf{f}}_1 - \vec{\mathbf{f}}_{p2} - \vec{\mathbf{f}}_{p3} \qquad \text{Eqn C.19}$$

and for R_i (i = 2..5)

$$\vec{\mathbf{p}}_i^{\,*} = \vec{\mathbf{f}}_i + \vec{\mathbf{f}}_{pi} - \vec{\mathbf{f}}_{pj} \qquad \text{Eqn C.20}$$

Adding Eqns C.19 and C.20 for all the individual bodies results in the force equations of motion for the system

$$\sum_{i=1}^{5} \vec{\mathbf{p}}_i^{\,*} = \vec{\mathbf{p}}^{\,*} = \sum_{i=1}^{5} \vec{\mathbf{f}}_i = \vec{\mathbf{f}} \qquad \text{Eqn C.21}$$

C.7 MOMENT EQUATIONS

The moment equation for R_1 is given by

$$\vec{\mathbf{h}}_1^{\,*} + \vec{\mathbf{v}}_1 \times \vec{\mathbf{p}} = \vec{\mathbf{g}}_1 - \vec{\mathbf{g}}_{p1} - \vec{\mathbf{g}}_{p2} - \vec{\mathbf{b}}_2 \times \vec{\mathbf{f}}_{p2} - \vec{\mathbf{b}}_3 \times \vec{\mathbf{f}}_{p3} \qquad \text{Eqn C.22}$$

and for R_i (i = 2..5) by

$$\vec{\mathbf{h}}_i^{\,*} + \left[\vec{\mathbf{v}}_1 + \vec{\omega}_1 \times \left(\vec{\mathbf{b}}_h + \vec{\mathbf{b}}_i\right) + \vec{\omega}_{ph} \times \vec{\mathbf{b}}_i\right] \times \vec{\mathbf{p}}_i = \vec{\mathbf{g}}_i + \vec{\mathbf{g}}_{pi} - \vec{\mathbf{g}}_{pj} - \vec{\mathbf{b}}_j \times \vec{\mathbf{f}}_{pj} \qquad \text{Eqn C.23}$$

Adding Eqns C.22 and C.23 results in the moment equations of motion for the system

$$\sum_{i=1}^{5} \vec{\mathbf{h}}_i^{\,*} + \vec{\mathbf{v}}_0 \times \sum_{i=1}^{5} \vec{\mathbf{p}}_i + \sum_{i=2}^{5} \left[\vec{\omega}_1 \times \left(\vec{\mathbf{b}}_h + \vec{\mathbf{b}}_i\right)\right] \times \vec{\mathbf{p}}_i + \sum_{i=4}^{5} \left(\vec{\omega}_{ph} \times \vec{\mathbf{b}}_i\right) \times \vec{\mathbf{p}}_i = \sum_{i=1}^{5} \vec{\mathbf{g}}_i - \sum_{i=1}^{3} \vec{\mathbf{b}}_j \times \vec{\mathbf{f}}_{pj}$$

Eqn C.24

Taking the time derivative of Eqn C.12 gives

$$\overset{*}{\vec{h}}_{P_1} = \sum_{i=1}^{5} \overset{*}{\vec{h}}_i + \sum_{i=2}^{5} \left[\vec{\omega}_1 \times \left(\vec{b}_h + \vec{b}_i\right)\right] \times \vec{p}_i + \sum_{i=2}^{5} \left(\vec{\omega}_{ph} \times \vec{b}_i\right) \times \vec{p}_i + \sum_{i=2}^{5} \left(\vec{b}_h + \vec{b}_i\right) \times \overset{*}{\vec{p}}_i \qquad \text{Eqn C.25}$$

since $\overset{*}{\vec{b}}_i = \dot{\vec{b}}_i + \vec{\omega}_1 \times \vec{b}_i = \vec{\omega}_1 \times \vec{b}_i$.

Rearranging Eqn C.25 results in

$$\sum_{i=1}^{5} \overset{*}{\vec{h}}_i = \overset{*}{\vec{h}}_{P_1} - \sum_{i=2}^{5} \left[\vec{\omega}_1 \times \left(\vec{b}_h + \vec{b}_i\right)\right] \times \vec{p}_i - \sum_{i=2}^{5} \left(\vec{\omega}_{ph} \times \vec{b}_i\right) \times \vec{p}_i - \sum_{i=2}^{5} \left(\vec{b}_h + \vec{b}_i\right) \times \overset{*}{\vec{p}}_i \qquad \text{Eqn C.26}$$

The force $\vec{f}_{pi}$ acting on the joint P_i, for i = 2 and 3, can be obtained by rearranging the Eqn C.20

$$\vec{f}_{pi} = \overset{*}{\vec{p}}_i + \vec{f}_{pj} - \vec{f}_i \qquad \text{Eqn C.27}$$

The index given to the wings relative to the stroke plane actuators is j. Thus, relative to the stroke plane actuators, the forces acting on the outboard joint P_j of the stroke plane actuators will be

$$\vec{f}_{pj} = \overset{*}{\vec{p}}_j - \vec{f}_j \qquad \text{Eqn C.28}$$

Combining Eqn C.27 and C.28 results in the general form for i = 2..5

$$\vec{f}_{pi} = \overset{*}{\vec{p}}_i + \overset{*}{\vec{p}}_j - \vec{f}_j - \vec{f}_i \qquad \text{Eqn C.29}$$

The last term on the RHS of Eqn C.24, $-\sum_{i=1}^{3} \vec{b}_j \times \vec{f}_{pj}$, can be written as

$$-\sum_{i=1}^{3} \vec{b}_j \times \vec{f}_{pj} = -\sum_{i=2}^{5} \vec{b}_i \times \vec{f}_{pi} = \sum_{i=2}^{5} \vec{b}_i \times \left(\vec{f}_i + \vec{f}_j\right) - \sum_{i=2}^{5} \vec{b}_i \times \left(\vec{p}_i + \vec{p}_j\right) \qquad \text{Eqn C.30}$$

Substituting Eqns C.26 and C.30 into Eqn C.24 results in

$$\vec{\mathbf{h}}^{*}_{P_1} = \sum_{i=1}^{5}\vec{\mathbf{g}}_i + \sum_{i=2}^{5}\vec{\mathbf{b}}_i \times \left(\vec{\mathbf{f}}_i + \vec{\mathbf{f}}_j\right) - \sum_{i=2}^{5}\vec{\mathbf{b}}_i \times \left(\vec{\mathbf{p}}^{*}_i + \vec{\mathbf{p}}^{*}_j\right) - \sum_{i=2}^{5}\left(\vec{\mathbf{b}}_h + \vec{\mathbf{b}}_i\right) \times \vec{\mathbf{p}}^{*}_i - \vec{\mathbf{v}}_1 \times \sum_{i=1}^{5}\vec{\mathbf{p}}_i$$

$$= \sum_{i=1}^{5}\vec{\mathbf{g}}_i + \sum_{i=2}^{5}\left[\vec{\mathbf{b}}_i \times \left(\vec{\mathbf{f}}_i + \vec{\mathbf{f}}_j\right)\right] - \vec{\mathbf{v}}_1 \times \sum_{i=1}^{5}\vec{\mathbf{p}}_i$$

Eqn C.31

since it can be shown by expanding the indices that $\sum_{i=2}^{5}\vec{\mathbf{b}}_i \times \vec{\mathbf{p}}^{*}_j = \sum_{i=2}^{5}\vec{\mathbf{b}}_h \times \vec{\mathbf{p}}^{*}_i$.

Similarly, it can be shown that $\sum_{i=2}^{5}\vec{\mathbf{b}}_i \times \left(\vec{\mathbf{f}}_j + \vec{\mathbf{f}}_i\right) = \sum_{i=2}^{5}\left(\vec{\mathbf{b}}_i + \vec{\mathbf{b}}_h\right) \times \vec{\mathbf{f}}_i$, which allows Eqn C.31 to be written as

$$\vec{\mathbf{h}}^{*}_{P_1} = \sum_{i=1}^{5}\vec{\mathbf{g}}_i + \sum_{i=2}^{5}\left(\vec{\mathbf{b}}_i + \vec{\mathbf{b}}_h\right) \times \vec{\mathbf{f}}_i - \vec{\mathbf{v}}_1 \times \sum_{i=1}^{5}\vec{\mathbf{p}}_i \qquad \text{Eqn C.32}$$

C.8 TRANSFORMATION TO BODY FRAME

The force and moment equations of the system of rigid bodies R_1, R_2 and R_3 in inertial frame are given in Eqns C.21 and C32.

To transform them to the body frame, the identities for a vector $\vec{\mathbf{a}}_i$ are applied

$$\overset{o}{\vec{\mathbf{a}}}_i = \overset{+}{\vec{\mathbf{a}}}_i + \vec{\omega}_{pn} \times \vec{\mathbf{a}}_i \qquad \text{Eqn C.33}$$

$$\dot{\vec{\mathbf{a}}}_i = \overset{o}{\vec{\mathbf{a}}}_i + \vec{\omega}_{pm} \times \vec{\mathbf{a}}_i = \overset{+}{\vec{\mathbf{a}}}_i + \left(\vec{\omega}_{pm} + \vec{\omega}_{pn}\right) \times \vec{\mathbf{a}}_i \qquad \text{Eqn C.34}$$

$$\vec{\mathbf{a}}^{*}_i = \dot{\vec{\mathbf{a}}}_i + \vec{\omega}_1 \times \vec{\mathbf{a}}_i = \overset{o}{\vec{\mathbf{a}}}_i + \left(\vec{\omega}_1 + \vec{\omega}_{pm}\right) \times \vec{\mathbf{a}}_i = \overset{+}{\vec{\mathbf{a}}}_i + \left(\vec{\omega}_1 + \vec{\omega}_{pm} + \vec{\omega}_{pn}\right) \times \vec{\mathbf{a}}_i \qquad \text{Eqn C.35}$$

where i, m and n have the following relationship shown in Table C.2.

i	m	n
1	-	-
2	2	-
3	3	-
4	2	4
5	3	5

Table C.2 Relationship between Indices i, m and n

C.8.1 Force Equations of Motion

Eqn B.21 can thus be written as

$$\vec{\mathbf{p}} = \vec{\mathbf{p}} + \vec{\omega}_1 \times \vec{\mathbf{p}} = \vec{\mathbf{f}} \qquad \text{Eqn C.36}$$

or

$$\vec{\mathbf{p}} = \vec{\mathbf{f}} - \vec{\omega}_1 \times \vec{\mathbf{p}} \qquad \text{Eqn C.37}$$

C.8.2 Moment Equations of Motion

Similarly, Eqn C.32 will be after rearranging

$$\dot{\vec{\mathbf{h}}}_{P_1} = \sum_{i=1}^{5} \vec{\mathbf{g}}_i + \sum_{i=2}^{5} \left(\vec{\mathbf{b}}_i + \vec{\mathbf{b}}_h\right) \times \vec{\mathbf{f}}_i - \vec{\mathbf{v}}_0 \times \sum_{i=1}^{5} \vec{\mathbf{p}}_i - \vec{\omega}_i \times \vec{\mathbf{h}}_{P_1} \qquad \text{Eqn C.38}$$

The angular momentum equation for R_i (i = 2..5) is given by Eqn C.23, which can be transformed into the frame of R_i and expressed by Eqn C.39 for i = 2 and 3, and Eqn C.40 for i = 4 and 5

$$\overset{o}{\vec{\mathbf{h}}}_i + \left(\vec{\omega}_1 + \vec{\omega}_{pm}\right) \times \vec{\mathbf{h}}_i + \left[\vec{\mathbf{v}}_1 + \vec{\omega}_1 \times \left(\vec{\mathbf{b}}_h + \vec{\mathbf{b}}_i\right) + \vec{\omega}_{ph} \times \vec{\mathbf{b}}_i\right] \times \vec{\mathbf{p}}_i = \vec{\mathbf{g}}_i + \vec{\mathbf{g}}_{pi} - \vec{\mathbf{g}}_{pj} - \vec{\mathbf{b}}_j \times \vec{\mathbf{f}}_{pj} \qquad \text{Eqn C.39}$$

$$\overset{+}{\vec{\mathbf{h}}}_i + \left(\vec{\omega}_1 + \vec{\omega}_{pm} + \vec{\omega}_{pn}\right) \times \vec{\mathbf{h}}_i + \left[\vec{\mathbf{v}}_0 + \vec{\omega}_1 \times \left(\vec{\mathbf{b}}_h + \vec{\mathbf{b}}_i\right) + \vec{\omega}_{ph} \times \vec{\mathbf{b}}_i\right] \times \vec{\mathbf{p}}_i = \vec{\mathbf{g}}_i + \vec{\mathbf{g}}_{pi} - \vec{\mathbf{g}}_{pj} - \vec{\mathbf{b}}_j \times \vec{\mathbf{f}}_{pj} \qquad \text{Eqn C.40}$$

Denoting the wings R_4 and R_5 as R_j relative to R_2 and R_3 respectively, Eqn B.38 can be rewritten by substituting the index i with j, etc

$$\overset{o}{\vec{\mathbf{h}}}_j + (\vec{\omega}_1 + \vec{\omega}_{pm}) \times \vec{\mathbf{h}}_j + \left[\vec{\mathbf{v}}_1 + \vec{\omega}_1 \times (\vec{\mathbf{b}}_i + \vec{\mathbf{b}}_j) + \vec{\omega}_{pi} \times \vec{\mathbf{b}}_j\right] \times \vec{\mathbf{p}}_j = \vec{\mathbf{g}}_j + \vec{\mathbf{g}}_{pj}$$

or

$$\vec{\mathbf{g}}_{pj} = \overset{o}{\vec{\mathbf{h}}}_j - \vec{\mathbf{h}}_j \times (\vec{\omega}_1 + \vec{\omega}_{pm}) + \left[\vec{\mathbf{v}}_1 + \vec{\omega}_1 \times (\vec{\mathbf{b}}_i + \vec{\mathbf{b}}_j) + \vec{\omega}_{pi} \times \vec{\mathbf{b}}_j\right] \times \vec{\mathbf{p}}_j - \vec{\mathbf{g}}_j \qquad \text{Eqn C.40}$$

Using Eqn C.35 to transform $\dot{\vec{\mathbf{p}}}_j$, Eqn C.28 becomes

$$\vec{\mathbf{f}}_{pj} = \dot{\vec{\mathbf{p}}}_j + \vec{\omega}_1 \times \vec{\mathbf{p}}_j - \vec{\mathbf{f}}_j \qquad \text{Eqn C.41}$$

This is then substituted in Eqn C.39, resulting in

$$\begin{aligned} \overset{o}{\vec{\mathbf{h}}}_i = {} & \vec{\mathbf{h}}_i \times (\vec{\omega}_1 + \vec{\omega}_{pm}) - \left[\vec{\mathbf{v}}_1 + \vec{\omega}_1 \times (\vec{\mathbf{b}}_h + \vec{\mathbf{b}}_i) + \vec{\omega}_{ph} \times \vec{\mathbf{b}}_i\right] \times \vec{\mathbf{p}}_i \\ & + \vec{\mathbf{g}}_i + \vec{\mathbf{g}}_{pi} - \vec{\mathbf{g}}_{pj} - \vec{\mathbf{b}}_j \times (\dot{\vec{\mathbf{p}}}_j + \vec{\omega}_1 \times \vec{\mathbf{p}}_j - \vec{\mathbf{f}}_j) \end{aligned} \qquad \text{Eqn C.42}$$

Substituting Eqn C.40 into Eqn C.42 results in

$$\begin{aligned} \overset{o}{\vec{\mathbf{h}}}_i = {} & \vec{\mathbf{h}}_i \times (\vec{\omega}_1 + \vec{\omega}_{pm}) - \left[\vec{\mathbf{v}}_1 + \vec{\omega}_1 \times (\vec{\mathbf{b}}_h + \dot{\vec{\mathbf{b}}}_i) + \vec{\omega}_{ph} \times \vec{\mathbf{b}}_i\right] \times \vec{\mathbf{p}}_i + \vec{\mathbf{g}}_i + \vec{\mathbf{g}}_{pi} \\ & - \overset{o}{\vec{\mathbf{h}}}_j + \vec{\mathbf{h}}_j \times (\vec{\omega}_1 + \vec{\omega}_{pm}) - \left[\vec{\mathbf{v}}_1 + \vec{\omega}_1 \times (\vec{\mathbf{b}}_j + \vec{\mathbf{b}}_j) + \vec{\omega}_{pi} \times \vec{\mathbf{b}}_j\right] \times \vec{\mathbf{p}}_j \\ & + \vec{\mathbf{g}}_j - \vec{\mathbf{b}}_j \times (\dot{\vec{\mathbf{p}}}_j + \vec{\omega}_1 \times \vec{\mathbf{p}}_j - \vec{\mathbf{f}}_j) \end{aligned} \qquad \text{Eqn C.43}$$

This can be rewritten as

$$\overset{\circ}{\vec{\mathbf{h}}}_i = \left(\vec{\mathbf{h}}_i + \vec{\mathbf{h}}_j\right)\times\left(\vec{\omega}_1 + \vec{\omega}_{pm}\right) - \overset{\circ}{\vec{\mathbf{h}}}_j - \left[\vec{\mathbf{v}}_1 + \vec{\omega}_1 \times \left(\vec{\mathbf{b}}_h + \vec{\mathbf{b}}_i\right) + \vec{\omega}_{ph} \times \vec{\mathbf{b}}_i\right]\times \vec{\mathbf{p}}_i$$

$$- \left[\vec{\mathbf{v}}_1 + \vec{\omega}_1 \times \left(\vec{\mathbf{b}}_i + \vec{\mathbf{b}}_j\right) + \vec{\omega}_{pi} \times \vec{\mathbf{b}}_j\right]\times \vec{\mathbf{p}}_j + \vec{\mathbf{g}}_i + \vec{\mathbf{g}}_{pi} + \vec{\mathbf{g}}_j \qquad \text{Eqn C.44}$$

$$- \vec{\mathbf{b}}_j \times \left(\dot{\vec{\mathbf{p}}}_j + \vec{\omega}_1 \times \vec{\mathbf{p}}_j - \vec{\mathbf{f}}_j\right)$$

Finally putting Eqn C.3 into Eqn C.44 results in

$$\overset{\circ}{\vec{\mathbf{h}}}_i = \left(\vec{\mathbf{h}}_i + \vec{\mathbf{h}}_j\right)\times\left(\vec{\omega}_1 + \vec{\omega}_{pm}\right) - \overset{\circ}{\vec{\mathbf{h}}}_j + \vec{\mathbf{g}}_i + \vec{\mathbf{g}}_{pi} + \vec{\mathbf{g}}_j - \vec{\mathbf{b}}_j \times \left(\dot{\vec{\mathbf{p}}}_j + \vec{\omega}_1 \times \vec{\mathbf{p}}_j - \vec{\mathbf{f}}_j\right)$$

$$+ \left[\vec{\mathbf{v}}_1 + \vec{\omega}_1 \times \left(\vec{\mathbf{b}}_h + \vec{\mathbf{b}}_i\right) + \vec{\omega}_{ph} \times \vec{\mathbf{b}}_i\right]\times\left[\vec{\mathbf{c}}_i \times \left(\vec{\omega}_1 + \vec{\omega}_{ph} + \vec{\omega}_{pi}\right)\right] \qquad \text{Eqn C.45}$$

$$+ \left[\vec{\mathbf{v}}_1 + \vec{\omega}_1 \times \left(\vec{\mathbf{b}}_i + \vec{\mathbf{b}}_j\right) + \vec{\omega}_{pi} \times \vec{\mathbf{b}}_j\right]\times\left[\vec{\mathbf{c}}_j \times \left(\vec{\omega}_1 + \vec{\omega}_{pi} + \vec{\omega}_{pj}\right)\right]$$

since

$$\vec{\mathbf{v}} \times \vec{\mathbf{p}}_i = \vec{\mathbf{v}} \times \left[m_i \vec{\mathbf{v}} - \vec{\mathbf{c}}_i \times \left(\vec{\omega}_1 + \vec{\omega}_{ph} + \vec{\omega}_{pi}\right)\right]$$

$$= \vec{\mathbf{v}} \times \left[\vec{\mathbf{c}}_i \times \left(\vec{\omega}_1 + \vec{\omega}_{ph} + \vec{\omega}_{pi}\right)\right]$$

and $\quad \vec{\mathbf{v}} = \vec{\mathbf{v}}_0 + \vec{\omega}_1 \times \left(\vec{\mathbf{b}}_h + \vec{\mathbf{b}}_i\right) + \vec{\omega}_{ph} \times \vec{\mathbf{b}}_i$

C.9 EQUATIONS IN SCALAR FORM

C.9.1 System Force Equations

Eqn B.37 represents the system force equation which relates the time derivative of the system linear momentum with the applied force

$$\dot{\vec{p}} = \vec{f} - \vec{\omega}_1 \times \vec{p} \qquad \text{Eqn C.37}$$

The linear momentum $\vec{p}_i$ of R_i (i = 1..5) is given by Eqn C.3

$$\vec{p}_i = m_i\left[\vec{v}_1 - \vec{b}_h \times \vec{\omega}_1 - \vec{b}_i \times \left(\vec{\omega}_1 + \vec{\omega}_{ph}\right)\right] - \vec{c}_i \times \left(\vec{\omega}_1 + \vec{\omega}_{ph} + \vec{\omega}_{pi}\right) \qquad \text{Eqn C.3}$$

Differentiating this in the frame of R_1 yields

$$\begin{aligned}\dot{\vec{p}}_i = m_i\Big[&\dot{\vec{v}}_1 - \vec{b}_h \times \dot{\vec{\omega}}_1 - \left(\vec{\omega}_{ph} \times \vec{b}_i\right) \times \left(\vec{\omega}_1 + \vec{\omega}_{ph}\right) - \vec{b}_i \times \left(\dot{\vec{\omega}}_1 + \dot{\vec{\omega}}_{ph}\right)\Big] \\ &- \vec{c}_i \times \left(\dot{\vec{\omega}}_1 + \dot{\vec{\omega}}_{ph} + \dot{\vec{\omega}}_{pi}\right) - \left[\left(\vec{\omega}_{pm} + \vec{\omega}_{pn}\right) \times \vec{c}_i\right] \times \left(\vec{\omega}_1 + \vec{\omega}_{ph} + \vec{\omega}_{pi}\right)\end{aligned} \qquad \text{Eqn C.46}$$

since $\vec{b}_h = \vec{0}$ for i = 2,3 and $\dot{\vec{b}}_h = \vec{0}$ for i = 4,5. Also, $\dot{\vec{c}}_i = \left(\vec{\omega}_{pm} + \vec{\omega}_{pn}\right) \times \vec{c}_i$.

Written in the frame of R_1 as described in Appendix A, Eqn C.46 becomes

$$\begin{aligned}\dot{\mathbf{p}}_i = m_i \dot{\mathbf{v}}_1 &- \left[m_i\left(\mathbf{b}_h^{\times} + \mathbf{C}_{1h}\mathbf{b}_i^{\times}\mathbf{C}_{hl}\right) + \mathbf{C}_{1i}\mathbf{c}_i^{\times}\mathbf{C}_{il}\right]\dot{\boldsymbol{\omega}}_1 - \left[m_i\mathbf{C}_{1h}\mathbf{b}_i^{\times} + \mathbf{C}_{1i}\mathbf{c}_i^{\times}\mathbf{C}_{ih}\right]\dot{\boldsymbol{\omega}}_{ph} \\ &- \mathbf{C}_{1i}\mathbf{c}_i^{\times}\dot{\boldsymbol{\omega}}_{pi} + m_i\left(\boldsymbol{\omega}_1 + \mathbf{C}_{1h}\boldsymbol{\omega}_{ph}\right)^{\times}\mathbf{C}_{1h}\boldsymbol{\omega}_{ph}^{\times}\mathbf{b}_i \\ &- \left[\left(\mathbf{C}_{1m}\boldsymbol{\omega}_{pm} + \mathbf{C}_{1n}\boldsymbol{\omega}_{pn}\right)^{\times}\mathbf{C}_{1i}\mathbf{c}_i\right]^{\times}\left(\boldsymbol{\omega}_1 + \mathbf{C}_{1h}\boldsymbol{\omega}_{ph} + \mathbf{C}_{1i}\boldsymbol{\omega}_{pi}\right)\end{aligned} \qquad \text{Eqn C.47}$$

The linear momentum of the system is the sum of the individual momenta

$$\begin{aligned}\dot{\mathbf{p}} = \sum_{i=1}^{5} m_i \dot{\mathbf{v}}_1 &- \sum_{i=1}^{5}\left[m_i\left(\mathbf{b}_h^{\times} + \mathbf{C}_{1h}\mathbf{b}_i^{\times}\mathbf{C}_{hl}\right) + \mathbf{C}_{1i}\mathbf{c}_i^{\times}\mathbf{C}_{il}\right]\dot{\boldsymbol{\omega}}_1 - \sum_{i=4}^{5}\left[m_i\mathbf{C}_{1h}\mathbf{b}_i^{\times} + \mathbf{C}_{1i}\mathbf{c}_i^{\times}\mathbf{C}_{ih}\right]\dot{\boldsymbol{\omega}}_{ph} \\ &- \sum_{i=1}^{5}\mathbf{C}_{1i}\mathbf{c}_i^{\times}\dot{\boldsymbol{\omega}}_{pi} + \sum_{i=1}^{5} m_i\left(\boldsymbol{\omega}_1 + \mathbf{C}_{1h}\boldsymbol{\omega}_{ph}\right)^{\times}\mathbf{C}_{1h}\boldsymbol{\omega}_{ph}^{\times}\mathbf{b}_i \\ &- \sum_{i=1}^{5}\left[\left\{\left(\mathbf{C}_{1m}\boldsymbol{\omega}_{pm}\right) + \left(\mathbf{C}_{1n}\boldsymbol{\omega}_{pn}\right)\right\}^{\times}\mathbf{C}_{1i}\mathbf{c}_i\right]^{\times}\left(\boldsymbol{\omega}_1 + \mathbf{C}_{1h}\boldsymbol{\omega}_{ph} + \mathbf{C}_{1i}\boldsymbol{\omega}_{pi}\right)\end{aligned}$$

or

$$\dot{\mathbf{p}} = m\dot{\mathbf{v}}_1 - \mathbf{c}^{\times}\dot{\vec{\omega}}_1 - \sum_{i=1}^{5}\left[m_i\mathbf{C}_{1h}\mathbf{b}_i^{\times} + \mathbf{C}_{1i}\mathbf{c}_i^{\times}\mathbf{C}_{ih}\right]\dot{\vec{\omega}}_{ph} - \sum_{i=1}^{5}\mathbf{C}_{1i}\mathbf{c}_i^{\times}\dot{\vec{\omega}}_{pi}$$
$$+ \sum_{i=1}^{5} m_i\left(\boldsymbol{\omega}_1 + \mathbf{C}_{1h}\boldsymbol{\omega}_{ph}\right)^{\times}\mathbf{C}_{1h}\boldsymbol{\omega}_{ph}^{\times}\mathbf{b}_i$$
$$- \sum_{i=1}^{5}\left[\left\{\left(\mathbf{C}_{1m}\boldsymbol{\omega}_{pm}\right) + \left(\mathbf{C}_{1n}\boldsymbol{\omega}_{pn}\right)\right\}^{\times}\mathbf{C}_{1i}\mathbf{c}_i\right]^{\times}\left(\boldsymbol{\omega}_1 + \mathbf{C}_{1h}\boldsymbol{\omega}_{ph} + \mathbf{C}_{1i}\boldsymbol{\omega}_{pi}\right) \qquad \text{Eqn C.48}$$
$$= m\dot{\mathbf{v}}_1 - \mathbf{c}^{\times}\dot{\vec{\omega}}_1 - \sum_{i=1}^{5}\left[m_i\mathbf{C}_{1h}\mathbf{b}_i^{\times} + \mathbf{C}_{1i}\mathbf{c}_i^{\times}\mathbf{C}_{ih}\right]\dot{\vec{\omega}}_{ph} - \sum_{i=1}^{5}\mathbf{C}_{1i}\mathbf{c}_i^{\times}\dot{\vec{\omega}}_{pi} - \mathbf{BB}$$

where

$$\mathbf{BB} = \sum_{i=1}^{5}\left[\left\{\left(\mathbf{C}_{1m}\boldsymbol{\omega}_{pm}\right) + \left(\mathbf{C}_{1n}\boldsymbol{\omega}_{pn}\right)\right\}^{\times}\mathbf{C}_{1i}\mathbf{c}_i\right]^{\times}\left(\boldsymbol{\omega}_1 + \mathbf{C}_{1h}\boldsymbol{\omega}_{ph} + \mathbf{C}_{1i}\boldsymbol{\omega}_{pi}\right)$$
$$- \sum_{i=1}^{5} m_i\left(\boldsymbol{\omega}_1 + \mathbf{C}_{1h}\boldsymbol{\omega}_{ph}\right)^{\times}\mathbf{C}_{1h}\boldsymbol{\omega}_{ph}^{\times}\mathbf{b}_i \qquad \text{Eqn C.49}$$

Substituting Eqn C.48 into Eqn C.37 results in

$$m\dot{\mathbf{v}}_1 - \mathbf{c}^{\times}\dot{\vec{\omega}}_1 - \sum_{i=1}^{5}\left[m_i\mathbf{C}_{1h}\mathbf{b}_i^{\times} + \mathbf{C}_{1i}\mathbf{c}_i^{\times}\mathbf{C}_{ih}\right]\dot{\vec{\omega}}_{ph} - \sum_{i=1}^{5}\mathbf{C}_{1i}\mathbf{c}_i^{\times}\dot{\vec{\omega}}_{pi} = \sum_{i=1}^{5}\mathbf{C}_{1i}\mathbf{f}_i - \boldsymbol{\omega}_1^{\times}\mathbf{p} + \mathbf{BB} \qquad \text{Eqn C.50}$$

where $\mathbf{p}$ is obtained by transforming Eqn C.4 into the frame of R_1 as follows

$$\mathbf{p} = m\mathbf{v}_1 - \mathbf{c}^{\times}\boldsymbol{\omega}_1 - \sum_{i=2}^{5}\left(\mathbf{C}_{1i}\mathbf{c}_i^{\times} + \mathbf{C}_{1j}\mathbf{c}_j^{\times}\mathbf{C}_{ji} + m_j\mathbf{C}_{1i}\mathbf{b}_j^{\times}\right)\boldsymbol{\omega}_{pi} \qquad \text{Eqn C.51}$$

and $\mathbf{c}^{\times}$ is obtained by transforming Eqn C.5

$$\mathbf{c}^{\times} = \sum_{i=1}^{5}\left[\mathbf{C}_{1i}\mathbf{c}_i^{\times}\mathbf{C}_{i1} + m_i\left(\mathbf{b}_h^{\times} + \mathbf{C}_{1h}\mathbf{b}_i^{\times}\mathbf{C}_{h1}\right)\right] \qquad \text{Eqn C.52}$$

C.9.2 System Moment Equations

For convenience, the inertia dyads $\tilde{\mathbf{J}}$, $\tilde{\mathbf{J}}_{1i}$ and $\tilde{\mathbf{J}}_{1ih}$ are to be expressed in the frame of R_1 while $\tilde{\mathbf{J}}_{ih}$ and $\tilde{\mathbf{J}}_i$ will be expressed in the frame of R_i. Now consider Eqn C.38.

$$\dot{\vec{\mathbf{h}}}_{P_1} = \sum_{i=1}^{5} \vec{\mathbf{g}}_i + \sum_{i=2}^{5} \left(\vec{\mathbf{b}}_i + \vec{\mathbf{b}}_h\right) \times \vec{\mathbf{f}}_i - \vec{\mathbf{v}}_1 \times \sum_{i=1}^{5} \vec{\mathbf{p}}_i - \vec{\boldsymbol{\omega}}_1 \times \vec{\mathbf{h}}_{P_1} \qquad \text{Eqn C.38}$$

The time derivative of Eqn C.18 yields the left hand side of Eqn C.38, which when written in the frame of R_1, becomes

$$\begin{aligned} \dot{\mathbf{h}}_{P_1} =& \dot{\mathbf{c}}^{\times} \mathbf{v}_1 + \mathbf{c}^{\times} \dot{\mathbf{v}}_1 + \dot{\mathbf{J}} \boldsymbol{\omega}_1 + \mathbf{J} \dot{\boldsymbol{\omega}}_1 + \sum_{i=4}^{5} \left(\dot{\mathbf{J}}_{1h} + \dot{\mathbf{J}}_{1ih}\right) \mathbf{C}_{1h} \boldsymbol{\omega}_{ph} \\ &+ \sum_{i=4}^{5} \left(\mathbf{J}_{1h} + \mathbf{J}_{1ih}\right) \mathbf{C}_{1h} \dot{\boldsymbol{\omega}}_{ph} + \sum_{i=4}^{5} \dot{\mathbf{J}}_{1i} \mathbf{C}_{1i} \boldsymbol{\omega}_{pi} + \sum_{i=4}^{5} \mathbf{J}_{1i} \mathbf{C}_{1i} \dot{\boldsymbol{\omega}}_{pi} \end{aligned} \qquad \text{Eqn C.53}$$

The terms on the right hand side of Eqn C.38 will have to be written in the frame of R_1 as well. From Eqn C.18,

$$\mathbf{h}_{P_1} = \mathbf{c}^{\times} \mathbf{v}_1 + \mathbf{J} \boldsymbol{\omega}_1 + \sum_{i=4}^{5} \left(\mathbf{J}_{1h} + \mathbf{J}_{1ih}\right) \mathbf{C}_{1h} \boldsymbol{\omega}_{ph} + \sum_{i=4}^{5} \mathbf{J}_{1i} \mathbf{C}_{1i} \boldsymbol{\omega}_{pi} \qquad \text{Eqn C.54}$$

and $-\vec{\boldsymbol{\omega}}_1 \times \vec{\mathbf{h}}_{P_1}$ becomes $-\boldsymbol{\omega}_1^{\times} \mathbf{h}_{P_1}$.

Next, $-\vec{\mathbf{v}}_1 \times \vec{\mathbf{p}}$ can be written as $\mathbf{v}_1^{\times} \mathbf{p}$, where $\mathbf{p}$ is given by Eqn C.51 or as

$$\mathbf{v}_1^{\times} \left[\mathbf{c}^{\times} \boldsymbol{\omega}_1 + \sum_{i=2}^{5} \left(\mathbf{C}_{1i} \mathbf{c}_i^{\times} + \mathbf{C}_{1i} \mathbf{c}_j^{\times} \mathbf{C}_{ji} + \mathbf{m}_j \mathbf{C}_{1i} \mathbf{b}_j^{\times} \right) \boldsymbol{\omega}_{pi} \right] \qquad \text{Eqn C.55}$$

Finally, $\sum_{i=1}^{5} \vec{\mathbf{g}}_i + \sum_{i=2}^{5} \left(\vec{\mathbf{b}}_i + \vec{\mathbf{b}}_h\right) \times \vec{\mathbf{f}}_i$ can be written as

$$\sum_{i=1}^{5} \mathbf{C}_{1i} \mathbf{g}_i + \sum_{i=2}^{5} \left(\mathbf{C}_{1g} \mathbf{b}_h^{\times} \mathbf{C}_{1i} + \mathbf{C}_{1h} \mathbf{b}_i^{\times} \mathbf{C}_{hi} \right) \mathbf{f}_i \qquad \text{Eqn C.56}$$

with the subscript g in $\mathbf{C}_{1g}$ in Eqn C.56 denotes the reference frame of $\mathbf{b}_h$.

Substituting Eqn C.54 to C.56 into the RHS and substituting Eqn C.53 into the left hand side of Eqn C.38 results in

$$\mathbf{c}^{\times}\dot{\mathbf{v}}_1 + \mathbf{J}\dot{\boldsymbol{\omega}}_1 + \sum_{i=4}^{5}\left(\mathbf{J}_{1h} + \mathbf{J}_{1ih}\right)\mathbf{C}_{1h}\dot{\boldsymbol{\omega}}_{ph} + \sum_{i=4}^{5}\mathbf{J}_{1i}\mathbf{C}_{1i}\dot{\boldsymbol{\omega}}_{pi}$$

$$= \sum_{i=1}^{5}\mathbf{C}_{1i}\mathbf{g}_i + \sum_{i=1}^{5}\left(\mathbf{C}_{1g}\mathbf{b}_h^{\times}\mathbf{C}_{1i} + \mathbf{C}_{1h}\mathbf{b}_i^{\times}\mathbf{C}_{hi}\right)\mathbf{f}_i - \boldsymbol{\omega}_1^{\times}\mathbf{h}_{P_1} - \mathbf{v}_1^{\times}\mathbf{p} - \dot{\mathbf{c}}^{\times}\mathbf{v}_1 - \mathbf{J}\boldsymbol{\omega}_1$$
$$- \sum_{i=4}^{5}\left(\dot{\mathbf{J}}_{1h} + \dot{\mathbf{J}}_{1ih}\right)\mathbf{C}_{1h}\boldsymbol{\omega}_{ph} - \sum_{i=4}^{5}\dot{\mathbf{J}}_{1h}\mathbf{C}_{1i}\boldsymbol{\omega}_{pi}$$

Eqn C.57

The term $\mathbf{c}^{\times}$ was given in Eqn C.52. The time derivative of Eqn C.5 allows us to obtain $\dot{\mathbf{c}}^{\times}$, noting that $\dot{\vec{\mathbf{c}}}_1 = \dot{\vec{\mathbf{b}}}_h = \vec{\mathbf{0}}$ and $\dot{\vec{\mathbf{c}}}_i = \left(\vec{\boldsymbol{\omega}}_{pm} + \vec{\boldsymbol{\omega}}_{pn}\right)\times\vec{\mathbf{c}}_i$ for i =2..5 where m and n are as given in Table C.2. Hence

$$\dot{\mathbf{c}}^{\times} = -\sum_{i=2}^{5}\mathbf{C}_{1i}\left[\mathbf{c}_i^{\times}\left(\mathbf{C}_{im}\boldsymbol{\omega}_{pm} + \mathbf{C}_{in}\boldsymbol{\omega}_{pn}\right)\right]^{\times}\mathbf{C}_{il} - \sum_{i=4}^{5}m_i\mathbf{C}_{1m}\left(\mathbf{b}_i^{\times}\boldsymbol{\omega}_{pm}\right)^{\times}\mathbf{C}_{ml} \qquad \text{Eqn C.58}$$

since $\dot{\vec{\mathbf{b}}}_i = \vec{\mathbf{0}}$ for i = 1..3 and $m_j = 0$ for i = 4,5.

C.9.3 Scalar Equations of R_2 and R_3

The scalar form of the moment equation for R_2 and R_3 was developed in the frame of R_i (i = 2, 3) and given by Eqn C.42, which can be simplified as:

$$\overset{o}{\vec{\mathbf{h}}}_i = \vec{\mathbf{h}}_i \times \left(\vec{\omega}_1 + \vec{\omega}_{pm}\right) - \left[\vec{\mathbf{v}}_1 + \vec{\omega}_1 \times \vec{\mathbf{b}}_i\right] \times \vec{\mathbf{p}}_i + \vec{\mathbf{g}}_i + \vec{\mathbf{g}}_{pi} - \vec{\mathbf{g}}_{pj} - \vec{\mathbf{b}}_j \times \left(\dot{\vec{\mathbf{p}}}_j + \vec{\omega}_1 \times \vec{\mathbf{p}}_j - \vec{\mathbf{f}}_j\right) \qquad \text{Eqn C.59}$$

since terms associated with the index h becomes zero.

The angular momentum of R_i (i = 2,3) appearing as the first term on the RHS of Eqn C.59 is given by Eqn C.7, which after omitting terms associated with the index h and transforming to the frame of R_i, becomes

$$\mathbf{h}_i = \mathbf{c}_i^{\times} \mathbf{C}_{i1} \mathbf{v}_1 + \mathbf{J}_{i1} \mathbf{C}_{i1} \boldsymbol{\omega}_1 + \mathbf{J}_i \boldsymbol{\omega}_{pi} \qquad \text{Eqn C.60}$$

The second term on the right hand side of Eqn C.59 can be obtained from Eqn C.3 with i = 2,3 (again omitting terms associated with the index h). After being transformed to the frame of R_i, this becomes

$$\left[\vec{\mathbf{v}}_1 + \vec{\omega}_1 \times \vec{\mathbf{b}}_i\right] \times \vec{\mathbf{p}}_i = -\mathbf{C}_{i1} \left[\mathbf{v}_1 + \boldsymbol{\omega}_1^{\times} \mathbf{b}_i\right]^{\times} \mathbf{C}_{1i} \mathbf{c}_i^{\times} \left(\mathbf{C}_{i1} \boldsymbol{\omega}_1 + \boldsymbol{\omega}_{pi}\right) \qquad \text{Eqn C.61}$$

The last term on the RHS of Eqn C.59 can be subdivided into 3 parts and developed further. First, using Eqn C.46 (replacing the indices h and i with i and j respectively):

$$\vec{\mathbf{b}}_j \times \dot{\vec{\mathbf{p}}}_j = m_j \vec{\mathbf{b}}_j \times \left[\dot{\vec{\mathbf{v}}}_1 - \vec{\mathbf{b}}_i \times \dot{\vec{\omega}}_1 - \left(\vec{\omega}_{pi} \times \vec{\mathbf{b}}_j\right) \times \left(\vec{\omega}_1 + \vec{\omega}_{pi}\right) - \vec{\mathbf{b}}_j \times \left(\dot{\vec{\omega}}_1 + \dot{\vec{\omega}}_{pi}\right)\right] - \vec{\mathbf{b}}_j \times \left[\vec{\mathbf{c}}_i \times \left(\dot{\vec{\omega}}_1 + \dot{\vec{\omega}}_{pi} + \dot{\vec{\omega}}_{pj}\right) - \left[\left(\vec{\omega}_{pi} + \vec{\omega}_{pj}\right) \times \vec{\mathbf{c}}_j\right] \times \left(\vec{\omega}_1 + \vec{\omega}_{pi} + \vec{\omega}_{pj}\right)\right] \qquad \text{Eqn C.62}$$

In the frame of R_i, this becomes

$$\begin{aligned}\left[\vec{\mathbf{b}}_j^{\times}\dot{\mathbf{p}}_j\right] &= m_j\mathbf{b}_j^{\times}\mathbf{C}_{i1}\dot{\mathbf{v}}_1 - \left[m_j\mathbf{b}_j^{\times}\mathbf{C}_{i1}\left(\mathbf{b}_i^{\times}+\mathbf{C}_{1i}\mathbf{b}_j^{\times}\mathbf{C}_{i1}\right)+\mathbf{b}_j^{\times}\mathbf{C}_{ij}\mathbf{c}_j^{\times}\mathbf{C}_{j1}\right]\dot{\boldsymbol{\omega}}_1 \\ &\quad -\mathbf{b}_j^{\times}\mathbf{C}_{ij}\mathbf{c}_j^{\times}\mathbf{C}_{j1}\dot{\boldsymbol{\omega}}_{pi} - \mathbf{b}_j^{\times}\mathbf{C}_{ij}\mathbf{c}_j^{\times}\dot{\boldsymbol{\omega}}_{pj} + m_j\mathbf{b}_j^{\times}\mathbf{C}_{i1}\left(\boldsymbol{\omega}_1+\mathbf{C}_{1i}\boldsymbol{\omega}_{pi}\right)^{\times}\left(\boldsymbol{\omega}_{pi}^{\times}\mathbf{b}_j\right) \\ &\quad -\mathbf{b}_j^{\times}\mathbf{C}_{i1}\left[\left(\boldsymbol{\omega}_1^{\times}\mathbf{C}_{1j}+\mathbf{C}_{1i}\boldsymbol{\omega}_{pi}^{\times}\mathbf{C}_{ij}+\mathbf{C}_{1j}\boldsymbol{\omega}_{pj}^{\times}\right)\mathbf{c}_j\right]^{\times}\left(\mathbf{C}_{jm}\boldsymbol{\omega}_{pm}+\mathbf{C}_{jn}\boldsymbol{\omega}_{pn}\right)\end{aligned}$$

$$\begin{aligned}&= m_j\mathbf{b}_j^{\times}\mathbf{C}_{i1}\dot{\mathbf{v}}_1 - \left[m_j\mathbf{b}_j^{\times}\mathbf{C}_{i1}\left(\mathbf{b}_i^{\times}+\mathbf{C}_{1i}\mathbf{b}_j^{\times}\mathbf{C}_{i1}\right)+\mathbf{b}_j^{\times}\mathbf{C}_{ij}\mathbf{c}_j^{\times}\mathbf{C}_{j1}\right]\dot{\boldsymbol{\omega}}_1 \\ &\quad -\mathbf{b}_j^{\times}\mathbf{C}_{ij}\mathbf{c}_j^{\times}\mathbf{C}_{ji}\dot{\boldsymbol{\omega}}_{pi} - \mathbf{b}_j^{\times}\mathbf{C}_{ij}\mathbf{c}_j^{\times}\dot{\boldsymbol{\omega}}_{pj} + \mathbf{A}_1\end{aligned}$$

Eqn C.63

where

$$\begin{aligned}\mathbf{A}_1 &= +m_j\mathbf{b}_j^{\times}\mathbf{C}_{i1}\left(\boldsymbol{\omega}_1+\mathbf{C}_{1i}\boldsymbol{\omega}_{pi}\right)^{\times}\left(\boldsymbol{\omega}_{pi}^{\times}\mathbf{b}_j\right) \\ &\quad -\mathbf{b}_j^{\times}\mathbf{C}_{i1}\left[\left(\boldsymbol{\omega}_1^{\times}\mathbf{C}_{1j}+\mathbf{C}_{1i}\boldsymbol{\omega}_{pi}^{\times}\mathbf{C}_{ij}+\mathbf{C}_{1j}\boldsymbol{\omega}_{pj}^{\times}\right)\mathbf{c}_j\right]^{\times}\left(\mathbf{C}_{jm}\boldsymbol{\omega}_{pm}+\mathbf{C}_{jn}\boldsymbol{\omega}_{pn}\right)\end{aligned}$$

Eqn C.64

Substituting Eqn C.3 for the linear momentum term in $\vec{\mathbf{b}}_j\times\left(\vec{\boldsymbol{\omega}}_1\times\vec{\mathbf{p}}_j\right)$ and again replacing the indices h and i with i and j respectively results in the following expression in the frame of R_i

$$\begin{aligned}\mathbf{b}_j^{\times}\mathbf{C}_{i1}\boldsymbol{\omega}_1^{\times}\mathbf{C}_{1j}\mathbf{p}_j &= \mathbf{b}_j^{\times}\mathbf{C}_{i1}\left\{m_j\left[\boldsymbol{\omega}_1^{\times}\mathbf{v}_0-\boldsymbol{\omega}_1^{\times}\mathbf{b}_i^{\times}\boldsymbol{\omega}_1-\boldsymbol{\omega}_1^{\times}\mathbf{C}_{i1}\mathbf{b}_j^{\times}\left(\mathbf{C}_{i1}\boldsymbol{\omega}_1+\boldsymbol{\omega}_{pi}\right)\right]\right\} \\ &\quad -\mathbf{b}_j^{\times}\mathbf{C}_{i1}\left[\boldsymbol{\omega}_1^{\times}\mathbf{C}_{1j}\mathbf{c}_j^{\times}\left(\mathbf{C}_{j1}\boldsymbol{\omega}_1+\mathbf{C}_{ji}\boldsymbol{\omega}_{pi}+\boldsymbol{\omega}_{pj}\right)\right]\end{aligned}$$

Eqn C.65

Finally, differentiating $\vec{\mathbf{h}}_i$ in Eqn B.7 with respect to time in the frame of R_i, for i = 2 and 3, results in

$$\mathring{\vec{\mathbf{h}}}_i = \vec{\mathbf{c}}_i\times\left(\dot{\vec{\mathbf{v}}}_1-\vec{\boldsymbol{\omega}}_{pm}\times\vec{\mathbf{v}}_1\right)+\mathring{\tilde{\mathbf{J}}}_{i1}\cdot\vec{\boldsymbol{\omega}}_1+\tilde{\mathbf{J}}_{i1}\cdot\left(\dot{\vec{\boldsymbol{\omega}}}_1-\vec{\boldsymbol{\omega}}_{pm}\times\vec{\boldsymbol{\omega}}_1\right)+\mathring{\tilde{\mathbf{J}}}_i\cdot\vec{\boldsymbol{\omega}}_{pi}+\tilde{\mathbf{J}}_i\cdot\dot{\vec{\boldsymbol{\omega}}}_{pi} \quad \text{Eqn C.66}$$

since $\mathring{\vec{\mathbf{v}}}_1=\left(\dot{\vec{\mathbf{v}}}_1-\vec{\boldsymbol{\omega}}_{pm}\times\vec{\mathbf{v}}_1\right)$ and $\mathring{\vec{\boldsymbol{\omega}}}_1=\left(\dot{\vec{\boldsymbol{\omega}}}_1-\vec{\boldsymbol{\omega}}_{pm}\times\vec{\boldsymbol{\omega}}_1\right)$.

Also, because the moment of inertia is constant in its frame, its time derivative $\overset{\circ}{\tilde{\mathbf{J}}}_i = \tilde{\mathbf{0}}$. The above can be written in the frame of R_i as follows:

$$\begin{aligned}\overset{\circ}{\mathbf{h}}_i &= \mathbf{c}_i^{\times}\left(\mathbf{C}_{i1}\dot{\mathbf{v}}_1 - \boldsymbol{\omega}_{pm}^{\times}\mathbf{C}_{i1}\mathbf{v}_1\right) + \overset{\circ}{\mathbf{J}}_{i1}\mathbf{C}_{i1}\boldsymbol{\omega}_1 + \mathbf{J}_{i1}\left(\mathbf{C}_{i1}\dot{\boldsymbol{\omega}}_1 - \boldsymbol{\omega}_{pm}^{\times}\mathbf{C}_{i1}\boldsymbol{\omega}_1\right) + \mathbf{J}_i\cdot\dot{\boldsymbol{\omega}}_{pi} \\ &= \mathbf{c}_i^{\times}\mathbf{C}_{i1}\dot{\mathbf{v}}_1 + \mathbf{J}_{i1}\mathbf{C}_{i1}\dot{\boldsymbol{\omega}}_1 + \mathbf{J}_i\cdot\dot{\boldsymbol{\omega}}_{pi} - \mathbf{c}_i^{\times}\boldsymbol{\omega}_{pm}^{\times}\mathbf{C}_{i1}\mathbf{v}_1 + \overset{\circ}{\mathbf{J}}_{i1}\mathbf{C}_{i1}\boldsymbol{\omega}_1 - \mathbf{J}_{i1}\boldsymbol{\omega}_{pm}^{\times}\mathbf{C}_{i1}\boldsymbol{\omega}_1 \quad \text{Eqn C.67} \\ &= \mathbf{c}_i^{\times}\mathbf{C}_{i1}\dot{\mathbf{v}}_1 + \mathbf{J}_{i1}\mathbf{C}_{i1}\dot{\boldsymbol{\omega}}_1 + \mathbf{J}_i\cdot\dot{\boldsymbol{\omega}}_{pi} + \mathbf{A}_2\end{aligned}$$

where $\mathbf{A}_2 = -\mathbf{c}_i^{\times}\boldsymbol{\omega}_{pm}^{\times}\mathbf{C}_{i1}\mathbf{v}_1 + \overset{\circ}{\mathbf{J}}_{i1}\mathbf{C}_{i1}\boldsymbol{\omega}_1 - \mathbf{J}_{i1}\boldsymbol{\omega}_{pm}^{\times}\mathbf{C}_{i1}\boldsymbol{\omega}_1$ Eqn C.68

The above equation has taken into consideration that i = m and j = n where applicable according to Tables C.1 and C.2, such that the direction cosine matrices $\mathbf{C}_{im} = \mathbf{C}_{jn} = \mathbf{I}$.

Now, Eqns C.60 to C.68 can be substituted into Eqn B.59 to obtain

$$\begin{aligned}&\left(\mathbf{c}_i^{\times}\mathbf{C}_{i1} + \mathrm{m}_j\mathbf{b}_j^{\times}\mathbf{C}_{i1}\right)\dot{\mathbf{v}}_1 + \left[\mathbf{J}_{i1}\mathbf{C}_{i1} - \mathrm{m}_j\mathbf{b}_j^{\times}\mathbf{C}_{i1}\left(\mathbf{b}_i^{\times} + \mathbf{C}_{1i}\mathbf{b}_j^{\times}\mathbf{C}_{i1}\right) - \mathbf{b}_j^{\times}\mathbf{C}_{ij}\mathbf{c}_j^{\times}\mathbf{C}_{j1}\right]\dot{\boldsymbol{\omega}}_1 \\ &+ \left(\mathbf{J}_i - \mathbf{b}_j^{\times}\mathbf{C}_{ij}\mathbf{c}_j^{\times}\mathbf{C}_{ji}\right)\dot{\boldsymbol{\omega}}_{pi} - \mathbf{b}_j^{\times}\mathbf{C}_{ij}\mathbf{c}_j^{\times}\dot{\boldsymbol{\omega}}_{pj} \\ &\qquad = \mathbf{g}_i + \mathbf{g}_{pi} - \mathbf{C}_{ij}\mathbf{g}_{pj} + \mathbf{b}_j^{\times}\mathbf{C}_{ij}\mathbf{f}_j + \left[\mathbf{h}_i^{\times} + \mathbf{C}_{i1}\left(\mathbf{v}_0 + \boldsymbol{\omega}_1^{\times}\mathbf{b}_i\right)^{\times}\mathbf{C}_{1i}\mathbf{c}_i^{\times}\right]\left(\mathbf{C}_{i1}\boldsymbol{\omega}_1 + \boldsymbol{\omega}_{pi}\right) \\ &\qquad\qquad - \mathbf{b}_j^{\times}\mathbf{C}_{i1}\boldsymbol{\omega}_1^{\times}\mathbf{C}_{1j}\mathbf{p}_j - \mathbf{A}_1 - \mathbf{A}_2\end{aligned}$$

Eqn C.69

C.9.4 Scalar Equations of R_4 and R_5

For R_i (i = 4,5), the moment equation is given by Eqn C.40, which can be rearranged as

$$\overset{+}{\vec{\mathbf{h}}}_i + \left(\vec{\omega}_1 + \vec{\omega}_{pm} + \vec{\omega}_{pn}\right)\times\vec{\mathbf{h}}_i + \left[\vec{\mathbf{v}}_1 + \vec{\omega}_1 \times \left(\vec{\mathbf{b}}_h + \vec{\mathbf{b}}_i\right) + \vec{\omega}_{ph} \times \vec{\mathbf{b}}_i\right]\times\vec{\mathbf{p}}_i = \vec{\mathbf{g}}_i + \vec{\mathbf{g}}_{pi} \quad \text{Eqn C.70}$$

and the angular momentum is given by Eqn C.7, which when written in the frame of R_i becomes

$$\mathbf{h}_i = \mathbf{c}_i^{\times}\mathbf{C}_{il}\mathbf{v}_1 + \mathbf{J}_{il}\mathbf{C}_{il}\boldsymbol{\omega}_1 + \mathbf{J}_{ih}\mathbf{C}_{ih}\boldsymbol{\omega}_{ph} + \mathbf{J}_i\boldsymbol{\omega}_{pi} \quad \text{Eqn C.71}$$

Differentiating Eqn C.7 with respect to time and the frame of R_i, we obtain

$$\begin{aligned}\overset{+}{\vec{\mathbf{h}}}_i = {} & \vec{\mathbf{c}}_i \times \left[\dot{\vec{\mathbf{v}}}_1 - \left(\vec{\omega}_{pm} + \vec{\omega}_{pn}\right)\times\vec{\mathbf{v}}_1\right] + \overset{+}{\vec{\mathbf{J}}}_{il}\cdot\vec{\omega}_1 + \tilde{\mathbf{J}}_{il}\cdot\left[\dot{\vec{\omega}}_1 - \left(\vec{\omega}_{pm} + \vec{\omega}_{pn}\right)\times\vec{\omega}_1\right] \\ & + \overset{+}{\vec{\mathbf{J}}}_{ih}\cdot\vec{\omega}_{ph} + \tilde{\mathbf{J}}_{ih}\cdot\left[\dot{\vec{\omega}}_{ph} - \dot{\vec{\omega}}_{pn}\times\vec{\omega}_{ph}\right] + \overset{+}{\vec{\mathbf{J}}}_i\cdot\vec{\omega}_{pi} + \tilde{\mathbf{J}}_i\cdot\left[\dot{\vec{\omega}}_{pi} - \vec{\omega}_{pm}\times\vec{\omega}_{pi}\right]\end{aligned} \quad \text{Eqn C.72}$$

since $\overset{+}{\vec{\mathbf{v}}}_1 = \left[\dot{\vec{\mathbf{v}}}_1 - \left(\vec{\omega}_{pm} + \vec{\omega}_{pn}\right)\times\vec{\mathbf{v}}_0\right]$, $\overset{+}{\vec{\omega}}_1 = \left[\dot{\vec{\omega}}_1 - \left(\vec{\omega}_{pm} + \vec{\omega}_{pn}\right)\times\vec{\omega}_1\right]$ etc.

As the moment of inertia is constant when referred to in its own frame, its time derivative $\overset{+}{\tilde{\mathbf{J}}}_i = \tilde{\mathbf{0}}$. Hence Eqn C.72 can be transformed into the frame of R_i and rearranged as

$$\begin{aligned}\overset{+}{\mathbf{h}}_i = {} & \mathbf{c}_i^{\times}\mathbf{C}_{il}\dot{\mathbf{v}}_1 + \mathbf{J}_{il}\mathbf{C}_{il}\dot{\boldsymbol{\omega}}_1 + \mathbf{J}_{ih}\mathbf{C}_{ih}\dot{\boldsymbol{\omega}}_{ph} + \mathbf{J}_i\dot{\boldsymbol{\omega}}_{pi} - \mathbf{c}_i^{\times}\left[\left(\mathbf{C}_{im}\boldsymbol{\omega}_{pm} + \mathbf{C}_{in}\boldsymbol{\omega}_{pn}\right)^{\times}\mathbf{C}_{il}\mathbf{v}_1\right] \\ & + \overset{+}{\mathbf{J}}_{il}\,\mathbf{C}_{il}\boldsymbol{\omega}_1 + \mathbf{J}_{il}\left(\mathbf{C}_{il}\boldsymbol{\omega}_1\right)^{\times}\left(\mathbf{C}_{im}\boldsymbol{\omega}_{pm} + \mathbf{C}_{in}\boldsymbol{\omega}_{pn}\right) \\ & + \overset{+}{\mathbf{J}}_{ih}\,\mathbf{C}_{ih}\boldsymbol{\omega}_{ph} + \mathbf{J}_{ih}\mathbf{C}_{ih}\left(\boldsymbol{\omega}_{ph}^{\times}\mathbf{C}_{hn}\boldsymbol{\omega}_{pn}\right) + \mathbf{J}_i\boldsymbol{\omega}_{pi}^{\times}\mathbf{C}_{im}\boldsymbol{\omega}_{pm} \\ = {} & \mathbf{c}_i^{\times}\mathbf{C}_{il}\dot{\mathbf{v}}_1 + \mathbf{J}_{il}\mathbf{C}_{il}\dot{\boldsymbol{\omega}}_1 + \mathbf{J}_{ih}\mathbf{C}_{ih}\dot{\boldsymbol{\omega}}_{ph} + \mathbf{J}_i\cdot\dot{\boldsymbol{\omega}}_{pi} - \mathbf{A}_3\end{aligned} \quad \text{Eqn C.73}$$

where

$$\begin{aligned}\mathbf{A}_3 = {} & \mathbf{c}_i^{\times}\left[\left(\mathbf{C}_{im}\boldsymbol{\omega}_{pm} + \mathbf{C}_{in}\boldsymbol{\omega}_{pn}\right)^{\times}\mathbf{C}_{il}\mathbf{v}_1\right] - \overset{+}{\mathbf{J}}_{il}\,\mathbf{C}_{il}\boldsymbol{\omega}_1 - \mathbf{J}_{il}\left(\mathbf{C}_{il}\boldsymbol{\omega}_1\right)^{\times}\left(\mathbf{C}_{im}\boldsymbol{\omega}_{pm} + \mathbf{C}_{in}\boldsymbol{\omega}_{pn}\right) \\ & - \overset{+}{\mathbf{J}}_{ih}\,\mathbf{C}_{ih}\boldsymbol{\omega}_{ph} - \mathbf{J}_{ih}\mathbf{C}_{ih}\left(\boldsymbol{\omega}_{ph}^{\times}\mathbf{C}_{hn}\boldsymbol{\omega}_{pn}\right) - \mathbf{J}_i\boldsymbol{\omega}_{pi}^{\times}\mathbf{C}_{im}\boldsymbol{\omega}_{pm}\end{aligned} \quad \text{Eqn C.74}$$

Transforming Eqn C.40 into the frame of R_i, and then substituting Eqn C.73 in it results in

$$\mathbf{c}_i^{\times}\mathbf{C}_{il}\dot{\mathbf{v}}_l + \mathbf{J}_{il}\mathbf{C}_{il}\dot{\boldsymbol{\omega}}_l + \mathbf{J}_{ih}\mathbf{C}_{ih}\dot{\boldsymbol{\omega}}_{ph} + \mathbf{J}_i \cdot \dot{\boldsymbol{\omega}}_{pi}$$

$$\begin{aligned} &= \left\{\mathbf{C}_{il}\left[\mathbf{v}_l^{\times} + \left(\boldsymbol{\omega}_l^{\times}\mathbf{b}_h\right)^{\times} + \left(\boldsymbol{\omega}_l^{\times}\mathbf{C}_{lh}\mathbf{b}_i\right)^{\times}\right]\mathbf{C}_{li}\mathbf{c}_i^{\times}\right\}\left(\mathbf{C}_{il}\boldsymbol{\omega}_l + \mathbf{C}_{im}\boldsymbol{\omega}_{pm} + \mathbf{C}_{in}\boldsymbol{\omega}_{pn}\right) \\ &+ \left\{\mathbf{C}_{lh}\left(\boldsymbol{\omega}_{ph}^{\times}\mathbf{b}_i\right)^{\times}\mathbf{C}_{hi}\mathbf{c}_i^{\times}\right\}\left(\mathbf{C}_{il}\boldsymbol{\omega}_l + \mathbf{C}_{im}\boldsymbol{\omega}_{pm} + \mathbf{C}_{in}\boldsymbol{\omega}_{pn}\right) \\ &+ \mathbf{h}_i^{\times}\left(\mathbf{C}_{il}\boldsymbol{\omega}_l + \mathbf{C}_{im}\boldsymbol{\omega}_{pm} + \mathbf{C}_{in}\boldsymbol{\omega}_{pn}\right) + \mathbf{g}_i + \mathbf{g}_{pi} + \mathbf{A}_3 \end{aligned} \qquad \text{Eqn C.75}$$

C.10 MATRIX FORMULATION OF EQUATIONS OF MOTION

The equations of motion for the multi-body system of the vehicle comprising of five bodies R_1 to R_5, with a total of 12 degrees of freedom are given in Eqns C.50, C.57, C.69 and C.75.

$$m\dot{\mathbf{v}}_1 - \mathbf{c}^{\times}\dot{\tilde{\boldsymbol{\omega}}}_1 - \sum_{i=1}^{5}\left[m_i\mathbf{C}_{1h}\mathbf{b}_i^{\times} + \mathbf{C}_{1i}\mathbf{c}_i^{\times}\mathbf{C}_{ih}\right]\dot{\tilde{\boldsymbol{\omega}}}_{ph} - \sum_{i=1}^{5}\mathbf{C}_{1i}\mathbf{c}_i^{\times}\dot{\tilde{\boldsymbol{\omega}}}_{pi} = \sum_{i=1}^{5}\mathbf{C}_{1i}\mathbf{f}_i - \boldsymbol{\omega}_1^{\times}\mathbf{p} + \mathbf{BB}$$

Eqn C.50

$$\mathbf{c}^{\times}\dot{\mathbf{v}}_1 + \mathbf{J}\dot{\boldsymbol{\omega}}_1 + \sum_{i=4}^{5}\left(\mathbf{J}_{1h} + \mathbf{J}_{1ih}\right)\mathbf{C}_{1h}\dot{\boldsymbol{\omega}}_{ph} + \sum_{i=4}^{5}\mathbf{J}_{1i}\mathbf{C}_{1i}\dot{\boldsymbol{\omega}}_{pi}$$

$$= \sum_{i=1}^{5}\mathbf{C}_{1i}\mathbf{g}_i + \sum_{i=1}^{5}\left(\mathbf{C}_{1g}\mathbf{b}_h^{\times}\mathbf{C}_{1i} + \mathbf{C}_{1h}\mathbf{b}_i^{\times}\mathbf{C}_{hi}\right)\mathbf{f}_i - \boldsymbol{\omega}_1^{\times}\mathbf{h}_{P_1} - \mathbf{v}_1^{\times}\mathbf{p} - \dot{\mathbf{c}}^{\times}\mathbf{v}_1 - \dot{\mathbf{J}}\boldsymbol{\omega}_1$$
$$- \sum_{i=4}^{5}\left(\dot{\mathbf{J}}_{1h} + \dot{\mathbf{J}}_{1ih}\right)\mathbf{C}_{1h}\boldsymbol{\omega}_{ph} - \sum_{i=4}^{5}\dot{\mathbf{J}}_{1h}\mathbf{C}_{1i}\boldsymbol{\omega}_{pi}$$

Eqn C.57

$$\left(\mathbf{c}_i^{\times}\mathbf{C}_{i1} + m_j\mathbf{b}_j^{\times}\mathbf{C}_{i1}\right)\dot{\mathbf{v}}_1 + \left[\mathbf{J}_{i1}\mathbf{C}_{i1} - m_j\mathbf{b}_j^{\times}\mathbf{C}_{i1}\left(\mathbf{b}_i^{\times} + \mathbf{C}_{1i}\mathbf{b}_j^{\times}\mathbf{C}_{i1}\right) - \mathbf{b}_j^{\times}\mathbf{C}_{ij}\mathbf{c}_j^{\times}\mathbf{C}_{j1}\right]\dot{\boldsymbol{\omega}}_1$$
$$+ \left(\mathbf{J}_i - \mathbf{b}_j^{\times}\mathbf{C}_{ij}\mathbf{c}_j^{\times}\mathbf{C}_{ji}\right)\dot{\boldsymbol{\omega}}_{pi} - \mathbf{b}_j^{\times}\mathbf{C}_{ij}\mathbf{c}_j^{\times}\dot{\boldsymbol{\omega}}_{pj}$$
$$= \mathbf{g}_i + \mathbf{g}_{pi} - \mathbf{C}_{ij}\mathbf{g}_{pj} + \mathbf{b}_j^{\times}\mathbf{C}_{ij}\mathbf{f}_j + \left[\mathbf{h}_i^{\times} + \mathbf{C}_{i1}\left(\mathbf{v}_1 + \boldsymbol{\omega}_1^{\times}\mathbf{b}_i\right)^{\times}\mathbf{C}_{1i}\mathbf{c}_i^{\times}\right]\left(\mathbf{C}_{i1}\boldsymbol{\omega}_1 + \boldsymbol{\omega}_{pi}\right)$$
$$- \mathbf{b}_j^{\times}\mathbf{C}_{i1}\boldsymbol{\omega}_1^{\times}\mathbf{C}_{1j}\mathbf{p}_j - \mathbf{A}_1 - \mathbf{A}_2$$

Eqn C.69

$$\mathbf{c}_i^{\times}\mathbf{C}_{i1}\dot{\mathbf{v}}_1 + \mathbf{J}_{i1}\mathbf{C}_{i1}\dot{\boldsymbol{\omega}}_1 + \mathbf{J}_{ih}\mathbf{C}_{ih}\dot{\boldsymbol{\omega}}_{ph} + \mathbf{J}_i\cdot\dot{\boldsymbol{\omega}}_{pi}$$

$$= \left\{\mathbf{C}_{i1}\left[\mathbf{v}_1^{\times} + \left(\boldsymbol{\omega}_1^{\times}\mathbf{b}_h\right)^{\times} + \left(\boldsymbol{\omega}_1^{\times}\mathbf{C}_{1h}\mathbf{b}_i\right)^{\times}\right]\mathbf{C}_{1i}\mathbf{c}_i^{\times}\right\}\left(\mathbf{C}_{i1}\boldsymbol{\omega}_1 + \mathbf{C}_{im}\boldsymbol{\omega}_{pm} + \mathbf{C}_{in}\boldsymbol{\omega}_{pn}\right) \quad \text{Eqn C.75}$$
$$+ \left\{\mathbf{C}_{1h}\left(\boldsymbol{\omega}_{ph}^{\times}\mathbf{b}_i\right)^{\times}\mathbf{C}_{hi}\mathbf{c}_i^{\times}\right\}\left(\mathbf{C}_{i1}\boldsymbol{\omega}_1 + \mathbf{C}_{im}\boldsymbol{\omega}_{pm} + \mathbf{C}_{in}\boldsymbol{\omega}_{pn}\right)$$
$$+ \mathbf{h}_i^{\times}\left(\mathbf{C}_{i1}\boldsymbol{\omega}_1 + \mathbf{C}_{im}\boldsymbol{\omega}_{pm} + \mathbf{C}_{in}\boldsymbol{\omega}_{pn}\right) + \mathbf{g}_i + \mathbf{g}_{pi} + \mathbf{A}_3$$

They can be put together in a matrix equation of order 18 as shown in Eqn C.76 :

$$\dot{\mathbf{V}} = \mathbf{M}^{-1}\left(\mathbf{F} + \mathbf{F}_{dyn}\right) \qquad \text{Eqn C.76}$$

with

$$\dot{\mathbf{V}} = \begin{bmatrix} \dot{\mathbf{v}}_1 & \dot{\boldsymbol{\omega}}_1 & \dot{\boldsymbol{\omega}}_{p2} & \dot{\boldsymbol{\omega}}_{p3} & \dot{\boldsymbol{\omega}}_{p4} & \dot{\boldsymbol{\omega}}_{p5} \end{bmatrix}^T, \qquad \text{Eqn C.77}$$

$$\mathbf{F} = \begin{bmatrix} \sum_{i=1}^{5} \mathbf{C}_{1i}\mathbf{f}_i \\ \sum_{i=1}^{5} \mathbf{C}_{1i}\mathbf{g}_i + \sum_{i=1}^{5}\left(\mathbf{C}_{1g}\mathbf{b}_h^{\times}\mathbf{C}_{1i} + \mathbf{C}_{1h}\mathbf{b}_i^{\times}\mathbf{C}_{hi}\right)\mathbf{f}_i \\ \mathbf{g}_2 + \mathbf{g}_{p2} - \mathbf{C}_{24}\mathbf{g}_{p4} + \mathbf{b}_4^{\times}\mathbf{C}_{24}\mathbf{f}_4 \\ \mathbf{g}_3 + \mathbf{g}_{p3} - \mathbf{C}_{35}\mathbf{g}_{p5} + \mathbf{b}_5^{\times}\mathbf{C}_{35}\mathbf{f}_5 \\ \mathbf{g}_4 + \mathbf{g}_{p4} \\ \mathbf{g}_5 + \mathbf{g}_{p5} \end{bmatrix} \qquad \text{Eqn C.78}$$

$$\mathbf{F}_{dyn} = \begin{bmatrix} -\boldsymbol{\omega}_1^{\times}\mathbf{p} + \mathbf{BB} \\ -\boldsymbol{\omega}_1^{\times}\mathbf{h}_{P_1} - \mathbf{v}_1^{\times}\mathbf{p} - \dot{\mathbf{c}}^{\times}\mathbf{v}_1 - \dot{\mathbf{J}}\boldsymbol{\omega}_1 - \left(\dot{\mathbf{J}}_{12} + \dot{\mathbf{J}}_{142}\right)\mathbf{C}_{12}\boldsymbol{\omega}_{p2} - \left(\dot{\mathbf{J}}_{13} + \dot{\mathbf{J}}_{153}\right)\mathbf{C}_{13}\boldsymbol{\omega}_{p3} - \dot{\mathbf{J}}_{14}\mathbf{C}_{14}\boldsymbol{\omega}_{p4} - \dot{\mathbf{J}}_{15}\mathbf{C}_{15}\boldsymbol{\omega} \\ \left\{\mathbf{h}_2^{\times} + \mathbf{C}_{21}\left(\mathbf{v}_1 + \boldsymbol{\omega}_1^{\times}\mathbf{b}_2\right)^{\times}\mathbf{C}_{12}\mathbf{c}_4^{\times}\right\}\left(\mathbf{C}_{21}\boldsymbol{\omega}_1 + \boldsymbol{\omega}_{p2}\right) - \mathbf{b}_4^{\times}\mathbf{C}_{21}\boldsymbol{\omega}_1^{\times}\mathbf{C}_{14}\mathbf{p}_4 - \mathbf{A}_{1,2} - \mathbf{A}_{2,2} \\ \left\{\mathbf{h}_3^{\times} + \mathbf{C}_{31}\left(\mathbf{v}_1 + \boldsymbol{\omega}_1^{\times}\mathbf{b}_3\right)^{\times}\mathbf{C}_{13}\mathbf{c}_5^{\times}\right\}\left(\mathbf{C}_{31}\boldsymbol{\omega}_1 + \boldsymbol{\omega}_{p3}\right) - \mathbf{b}_5^{\times}\mathbf{C}_{31}\boldsymbol{\omega}_1^{\times}\mathbf{C}_{15}\mathbf{p}_5 - \mathbf{A}_{1,3} - \mathbf{A}_{2,3} \\ \left\{\mathbf{h}_4^{\times} + \left[\mathbf{C}_{41}\left(\mathbf{v}_1 + \boldsymbol{\omega}_1^{\times}\mathbf{b}_2 + \boldsymbol{\omega}_1^{\times}\mathbf{C}_{12}\mathbf{b}_4\right)^{\times}\mathbf{C}_{14} + \mathbf{C}_{42}\left(\boldsymbol{\omega}_{p2}^{\times}\mathbf{b}_4\right)^{\times}\mathbf{C}_{24}\right]\mathbf{c}_4^{\times}\right\}\left(\mathbf{C}_{41}\boldsymbol{\omega}_1 + \mathbf{C}_{42}\boldsymbol{\omega}_{p2} + \boldsymbol{\omega}_{p4}\right) + \mathbf{A}_3 \\ \left\{\mathbf{h}_5^{\times} + \left[\mathbf{C}_{51}\left(\mathbf{v}_1 + \boldsymbol{\omega}_1^{\times}\mathbf{b}_3 + \boldsymbol{\omega}_1^{\times}\mathbf{C}_{13}\mathbf{b}_5\right)^{\times}\mathbf{C}_{15} + \mathbf{C}_{53}\left(\boldsymbol{\omega}_{p3}^{\times}\mathbf{b}_5\right)^{\times}\mathbf{C}_{25}\right]\mathbf{c}_5^{\times}\right\}\left(\mathbf{C}_{51}\boldsymbol{\omega}_1 + \mathbf{C}_{53}\boldsymbol{\omega}_{p3} + \boldsymbol{\omega}_{p5}\right) + \mathbf{A}_3 \end{bmatrix}$$

Eqn C.79

and

$$M = \begin{bmatrix} m & -c^{x} & -\left\{C_{12}\left(m_2 b_4^{x} + c_2^{x}\right) + C_{14} c_4^{x} C_{42}\right\} & -\left\{C_{13}\left(m_3 b_5^{x} + c_3^{x}\right) + C_{15} c_5^{x} C_{53}\right\} & -C_{14} c_4^{x} & -C_{15} c_5^{x} \\ c^{x} & J & \left(J_{12} + J_{142}\right) & \left(J_{13} + J_{153}\right) & J_{14} C_{14} & J_{15} C_{15} \\ c_2^{x} C_{21} + m_2 b_4^{x} C_{21} & J_{21} C_{21} - m_4 b_4^{x} C_{21} b_2^{x} - b_4^{x} C_{24} c_4^{x} C_{41} & J_2 - b_4^{x} C_{24} c_4^{x} C_{42} & 0 & -b_4^{x} C_{24} c_4^{x} & 0 \\ c_3^{x} C_{31} + m_3 b_5^{x} C_{31} & J_{31} C_{31} - m_5 b_5^{x} C_{31} b_3^{x} - b_5^{x} C_{35} c_5^{x} C_{51} & 0 & J_3 - b_5^{x} C_{35} c_5^{x} C_{53} & 0 & -b_5^{x} C_{35} c_5^{x} \\ c_4^{x} C_{41} & J_{41} C_{41} & J_{42} C_{42} & 0 & J_4 & 0 \\ c_5^{x} C_{51} & J_{51} C_{51} & 0 & J_{53} C_{53} & 0 & J_5 \end{bmatrix}$$

Eqn C.80

APPENDIX D EVALUATION OF MASS AND INERTIA

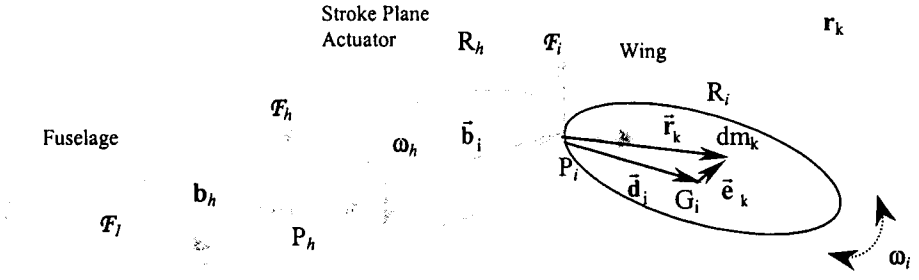

Fig D.1 Schematic Representation of the MAV

Fig D.1 shows three of the five bodies in the multi-body system of the vehicle. P_h and P_i are the joints / origins of the bodies denoted by R_h and R_i. The vector from P_h to P_i is $\vec{b}_i$. G_i is the location of the centre of gravity of R_i and the vector from P_i to G_i is given by $\vec{d}_i$. The vectors from P_i and G_i to a particle with mass dm_k on the body are given by $\vec{r}_k$ and $\vec{e}_k$ respectively.

D.1 MASSES

Let m_i be the total mass of the body R_i and $m_i = \sum_{k=1}^{n} dm_k$.

The total mass of the vehicle, which consists of the fuselage, stroke plane actuators and wings, is given by

$$m = \sum_{i=1}^{5} m_i \qquad \text{Eqn D.1}$$

The components of the element in the first column and first row of the matrix **M** of Eqn C.80, ie **M**(1,1) = **m**, is in itself a 3×3 matrix given by

$$\mathbf{m} = \begin{bmatrix} m & 0 & 0 \\ 0 & m & 0 \\ 0 & 0 & m \end{bmatrix} \qquad \text{Eqn D.2}$$

D.2 FIRST MOMENTS OF INERTIA

The first moment of inertia $\vec{\mathbf{c}}_i$ of a body R_i is defined as follows:

$$\vec{\mathbf{c}}_i = \int_{R_i} \vec{\mathbf{r}}_k \, dm_k \qquad \text{Eqn D.3}$$

or expressed in the frame of R_i

$$\mathbf{c}_i = \sum_{k=1}^{n} (\mathbf{r}_k \, dm_k) = m_i \mathbf{d}_i \qquad \text{Eqn D.4}$$

D.3 TENSOR OF SECOND MOMENTS OF INERTIA

The tensor of the second moment of inertia $\tilde{\mathbf{J}}_i$ of a body R_i is defined as

$$\begin{aligned} \tilde{\mathbf{J}}_i \cdot \vec{\omega}_i &\doteq \int_{R_i} [\vec{\mathbf{r}}_k \times (\vec{\omega}_i \times \vec{\mathbf{r}}_k)] dm_k \\ &= \left(\int_{R_i} [(\vec{\mathbf{r}}_k \cdot \vec{\mathbf{r}}_k)\tilde{\mathbf{I}} - \vec{\mathbf{r}}_k \vec{\mathbf{r}}_k] dm_k \right) \cdot \vec{\omega}_i \end{aligned} \qquad \text{Eqn D.5}$$

The term $\vec{\omega}_i$ in the above definition is replaceable with any angular velocity such as $\vec{\omega}_{pi}$, etc.

Evaluating the terms of Eqn D.5 within the outermost parentheses in $\mathcal{F}_i$ results in

$$\begin{aligned} \left(\int_{R_i} [(\vec{\mathbf{r}}_k \cdot \vec{\mathbf{r}}_k)\tilde{\mathbf{I}} - \vec{\mathbf{r}}_k \vec{\mathbf{r}}_k] dm_k \right) &= \left(\int_{R_i} [(\mathbf{r}_k^T \mathcal{F}_i \cdot \mathcal{F}_i^T \mathbf{r}_k)\mathbf{F}_i^T \cdot \mathbf{I} \cdot \mathcal{F}_i - \mathcal{F}_i^T \mathbf{r}_k \mathbf{r}_k^T \mathcal{F}_i] dm_k \right) \\ &= \mathcal{F}_i^T \cdot \left(\int_{R_i} [(\mathbf{r}_k^T \mathbf{r}_k)\mathbf{I} - \mathbf{r}_k \mathbf{r}_k^T] dm_k \right) \cdot \mathcal{F}_i \\ &= \mathcal{F}_i^T \cdot \mathbf{J}_i \cdot \mathcal{F}_i \end{aligned} \qquad \text{Eqn D.6}$$

with

$$\mathbf{J}_i = \int_{R_i} [(\mathbf{r}_k^T \mathbf{r}_k)\mathbf{I} - \mathbf{r}_k \mathbf{r}_k^T] dm_k \qquad \text{Eqn D.7}$$

where $\mathbf{I}$ is the unit dyad.

Eqn D.7 can be written in matrix formulation as follows:

$$\mathbf{J}_i = \begin{bmatrix} \sum_{k=1}^{n} m_k\left(r_{kx}^2 + r_{ky}^2 + r_{kz}^2\right) & 0 & 0 \\ 0 & \sum_{k=1}^{n} m_k\left(r_{kx}^2 + r_{ky}^2 + r_{kz}^2\right) & 0 \\ 0 & 0 & \sum_{k=1}^{n} m_k\left(r_{kx}^2 + r_{ky}^2 + r_{kz}^2\right) \end{bmatrix} - \begin{bmatrix} \sum_{k=1}^{n} m_k r_{kx}^2 & \sum_{i=1}^{n} m_k r_{kx} r_{ky} & \sum_{i=1}^{n} m_k r_{kx} r_{kz} \\ \sum_{i=1}^{n} m_k r_{kx} r_{ky} & \sum_{k=1}^{n} m_k r_{ky}^2 & \sum_{i=1}^{n} m_k r_{ky} r_{kz} \\ \sum_{i=1}^{n} m_k r_{kx} r_{kz} & \sum_{i=1}^{n} m_k r_{ky} r_{kz} & \sum_{k=1}^{n} m_k r_{kz}^2 \end{bmatrix}$$

$$= \begin{bmatrix} \sum_{k=1}^{n} m_k\left(r_{ky}^2 + r_{kz}^2\right) & -\sum_{i=1}^{n} m_k r_{kx} r_{ky} & -\sum_{i=1}^{n} m_k r_{kx} r_{kz} \\ -\sum_{i=1}^{n} m_k r_{kx} r_{ky} & \sum_{k=1}^{n} m_k\left(r_{kx}^2 + r_{kz}^2\right) & -\sum_{i=1}^{n} m_k r_{ky} r_{kz} \\ -\sum_{i=1}^{n} m_k r_{kx} r_{kz} & -\sum_{i=1}^{n} m_k r_{ky} r_{kz} & \sum_{k=1}^{n} m_k\left(r_{kx}^2 + r_{ky}^2\right) \end{bmatrix}$$

or simply as

$$\mathbf{J}_i = \begin{bmatrix} I_{xx} & -I_{xy} & -I_{xz} \\ -I_{xy} & I_{yy} & -I_{yz} \\ -I_{xz} & -I_{xz} & I_{zz} \end{bmatrix}_{R_i} \qquad \text{Eqn D.8}$$

with I_{xx}, I_{yy} and I_{zz} being the second moments of inertia, and I_{xy}, I_{xz} and I_{yz} being the products of inertia referred to at the origin of the frame of R_i.

Note also that $\vec{\mathbf{r}}_k = \vec{\mathbf{d}}_i + \vec{\mathbf{e}}_k$. Hence,

$$\begin{aligned} \tilde{\mathbf{J}}_i \cdot \vec{\omega}_i &= \int_{R_i} \left(\vec{\mathbf{d}}_i + \vec{\mathbf{e}}_k\right) \times \left[\vec{\omega}_i \times \left(\vec{\mathbf{d}}_i + \vec{\mathbf{e}}_k\right)\right] dm_k \\ &= \int_{R_i} \vec{\mathbf{d}}_i \times \left(\vec{\omega}_i \times \vec{\mathbf{d}}_i\right) dm_k + \int_{R_i} \vec{\mathbf{e}}_k \times \left(\vec{\omega}_i \times \vec{\mathbf{e}}_k\right) dm_k \qquad \text{Eqn D.9} \\ &= \int_{R_i} \vec{\mathbf{d}}_i \times \left(\vec{\omega}_i \times \vec{\mathbf{d}}_i\right) dm_k + \tilde{\mathbf{J}}_{Gi} \cdot \vec{\omega}_i \end{aligned}$$

since it can be shown that $\int_{R_i} \vec{\mathbf{e}}_k \times \left(\vec{\omega}_i \times \vec{\mathbf{d}}_i\right) dm_k = \vec{\mathbf{0}}$ and $\int_{R_i} \vec{\mathbf{d}}_i \times \left(\vec{\omega}_i \times \vec{\mathbf{e}}_k\right) dm_k = \vec{\mathbf{0}}$ because $\int_{R_i} \vec{\mathbf{e}}_k dm_k = \vec{\mathbf{0}}$.

$\tilde{\mathbf{J}}_{Gi}$ is the inertia tensor referred to at the origin G_i of the body R_i. Rearranging Eqn D.9 leads to

$$\tilde{\mathbf{J}}_{Gi} \cdot \vec{\omega}_i = \tilde{\mathbf{J}}_i \cdot \vec{\omega}_i - \int_{R_i} \vec{\mathbf{d}}_i \times \left(\vec{\omega}_i \times \vec{\mathbf{d}}_i\right) dm_k \qquad \text{Eqn D.10}$$

where

$$\mathbf{J}_{G_i} = \int_{R_i} \left[\left(\mathbf{e}_k^T \mathbf{e}_k\right)\mathbf{I} - \mathbf{e}_k \mathbf{e}_k^T\right] dm_k$$

or

$$\mathbf{J}_{G_i} = \begin{bmatrix} I_{XX} & -I_{XY} & -I_{XZ} \\ -I_{XY} & I_{YY} & -I_{YZ} \\ -I_{XZ} & -I_{YZ} & I_{ZZ} \end{bmatrix}_{R_i} \qquad \text{Eqn D.11}$$

and I_{XX}, I_{YY} and I_{ZZ} being the second moments of inertia, and I_{XY}, I_{XZ} and I_{YZ} being the products of inertia referred to at the centre of gravity G_i of the frame of R_i.

D.4 TENSOR $\tilde{\mathbf{J}}_{1i}$

The term $\tilde{\mathbf{J}}_{1i} \cdot \vec{\omega}_{pi}$ was defined in Eqn C.15 as

$$\begin{aligned} \tilde{\mathbf{J}}_{1i} \cdot \vec{\omega}_{pi} &= \int_{R_i} \left[\left(\vec{\mathbf{b}}_h + \vec{\mathbf{b}}_i + \vec{\mathbf{r}}_k\right) \times \left(\vec{\omega}_{pi} \times \vec{\mathbf{r}}_k\right)\right] dm_k \\ &= \int_{R_i} \left[\left(\vec{\mathbf{b}}_h + \vec{\mathbf{b}}_i\right) \times \left(\vec{\omega}_{pi} \times \vec{\mathbf{r}}_k\right)\right] dm_i + \int_{R_i} \left[\vec{\mathbf{r}}_k \times \left(\vec{\omega}_{pi} \times \vec{\mathbf{r}}_k\right)\right] dm_k \end{aligned} \qquad \text{Eqn C.15}$$

The first term on the RHS of the above equation can be written as follows

$$\begin{aligned} \int_{R_i} \left[\left(\vec{\mathbf{b}}_h + \vec{\mathbf{b}}_i\right) \times \left(\tilde{}_{pi} \times \vec{\mathbf{r}}_k\right)\right] dm_k &= \int_{R_i} \left[\left(\vec{\mathbf{b}}_h + \vec{\mathbf{b}}_i\right) \times \tilde{}_{pi} \times \left(\vec{\mathbf{d}}_i + \vec{\mathbf{e}}_k\right)\right] dm_k \\ &= \int_{R_i} \left[\left(\vec{\mathbf{b}}_h + \vec{\mathbf{b}}_i\right) \times \left(\tilde{}_{pi} \times \vec{\mathbf{d}}_i\right)\right] dm_k \end{aligned} \qquad \text{Eqn D.12}$$

Evaluating in the frame of R_1, Eqn D.12 can be written as

$$\int_{R_i}\left[\left(\vec{b}_h+\vec{b}_i\right)\times\left(\vec{\omega}_{pi}\times\vec{r}_k\right)\right]dm_k \equiv \left(\int_{R_i}\left[\left(\vec{b}_h+\vec{b}_i\right)\cdot\vec{d}_i\tilde{I}-\vec{d}_i\left(\vec{b}_h+\vec{b}_i\right)\right]dm_k\right)\cdot\vec{\omega}_{pi}$$

Eqn D.13

$$=\mathcal{F}_1^T\cdot\left(\int_{R_i}\left[\left(\mathbf{b}_h^T+\left\{\mathbf{C}_{1h}\mathbf{b}_i\right\}^T\right)\mathbf{C}_{1i}\mathbf{d}_i\mathbf{I}-\mathbf{C}_{1i}\mathbf{d}_i\left(\mathbf{b}_h^T+\left\{\mathbf{C}_{1h}\mathbf{b}_i\right\}^T\right)\right]dm_i\right)\cdot\mathcal{F}_1\cdot\vec{\omega}_{pi}$$

Substituting Eqn D.6 and D.13 into Eqn C.15 and writing in the frame of R_1 leads to

$$\tilde{\mathbf{J}}_{1i}\cdot\vec{\omega}_{pi}=\mathcal{F}_1^T\cdot\left(\int_{R_i}\left[\left(\mathbf{b}_h^T+\left\{\mathbf{C}_{1h}\mathbf{b}_i\right\}^T\right)\mathbf{C}_{1i}\mathbf{d}_i\mathbf{I}-\mathbf{C}_{1i}\mathbf{d}_i\left(\mathbf{b}_h^T+\left\{\mathbf{C}_{1h}\mathbf{b}_i\right\}^T\right)\right]dm_k+\mathbf{C}_{1i}\int_{R_i}\left[\left(\mathbf{r}_k^T\mathbf{r}_k\right)\mathbf{I}-\mathbf{r}_k\mathbf{r}_k^T\right]dm_k\mathbf{C}_{i1}\right)\cdot\mathcal{F}_1\cdot\vec{\omega}_{pi}$$

$$=\mathcal{F}_1^T\cdot\left(\int_{R_i}\left[\left(\mathbf{b}_h^T+\left\{\mathbf{C}_{1h}\mathbf{b}_i\right\}^T\right)\mathbf{C}_{1i}\mathbf{d}_i\mathbf{I}-\mathbf{C}_{1i}\mathbf{d}_i\left(\mathbf{b}_h^T+\left\{\mathbf{C}_{1h}\mathbf{b}_i\right\}^T\right)\right]dm_k+\mathbf{C}_{1i}\mathbf{J}_i\mathbf{C}_{i1}\right)\cdot\mathcal{F}_1\cdot\vec{\omega}_{pi}$$

Eqn D.14

or

$$\mathbf{J}_{1i}=\left(\int_{R_i}\left[\left(\mathbf{b}_h^T+\left\{\mathbf{C}_{1h}\mathbf{b}_i\right\}^T\right)\mathbf{C}_{1i}\mathbf{d}_i\mathbf{I}-\mathbf{C}_{1i}\mathbf{d}_i\left(\mathbf{b}_h^T+\left\{\mathbf{C}_{1h}\mathbf{b}_i\right\}^T\right)\right]dm_k+\mathbf{C}_{1i}\mathbf{J}_i\mathbf{C}_{i1}\right)$$ Eqn D.15

D.5 TENSOR $\tilde{J}_{il}$

Similarly, it was implied in Eqn C.16 that

$$\tilde{\mathbf{J}}_{il}\cdot\vec{\omega}_1=\int_{R_i}\left[\vec{r}_k\times\vec{\omega}_1\times\left(\vec{b}_h+\vec{b}_i+\vec{r}_k\right)\right]dm_k$$

$$\equiv\int_{R_i}\left[\vec{d}_i\times\vec{\omega}_1\times\left(\vec{b}_h+\vec{b}_i\right)\right]dm_k+\int_{R_i}\left[\vec{r}_k\times\left(\vec{\omega}_1\times\vec{r}_k\right)\right]dm_k$$

Eqn D.16

Evaluating in the frame of R_i, the first term on the RHS of Eqn D.16 can be written as

$$\int_{R_i}\left[\vec{d}_i\times\vec{\omega}_1\times\left(\vec{b}_h+\vec{b}_i\right)\right]dm_k=\left(\int_{R_i}\left[\vec{d}_i\cdot\left(\vec{b}_h+\vec{b}_i\right)\tilde{I}-\left(\vec{b}_h+\vec{b}_i\right)\vec{d}_i\right]dm_k\right)\cdot\vec{\omega}_1$$

$$=\mathcal{F}_i^T\cdot\left(\int_{R_i}\left[\mathbf{d}_i^T\left(\mathbf{C}_{il}\mathbf{b}_h+\mathbf{C}_{ih}\mathbf{b}_i\right)\mathbf{I}-\left(\mathbf{C}_{il}\mathbf{b}_h+\mathbf{C}_{ih}\mathbf{b}_i\right)\mathbf{d}_i^T\right]dm_k\right)\cdot\mathcal{F}_i\cdot\vec{\omega}_1$$

Eqn D.17

Substituting Eqn D.6 and D.17 back into Eqn D.16 and writing in the frame of R_i results in

$$\tilde{\mathbf{J}}_{il}\cdot\vec{\omega}_l = \mathcal{F}_i^T\cdot\left(\int_{R_i}\left[\mathbf{d}_i^T\left(\mathbf{C}_{il}\mathbf{b}_h+\mathbf{C}_{ih}\mathbf{b}_i\right)\mathbf{I}-\left(\mathbf{C}_{il}\mathbf{b}_h+\mathbf{C}_{ih}\mathbf{b}_i\right)\mathbf{d}_i^T\right]dm_k+\int_{R_i}\left[\left(\mathbf{r}_k^T\mathbf{r}_k\right)\mathbf{I}-\mathbf{r}_k\mathbf{r}_k^T\right]dm_i\right)\cdot\mathcal{F}_i\cdot\vec{\omega}_l$$
$$= \mathcal{F}_i^T\cdot\left(\int_{R_i}\left[\mathbf{d}_i^T\left(\mathbf{C}_{il}\mathbf{b}_h+\mathbf{C}_{ih}\mathbf{b}_i\right)\mathbf{I}-\left(\mathbf{C}_{il}\mathbf{b}_h+\mathbf{C}_{ih}\mathbf{b}_i\right)\mathbf{d}_i^T\right]dm_k+\mathbf{J}_i\right)\cdot\mathcal{F}_i\cdot\vec{\omega}_l$$

Eqn D.18

or

$$\mathbf{J}_{il} = \int_{R_i}\left[\mathbf{d}_i^T\left(\mathbf{C}_{il}\mathbf{b}_h+\mathbf{C}_{ih}\mathbf{b}_i\right)\mathbf{I}-\left(\mathbf{C}_{il}\mathbf{b}_h+\mathbf{C}_{ih}\mathbf{b}_i\right)\mathbf{d}_i^T\right]dm_k+\mathbf{J}_i \qquad \text{Eqn D.19}$$

D.6 TENSOR $\tilde{\mathbf{J}}_{ih}$

For R_i (i = 4,5), the term $\tilde{\mathbf{J}}_{ih}$ was also implied in Eqn C.7

$$\tilde{\mathbf{J}}_{ih}\cdot\vec{\omega}_{ph} = \int_{R_i}\left[\vec{r}_k\times\vec{\omega}_{ph}\times\left(\vec{b}_i+\vec{r}_k\right)\right]dm_k$$
$$\equiv \int_{R_i}\left[\vec{d}_i\times\left(\vec{\omega}_{ph}\times\vec{b}_i\right)\right]dm_k+\int_{R_i}\left[\vec{r}_k\times\left(\vec{\omega}_{ph}\times\vec{r}_k\right)\right]dm_k \qquad \text{Eqn D.20}$$

Evaluating in the frame of R_i, the first term on the RHS of Eqn D.20 can written as follows:

$$\int_{R_i}\left[\vec{d}_i\times\left(\vec{\omega}_{ph}\times\vec{b}_i\right)\right]dm_k = \left(\int_{R_i}\left[\vec{d}_i\cdot\vec{b}_i\tilde{I}-\vec{b}_i\vec{d}_i\right]dm_k\right)\cdot\vec{\omega}_{ph}$$
$$= \mathcal{F}_i^T\cdot\left(\int_{R_i}\left[\mathbf{d}_i^T\mathbf{C}_{ih}\mathbf{b}_i\mathbf{I}-\mathbf{C}_{ih}\mathbf{b}_i\mathbf{d}_i^T\right]dm_k\right)\cdot\mathcal{F}_i\cdot\vec{\omega}_{ph} \qquad \text{Eqn D.21}$$

hence

$$\mathbf{J}_{ih} = m_i\left(\mathbf{d}_i^T\mathbf{C}_{ih}\mathbf{b}_i\mathbf{I}-\mathbf{C}_{ih}\mathbf{b}_i\mathbf{d}_i^T\right)+\mathbf{J}_i \qquad \text{Eqn D.22}$$

D.7 TENSOR $\tilde{\mathbf{J}}_{1ih}$

For R_i (i = 4,5), the term $\tilde{\mathbf{J}}_{1ih}$ was defined in Eqn C.17

$$\begin{aligned}\tilde{\mathbf{J}}_{1ih}\cdot\vec{\omega}_{ph} &= \int_{R_i}\left(\vec{b}_h+\vec{b}_i\right)\times\vec{\omega}_{ph}\times\left(\vec{r}_k+\vec{b}_i\right)dm_k+\tilde{\mathbf{J}}_{ih}\cdot\vec{\omega}_{ph}\\ &\equiv\int_{R_i}\left(\vec{b}_h+\vec{b}_i\right)\times\vec{\omega}_{ph}\times\left(\vec{d}_i+\vec{b}_i\right)dm_k+\tilde{\mathbf{J}}_{ih}\cdot\vec{\omega}_{ph}\end{aligned}$$

Eqn C.17

The first term on the right hand side of the above equation can be expressed in the frame of R_h as

$$\begin{aligned}\int_{R_i}\left[\left(\vec{b}_h+\vec{b}_i\right)\times\vec{\omega}_{ph}\times\left(\vec{d}_i+\vec{b}_i\right)\right]dm_k &= \int_{R_i}\left[\left(\vec{b}_h+\vec{b}_i\right)\cdot\left(\vec{d}_i+\vec{b}_i\right)\tilde{\mathbf{I}}-\left(\vec{d}_i+\vec{b}_i\right)\left(\vec{b}_h+\vec{b}_i\right)\right]dm_k\cdot\vec{\omega}_{ph}\\ &= \mathcal{F}_{fi}^{T}m_i\left[\left(\mathbf{b}_h^{T}\mathbf{C}_{1h}+\mathbf{b}_i^{T}\right)\left(\mathbf{b}_i+\mathbf{C}_{hi}\mathbf{d}_i\right)\mathbf{I}-\left(\mathbf{b}_i+\mathbf{C}_{hi}\mathbf{d}_i\right)\left(\mathbf{b}_h^{T}\mathbf{C}_{1h}+\mathbf{b}_i^{T}\right)\right]\mathcal{F}_{fi}\cdot\vec{\omega}_{ph}\end{aligned}$$

Eqn D.23

Note that $\tilde{\mathbf{J}}_{ih}$ is expressed in the frame of R_i in Eqn D.22. Substituting Eqn D.23 into Eqn C.17 and then transforming into R_i results in

$$\mathbf{J}_{1ih}=\left\{m_i\mathbf{C}_{1h}\left[\left(\mathbf{b}_h^{T}\mathbf{C}_{1h}+\mathbf{b}_i^{T}\right)\left(\mathbf{b}_i+\mathbf{C}_{hi}\mathbf{d}_i\right)\mathbf{I}-\left(\mathbf{b}_i+\mathbf{C}_{hi}\mathbf{d}_i\right)\left(\mathbf{b}_h^{T}\mathbf{C}_{1h}+\mathbf{b}_i^{T}\right)\right]\mathbf{C}_{h1}+\mathbf{C}_{1i}\mathbf{J}_{ih}\mathbf{C}_{i1}\right\}$$

Eqn D.24

D.8 TENSOR $\tilde{\mathbf{J}}$

The tensor $\tilde{\mathbf{J}}$ defined in Eqn C.16 can be evaluated in $\mathcal{F}_i$ as follows

$$\begin{aligned}\tilde{\mathbf{J}}\cdot\vec{\omega}_1 &= \tilde{\mathbf{J}}_1\cdot\vec{\omega}_1+\sum_{i=2}^{5}\tilde{\mathbf{J}}_{i1}\cdot\vec{\omega}_i+\sum_{i=2}^{5}\int\left[\left(\vec{b}_h+\vec{b}_i\right)\times\left\{\vec{\omega}_1\times\left(\vec{b}_h+\vec{b}_i+\vec{r}_k\right)\right\}\right]dm_k\\ &=\tilde{\mathbf{J}}_1\cdot\vec{\omega}_1+\sum_{i=2}^{5}\tilde{\mathbf{J}}_{i1}\cdot\vec{\omega}_1+\sum_{i=2}^{5}\int\left[\left(\vec{b}_h+\vec{b}_i\right)\times\left\{\vec{\omega}_1\times\vec{r}_k\right\}\right]dm_k+\sum_{i=2}^{5}\int\left[\left(\vec{b}_h+\vec{b}_i\right)\times\left\{\vec{\omega}_1\times\left(\vec{b}_h+\vec{b}_i\right)\right\}\right]dm_k\end{aligned}$$

Eqn D.25

Replacing $\vec{\omega}_{pi}$ with $\vec{\omega}_1$ in Eqn C.15 and rearranging it yields the following

$$\sum_{i=2}^{5}\int\left[\left(\vec{b}_h+\vec{b}_i\right)\times\left\{\vec{\omega}_1\times\vec{r}_k\right\}\right]dm_k=\tilde{\mathbf{J}}_{1i}\cdot\vec{\omega}_1-\tilde{\mathbf{J}}_i\cdot\vec{\omega}_1 \qquad \text{Eqn D.26}$$

Substituting into Eqn D.25 results in

$$\begin{aligned}\tilde{\mathbf{J}}\cdot\vec{\omega}_1 &= \tilde{\mathbf{J}}_1\cdot\vec{\omega}_1+\sum_{i=2}^{5}\tilde{\mathbf{J}}_{i1}\cdot\vec{\omega}_1+\sum_{i=2}^{5}\left(\tilde{\mathbf{J}}_{1i}\cdot\vec{\omega}_1-\tilde{\mathbf{J}}_i\cdot\vec{\omega}_1\right)+\sum_{i=2}^{5}\int_{R_i}\left[\left(\vec{b}_h+\vec{b}_i\right)\times\left\{\vec{\omega}_1\times\left(\vec{b}_h+\vec{b}_i\right)\right\}\right]dm_k\\ &=\left[\tilde{\mathbf{J}}_1+\sum_{i=2}^{5}\tilde{\mathbf{J}}_{1i}+\sum_{i=2}^{5}\left(\tilde{\mathbf{J}}_{i1}-\tilde{\mathbf{J}}_i\right)\right]\cdot\vec{\omega}_1+\sum_{i=2}^{5}\int_{R_i}\left[\left(\vec{b}_h+\vec{b}_i\right)\times\left\{\vec{\omega}_1\times\left(\vec{b}_h+\vec{b}_i\right)\right\}\right]dm_k\end{aligned}$$

Eqn D.27

This can be written in the frame of R_1 after omitting the angular velocity term $\vec{\omega}_1$ as

$$\begin{aligned}\mathbf{J} &= \left[\mathbf{J}_1+\sum_{i=2}^{5}\mathbf{J}_{1i}+\sum_{i=2}^{5}\mathbf{C}_{1i}\left(\mathbf{J}_{i1}-\mathbf{J}_i\right)\mathbf{C}_{i1}\right]\\ &+\sum_{i=2}^{5}m_i\left[\left(\mathbf{b}_h+\mathbf{C}_{1h}\mathbf{b}_i\right)^T\left(\mathbf{b}_h+\mathbf{C}_{1h}\mathbf{b}_i\right)\mathbf{I}-\left(\mathbf{b}\mathbf{b}_h+\mathbf{C}_{1h}\mathbf{b}_i\right)\left(\mathbf{b}_h+\mathbf{C}_{1h}\mathbf{b}_i\right)^T\right]\end{aligned} \qquad \text{Eqn D.28}$$

APPENDIX E TIME DERIVATIVES OF INERTIA

E.1 TIME DERIVATIVE OF J_{1i}

Taking the time derivative of Eqn B.15 results in

$$\begin{aligned}\dot{\tilde{\mathbf{J}}}_{1i}\cdot\vec{\omega}_{pi}+\tilde{\mathbf{J}}_{1i}\cdot\dot{\vec{\omega}}_{pi} &= \int_{R_i}\left[\left(\dot{\vec{b}}_h+\dot{\vec{b}}_i\right)\times\left(\vec{\omega}_{pi}\times\vec{r}_k\right)\right]dm_k+\dot{\tilde{J}}_i\cdot\vec{\omega}_{pi}\\ &+\int_{R_i}\left[\left(\vec{b}_h+\vec{b}_i\right)\times\left(\dot{\vec{\omega}}_{pi}\times\vec{r}_k\right)\right]dm_k+\tilde{J}_i\cdot\dot{\vec{\omega}}_{pi}\\ &+\int_{R_i}\left[\left(\vec{b}_h+\vec{b}_i\right)\times\left(\vec{\omega}_{pi}\times\dot{\vec{r}}_k\right)\right]dm_k\end{aligned}$$

Eqn E.1

Removing the terms related to $\dot{\vec{\omega}}_{pi}$ results in

$$\dot{\tilde{\mathbf{J}}}_{1i}\cdot\vec{\omega}_{pi}=\int_{R_i}\left[\left(\dot{\vec{b}}_h+\dot{\vec{b}}_i\right)\times\left(\vec{\omega}_{pi}\times\vec{r}_k\right)\right]dm_k+\dot{\tilde{J}}_i\cdot\vec{\omega}_{pi}+\int_{R_i}\left[\left(\vec{b}_h+\vec{b}_i\right)\times\left(\vec{\omega}_{pi}\times\dot{\vec{r}}_k\right)\right]dm_k$$

Eqn E.2

Noting that $\dot{\vec{b}}_h=\vec{0}$, $\dot{\vec{b}}_i=\vec{\omega}_{ph}\times\vec{b}_i$ and $\dot{\vec{r}}_k=\left(\vec{\omega}_{ph}+\vec{\omega}_{pi}\right)\times\vec{r}_k$, Eqn E.2 can be written as

$$\begin{aligned}\dot{\tilde{\mathbf{J}}}_{1i}\cdot\vec{\omega}_{pi} &= \int_{R_i}\left[\left(\vec{\omega}_{ph}\times\vec{b}_i\right)\times\left(\vec{\omega}_{pi}\times\vec{r}_k\right)\right]dm_k+\int_{R_i}\left(\vec{b}_h+\vec{b}_i\right)\times\left\{\vec{\omega}_{pi}\times\left[\left(\vec{\omega}_{ph}+\vec{\omega}_{pi}\right)\times\vec{r}_k\right]\right\}dm_k\\ &+\dot{\tilde{J}}_i\cdot\vec{\omega}_{pi}\\ &=\int_{R_i}\left[\vec{\omega}_{ph}\cdot\left(\vec{b}_i\times\vec{r}_k\right)\tilde{I}-\vec{r}_k\left(\vec{\omega}_{ph}\times\vec{b}_i\right)\right]dm_k\cdot\vec{\omega}_{pi}+\dot{\tilde{J}}_i\cdot\vec{\omega}_{pi}\\ &+\int_{R_i}\left(\vec{b}_h+\vec{b}_i\right)\times\left\{\left[\left(\vec{\omega}_{ph}+\vec{\omega}_{pi}\right)\vec{r}_k-\vec{r}_k\left(\vec{\omega}_{ph}+\vec{\omega}_{pi}\right)\right]\right\}dm_k\cdot\vec{\omega}_{pi}\end{aligned}$$

Eqn E.3

Differentiating Eqn D.5 with respect to time, and removing terms related to $\dot{\vec{\omega}}_{pi}$ allows the second term on the RHS of Eqn E.2 to be found

$$\begin{aligned}
\dot{\tilde{\mathbf{J}}}_i \cdot \vec{\omega}_{pi} &= \int_{R_i} \left[\dot{\vec{r}}_k \times \left(\vec{\omega}_{pi} \times \vec{r}_k\right)\right] dm_k + \int_{R_i} \left[\vec{r}_k \times \left(\vec{\omega}_{pi} \times \dot{\vec{r}}_k\right)\right] dm_k \\
&= \int_{R_i} \left[\left(\vec{\omega}_{pi} + \vec{\omega}_{ph}\right) \times \vec{r}_k\right] \times \left(\vec{\omega}_{pi} \times \vec{r}_k\right) dm_k + \int_{R_i} \vec{r}_k \times \left\{ \vec{\omega}_{pi} \times \left[\left(\vec{\omega}_{pi} + \vec{\omega}_{ph}\right) \times \vec{r}_k\right] \right\} dm_k \\
&= \int_{R_i} \left[\left(\vec{\omega}_{pi} + \vec{\omega}_{ph}\right) \times \left(\vec{d}_i + \vec{e}_k\right)\right] \times \left[\vec{\omega}_{pi} \times \left(\vec{d}_i + \vec{e}_k\right)\right] dm_k \\
&\quad + \int_{R_i} \left(\vec{d}_i + \vec{e}_k\right) \times \left\{ \vec{\omega}_{pi} \times \left[\left(\vec{\omega}_{pi} + \vec{\omega}_{ph}\right) \times \left(\vec{d}_i + \vec{e}_k\right)\right] \right\} dm_k \\
&= \int_{R_i} \left[\left(\vec{\omega}_{pi} + \vec{\omega}_{ph}\right) \times \vec{d}_i\right] \times \left(\vec{\omega}_{pi} \times \vec{d}_i\right) dm_k + \int_{R_i} \left[\left(\vec{\omega}_{pi} + \vec{\omega}_{ph}\right) \times \vec{e}_k\right] \times \left(\vec{\omega}_{pi} \times \vec{e}_k\right) dm_k \\
&\quad + \int_{R_i} \vec{d}_i \times \left\{ \vec{\omega}_{pi} \times \left[\left(\vec{\omega}_{pi} + \vec{\omega}_{ph}\right) \times \vec{d}_i\right] \right\} dm_k + \int_{R_i} \vec{e}_k \times \left\{ \vec{\omega}_{pi} \times \left[\left(\vec{\omega}_{pi} + \vec{\omega}_{ph}\right) \times \vec{e}_k\right] \right\} dm_k
\end{aligned}$$

Eqn E.4

This can be rewritten as

$$\begin{aligned}
\dot{\tilde{\mathbf{J}}}_i \cdot \vec{\omega}_{pi} &= \int_{R_i} \left\{ \left[\vec{\omega}_{i*} \cdot \left(\vec{d}_i \times \vec{d}_i\right)\tilde{\mathbf{I}}\right] - \vec{d}_i \left[\vec{\omega}_{i*} \times \vec{d}_i\right] \right\} dm_k \cdot \vec{\omega}_{pi} \\
&\quad + \int_{R_i} \left\{ \left[\vec{\omega}_{i*} \cdot \left(\vec{e}_k \times \vec{e}_k\right)\tilde{\mathbf{I}}\right] - \vec{e}_k \left[\vec{\omega}_{i*} \times \vec{e}_k\right] \right\} dm_k \cdot \vec{\omega}_{pi} \\
&\quad + \int_{R_i} \vec{d}_i \times \left[\vec{\omega}_{i*} \vec{d}_i - \vec{d}_i \vec{\omega}_{i*}\right] dm_k \cdot \vec{\omega}_{pi} \\
&\quad + \int_{R_i} \vec{e}_k \times \left[\vec{\omega}_{i*} \vec{e}_k - \vec{e}_k \vec{\omega}_{i*}\right] dm_k \cdot \vec{\omega}_{pi}
\end{aligned}$$

Eqn E.5

$$\begin{aligned}
&= -\left\{ \int_{R_i} \vec{d}_i \left[\vec{\omega}_{i*} \times \vec{d}_i\right] dm_k + \int_{R_i} \vec{e}_k \left[\vec{\omega}_{i*} \times \vec{e}_k\right] dm_k \right\} \cdot \vec{\omega}_{pi} \\
&\quad + \left\{ \int_{R_i} \vec{d}_i \times \left[\vec{\omega}_{i*} \vec{d}_i - \vec{d}_i \vec{\omega}_{i*}\right] dm_k + \int_{R_i} \vec{e}_k \times \left[\vec{\omega}_{i*} \vec{e}_k - \vec{e}_k \vec{\omega}_{i*}\right] dm_k \right\} \cdot \vec{\omega}_{pi}
\end{aligned}$$

with $\vec{\omega}_{i*} = \left(\vec{\omega}_{pi} + \vec{\omega}_{ph}\right)$.

Written in the frame of R_i, Eqn E.5 becomes

$$\dot{\mathbf{J}}_i \cdot \boldsymbol{\omega}_{pi} = \left\{ -m_i \mathbf{d}_i \left[\boldsymbol{\omega}_{i*}^{\times} \mathbf{d}_i\right]^T - \int_{R_i} \mathbf{e}_k \left[\boldsymbol{\omega}_{i*}^{\times} \mathbf{e}_k\right]^T dm_k + m_i \mathbf{d}_i^{\times} \left[\boldsymbol{\omega}_{i*} \mathbf{d}_i^T - \mathbf{d}_i \boldsymbol{\omega}_{i*}^T\right] + \int_{R_i} \mathbf{e}_i^{\times} \left[\boldsymbol{\omega}_{i*} \mathbf{e}_i^T - \mathbf{e}_k \boldsymbol{\omega}_{i*}^T\right] dm_k \right\} \cdot \boldsymbol{\omega}_{pi}$$

Eqn E.6

with $\boldsymbol{\omega}_{i*} = \left(\boldsymbol{\omega}_{pi} + \mathbf{C}_{ih} \boldsymbol{\omega}_{ph}\right)$. The first and third terms on the RHS of Eqn E.6 can be easily evaluated since $\mathbf{d}_i$ (the centre of gravity location of R_i from the origin of $\mathcal{F}_i$) is probably known.

The second term in parenthesis on the RHS of Eqn E.6 can be represented as follows:

$$\sum_{k=1}^{n} dm_k \mathbf{e}_k \left(\boldsymbol{\omega}_{i*}^{\times} \mathbf{e}_k\right)^T = \sum_{k=1}^{n} dm_k \begin{bmatrix} e_{kx} \\ e_{ky} \\ ek \end{bmatrix} \begin{bmatrix} -\omega_{i*,z} e_{ky} + \omega_{i*,y} e_{kz} & \omega_{i*,z} e_{kx} - \omega_{i*,x} e_{kz} & -\omega_{i*,y} e_{kx} + \omega_{i*,x} e_{ky} \end{bmatrix}$$

$$= \begin{bmatrix} \sum_{k=1}^{n} dm_k e_{kx} \left(\omega_{i*,y} e_{kz} - \omega_{i*,z} e_{ky}\right) & \sum_{k=1}^{n} dm_k e_{kx} \left(\omega_{i*,z} e_{kx} - \omega_{i*,x} e_{kz}\right) & \sum_{k=1}^{n} dm_k e_{kx} \left(\omega_{i*,x} e_{ky} - \omega_{i*,y} e_{kx}\right) \\ \sum_{k=1}^{n} dm_k e_{ky} \left(\omega_{i*,y} e_{kz} - \omega_{i*,z} e_{ky}\right) & \sum_{k=1}^{n} dm_k e_{ky} \left(\omega_{i*,z} e_{kx} - \omega_{i*,x} e_{kz}\right) & \sum_{k=1}^{n} dm_k e_{ky} \left(\omega_{i*,x} e_{ky} - \omega_{i*,y} e_{kx}\right) \\ \sum_{k=1}^{n} dm_k e_{kz} \left(\omega_{i*,y} e_{kz} - \omega_{i*,z} e_{ky}\right) & \sum_{k=1}^{n} dm_k e_{kz} \left(\omega_{i*,z} e_{kx} - \omega_{i*,x} e_{kz}\right) & \sum_{k=1}^{n} dm_k e_{kz} \left(\omega_{i*,x} e_{ky} - \omega_{i*,y} e_{kx}\right) \end{bmatrix}$$

Eqn E.7

The following equation can be written

$$\begin{aligned} I_{ZZ} + I_{YY} &= \sum_{k=1}^{n} dm_k \left(e_{kx}^2 + e_{ky}^2\right) + \sum_{k=1}^{n} dm_k \left(e_{kx}^2 + e_{kz}^2\right) \\ &= \sum_{k=1}^{n} dm_k \left(e_{ky}^2 + e_{kz}^2\right) + 2 \sum_{k=1}^{n} dm_k e_{kx}^2 \\ &= I_{XX} + 2 \sum_{k=1}^{n} dm_k e_{kx}^2 \end{aligned}$$

Eqn E.8

which can be rearranged as

$$\sum_{k=1}^{n} dm_k e_{kx}^2 = \frac{1}{2} \left(I_{ZZ} + I_{YY} - I_{XX}\right)$$

Eqn E.9

Similarly, for the y- and z-components of the vector **e**

$$\sum_{k=1}^{n} dm_k e_{ky}^2 = \frac{1}{2}(I_{XX} + I_{ZZ} - I_{YY}) \qquad \text{Eqn E.10}$$

$$\sum_{k=1}^{n} dm_k e_{kz}^2 = \frac{1}{2}(I_{XX} + I_{YY} - I_{ZZ}) \qquad \text{Eqn E.11}$$

Substituting Eqns E.9 to E.11 into Eqn E.7 results in

$$\sum_{k=1}^{n} dm_k \mathbf{e}_k \left(\omega_{i^*}^{\times} \mathbf{e}_k\right)^T = \begin{bmatrix} \omega_{i^*,y} I_{XZ} - \omega_{i^*,z} I_{XY} & \frac{1}{2}\omega_{i^*,z}[I_{YY} + I_{ZZ} - I_{XX}] - \omega_{i^*,x} I_{XZ} & \omega_{i^*,x} I_{XY} - \frac{1}{2}\omega_{i^*,y}[I_{YY} + I_{ZZ} - I_{XX}] \\ \omega_{i^*,y} I_{YZ} - \frac{1}{2}\omega_{i^*,z}[I_{XX} + I_{ZZ} - I_{YY}] & \omega_{i^*,z} I_{XY} - \omega_{i^*,x} I_{YZ} & \frac{1}{2}\omega_{i^*,x}[I_{XX} + I_{ZZ} - I_{YY}] - \omega_{i^*,y} I_{XY} \\ \frac{1}{2}\omega_{i^*,y}[I_{XX} + I_{YY} - I_{ZZ}] - \omega_{i^*,z} I_{YZ} & \omega_{i^*,z} I_{XZ} - \frac{1}{2}\omega_{i^*,x}[I_{XX} + I_{YY} - I_{ZZ}] & \omega_{i^*,x} I_{YZ} - \omega_{i^*,y} I_{XZ} \end{bmatrix}$$

Eqn E.12

The last term of Eqn E.6 is

$$\sum_{k=1}^{n} dm_k \mathbf{e}_k^{\times} \left(\omega_{i^*} \mathbf{e}_k^T - \mathbf{e}_k \omega_{i^*}^T\right) = \sum_{k=1}^{n} dm_k \mathbf{e}_k^{\times} \omega_p \mathbf{e}_k^T$$

$$= \begin{bmatrix} \sum_{k=1}^{n} dm_k \left(e_{ky}\omega_{i^*,z} e_{kx} - e_{kz}\omega_{i^*,y} e_{kx}\right) & \sum_{k=1}^{n} dm_k \left(e_{ky}\omega_{i^*,z} e_{ky} - e_{kz}\omega_{i^*,y} e_{ky}\right) & \sum_{k=1}^{n} dm_k \left(e_{ky}\omega_{i^*,z} e_{kz} - e_{kz}\omega_{i^*,y} e \right. \\ \sum_{k=1}^{n} dm_k \left(e_{kz}\omega_{i^*,x} e_{kx} - e_{kx}\omega_{i^*,z} e_{kx}\right) & \sum_{k=1}^{n} dm_k \left(e_{kz}\omega_{i^*,x} e_{ky} - e_{kx}\omega_{i^*,z} e_{ky}\right) & \sum_{k=1}^{n} dm_k \left(e_{kz}\omega_{i^*,x} e_{kz} - e_{kx}\omega_{i^*,z} e \right. \\ \sum_{k=1}^{n} dm_k \left(e_{kx}\omega_{i^*,y} e_{kx} - e_{ky}\omega_{i^*,x} e_{kx}\right) & \sum_{k=1}^{n} dm_k \left(e_{kx}\omega_{i^*,y} e_{ky} - e_{ky}\omega_{i^*,x} e_{ky}\right) & \sum_{k=1}^{n} dm_k \left(ek_x\omega_{i^*,y} e_{kz} - e_{ky}\omega_{i^*,x} \right. \end{bmatrix}$$

$$= \begin{bmatrix} \omega_{i^*,z} I_{XY} - \omega_{i^*,y} I_{XZ} & \frac{1}{2}\omega_{i^*,z}[I_{XX} + I_{ZZ} - I_{YY}] - \omega_{i^*,y} I_{YZ} & \omega_{i^*,z} I_{YZ} - \frac{1}{2}\omega_{i^*,y}[I_{XX} + I_{YY} - I_{Z} \\ \omega_{i^*,x} I_{XZ} - \frac{1}{2}\omega_{i^*,z}[I_{YY} + I_{ZZ} - I_{XX}] & \omega_{i^*,x} I_{YZ} - \omega_{i^*,z} I_{XY} & \frac{1}{2}\omega_{i^*,x}[I_{XX} + I_{YY} - I_{ZZ}] - \omega_{i^*,z} I_{X} \\ \frac{1}{2}\omega_{i^*,y}[I_{YY} + I_{ZZ} - I_{XX}] - \omega_{i^*,x} I_{XY} & \omega_{i^*,y} I_{XY} - \frac{1}{2}\omega_{i^*,x}[I_{XX} + I_{ZZ} - I_{YY}] & \omega_{i^*,y} I_{XZ} - \omega_{i^*,x} I_{YZ} \end{bmatrix}$$

Eqn E.13

Combining Eqn E.12 and E.13 as follows

$$\mathbf{D} = \sum_{k=1}^{n} dm_k \mathbf{e}_k^{\times}\left(\boldsymbol{\omega}_{i^*} \mathbf{e}_k^{T} - \mathbf{e}_k \boldsymbol{\omega}_{i^*}^{T}\right) - \sum_{k=1}^{n} dm_k \mathbf{e}_k \left(\boldsymbol{\omega}_{i^*}^{\times} \mathbf{e}_k\right)^{T}$$

$$= \begin{bmatrix} 2\left(\omega_{i^*,z} I_{XY} - \omega_{i^*,y} I_{XZ}\right) & \omega_{i^*,z}\left[I_{XX} - I_{YY}\right] + \omega_{i^*,x} I_{XZ} - \omega_{i^*,y} I_{YZ} & \omega_{i^*,z} I_{YZ} - \omega_{i^*,x} I_{XY} - \omega_{i^*,y}\left[I_{XX}\right. \\ \omega_{i^*,x} I_{XZ} - \omega_{i^*,y} I_{YZ} - \omega_{i^*,z}\left[I_{YY} - I_{XX}\right] & 2\left(\omega_{i^*,x} I_{YZ} - \omega_{i^*,z} I_{XY}\right) & \omega_{i^*,x}\left[I_{YY} - I_{ZZ}\right] + \omega_{i^*,y} I_{XY} - \omega \\ \omega_{i^*,y}\left[I_{ZZ} - I_{XX}\right] + \omega_{i^*,z} I_{YZ} - \omega_{i^*,x} I_{XY} & \omega_{i^*,y} I_{XY} - \omega_{i^*,z} I_{XZ} - \omega_{i^*,x}\left[I_{ZZ} - I_{YY}\right] & 2\left(\omega_{i^*,y} I_{XZ} - \omega_{i^*,x} I_{YZ}\right) \end{bmatrix}$$

$$= \boldsymbol{\omega}_{i^*}^{\times} \mathbf{J}_{G_i} - \mathbf{J}_{G_i} \boldsymbol{\omega}_{i^*}^{\times}$$

Eqn E.14

Hence Eqn E.6 can be rewritten as follows

$$\dot{\mathbf{J}}_i \cdot \boldsymbol{\omega}_{pi} = \left\{ -m_i \mathbf{d}_i \left[\boldsymbol{\omega}_{i^*}^{\times} \mathbf{d}_i\right]^{T} + m_i \mathbf{d}_i^{\times}\left[\boldsymbol{\omega}_{i^*} \mathbf{d}_i^{T} - \mathbf{d}_i \boldsymbol{\omega}_{i^*}^{T}\right] + \mathbf{D} \right\} \cdot \boldsymbol{\omega}_{pi} \qquad \text{Eqn E.15}$$

Substituting Eqn E.15 and omitting $\bar{\boldsymbol{\omega}}_{pi}$ from the equation, Eqn E.3 can be written in the frame of R_1 as

$$\begin{aligned} \dot{\mathbf{J}}_{1i} = m_i & \left\{ \left(\mathbf{C}_{1h} \boldsymbol{\omega}_{ph}\right)^{T} \left[\left(\mathbf{C}_{1h} \mathbf{b}_i\right)^{\times} \left(\mathbf{C}_{1i} \mathbf{d}_i\right)\right] \mathbf{I} - \left(\mathbf{C}_{1i} \mathbf{d}_i\right)\left(\mathbf{C}_{1h} \boldsymbol{\omega}_{ph}^{\times} \mathbf{b}_i\right)^{T} \right\} \\ & + m_i \left(\mathbf{C}_{1h} \mathbf{b}_i + \mathbf{b}_h\right)^{\times} \left[\left(\mathbf{C}_{1h} \boldsymbol{\omega}_{ph} + \mathbf{C}_{1i} \boldsymbol{\omega}_{pi}\right)\left(\mathbf{C}_{1i} \mathbf{d}_i\right)^{T} - \left(\mathbf{C}_{1i} \mathbf{d}_i\right)\left(\mathbf{C}_{1h} \boldsymbol{\omega}_{ph} + \mathbf{C}_{1i} \boldsymbol{\omega}_{pi}\right)^{T}\right] \\ & + \mathbf{C}_{1i} \left\{ m_i \mathbf{d}_i^{\times} \left[\boldsymbol{\omega}_{i^*}^{\times} \mathbf{d}_i^{T} - \mathbf{d}_i \boldsymbol{\omega}_{i^*}^{T}\right] - m_i \mathbf{d}_i \left[\boldsymbol{\omega}_{i^*}^{\times} \mathbf{d}_i\right]^{T} + \mathbf{D} \right\} \mathbf{C}_{i1} \end{aligned}$$

Eqn E.16

E.2 TIME DERIVATIVE OF J_{il}

Differentiating Eqn D.16 in the frame of R_l and eliminating the terms associated with $\dot{\vec{\omega}}_l$ results in

$$\begin{aligned}\dot{\tilde{\mathbf{J}}}_{il}\cdot\vec{\omega}_l &= \int_{R_i}\left[\dot{\vec{d}}_i\times\vec{\omega}_l\times\left(\vec{b}_h+\vec{b}_i\right)\right]dm_k+\int_{R_i}\left[\vec{d}_i\times\vec{\omega}_l\times\left(\dot{\vec{b}}_h+\dot{\vec{b}}_i\right)\right]dm_k+\dot{\tilde{\mathbf{J}}}_i\cdot\vec{\omega}_l\\ &= \int_{R_i}\left[\left(\vec{\omega}_{i*}\times\vec{d}_i\right)\times\vec{\omega}_l\times\left(\vec{b}_h+\vec{b}_i\right)\right]dm_k+\int_{R_i}\left[\vec{r}_k\times\vec{\omega}_l\times\left(\vec{\omega}_{ph}\times\vec{b}_i\right)\right]dm_k+\dot{\tilde{\mathbf{J}}}_i\cdot\vec{\omega}_l\\ &= \int_{R_i}\left\{\vec{\omega}_{i*}\cdot\left[\vec{d}_i\times\left(\vec{b}_h+\vec{b}_i\right)\right]\tilde{\mathbf{I}}-\left(\vec{b}_h+\vec{b}_i\right)\left[\vec{\omega}_{i*}\times\vec{d}_i\right]\right\}dm_k\cdot\vec{\omega}_l\\ &\quad+\int_{R_i}\vec{d}_i\times\left[\vec{\omega}_{ph}\cdot\vec{b}_i-\vec{b}_i\vec{\omega}_{ph}\right]dm_k\cdot\vec{\omega}_l+\dot{\tilde{\mathbf{J}}}_i\cdot\vec{\omega}_l\end{aligned}$$

Eqn E.17

The last term on the left hand side of Eqn E.17 is given in the frame of R_i by Eqn E.15, replacing $\vec{\omega}_{pi}$ with $\vec{\omega}_l$.

Eliminating $\vec{\omega}_l$ and expressing in the frame of R_i, Eqn E.17 becomes

$$\begin{aligned}\dot{\mathbf{J}}_{il} &= m_i\left\{\boldsymbol{\omega}_{i*}^T\left[\mathbf{d}_i^\times\left(\mathbf{C}_{il}\mathbf{b}_h+\mathbf{C}_{ih}\mathbf{b}_i\right)\right]\mathbf{I}-\left(\mathbf{C}_{il}\mathbf{b}_h+\mathbf{C}_{ih}\mathbf{b}_i+\mathbf{d}_i\right)\left[\boldsymbol{\omega}_{i*}^\times\mathbf{d}_i\right]^T\right\}\\ &\quad+m_i\mathbf{d}_i^\times\mathbf{C}_{ih}\left(\boldsymbol{\omega}_{ph}\mathbf{b}_i^T-\mathbf{b}_i\boldsymbol{\omega}_{ph}^T\right)+m_i\mathbf{d}_i^\times\left[\boldsymbol{\omega}_{i*}\mathbf{d}_i^T-\mathbf{d}_i\boldsymbol{\omega}_{i*}^T\right]+\mathbf{D}\end{aligned}$$

Eqn E.18

where $\mathbf{E}$ is given in Eqn E.14.

E.3 TIME DERIVATIVE OF J_{ih}

Differentiating Eqn D.20 in the frame of R_1 and eliminating the terms associated with $\dot{\vec{\omega}}_1$, results in the following expression

$$\begin{aligned}\dot{\tilde{\mathbf{J}}}_{ih}\cdot\vec{\omega}_1 &= \int_{R_i}\left[\dot{\vec{\mathbf{d}}}_i\times\left(\vec{\omega}_1\times\vec{\mathbf{b}}_i\right)\right]dm_k+\int_{R_i}\left[\vec{\mathbf{d}}_i\times\left(\vec{\omega}_1\times\dot{\vec{\mathbf{b}}}_i\right)\right]dm_k+\dot{\tilde{\mathbf{J}}}_i\cdot\vec{\omega}_1\\ &= \int_{R_i}\left[\left(\vec{\omega}_{i*}\times\vec{\mathbf{d}}_i\right)\times\left(\vec{\omega}_1\times\vec{\mathbf{b}}_i\right)\right]dm_k+\int_{R_i}\left[\vec{\mathbf{d}}_i\times\vec{\omega}_1\times\left(\vec{\omega}_{ph}\times\vec{\mathbf{b}}_i\right)\right]dm_k+\dot{\tilde{\mathbf{J}}}_i\cdot\vec{\omega}_1\\ &= \int_{R_i}\left[\vec{\omega}_{i*}\cdot\left(\vec{\mathbf{d}}_i\times\vec{\mathbf{b}}_i\right)\tilde{\mathbf{I}}-\vec{\mathbf{b}}_i\left(\vec{\omega}_{i*}\times\vec{\mathbf{d}}_i\right)\right]dm_k\cdot\vec{\omega}_1\\ &\quad+\int_{R_i}\vec{\mathbf{d}}_i\times\left[\vec{\omega}_{ph}\cdot\vec{\mathbf{b}}_i-\vec{\mathbf{b}}_i\vec{\omega}_{ph}\right]dm_k\cdot\vec{\omega}_1+\dot{\tilde{\mathbf{J}}}_i\cdot\vec{\omega}_1\end{aligned}\qquad\text{Eqn E.19}$$

As in Eqn E.17, the last term on the left hand side of Eqn E.19 is given by Eqn E.15 in the frame of R_i, if $\vec{\omega}_{pi}$ is replaced with $\vec{\omega}_1$.

Eliminating $\vec{\omega}_1$ and expressing in the frame of R_i, Eqn E.19 becomes

$$\begin{aligned}\dot{\mathbf{J}}_{ih} &= m_i\left\{\omega_{i*}^T\left(\mathbf{d}_i^\times\mathbf{C}_{ih}\mathbf{b}_i\right)\mathbf{I}-\left(\mathbf{C}_{ih}\mathbf{b}_i+\mathbf{d}_i\right)\left[\omega_{i*}^\times\mathbf{d}_i\right]^T\right\}\\ &\quad+m_i\mathbf{d}_i^\times\mathbf{C}_{ih}\left(\omega_{ph}\mathbf{b}_i^T-\mathbf{b}_i\omega_{ph}^T\right)+m_i\mathbf{d}_i^\times\left[\omega_{i*}\mathbf{d}_i^T-\mathbf{d}_i\omega_{i*}^T\right]+\mathbf{D}\end{aligned}\qquad\text{Eqn E.20}$$

where **D** is given in Eqn E.14

E.4 TIME DERIVATIVE OF J_{1ih}

Making use of Eqn D.26, with $\vec{\omega}_1$ being replaced by $\vec{\omega}_{ph}$, Eqn B.17 can also be expanded and rewritten as

$$\begin{aligned}\tilde{\mathbf{J}}_{1ih}\cdot\vec{\omega}_{ph} &= \int_{R_i}\left(\vec{b}_h+\vec{b}_i\right)\times\left(\vec{\omega}_{ph}\times\vec{b}_i\right)dm_k+\int_{R_i}\left(\vec{b}_h+\vec{b}_i\right)\times\left(\vec{\omega}_{ph}\times\vec{r}_k\right)dm_k+\tilde{\mathbf{J}}_{ih}\cdot\vec{\omega}_{ph}\\ &= \int_{R_i}\left(\vec{b}_h+\vec{b}_i\right)\times\left(\vec{\omega}_{ph}\times\vec{b}_i\right)dm_k+\left(\tilde{\mathbf{J}}_{1i}-\tilde{\mathbf{J}}_i\right)\cdot\vec{\omega}_{ph}+\tilde{\mathbf{J}}_{ih}\cdot\vec{\omega}_{ph}\end{aligned}$$

Eqn E.21

Differentiating the above equation in the frame of R_1 and eliminating the terms associated with $\dot{\vec{\omega}}_{ph}$, results in the following expression

$$\begin{aligned}\dot{\tilde{\mathbf{J}}}_{1ih}\cdot\vec{\omega}_{ph} &= \int_{R_i}\left(\dot{\vec{b}}_h+\dot{\vec{b}}_i\right)\times\left(\vec{\omega}_{ph}\times\vec{b}_i\right)dm_k+\int_{R_i}\left(\vec{b}_h+\vec{b}_i\right)\times\left(\vec{\omega}_{ph}\times\dot{\vec{b}}_i\right)dm_k\\ &\quad+\left(\dot{\tilde{\mathbf{J}}}_{1i}-\dot{\tilde{\mathbf{J}}}_i\right)\cdot\vec{\omega}_{ph}+\dot{\tilde{\mathbf{J}}}_{ih}\cdot\vec{\omega}_{ph}\\ &= \int_{R_i}\left(\vec{\omega}_{ph}\times\vec{b}_i\right)\times\left(\vec{\omega}_{ph}\times\vec{b}_i\right)dm_k+\int_{R_i}\left(\vec{b}_h+\vec{b}_i\right)\times\left[\vec{\omega}_{ph}\times\left(\vec{\omega}_{ph}\times\vec{b}_i\right)\right]dm_k\\ &\quad+\left(\dot{\tilde{\mathbf{J}}}_{1i}-\dot{\tilde{\mathbf{J}}}_i\right)\cdot\vec{\omega}_{ph}+\dot{\tilde{\mathbf{J}}}_{ih}\cdot\vec{\omega}_{ph}\end{aligned}$$

Eqn E.22

or

$$\begin{aligned}\dot{\tilde{\mathbf{J}}}_{1ih}\cdot\vec{\omega}_{ph} &= \int_{R_i}\left[\vec{\omega}_{ph}\left(\vec{b}_i\times\vec{b}_i\right)\tilde{\mathbf{I}}-\vec{b}_i\times\left(\vec{\omega}_{ph}\times\vec{b}_i\right)\right]dm_k\cdot\vec{\omega}_{ph}\\ &\quad+\int_{R_i}\left(\vec{b}_h+\vec{b}_i\right)\times\left[\vec{\omega}_{ph}\vec{b}_i-\vec{b}_i\vec{\omega}_{ph}\right]dm_k\cdot\vec{\omega}_{ph}+\left(\dot{\tilde{\mathbf{J}}}_{1i}-\dot{\tilde{\mathbf{J}}}_i\right)\cdot\vec{\omega}_{ph}+\dot{\tilde{\mathbf{J}}}_{ih}\cdot\vec{\omega}_{ph}\\ &= \left(\dot{\tilde{\mathbf{J}}}_{1i}-\dot{\tilde{\mathbf{J}}}_i\right)\cdot\vec{\omega}_{ph}+\dot{\tilde{\mathbf{J}}}_{ih}\cdot\vec{\omega}_{ph}-\int_{R_i}\left[\vec{b}_i\times\left(\vec{\omega}_{ph}\times\vec{b}_i\right)\right]dm_k\cdot\vec{\omega}_{ph}\\ &\quad+\int_{R_i}\left(\vec{b}_h+\vec{b}_i\right)\times\left[\vec{\omega}_{ph}\vec{b}_i-\vec{b}_i\vec{\omega}_{ph}\right]dm_k\cdot\vec{\omega}_{ph}\end{aligned}$$

Eqn E.23

Written in the frame of R_1, Eqn E.23 becomes

$$\dot{\mathbf{J}}_{1ih} = \dot{\mathbf{J}}_{1i} - \mathbf{C}_{1i}\dot{\mathbf{J}}_i\mathbf{C}_{i1} + \mathbf{C}_{1i}\dot{\mathbf{J}}_{ih}\mathbf{C}_{i1} - m_i\mathbf{C}_{1h}\mathbf{b}_i^{\times}\boldsymbol{\omega}_{ph}^{\times}\mathbf{b}_i + (\mathbf{b}_h + \mathbf{C}_{1h}\mathbf{b}_i)^{\times}(\boldsymbol{\omega}_{ph}\mathbf{b}_i^T - \mathbf{b}_i\boldsymbol{\omega}_{ph}^T)$$

Eqn E.24

noting that $\dot{\mathbf{J}}_{ih}$ is given in the frame of R_i in Eqn E.20 and $\dot{\mathbf{J}}_{1i} - \mathbf{C}_{1i}\dot{\mathbf{J}}_i\mathbf{C}_{i1}$ can be extracted from Eqn E.16 as

$$\dot{\mathbf{J}}_{1i} - \mathbf{C}_{1i}\dot{\mathbf{J}}_i\mathbf{C}_{i1} = m_i\left\{(\mathbf{C}_{1h}\boldsymbol{\omega}_{ph})^T\left[(\mathbf{C}_{1h}\mathbf{b}_i)^{\times}(\mathbf{C}_{1i}\mathbf{d}_i)\right]\mathbf{I} - (\mathbf{C}_{1i}\mathbf{d}_i)(\mathbf{C}_{1h}\boldsymbol{\omega}_{ph}^{\times}\mathbf{b}_i)^T\right\}$$
$$+ m_i(\mathbf{C}_{1h}\mathbf{b}_i + \mathbf{b}_h)^{\times}\left[(\mathbf{C}_{1h}\boldsymbol{\omega}_{ph} + \mathbf{C}_{1i}\boldsymbol{\omega}_{pi})(\mathbf{C}_{1i}\mathbf{d}_i)^T - (\mathbf{C}_{1i}\mathbf{d}_i)(\mathbf{C}_{1h}\boldsymbol{\omega}_{ph} + \mathbf{C}_{1i}\boldsymbol{\omega}_{pi})^T\right]$$

Eqn E.25

E.5 TIME DERIVATIVE OF J

Differentiating Eqn D.27 in the frame of R_1 and eliminating the terms associated with $\dot{\vec{\omega}}_1$, results in the following expression

$$\dot{\tilde{\mathbf{J}}}\cdot\vec{\omega}_1 = \left[\sum_{i=2}^{5}\dot{\tilde{\mathbf{J}}}_{1i} + \sum_{i=2}^{5}\left(\dot{\tilde{\mathbf{J}}}_{il} - \dot{\tilde{\mathbf{J}}}_i\right)\right]\cdot\vec{\omega}_1 + \sum_{i=2}^{5}\int_{R_i}\left[\dot{\vec{b}}_i\times\left\{\vec{\omega}_1\times\left(\vec{b}_h+\vec{b}_i\right)\right\}\right]dm_k + \sum_{i=2}^{5}\int_{R_i}\left[\left(\vec{b}_h+\vec{b}_i\right)\times\left(\vec{\omega}_1\times\dot{\vec{b}}_i\right)\right]dm_k$$

$$= \left[\sum_{i=2}^{5}\dot{\tilde{\mathbf{J}}}_{1i} + \sum_{i=2}^{5}\left(\dot{\tilde{\mathbf{J}}}_{il} - \dot{\tilde{\mathbf{J}}}_i\right)\right]\cdot\vec{\omega}_1 + \sum_{i=2}^{5}\int_{R_i}\left[\left(\vec{\omega}_{ph}\times\vec{b}_i\right)\times\left\{\vec{\omega}_1\times\left(\vec{b}_h+\vec{b}_i\right)\right\}\right]dm_k$$
$$+\sum_{i=2}^{5}\int_{R_i}\left(\vec{b}_h+\vec{b}_i\right)\times\left[\vec{\omega}_1\times\left(\vec{\omega}_{ph}\times\vec{b}_i\right)\right]dm_k$$

$$= \left[\sum_{i=2}^{5}\dot{\tilde{\mathbf{J}}}_{1i} + \sum_{i=2}^{5}\left(\dot{\tilde{\mathbf{J}}}_{il} - \dot{\tilde{\mathbf{J}}}_i\right)\right]\cdot\vec{\omega}_1 + \sum_{i=2}^{5}\int_{R_i}\left\{\vec{\omega}_{ph}\left[\vec{b}_i\times\left(\vec{b}_h+\vec{b}_i\right)\right]\mathbf{I} - \left(\vec{b}_h+\vec{b}_i\right)\left(\vec{\omega}_{ph}\times\vec{b}_i\right)\right\}dm_k\cdot\vec{\omega}_1$$
$$+\sum_{i=2}^{5}\int_{R_i}\left(\vec{b}_h+\vec{b}_i\right)\times\left[\vec{\omega}_{ph}\vec{b}_i - \left(\vec{b}_i\vec{\omega}_{ph}\right)\right]dm_k\cdot\vec{\omega}_1$$

Eqn E.26

Written in the frame of R_1, this becomes

$$\dot{\mathbf{J}} = \left[\sum_{i=2}^{5}\mathbf{C}_{1i}\dot{\mathbf{J}}_{il}\mathbf{C}_{il} + \sum_{i=2}^{5}\left(\dot{\mathbf{J}}_{1i} - \mathbf{C}_{1i}\dot{\mathbf{J}}_i\mathbf{C}_{il}\right)\right] + \sum_{i=2}^{5}m_i\mathbf{C}_{1h}\left(\mathbf{C}_{hl}\mathbf{b}_h+\mathbf{b}_i\right)^{\times}\left[\vec{\omega}_{ph}\mathbf{b}_i^T - \mathbf{b}_i\vec{\omega}_{ph}^T\right]\mathbf{C}_{hl}$$
$$+\sum_{i=2}^{5}m_i\mathbf{C}_{1h}\left\{\vec{\omega}_{ph}^T\left[\mathbf{b}_i^{\times}\left(\mathbf{C}_{hl}\mathbf{b}_h+\mathbf{b}_i\right)\right]\mathbf{I} - \left(\mathbf{C}_{hl}\mathbf{b}_h+\mathbf{b}_i\right)\left(\vec{\omega}_{ph}^{\times}\mathbf{b}_i\right)^T\right\}\mathbf{C}_{hl}$$

Eqn E.27

noting that $\dot{\mathbf{J}}_{il}$ is given in the frame of R_i in Eqn E.18 and $\dot{\mathbf{J}}_{1i} - \mathbf{C}_{1i}\dot{\mathbf{J}}_i\mathbf{C}_{il}$ is given in Eqn E.25 in the frame of R_1.

E.6 TIME DERIVATIVES OF J_{il} IN THE FRAME OF R_2 OR R_3

The equations of motion derived in Appendix B require $\overset{\circ}{\tilde{J}}_{il}$ for i = 2 and 3 only.

Starting from Eqn D.16, differentiating in the frame of R_i (for i = 2 and 3) and omitting terms related to $\overset{\circ}{\vec{\omega}}_l$, the following expression results

$$\begin{aligned}\overset{\circ}{\tilde{J}}_{il}\cdot\vec{\omega}_l &= \int_{R_i}\left[\overset{\circ}{\vec{d}}_i\times\vec{\omega}_l\times\left(\vec{d}_i+\vec{b}_i\right)\right]dm_k+\int_{R_i}\left[\vec{d}_i\times\vec{\omega}_l\times\left(\overset{\circ}{\vec{d}}_i+\overset{\circ}{\vec{b}}_i\right)\right]dm_k\\ &= -\int_{R_i}\left[\vec{d}_i\times\vec{\omega}_l\times\left(\vec{\omega}_{pm}\times\vec{b}_i\right)\right]dm_k \qquad \text{Eqn E.28}\\ &= -\int_{R_i}\left[\vec{d}_i\times\left(\vec{\omega}_{pm}\vec{b}_i-\vec{b}_i\vec{\omega}_{pm}\right)\right]dm_k\cdot\vec{\omega}_l\end{aligned}$$

This can be expressed in the frame of R_i as

$$\overset{\circ}{J}_{il}=-m_i d_i^{\times}\left(\omega_{pm}b_i^{T}C_{lm}-C_{ml}b_i\omega_{pm}^{T}\right) \qquad \text{Eqn E.29}$$

where the relation between the indices h, i and m are given in Tables B.1 and B.2 in Appendix B.

E.7 TIME DERIVATIVES OF J_{i1} IN THE FRAME OF R_4 OR R_5

The equations of motion derived in Appendix B require $\overset{+}{\tilde{J}}_{i1}$ for i = 4 and 5 only.

Starting from Eqn D.16, differentiating in the frame of R_i (for i = 4 and 5) and omitting terms related to $\overset{+}{\vec{\omega}}_1$, the following expression results

$$\begin{aligned}
\overset{+}{\tilde{J}}_{i1}\cdot\vec{\omega}_1 &= \int_{R_i}\left[\overset{+}{\vec{d}}_i\times\vec{\omega}_1\times\left(\vec{d}_i+\vec{b}_i\right)\right]dm_k+\int_{R_i}\left[\vec{d}_i\times\vec{\omega}_1\times\left(\overset{+}{\vec{d}}_i+\overset{+}{\vec{b}}_h+\overset{+}{\vec{b}}_i\right)\right]dm_k\\
&=-\int_{R_i}\left[\vec{d}_i\times\vec{\omega}_1\times\left(\vec{\omega}_{pm}+\vec{\omega}_{pn}\right)\times\vec{b}_h\right]dm_k-\int_{R_i}\left[\vec{d}_i\times\vec{\omega}_1\times\left(\vec{\omega}_{pn}\times\vec{b}_i\right)\right]dm_k\\
&=-\int_{R_i}\vec{d}_i\times\left[\vec{\omega}_1\times\left(\vec{\omega}_{pm}\times\vec{b}_h\right)\right]dm_k-\int_{R_i}\vec{d}_i\times\left\{\vec{\omega}_1\times\left[\vec{\omega}_{pn}\times\left(\vec{b}_h+\vec{b}_i\right)\right]\right\}dm_k\\
&=-\left\{\int_{R_i}\vec{d}_i\times\left(\vec{\omega}_{pm}\vec{b}_h-\vec{b}_h\vec{\omega}_{pm}\right)dm_k+\int_{R_i}\vec{d}_i\times\left[\vec{\omega}_{pn}\left(\vec{b}_h+\vec{b}_i\right)-\left(\vec{b}_h+\vec{b}_i\right)\vec{\omega}_{pn}\right]dm_k\right\}\cdot\vec{\omega}_1
\end{aligned}$$

Eqn E.30

since

$$\overset{o}{\vec{b}}_i=\dot{\vec{b}}_h=\overset{+}{\vec{d}}_i=\vec{0}$$

$$\overset{+}{\vec{b}}_h=\dot{\vec{b}}_h-\left(\vec{\omega}_{pm}+\vec{\omega}_{pn}\right)\times\vec{b}_h=-\left(\vec{\omega}_{pm}+\vec{\omega}_{pn}\right)\times\vec{b}_h$$

and

$$\overset{+}{\vec{b}}_i=\overset{o}{\vec{b}}_i-\vec{\omega}_{pn}\times\vec{b}_i=-\vec{\omega}_{pn}\times\vec{b}_i$$

Eqn E.30 can be expressed in the frame of R_i (i = 4,5) as

$$\begin{aligned}
\overset{+}{\mathbf{J}}_{i1}=&-m_i\mathbf{d}_i^{\times}\left[\left(\mathbf{C}_{im}\boldsymbol{\omega}_{pm}\right)\left(\mathbf{C}_{i1}\mathbf{b}_h\right)^T-\left(\mathbf{C}_{i1}\mathbf{b}_h\right)\left(\mathbf{C}_{im}\boldsymbol{\omega}_{pm}\right)^T\right]\\
&-m_i\mathbf{d}_i^{\times}\left[\boldsymbol{\omega}_{pn}\left(\mathbf{C}_{i1}\mathbf{b}_h+\mathbf{C}_{ih}\mathbf{b}_i\right)^T-\left(\mathbf{C}_{i1}\mathbf{b}_h+\mathbf{C}_{ih}\mathbf{b}_i\right)\boldsymbol{\omega}_{pn}^T\right]
\end{aligned}$$

Eqn E.31

where the relation between the indices h, i, m and n are again given in Tables C.1 and C.2 in Appendix C.

E.8 TIME DERIVATIVES OF J_{ih} IN THE FRAME OF R_4 OR R_5

The equations of motion derived in Appendix B require $\overset{+}{\tilde{\mathbf{J}}}_{ih}$ for i = 4 and 5 only.

Starting from Eqn D.20, differentiating in the frame of R_i (for i = 4 and 5) and omitting terms related to $\overset{+}{\vec{\omega}}_{ph}$, the following expression results

$$\begin{aligned}\overset{+}{\tilde{\mathbf{J}}}_{ih}\cdot\vec{\omega}_{ph} &= \int_{R_i}\left[\overset{+}{\vec{d}}_i\times\left(\vec{\omega}_{ph}\times\vec{b}_i\right)\right]dm_k + \int_{R_i}\left[\vec{d}_i\times\left(\vec{\omega}_{ph}\times\overset{+}{\vec{b}}_i\right)\right]dm_k \\ &= -\int_{R_i}\vec{d}_i\times\left[\vec{\omega}_{ph}\times\left(\vec{\omega}_{pn}\times\vec{b}_i\right)\right]dm_k \\ &= -\int_{R_i}\vec{d}_i\times\left[\left(\vec{\omega}_{pn}\vec{b}_i-\vec{b}_i\vec{\omega}_{pn}\right)\right]dm_k\cdot\vec{\omega}_{ph}\end{aligned} \qquad \text{Eqn E.32}$$

This can be expressed in the frame of R_i as

$$\overset{+}{\mathbf{J}}_{ih} = -m_i\mathbf{d}_i^{\times}\left[\omega_{pn}\left(\mathbf{C}_{ih}\mathbf{b}_i\right)^T-\left(\mathbf{C}_{ih}\mathbf{b}_i\right)\omega_{pn}^T\right] \qquad \text{Eqn E.33}$$

where the relation between the indices h, i and n are given in Tables C.1 and C.2 in Appendix C.

APPENDIX F AERODYNAMIC DATA OF FLAPPING WING

Fourier Coefficients of Aerodynamic Coefficients

$n = 1.86$ Hz; $\hat{\delta} = \pm 50°$; $\overline{\delta} = 0°$; $\hat{\chi} = \pm 45°$; $\overline{\chi} = 0°$; $\varphi = 30°$

		i = 0	i = 1	i = 2	i = 3	i = 4	i = 5
C_x	a_i	0.3180	-0.2227	-0.6091	-0.0110	0.0117	-0.0013
	b_i		0.0511	0.1888	-0.0255	-0.0014	0.0008
C_y	a_i	-0.1786	-0.1347	0.4383	-0.0397	-0.0375	-0.0055
	b_i		0.0408	0.5785	0.0058	0.0021	0.0183
C_z	a_i	-0.2207	-0.4382	-0.1960	0.2563	-0.0044	-0.0077
	b_i		-1.05	0.1889	0.1030	-0.02796	0.0056

$n = 1.86$ Hz; $\hat{\delta} = \pm 50°$; $\overline{\delta} = 0°$; $\hat{\chi} = \pm 45°$; $\overline{\chi} = 0°$; $\varphi = 45°$

		i = 0	i = 1	i = 2	i = 3	i = 4	i = 5
C_x	a_i	0.2963	-0.2435	-0.5346	-0.0141	0.0086	-0.0008
	b_i		0.0410	0.3170	-0.0209	0.0005	0.0010
C_y	a_i	0.0085	-0.1129	0.4438	0.0153	-0.0509	-0.0053
	b_i		-0.0025	0.4773	0.0562	-0.0254	0.0244
C_z	a_i	-0.1910	-0.4282	-0.2103	0.2727	-0.0071	-0.0032
	b_i		-0.9653	0.1505	0.0882	-0.0169	0.0151

n = 1.86 Hz; $\hat{\delta} = \pm 50°$; $\overline{\delta} = 0°$; $\hat{\chi} = \pm 45°$; $\overline{\chi} = 0°$; $\varphi = 60°$

		i = 0	i = 1	i = 2	i = 3	i = 4	i = 5
C_x	a_i	0.2555	-0.2119	-0.4455	-0.01516	0.0075	-0.0017
	b_i		0.0380	0.4491	-0.0188	-0.0013	0.0009
C_y	a_i	-0.0234	-0.1310	0.3466	-0.0092	-0.0505	-0.0032
	b_i		0.0479	0.6394	0.0050	-0.0210	0.0093
C_z	a_i	-0.1615	-0.3311	-0.1619	0.2074	-0.0105	-0.0086
	b_i		-0.9227	0.1805	0.0812	-0.0091	0.0175

n = 1.86 Hz; $\hat{\delta} = \pm 50°$; $\overline{\delta} = 0°$; $\hat{\chi} = \pm 45°$; $\overline{\chi} = 0°$; $\varphi = 75°$

		i = 0	i = 1	i = 2	i = 3	i = 4	i = 5
C_x	a_i	0.2355	-0.2332	-0.2682	-0.0216	0.0040	0.0022
	b_i		0.0621	0.5452	-0.0088	-0.0047	0.0006
C_y	a_i	0.0132	-0.1187	0.5563	-0.0102	-0.0318	0.0031
	b_i		0.0439	0.6256	-0.0087	-0.0512	0.01772
C_z	a_i	-0.1185	-0.4123	-0.1338	0.2673	-0.0088	-0.0098
	b_i		-1.0130	0.2237	0.1452	-0.0169	0.0099

$n = 1.86$ Hz; $\hat{\delta} = \pm 50°$; $\overline{\delta} = 0°$; $\hat{\chi} = \pm 45°$; $\overline{\chi} = 0°$; $\varphi = 90°$

		i = 0	i = 1	i = 2	i = 3	i = 4	i = 5
C_x	a_i	0.2052	-0.2659	-0.1769	-0.0138	0.0062	-0.0009
	b_i		0.0886	0.5679	-0.0008	-0.0046	0.0018
C_y	a_i	-0.0191	-0.1629	0.5111	-0.0066	-0.0692	0.0044
	b_i		0.0627	0.6813	0.0195	-0.0102	0.0065
C_z	a_i	-0.0762	-0.3536	-0.2238	0.3068	0.0100	-0.0270
	b_i		-0.8769	0.1933	0.1194	0.0146	-0.0020

$n = 1.86$ Hz; $\hat{\delta} = \pm 50°$; $\overline{\delta} = 15°$; $\hat{\chi} = \pm 45°$; $\overline{\chi} = 0°$; $\varphi = 30°$

		i = 0	i = 1	i = 2	i = 3	i = 4	i = 5
C_x	a_i	0.4551	0.0731	-0.5474	0.0191	0.0070	0.0020
	b_i		-0.2314	0.2502	-0.0018	0.0005	-0.0007
C_y	a_i	-0.1794	0.0398	0.4624	-0.0034	-0.0493	0.0042
	b_i		-0.0562	0.5228	-0.0606	-0.0315	-0.0202
C_z	a_i	-0.2390	-0.5547	0.2607	0.2909	0.0052	-0.0150
	b_i		-1.0828	-0.1546	0.0877	0.0188	0.0068

$n = 1.86$ Hz; $\hat{\delta} = \pm 50°$; $\overline{\delta} = 15°$; $\hat{\chi} = \pm 45°$; $\overline{\chi} = 0°$; $\varphi = 60°$

		i = 0	i = 1	i = 2	i = 3	i = 4	i = 5
C_x	a_i	0.4285	0.1407	-0.4039	0.0096	0.0020	0.0018
	b_i		-0.1012	0.4226	-0.0007	-0.0017	-0.0027
C_y	a_i	-0.2253	0.1964	0.4504	0.0184	-0.0314	-0.0005
	b_i		-0.0609	0.5730	-0.0286	-0.0198	-0.0163
C_z	a_i	-0.2287	-0.4447	0.2402	0.2472	-0.0026	-0.0080
	b_i		-0.9338	-0.1832	0.1086	0.0110	0.0044

$n = 1.86$ Hz; $\hat{\delta} = \pm 50°$; $\overline{\delta} = 15°$; $\hat{\chi} = \pm 45°$; $\overline{\chi} = 0°$; $\varphi = 90°$

		i = 0	i = 1	i = 2	i = 3	i = 4	i = 5
C_x	a_i	0.0749	0.2215	-0.1453	-0.0064	0.0030	0.0015
	b_i		-0.1572	0.5285	0.0215	-0.0051	-0.0029
C_y	a_i	-0.1560	0.1568	0.2985	0.0122	-0.0522	0.0026
	b_i		-0.0032	0.5166	0.0080	-0.0144	-0.0078
C_z	a_i	-0.3412	-0.2388	0.2420	0.2495	-0.0010	-0.0025
	b_i		-0.7412	-0.1156	0.1205	0.0079	0.0130

n = 1.86 Hz; $\hat{\delta} = \pm 50°$; $\overline{\delta} = 30°$; $\hat{\chi} = \pm 45°$; $\overline{\chi} = 0°$; $\varphi = 30°$

		i = 0	i = 1	i = 2	i = 3	i = 4	i = 5
C_x	a_i	0.3387	0.0117	-0.4564	0.0378	0.0023	0.0009
	b_i		-0.3320	0.1770	-0.0006	0.0132	0.0020
C_y	a_i	-0.1356	0.1411	0.2305	-0.0293	-0.0339	0.0083
	b_i		-0.0785	0.4902	-0.0369	-0.0233	-0.0136
C_z	a_i	-0.0299	-0.2436	0.3826	0.2110	-0.0094	-0.0088
	b_i		-0.9599	-0.1731	0.1044	0.0121	0.0014

n = 1.86 Hz; $\hat{\delta} = \pm 50°$; $\overline{\delta} = 30°$; $\hat{\chi} = \pm 45°$; $\overline{\chi} = 0°$; $\varphi = 60°$

		i = 0	i = 1	i = 2	i = 3	i = 4	i = 5
C_x	a_i	0.2832	0.0270	-0.3460	-0.0029	0.0004	0.0018
	b_i		-0.2107	0.3851	-0.0139	0.0069	-0.0012
C_y	a_i	-0.0149	0.1148	0.3941	-0.03617	-0.0518	0.0050
	b_i		-0.0469	0.5015	-0.0123	0.0044	-0.0070
C_z	a_i	-0.2416	-0.2721	0.3008	0.2359	-0.0065	-0.0135
	b_i		-0.8122	-0.1976	0.1018	0.0251	0.0122

$n = 1.86$ Hz; $\hat{\delta} = \pm 50°$; $\overline{\delta} = 30°$; $\hat{\chi} = \pm 45°$; $\overline{\chi} = 0°$; $\varphi = 90°$

		i = 0	i = 1	i = 2	i = 3	i = 4	i = 5
C_x	a_i	0.0531	0.1632	-0.1746	-0.0165	0.0015	-0.0009
	b_i		-0.1301	0.4341	0.0200	0.0036	0.0002
C_y	a_i	-0.0290	0.2350	0.3592	-0.0089	-0.0706	0.0026
	b_i		-0.0063	0.4109	-0.0052	-0.0221	-0.0047
C_z	a_i	-0.4118	-0.2132	0.2259	0.2279	0.0177	-0.0065
	b_i		-0.7247	-0.2218	0.0924	0.0095	0.0107

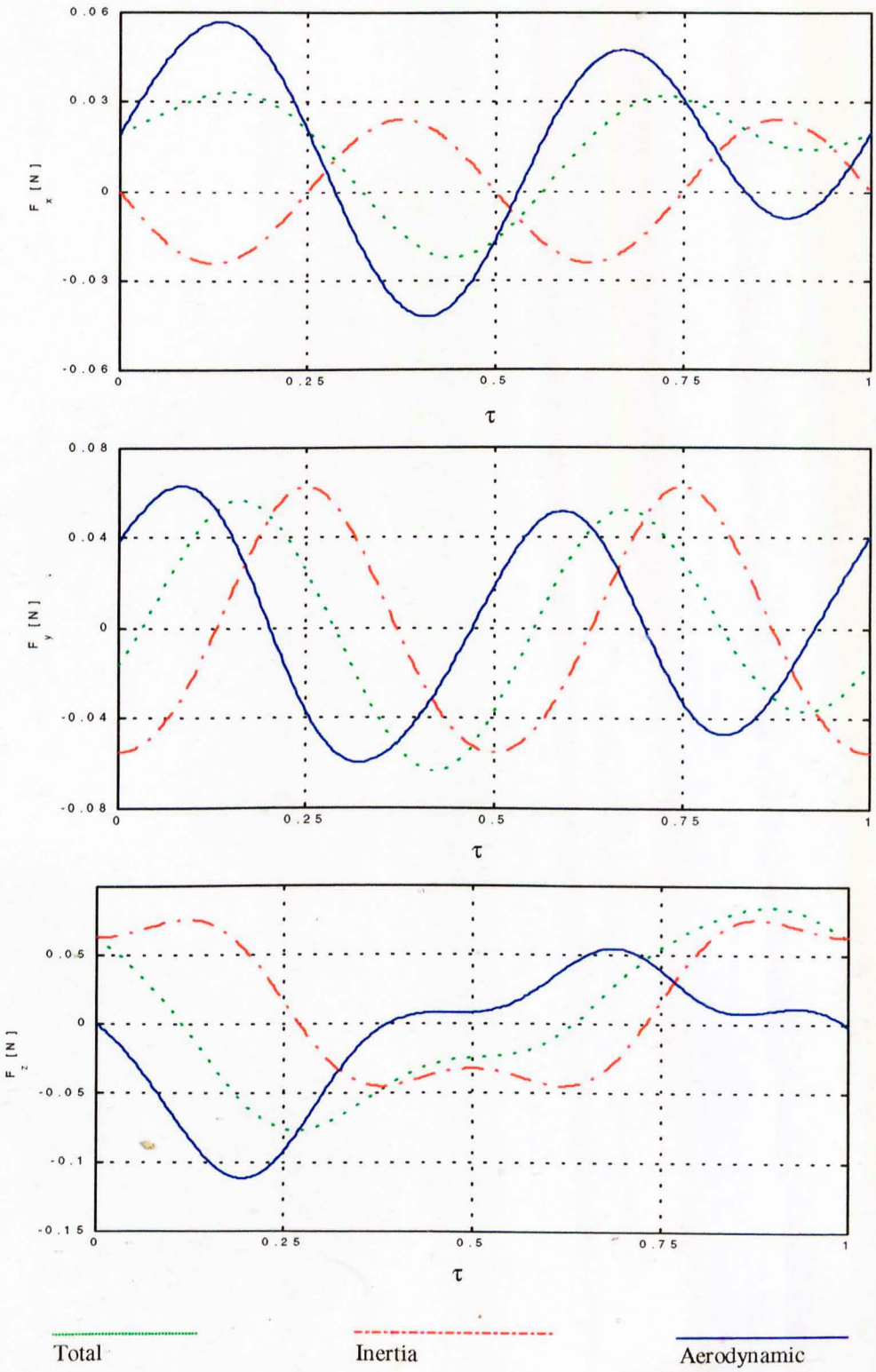

Fig F.5 Forces at n = 1.86 Hz $\varphi = 90°$, $\hat{\chi} = \pm 45°$, $\bar{\chi} = 0°$, $\hat{\delta} = \pm 50°$ and $\bar{\delta} = 0°$.